POLITECNICO DI TORINO

DEPARTMENT OF CONTROL AND COMPUTER ENGINEERING

Master's Degree in Mechatronic Engineering

MASTER'S DEGREE THESIS

Design of a PMSM Field-Oriented Control Algorithm with Flux-Weakening for Battery Electric Vehicles

Supervisor:

Prof. Massimo Violante

Candidate:

Riccardo Rossi

Academic Year 2018-2019

A Carlotta e alla mia Famiglia

Index

CHAPTER II
Electric AC machines

CHAPTER III
Control applications for PMSMs

CHAPTER IV
Development environment

CHAPTER V
Project of the FOC algorithm for a PMSM

Introduction

The thesis is focused on the design of a field-oriented control algorithm with flux-weakening for a permanent magnet synchronous motor (PMSM). The development of the controller is based on LabVIEW FPGA language, using a model-based approach to create the block scheme and to run the autogenerated code on the SPARK engine control unit of Alma Automotive. The realized control strategy takes into account possible automotive applications of this kind of electric motors, discussing and facing in particular the issues related to battery electric vehicles (BEVs). For the project, both interior permanent magnet and surface-mounted permanent magnet synchronous machines have been considered, analysing the behaviour of the first typology with torque loop and speed loop control mechanisms, while for the second one just the torque-based strategy is implemented. The plant and controller models are flashed on the field programmable gate array integrated circuit of the board, while the user interface – with all the commands and the programmable parameters – exploits the hardware real-time module. In the final part of the project, the battery management system and the dashboard are simulated, and the CAN communication protocol is included in order to show the obtained results.

In the first part, electric and hybrid-electric vehicles are analysed, classifying and evaluating them according to their powertrain systems and hybridization levels. An historical description of development and diffusion of these cars is provided, considering also their presence on the worldwide market nowadays. A short presentation of CAN bus is inserted for explaining its features and for describing its use in automotive applications. In the second chapter, the attention is focused on the electric AC machines: the discussion starts from their basic physical principles and their comparison with DC typology. For a complete analysis, asynchronous and synchronous motors are described, studying in particular the dynamic equations of the PMSM. In that section the mathematical models are reported, in order to explain the main properties of FOC algorithm. For what concerns the driving strategy, after an introduction about the inverters and their possible implementation and modulation mechanisms, the scalar regulation and the field-oriented control are presented to show the

differences among them. In the fourth chapter the practical aspects for the control development are introduced: the LabVIEW FPGA – used for the realization of the models – and LabVIEW Real-Time – for the creation of the user interface – modules are described together with the SPARK control prototyping system, concentrating the attention on the main features that are useful for the design. A short description of field programmable gate array system is included too.

The final chapter regards the implementation of the block diagrams for both controller and plant, reporting the relevant schemes and the final results obtained through the simulation of interior permanent magnet and surface-mounted permanent magnet synchronous motors. Moreover, in this part the practical aspects and the faced problems are considered, focusing the analysis on the adopted solutions and the optimization strategies of the algorithm. For a complete scenario of the possible automotive application, also the CAN communication is implemented in the real-time interface, in order to exchange messages with simulated nodes – in particular with the dashboard control unit and the battery management system, for analysing the use of the designed algorithm in a battery electric vehicle. The project has been developed in collaboration with the Automotive area of Teoresi Group S.p.A. in Turin, from March 2019 to October 2019.

List of abbreviations

ABS	–	Anti-lock Braking System
AC	–	Alternating Current
ASIC	–	Application-Specific Integrated Circuit
BC	–	Black Carbon
BCM	–	Body Computer Module
BEV	–	Battery Electric Vehicle
BJT	–	Bipolar Junction Transistor
BLDC	–	Brushless DC motor
BMS	–	Battery Management System
CAN	–	Controller Area Network
CAN FD	–	Controller Area Network with Flexible Data-rate
CHG	–	Compressed Hydrogen Gas
CO_2	–	Carbon Dioxide
CPU	–	Central Processing Unit
CSI	–	Current Source Inverter
DC	–	Direct Current
DSP	–	Digital Signal Processing
ECU	–	Engine Control Unit
EEPROM	–	Electrically Erasable Programmable Read-Only Memory
EMF	–	ElectroMotive Force
EPROM	–	Erasable Programmable Read-Only Memory
ESP	–	Electronic Stability Program
EV	–	Electric vehicle
FCEV	–	Fuel-Cell Electric Vehicle
FIFO	–	First-In First-Out
FOC	–	Field-Oriented Control
FPGA	–	Field Programmable Gate Array

FW	–	Flux-Weakening
FXP	–	Fixed-Point
HDL	–	Hardware Description Language
HEV	–	Hybrid-electric vehicle
HIL	–	Hardware-In-the-Loop
I/O	–	Input/Output
ICE	–	Internal Combustion Engine
IG	–	Interactive Generator
IGBT	–	Insulated Gate Bipolar Transistor
IM	–	Induction Motor
IPM	–	Interior Permanent Magnet
IPMSM	–	Interior Permanent Magnet Synchronous Motor
LED	–	Light Emitting Diode
Li-ion	–	Lithium-ion battery
LUT	–	Look-Up Table
MMF	–	MagnetoMotive Force
MOSFET	–	Metal-Oxide-Semiconductor Field-Effect transistor
MTPA	–	Maximum Torque Per Ampere
MTPV	–	Maximum Torque Per Voltage
Ni-MH	–	Nickel-Metal Hybride battery
NOx	–	Nitrous Oxides
PEMFC	–	Proton Exchange Membrane Fuel-Cell
PHEV	–	Plug-in Hybrid Electric Vehicle
PI	–	Proportional Integral controller/regulator
PM	–	Permanent Magnet
PMSM	–	Permanent Magnet Synchronous Motor
PROM	–	Programmable Read-Only Memory
PWM	–	Pulse-Width Modulation
RAM	–	Random-Access Memory
RF	–	Reference Frame
RIO	–	Reconfigurable Input/Output
RMF	–	Rotating Magnetic Field
RPM	–	Revolutions Per Minute
RT	–	Real-Time
SM	–	Synchronous Motor

SOC	–	State Of Charge
SPFC	–	Solid Polymer Fuel-Cell
SPM	–	Surface-mounted Permanent Magnet
SPMSM	–	Surface-mounted Permanent Magnet Synchronous Motor
SRAM	–	Static Random-Access Memory
SRM	–	Switched Reluctance Motor
SVPWM	–	Space Vector Pulse-Width Modulation
VI	–	Virtual Instrument
VSI	–	Voltage Source Inverter
ZEV	–	Zero-Emission Vehicle

Chapter I:
Electric and hybrid-electric vehicles

SUMMARY: 1.1 Automotive applications of electric motors – 1.1.1 History of electric and hybrid-electric vehicles – 1.1.2 Advantages and disadvantages of electric powertrains – 1.2 Electric vehicles – 1.2.1 Energy sources – 1.2.1.1 Batteries – 1.2.1.2 Fuel-cells – 1.2.1.3 Ultracapacitors – 1.2.1.4 Ultra-high-speed flywheels – 1.2.1.5 Fundamentals of regenerative braking – 1.2.2 Battery electric vehicles – 1.2.3 Fuel-Cell electric vehicles – 1.3 Hybrid-electric vehicles – 1.3.1 Classification of the powertrains – 1.3.1.1 Series hybrid – 1.3.1.2 Parallel hybrid – 1.3.1.3 Series-parallel hybrid – 1.3.2 Levels of hybridization – 1.3.2.1 Micro hybrid – 1.3.2.2 Mild hybrid – 1.3.2.3 Full hybrid – 1.4 Plug-in hybrid-electric vehicles – 1.5 Controller area network (CAN) protocol.

1.1 Automotive applications of electric motors

In recent years, electric and hybrid-electric vehicles development and control techniques are advancing, with important changes and innovations for what concerns the powertrain, the driver assistance systems of modern cars and their automation. The automotive industry is experiencing a global renovation, especially for the reduction of fuel consumption and pollution: in fact, many companies are actually decreasing the production of internal combustion engine cars to concentrate their efforts on the research of modern technologies to improve the environmental sustainability. Consequently, the industry is expending considerable efforts and resources to address the challenges associated with developing alternative solutions for transportation, reducing the emission of dangerous substances – that influences the air quality – and the dependence on petroleum products and non-renewable resources.[1]

[1] Khajepour, A., Fallah, S., & Goodarzi, A. (2014), *Electric and Hybrid vehicles. Technologies, Modeling and Control: A Mechatronic Approach,* Chichester, West Sussex, United Kingdom: Wiley, p.1.

«Electric vehicles (EVs) and hybrid-electric vehicles (HEVs) present many and complex design problems that are absent in the well-established conventional automotive technologies and transportation systems».[2] In order to counterbalance their drawbacks, the design of efficient and long-range cars is one of the major issues that automotive engineers are facing nowadays. For what concerns the electric powertrain system, the development of new powerful motors is fundamental for the increase of vehicles production, considering also the modern control algorithms that assure more reliability and efficiency for their use. Electric, hybrid-electric and fuel-cell-powered drivetrain technologies are the most promising vehicle solutions to replace conventional vehicles in near future.[3]

During past decades – when vehicles became accessible for all the citizens – the internal combustion engine has dominated the transportation industry and today it can be considered an essential part of human life. In fact, the ICE powertrain is actually perfectly known and optimized, while efficient simulation tools are used to describe its behaviour.[4] The combination of this powertrain with the transmission system – manual, automatic, automated or continuous – allows adapting the engine speed to the vehicle velocity: for example, in the manual one a set of gears can be shifted directly by the driver through a clutch pedal and a shift knob. This system operates safely with a high power to weight ratio. Moreover, an ICE vehicle can be also recharged in a very fast way; in fact, it's difficult to overcome the forms of energy that have the highest density and are easily accessible, like gasoline and diesel. The same cannot be said for battery-electric components, because an efficient infrastructure to support the demand of power stations doesn't already exist.

Despite the evolution of modern ICEs, some disadvantages are inevitably related to these systems: for example, the impossibility of generating torque from rest, the losses due to heat, the incomplete combustion and the friction between moving parts of the system. Practically, the real efficiency of this engine is around 35% for modern vehicle, because the remaining quantity is dissipated through the exhaust and cooling systems. A transmission mechanism is needed to connect the ICE to the driving wheels, increasing in this way the number of moving elements and consequently the friction losses and the overall inertia; also noises and vibrations are negative aspects that affect internal combustion engines and not the electric motors.

2 Khajepour, A., Fallah, S., & Goodarzi, A. (2014), *op. cit.,* p. 47.

3 Ehsani, M., Gao, Y., & Emadi, A. (2010), *Modern Electric, Hybrid Electric, and Fuel Cell Vehicles. Fundamentals, Theory, and Design (Second edition)*, Boca Raton, Florida, United States: CRC Press, p. 1.

4 Khajepour, A., Fallah, S., & Goodarzi, A. (2014), *op. cit.,* p. 47.

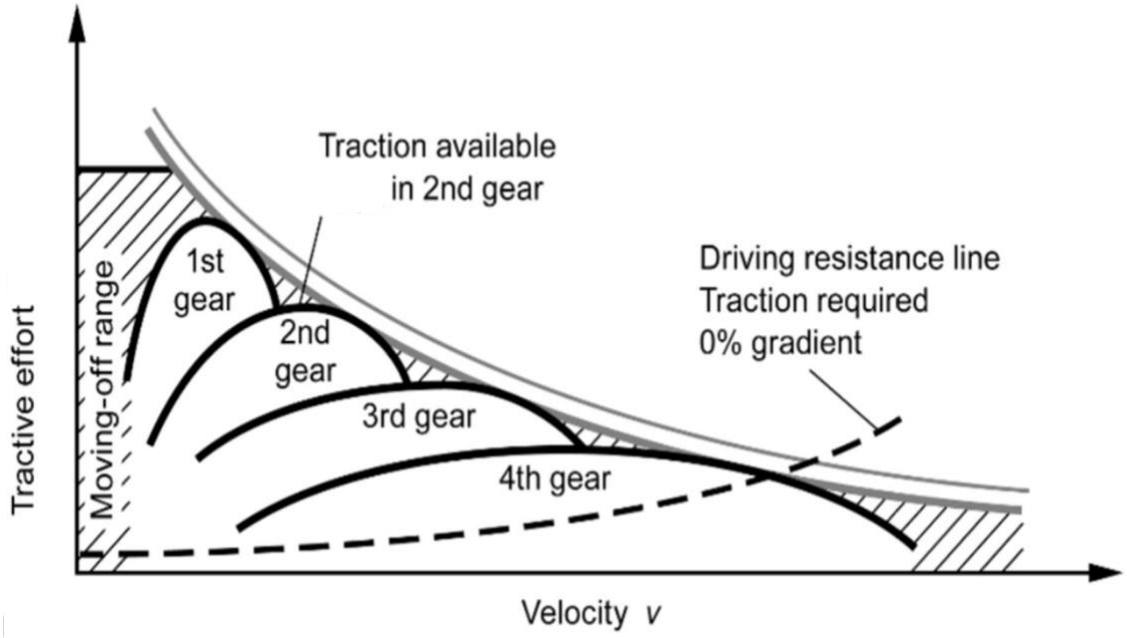

Figure 1.1: Engine torque - vehicle velocity characteristics of an ICE car.[5]

Obviously the most evident drawback is the emission of exhaust gas from the vehicles and the use of petroleum products as fuel; «conventional cars with internal combustion engines (ICE) are still a major source of air pollutants such as carbon dioxide (CO_2), nitrogen oxides (NOx), black carbon (BC) and fine particulate matter».[6] Moreover, the diesel emission scandal – that started in 2014, involving all the main car manufacturers for the exceeding of the legal European emission limits for nitrogen oxide by more than ten times – has given a further incentive to the development of electric vehicles. For all these reasons, the electric powertrains – applied in the automotive sector – are actually experiencing a substantial growth in terms of utilization, research and development.[7] However, the adoption of this kind of engine has only been rediscovered and improved, because the concept of electric vehicles preceded the diffusion of ICEs. The advantages of electricity for mobility applications have been studied since their introduction in the 19th century and their improvement at the beginning of the 20th, during the so-called Golden Age.

[5] Velardocchia, M. (2019), *Fundamentals of Longitudinal Dynamics (Technologies for Autonomous Vehicles),* Turin, Italy: Politecnico di Torino, p. 18.

[6] Buekers, J., Van Holderbeke, M., Bierkens, J., & Int Panis, L. (2014, December), *Health and environmental benefits related to electric vehicle introduction in EU countries*, In *Transportation Research Part D: Transport and Environment*, *33,* p. 26.

[7] Bayindir, K., Gözüküçük, M., & Teke, A. (2011, February), *A comprehensive overview of hybrid electric vehicle: Powertrain configurations, powertrain control techniques and electronic control units*, In *Energy Conversion and Management*, *52(2),* p. 1311.

1.1.1 History of electric and hybrid-electric vehicles

The electric vehicle has been one of the first cars to be invented around 1835 in the Netherlands by Sibrandus Stratingh and Christopher Becker, who created a small-scale electric car, powered by non-rechargeable primary cells. The evolution of batteries to store energy gave a significant improvement to the manufacturing of electric-based solutions for the mobility, in terms of vehicles and locomotives. English inventor Thomas Parker, responsible also for the electrification of London Underground, built the first production electric vehicle in 1884 in London, using rechargeable batteries; he was interested in fuel-efficient vehicles to reduce the malign effects of smoke and pollution in the city. Moreover, France, United Kingdom, Germany and the United States supported the widespread development of this electric cars and trains. The most significant technical advance of that era was the invention of the regenerative braking by M. A. Darraq in 1897: this method enhances the driving range, recuperating the vehicle's kinetic energy while braking and recharging the batteries. This can be defined as one of the major contributions to electric and hybrid-electric vehicles' efficiency.[8]

At the beginning of 20th century – during the Golden Age – electric vehicles obtained many speed and distance records: for example, in 1899 "La Jamais Contente", built by Frenchman Camille Jenatzy, was the first ever vehicle to reach 100 km/h.[9] EVs had many advantages with respect to first gasoline-based competitors: less vibration, smell and noise and obviously no gear shifting, giving the perception of very simple vehicles. These cars were preferred because they not required a manual effort to start, differently from gasoline cars which needed a hand crank to start the engine; moreover, many homes were wired for electricity in the early 1910s, increasing the popularity of electric solutions, that reach the peak production in 1912. In the USA in that period the 38% of registered vehicles were powered by electricity.

After the success of the "Golden Age" the decline of electric cars began in the 1920s due to the improvement of road infrastructure: the limitation of the autonomy was the biggest problem, because at the same time gasoline cars became more powerful, more flexible and they guaranteed the possibility of travelling faster and further.[10] The beginning of mass production brought the price of gas-powered vehicles down, while the price of electric cars

8 Ehsani, M., Gao, Y., & Emadi, A. (2010), *op. cit.,* p. 13.

9 *Ibidem*.

10 Khajepour, A., Fallah, S., & Goodarzi, A. (2014), *op. cit.,* p. 2.

continued to rise. The union of all these aspects caused the disappearance of electric automobile industry from the 1920s – except for some restricted applications (as golf carts and delivery vehicles) – and the internal combustion engine started to dominate the market, as well as nowadays. Moving forward in time, scientists began to worry about the environmental effects of ICE exhaust emissions. For this reason – combined with the fluctuations of hydrocarbon energy market – from the 1970s governments started to take several legislative and regulatory actions to moderate oil production dependency. In this way the conditions for the development of alternatively-powered vehicles were created, so many manufacturers renewed their attempts to produce electric cars. In 1974, The American company Sebring-Vangaurd designed the CitiCar, the first mass-produced electric vehicle. In that period, General Motors Company, Renault, Peugeot and Audi spent a massive effort for electric powertrain development and research.[11]

However, the electric vehicles market failed in the 1990s due to the limited autonomy and performance of these cars with respect to gasoline-powered ones. Moreover, the EVs' high initial and maintenance costs contributed to their commercial failure. Finally, from the 2000s many highway-capable electric vehicles arrived on the market: for example, in 2004 Tesla Motors began to develop the Tesla Roadster that was able to travel more than 320 km per charge, using lithium-ion battery cells. The demand of sustainable solutions to reduce the emissions of ICE vehicles – in particular the diesel ones – led to the diffusion of today electric cars: General Motors, Nissan, Tesla and Toyota, and all the main automakers from the 2010s began to produce zero-emission vehicles, using new technologies to increase their autonomy or to regenerate energy.

Another fundamental aspect was the appearance of hybrid cars on the market in the late 1990s, combining internal combustion engine with an electric motor. Toyota launched successfully the Prius in Japan in 1997, while the Honda Insight arrived on the market in 1999; in 2004 Ford produced the first hybrid SUV. These vehicles were the starters for HEVs' diffusion:[12] modern hybrid vehicles guarantee low emissions, high fuel economy and obviously performance comparable to ICEVs. They represent the perfect solution towards the full electrification of the mobility. HEVs reached success especially in Japan, which surpassed the United States as world's largest hybrid market in 2014. Nevertheless, the diffusion of EVs and HEVs is actually quite small if compared with ICE cars: every aspect

11 Khajepour, A., Fallah, S., & Goodarzi, A. (2014), *op. cit.,* p. 3.

12 Ehsani, M., Gao, Y., & Emadi, A. (2010), *op. cit.,* p. 17.

of human life and energy distribution is still based on petroleum products and the infrastructure are not enough adequate to support the demand of recharging stations.

1.1.2 Advantages and disadvantages of electric powertrains

From the previous historical analysis, the main advantages of the electric powertrain can be defined. First of all, the efficiency is huge with respect to ICE and it can reach peaks over 85%. The gearbox is no more needed because electric engines can operate at significantly high angular speed: consequently, an electric car has only one gear to connect the engine to the shafts. This typology of motor operates safely over a wide range of vehicle speed, guaranteeing always a high traction torque. Obviously, a fundamental advantage is the absence of emissions and the possibility to reduce air pollution. As described before, electric powertrain has the capability of generating instant torque from rest without using any starters, and it's quite lighter and smaller if compared to internal combustion engine; moreover, this motor can reach the idle state and maintain the zero-speed condition, so it doesn't rotate if it is not necessary – for example when the vehicle is stopped.

An electric motor is able to rotate in both directions – clockwise and anticlockwise – so the vehicle can go back and forth, without the need of a reverse gear system. The transmission can be further simplified, reducing the weight and the heat losses due to friction. The electric machine can also operate as generator, when torque and speed have opposite signs. This benefit is exploited for recovering the kinetic energy with the regenerative braking and the potential energy during downhill driving, in order to recharge the energy source and increase the autonomy range. The following figure 1.2 shows the four operational modes – the four quadrants – of this kind of machines. The use of external electric grid for recharging these vehicles is generally less costly than other fuels; moreover, maintenance and repair costs are estimated to be lower with respect to conventional gasoline vehicles. Obviously, the remarkable initial cost is seen as an obstacle for electric-based cars' diffusion.

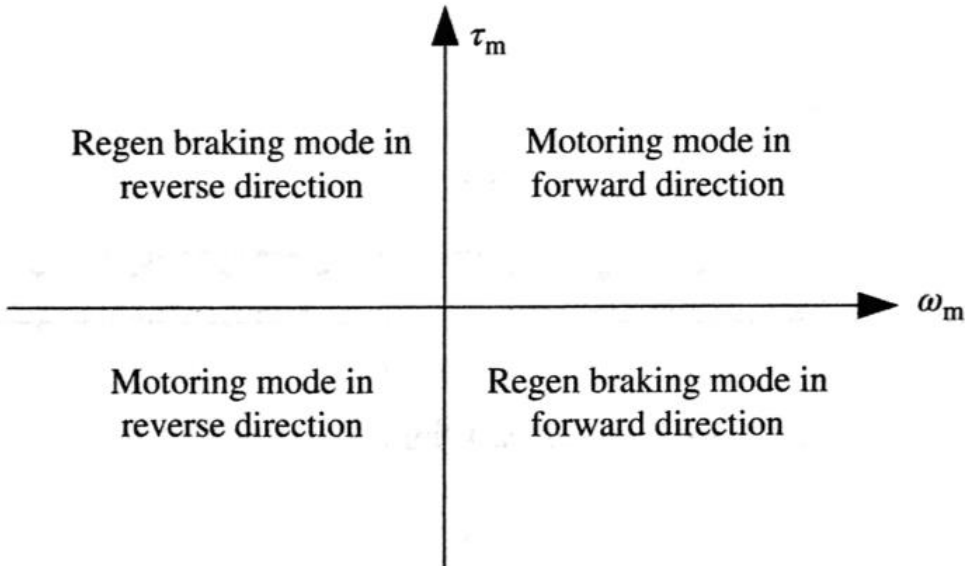

Figure 1.2: Four-quadrant operation modes of the electric machine (motor torque - mechanical speed characteristics).[13]

Regarding the application of the electric powertrains and the diffusion of HEVs and EVs, some interesting questions arise analysing their history, their success and their failure during the last century. In particular, the main problem is the origin of the electricity: actually, its production is still a relevant cause of pollution. Consequently, with EVs and HEVs the damages to the environment would be only partially reduced. The development of power stations based on renewable resources (solar energy, wind, water, geothermal energy) will consistently improve the air quality. The diffusion of this kind of vehicles cannot be split from the research of new solutions for the production of green energy.[14]

Secondly, one of the adopted solutions for energy storage is the use of batteries, in particular the lithium-ions cells – energy sources management will be analysed in next paragraphs. These elements are considered hazardous and they must operate in a specific condition of equilibrium, from electric and temperature points of view. These batteries are obviously subject to degradation and they must be replaced after a certain amount of time, because their capability is reduced. Consequently, the disposal is a critical aspect that is actually the argument of many studies:[15] the continuous development of new technologies

[13] Wei, L. (2017*), Hybrid electric vehicle system modeling and control (Second Edition)*, Chichester, West Sussex, United Kingdom: Wiley, p. 148.

[14] Buekers, J., Van Holderbeke, M., Bierkens, J., & Int Panis, L. (2014, December), *op. cit.,* p. 35.

[15] Gaines, L. (2014, December), *The future of automotive lithium-ion battery recycling: Charting a sustainable course*, In *Sustainable Materials and Technologies*, *1-2*, p 2.

implies that the batteries are difficult to be reused and recharged; moreover, the extraction of lithium from old ones is five times more expensive than mined lithium.

Finally – as considered before – the autonomy of this kind of vehicles is an essential problem that has always influenced their history and their diffusion: nowadays the electric vehicles cannot compete with the ICE ones or the hybrid cars, because the mileage is sufficient only for city driving. The mechanism of idle-off and the regenerative braking system are fundamental aspects to increase the autonomy.[16] The diffusion of charging stations will also greatly improve the use of electric vehicles, but the time needed for a complete recharge is obviously higher with respect to gasoline-based vehicles. An additional issue is the absence of noise that can be seen as an advantage from the driver and passengers' point of view, but as a danger for the pedestrians and other drivers; in many cases, sensors are mounted on these vehicles to advice surrounding people and cars.

In the following paragraphs, the main characteristics and the classification criteria of both electric and hybrid-electric vehicles will be analysed.

1.2 Electric vehicles

An electric vehicle – referred to as an electric drive vehicle – uses one or more electric motors for propulsion. An electric vehicle can be self-contained with battery or it can be powered by off-vehicle sources, depending on the application. EVs include road and rail vehicles, surface and underwater vessels and electric aircraft and spacecraft; despite the domination of ICE for almost 100 years, electric power remained fundamental for other mobility solutions, like trains and smaller vehicles. Recently, electric cars saw a fast and crucial development, thanks to the augmented focus on renewable energy and limitation of air pollution. From 2018 on the market there are almost 180 models of highway-capable all-electric passenger cars: Nissan Leaf is the world's top selling rechargeable electric car, followed by Tesla Model S and Model 3. To enlarge the diffusion of electric vehicles, several countries have recently established grants and subsidies for the purchase of the vehicle and for the advancement of the studies on cars and batteries. Electric vehicles are expected to increase from 2% of global share in 2016 to 22% in 2030, together with the development of new and more adequate infrastructure for energy distribution and more efficient mechanism for energy storage. «The price of the EVs is quite high compared to their ICE counterparts.

[16] Khajepour, A., Fallah, S., & Goodarzi, A. (2014), *op. cit.,* p. 49.

This is because of the high cost of batteries and fuel-cells. To make people overlook this factor, governments in different countries including the UK and Germany, have provided incentives and tax breaks which provide the buyers of EVs with subsidies. Mass production and technological advancements will lead to a decrease in the prices of batteries as well as fuel-cells».[17]

1.2.1 Energy sources

In contrast to vehicles powered by conventional ICE, energy storage systems are of crucial importance for electric vehicles.[18] Different technologies have been proposed and studied in recent years to guarantee the needed supply for the electric powertrain: batteries, fuel-cells, ultracapacitors and flywheels are the main adopted solutions. Batteries, capacitors and flywheels are systems where the electrical energy is stored during charging, while fuel-cells are energy generation systems based on chemical reaction. Actually, batteries are the fundamental elements of modern EVs because of their reasonable cost and their technological evolution.[19] Differently from ICE's high performance, these energy sources cannot provide high specific energy and high specific power simultaneously; the specific energy is the energy capacity per unit source weight, while the specific power is defined as the maximum power per unit energy source weight.[20] For this reason, hybridization techniques are actually being studied for combining two or more storages together so that the disadvantages of each can be compensated by others and the positive aspects can be exploited. [21] Basically, one energy storage provides high specific energy and the other high specific power. For high power demand operations, like acceleration or hill climbing, both basic energy sources deliver their power. In low power demand situations, like constant

[17] Un-Noor, F., *et al*. (2017, August), *A Comprehensive Study of Key Electric Vehicle (EV) Components, Technologies, Challenges, Impacts, and Future Direction of Development,* In *Energies*, *10(8),* p. 58.

[18] Eberle, U., & von Helmolt, R. (2010), *Fuel Cell Electric Vehicles, Battery Electric Vehicles, and their Impact on Energy Storage Technologies: An Overview,* In G. Pistoia, *Electric and Hybrid Vehicles. Power Sources, Models, Sustainability, Infrastructure and the Market (pp. 227-245),* Amsterdam, The Netherlands: Elseiver, p. 227.

[19] Chau, K., Wong, Y., & Chan, C. (1999, July), *An overview of energy sources for electric vehicle,* In *Energy Conversion & Management*, *40(10)*, p. 1023.

[20] Ehsani, M., Gao, Y., & Emadi, A. (2010), *op. cit.,* pp. 380-384.

[21] Chau, K., Wong, Y., & Chan, C. (1999, July), *op. cit.,* p. 1035.

speed operations, the high specific energy storage delivers its power to the load and charge also the high specific power storage. In case of negative power – regenerative braking situation – the peak power is absorbed by the high specific power element and only partially by the other.[22]

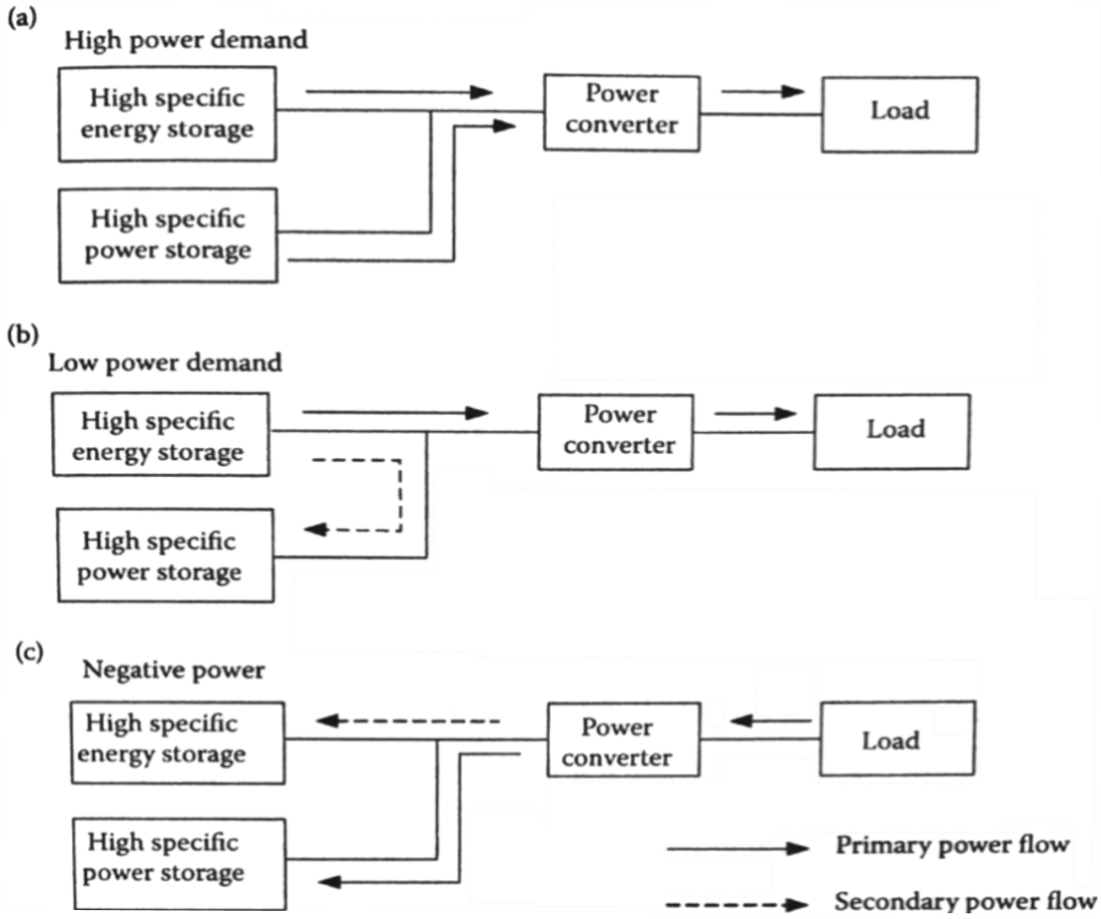

Figure 1.3: Hybridization concept in different operating conditions (a) hybrid powering, (b) power split, (c) hybrid recharging.[23]

1.2.1.1 Batteries

Battery systems are expected to be a safe and reliable source of energy that delivers the high performance that modern battery cells and chemistries have to offer. Electrochemical batteries are electrochemical device that convert electrical energy into potential chemical energy during charging and convert the stored chemical energy into

[22] Ehsani, M., Gao, Y., & Emadi, A. (2010), *op. cit.,* p. 404.

[23] *Ivi*, p. 405.

electric energy during discharging. Batteries are composed by several cells stacked together: each cell is an independent unit composed by two electrodes (positive and negative) immersed into electrolyte.[24]

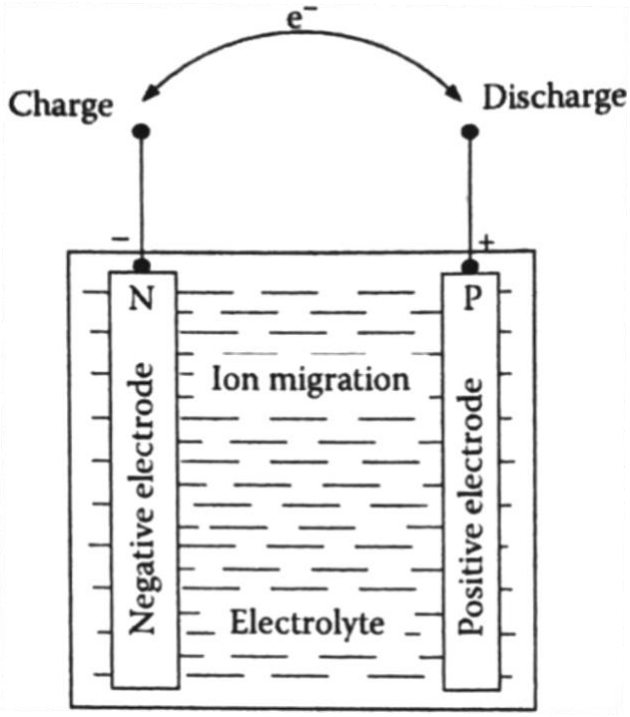

Figure 1.4: Electrochemical battery cell.[25]

One of the main parameters that are specified by manufacturers is the coulometric capacity (ampere-hours) that defines the number of ampere-hours gained when discharging the battery from a fully charged state until the terminal voltage drops reaches its cut-off voltage. Usually the discharging current rate influences the capacity – for example a large discharge rate causes a smaller capacity – so the manufacturers specify the discharge rate for a certain capacity. Another important value is the state of charge (SOC) of a battery, defined as the ratio of remaining capacity to fully charged capacity. The thermodynamic voltage of a battery cell is closely associated with the energy released and the number of electrons transferred in the chemical reaction; on the other hand, the efficiency expresses the cell operating voltage to the thermodynamic voltage, for evaluating the energy or power losses in terms of voltage losses. Finally, specific energy and specific power are two essential parameters for evaluating the performance of a battery.[26]

[24] Ehsani, M., Gao, Y., & Emadi, A. (2010), *op. cit.,* p. 375.

[25] *Ivi,* p. 376.

[26] *Ibidem*.

Different technologies have been used for developing adequate batteries for electric and hybrid-electric vehicles; the principal three solutions are: lead-acid batteries, nickel-based and nickel metal hybride batteries, lithium-ion batteries.[27] Lead-acid battery is the oldest rechargeable one and it has represented a successful commercial product for over a century; it's still widely used as electrical energy storage for many automotive applications, for example for starting the engine in conventional vehicles.[28] This technology requires lower cost compared with other solutions, high cell open-circuit voltage, easy recycling and accurate SOC indication. The principal drawbacks are related to the low energy density and short life cycle, high self-discharge rate and low charge/discharge efficiency.[29] Thanks to their high power, these energy storage systems are attractive for HEV applications; new lead-acid are actually being developed for improving the performance of electric and hybrid-electric cars: recently, the main disadvantages – as low specific energy, reduced lifetime and safety issue – have been overcome.

Nickel is a lighter metal than lead and guarantees good electrochemical properties for battery applications. Nickel/iron was the first nickel-based solution, but it suffered from gassing, corrosion and self-discharge problems, with a non-negligible initial cost; on the other hand, the higher power density with respect to lead-acid batteries was a huge benefit. Then nickel/cadmium batteries have been introduced, guaranteeing an enormous technical improvement for their high specific power, long life cycle, rapid charge capability, negligible corrosion and low self-discharge rate. The initial cost is still a problem, together with the environmental hazard due to cadmium: despite its recyclability, it can cause pollution if not properly disposed of.[30] A nickel-metal hybride (Ni-MH) battery uses hydrogen absorbed in a metal alloy for the active negative material; since a metal hybride electrode has a higher energy density than a cadmium electrode, this battery has higher capacity and longer life with respect to previous nickel-based technologies.[31] Ni-MH battery is free from toxicity or carcinogenicity – differently from cadmium – so it is actually a suitable choice for EV and HEV applications[32]; in fact, Ni-MH batteries are used for most

[27] Khajepour, A., Fallah, S., & Goodarzi, A. (2014), *op. cit.,* p. 59.

[28] Ehsani, M., Gao, Y., & Emadi, A. (2010), *op. cit.,* p. 385.

[29] Wei, L. (2017*), op. cit.*, p. 25.

[30] Khajepour, A., Fallah, S., & Goodarzi, A. (2014), *op. cit.,* p. 60.

[31] Wei, L. (2017*), op. cit.,* p. 26.

[32] Ehsani, M., Gao, Y., & Emadi, A. (2010), *op. cit.,* p. 388.

HEVs currently sold in the United States.[33] As drawbacks, limitations in energy and power density are not negligible, while the initial cost is an obstacle for their diffusion.

The lithium-ion (Li-Ion) battery is actually viewed as the battery that guarantees the long-term goals for EVs. It uses lithiated carbon intercalation material for the negative electrode, lithiated transition metal oxide for the positive electrode and liquid organic solution for the electrolyte: lithium ions are extracted from the negative electrode and inserted to the positive one on discharge and vice versa on charge operation.[34] This kind of battery exhibits high specific energy and specific power together with a long cycle life; the main drawback is related to the huge initial cost.[35]

New battery technologies will also create a need for new management capabilities; moreover, new active materials are continuously developed for improving energy capacity, cycle life and autonomy range.[36] Lithium-ion batteries are incorporated into advanced devices, from automotive to aviation, aerospace and defence, so a higher level of reliability and safety must be assured, reducing the risk of errors concerning the production and the operational mode of these batteries. «The field of Li-Ion solutions for energy storage is a fertile area for many years to come, leading to new advances in the fields of transportation and energy storage»[37]: management systems will need to cope with significant improvement in battery behaviour, maintaining always an accurate prediction of the battery condition and assuring the high reliability that all electronic control systems must guarantee.

1.2.1.2 Fuel-cells

Fuel-cells – and also ultracapacitors – have received attention recently and they have showed optimal performance in the mid-term.[38] Fuel-cells energy storage system is based on the conversion of the hydrogen and oxygen chemical energy directly into electrical

[33] Axsen, J., Burke, A. F., & Kurani, K. S. (2010), *Batteries for PHEVs: Comparing Goals and the State of Technology*, In G. Pistoia, *Electric and Hybrid Vehicles. Power Sources, Models, Sustainability, Infrastructure and the Market (pp. 405-427),* Amsterdam, The Netherlands: Elseiver, p. 418.

[34] Chau, K., Wong, Y., & Chan, C. (1999, July), *op. cit.,* p. 1028.

[35] Weicker, P. (2014), *A systems approach to Lithium-Ion Battery Management*, Norwood, Massachusetts, United States: Artech House, p. 25.

[36] Axsen, J., Burke, A. F., & Kurani, K. S. (2010), *op. cit.,* p. 420.

[37] Weicker, P. (2014), *op. cit.*, p. 23.

[38] Chau, K., Wong, Y., & Chan, C. (1999, July), *op. cit.,* p. 1023.

energy. In this case, the electricity-producing reactants are continually supplied from external sources to the fuel-cell itself: oxygen from the air and hydrogen from a separate onboard tank. Differently from batteries, the reactants are not regenerated by the recharging process.[39]

Solid polymer fuel-cells (SPFCs) – called also proton exchange membrane fuel-cells (PEMFCs) – are actually the most studied and developed technology for EVs. SPFC uses a solid polymer membrane as the electrolyte and has the advantage of the highest power density;[40] however, the cost of the catalyst is significant compared to ICE, because noble metals are needed due to low operating temperature of the fuel-cell and the acid nature of the electrolyte. Other critical issues are poisoning problem and water management because polymer membrane needs to be kept humid, otherwise there will not be enough acid ions to carry the protons; on the other hand, a too much wet membrane blocks reactant gases.[41] This technology guarantees advantages that motivate their future diffusion, such as low-temperature operation, fast start-up, high power density and reduced dimension.

Alternative fuel-cells are the alkaline ones, based on an aqueous solution of potassium hydroxide as electrolyte to conduct ions between electrodes, that are cheaper and guarantee high efficiency, but with a limited durability due to corrosive electrolyte.[42] Phosphoric acid fuel-cells are similar to PEMFCs, because they use an acid electrolyte to conduct hydrogen ions; they work at low temperature and guarantee fast start-up, but they need expensive catalyst and are subject to corrosion and carbon-monoxide poisoning.[43] Finally, molten carbonate fuel-cells work at high temperature and use a molten carbonate salt to conduct ions: differently from above technologies, these cells are supplied directly by hydrocarbons because the high temperature allows their decomposition to hydrogen on the electrodes. These fuel-cells require also low-cost catalyst and have improved efficiency, but they are slower and need only a particular set of materials due to high temperature.[44]

[39] Delucchi, M., & Lipman, T. (2010), *Lifetime Cost of Battery, Fuel-Cell, and Plug-in Hybrid Electric Vehicles*, In G. Pistoia, *Electric and Hybrid Vehicles. Power Sources, Models, Sustainability, Infrastructure and the Market (pp. 19-60)*, Amsterdam, The Netherlands: Elseiver, p. 45.

[40] Chau, K., Wong, Y., & Chan, C. (1999, July), *op. cit.,* p. 1029.

[41] Khajepour, A., Fallah, S., & Goodarzi, A. (2014), *op. cit.,* p. 68.

[42] Ehsani, M., Gao, Y., & Emadi, A. (2010), *op. cit.,* p. 444.

[43] *Ivi,* p. 447.

[44] Khajepour, A., Fallah, S., & Goodarzi, A. (2014), *op. cit.,* p. 70.

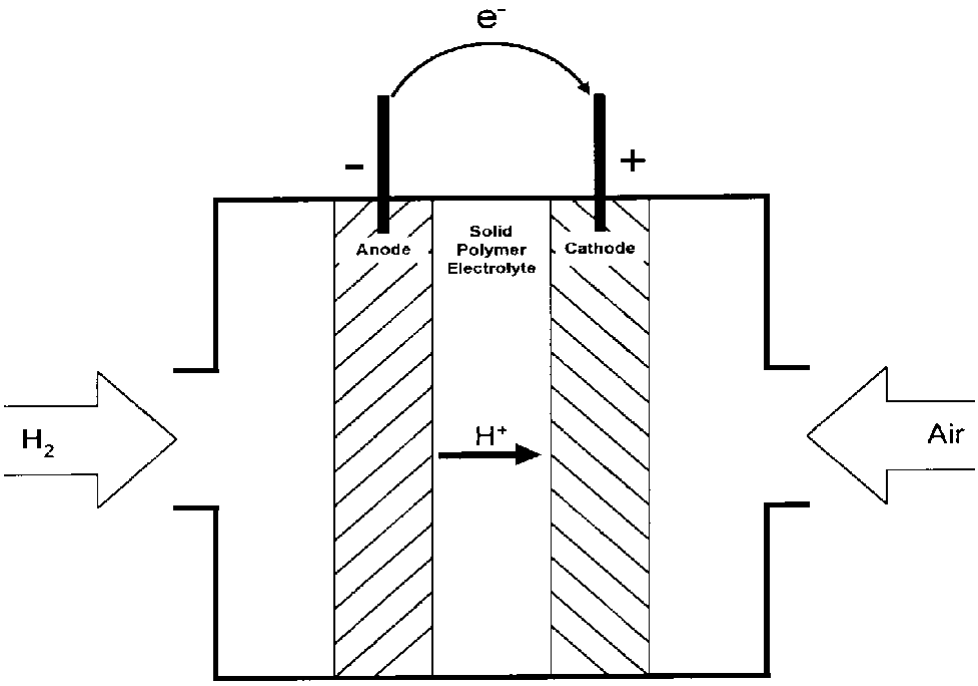

Figure 1.5: Schematic of a SPFC (or PEMFC).[45]

For hydrogen storage, the main adopted methods are three: storing it as a compressed gas (compressed hydrogen gas, CHG), so pure hydrogen is stored onboard the vehicle under pressure in a tank; in form of liquid hydrogen in cryogenic containers, a very hazardous application; using the metal hybrid technology, so hydrogen reacts with some metals like magnesium and vanadium. CHG solution and metal hybrids are still huge challenges for vehicle application, but they can guarantee optimal performances.[46]

1.2.1.3 Ultracapacitors

The difficulty in simultaneously obtaining high values of specific energy, specific power and cycle life has led to hybridization techniques. Fuel-cells and batteries have high specific energy, so a power source with high specific power is needed, and ultracapacitors received huge attention for this purpose.[47] These elements – based mainly on double-layer capacitor technology – are characterized by a specific power that can reach up to 3 kW/kg,

[45] Chau, K., Wong, Y., & Chan, C. (1999, July), *op. cit.,* p. 1030.

[46] *Ibidem*.

[47] *Ivi,* p. 1032.

much higher than any battery – so they can provide high output power within a short period of time, in case of huge power demand conditions.[48]

Moreover, the life cycle of batteries is affected by frequent start/stop operations of electric powertrain and by high peak power demands, jeopardizing the efficiency of regeneration system: ultracapacitors are able to minimize the huge discharging current and also the high charging current which arrives to the battery through the regenerative braking system, so the available energy, endurance and life of the battery can be greatly increased.[49] Therefore, the hybridization technique allows providing optimal energy recovery. On the other hand, ultracapacitors' implementation requires additional power electronics, increasing the initial costs of the vehicle. Actually, this mechanism is not enough powerful to support the power demand of an EV, but its evolution will significantly improve vehicles' performance. As additional issue, for an efficient hybridization an accurate control of the power flow between ultracapacitors, batteries, motors and power electronics is needed.[50]

1.2.1.4 Ultra-high-speed flywheels

Flywheels are not a new concept: they were introduced around 25 years ago for powering passenger buses, but they were heavy, and their rotor wasn't fast. Modern flywheels consist of a lightweight composite rotor, able to rotate at the order of ten thousand of revolutions per minute (RPM).[51] This energy storage system can achieve the requirements for EV applications, guaranteeing high specific power, high specific energy, high efficiency, quick recharging, reduced costs and almost unlimited life cycle. In case of hybridization, flywheels are used as an auxiliary energy source to store energy in mechanical form during period of cruise speed or regenerative braking. «To charge and discharge the ultra-high-speed flywheel, which is directly coupled to the machine rotor, the permanent magnet (PM) brushless machine has been accepted to be the most appropriate type».[52] Consequently, many benefits are associated to the use of this storage system, like also rapid short-term recharges and extension of vehicle range.

[48] Ehsani, M., Gao, Y., & Emadi, A. (2010), *op. cit.,* p. 390.

[49] Khajepour, A., Fallah, S., & Goodarzi, A. (2014), *op. cit.,* p. 61.

[50] *Ibidem*.

[51] Ehsani, M., Gao, Y., & Emadi, A. (2010), *op. cit.,* p. 397.

[52] Chau, K., Wong, Y., & Chan, C. (1999, July), *op. cit.,* p. 1034.

Despite the previous description, some problems affect their diffusion: first, the vehicle manoeuvrability could be reduced due to possible gyroscopic phenomena when the vehicle departs from its straight-line trajectory; secondly, in case of malfunctions the stored mechanical energy will be released very rapidly, causing severe damages to the other parts of the system. To overcome this inconvenient, the use of multiple flywheels will reduce the gyroscopic effects, while new safer failure containments are being developed. Ultra-High-speed flywheels are analysed as the main solution for the progress of long-term EVs.[53]

1.2.1.5 Fundamentals of regenerative braking

Regenerative braking is an energy recovery system that converts the vehicle kinetic energy into a form that can be stored, when the vehicle is braking. In conventional ICEVs, the braking system helps to decelerate or stop a moving vehicle by supplying a sufficient braking torque on all wheels and creating friction between the brake pads and the wheels; consequently, a substantial amount of energy is dissipated as excessive heat energy.[54] The electric motors of EVs and HEVs can be controlled to operate as generators to convert the kinetic energy into electric energy that can be stored and reused. This aspect is a unique feature of these vehicles that distinguishes them from gasoline-based cars. In fact, electric machines are able to work as motors or as generators – converting mechanical energy into electric energy[55] – depending on the operating mode. The main advantages due to regenerative braking are the improved efficiency and fuel economy, the reduction of brake and engine wear with respect to ICE, the attenuation of emissions thanks to the mitigation of dissipated energy and the increase of the operating range.[56]

Modern electric motors cannot provide the necessary braking torque in case of heavy braking. For this reason, hybrid braking system are implemented to guarantee optimal performance and to recover as much energy as possible.[57] When the regenerative braking is at maximum, the additional hydraulic system provides the required torque. In fact,

53 Ehsani, M., Gao, Y., & Emadi, A. (2010), *op. cit.,* p. 403.

54 *Ivi,* p. 411.

55 Bhandari, P., Dubey, S., Kandu, S., & Deshbhratar, R. (2017, February), *Regerative Braking Systems (RBS),* In *International Journal of Scientific & Engineering Research, 8(2),* p. 72.

56 Bhandari, P., Dubey, S., Kandu, S., & Deshbhratar, R. (2017, February), *op. cit.,* p. 73.

57 Ehsani, M., Gao, Y., & Emadi, A. (2010), *op. cit.,* p. 411.

regenerative braking is necessarily limited when the energy sources are fully recharged. For high-speed applications, regenerative braking doesn't work efficiently because electric machine – acting as generator – is in constant power region (also called flux-weakening region):[58] consequently, the torque capability is lower than the nominal one.

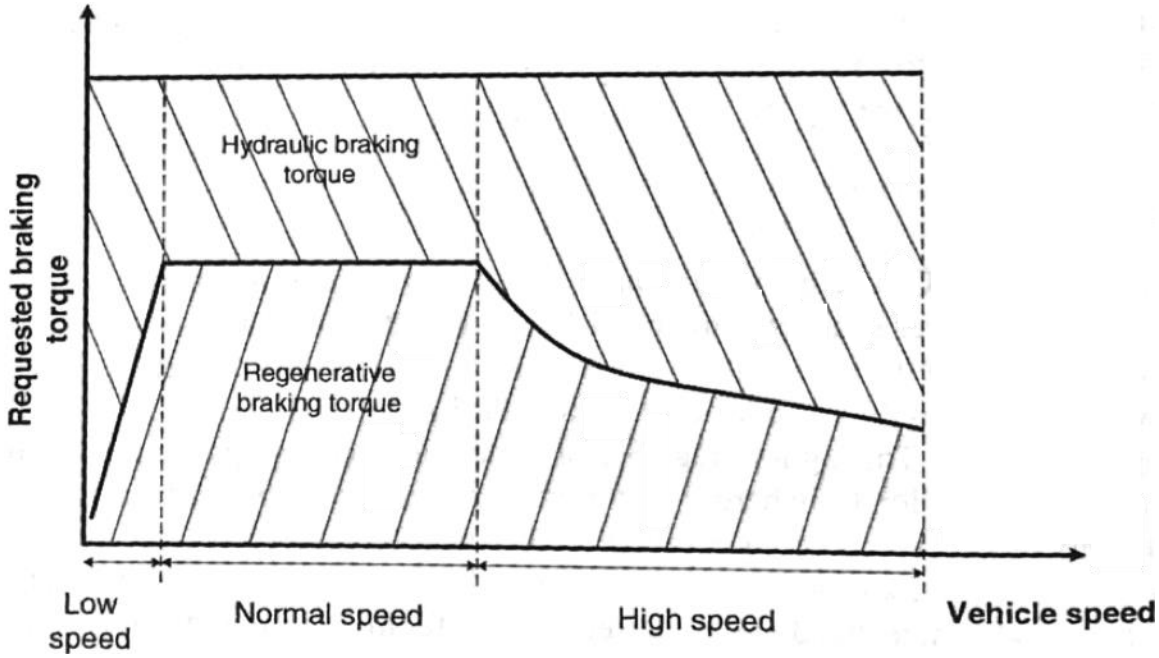

Figure 1.6: Hybridization of regenerative and hydraulic braking system battery cell.[59]

1.2.2 Battery electric vehicles

A battery electric vehicle runs entirely on a battery and electric drivetrain, without a conventional internal combustion engine; BEVs are the simplest type of electric vehicle from a conceptual perspective, because the electrical power of the electrochemical battery is exploited to power one or more electric machine. The typical configuration requires a single motor connected to the front axle through a simple gearbox; another significant variation is to use four hub motors attached to each wheel.[60] These vehicles must be plugged into an external source of electricity to recharge their batteries; they can be recharged from grid electricity at recharging stations or houses, non-grid sources as solar panels or using recuperative energy systems – as previously mentioned: potentially a BEV can emit zero

[58] Khajepour, A., Fallah, S., & Goodarzi, A. (2014), *op. cit.,* p. 65.

[59] *Ivi*, p. 64.

[60] Delucchi, M., & Lipman, T. (2010), *op. cit.,* p. 23.

greenhouse gases and air pollutants. In addition to environmental advantages, electric vehicles guarantee a higher efficiency with respect to internal combustion engine cars; moreover, the required maintenance is expected to be lower due to the reduction of mechanical and emission control components.[61] For example, muffler, tailpipe and gas tank are totally absent from electric vehicles.

Despite the benefits, some disadvantages are still related to BEV. First, the low energy and power density of batteries with respect to liquid fuels, i.e. gasoline or diesel. Second, once depleted, charging the battery pack takes quite a lot of time compared to refuelling an ICE vehicle – there are less time-consuming solutions, but none is comparable to the little time required to refill a fuel tank. Third, they can cover only 100-250 km on one charge, whereas the top-tier models can reach 500 km; these ranges depend on driving condition and style, vehicle configurations, road conditions, climate, battery type and age.[62] Modern BEVs have various configurations: some elements can be present in a vehicle and not in other one, depending on the design and providing consequently different performance in terms of autonomy, traction torque, recharging time, delivered power, weight and dimensions. Typically, the key components of this kind of cars are:

- one or more electric motors to convert the electric energy from energy sources into mechanical energy to provide the required traction force for the vehicle motion;[63]
- traction battery pack – regulated by the BMS – to store electricity for the electric motor;
- an auxiliary battery for providing the required electricity to power the accessories in the electric drive vehicle;
- battery management system (BMS) that is the control unit for monitoring the traction battery pack;
- charge port to connect the vehicle to an external supply;
- DC/DC converter to convert the higher-voltage DC power from the traction battery to the lower-voltage DC power needed to run vehicle accessories and recharge the battery;
- onboard charger that takes the incoming AC electricity via the charge port and converts it to DC power for charging the battery. Moreover, it monitors the battery status and operating condition for guaranteeing the correct current;

[61] Khajepour, A., Fallah, S., & Goodarzi, A. (2014), *op. cit.,* p. 48.

[62] Un-Noor, F., *et al.* (2017, August), *op. cit.*, p. 3.

[63] Khajepour, A., Fallah, S., & Goodarzi, A. (2014), *op. cit.,* p. 53.

- thermal system to maintain a proper operating temperature range in the engine;
- power electronics controller (inverter) to manage the flow of electric energy delivered by traction battery and to control the electric traction motor's speed and torque;
- regenerative braking system for exploiting the kinetic energy to recharge the battery, during braking;
- electric transmission for transferring the mechanical power from electric motor to the driving wheels. Motors can also be mounted inside the wheels.

Batteries are grouped into packs that can be realized in different ways, using series or parallel connections between groups of cells. BEV motors typically operate at a few hundred volts, that's why a minimum of about 100 cells is required (for example, considering a cell voltage of 3.6 V, 100 Li-Ion batteries can produce 360 V). Alternatively, some vehicles have many but smaller cells, up to tens of thousands. Battery pack is the largest and most expensive element of the BEV, because it is typically the unique power source. A fundamental concept for modern battery electric cars is to have a removable and replaceable battery pack: this can allow to extend the driving range through the use of swap stations, but obviously the substitution must be fast and non-complex.[64] In addition to the basic pack, thermal management and voltage-monitoring systems are required to prevent overcharging of the energy source and to detect degradation or failure. The powertrain of BEVs is simpler than that of ICE vehicles: power is transmitted to the driving wheels through few selected components, reducing the friction among mechanical elements. In addition, the rapid dynamics of electric motors enables accurate and precise control of wheel torque, giving the possibility of implementing faster, safer and more reliable stability and safety control systems – active cruise control, collision avoidance, etc. – with respect to conventional cars.[65]

[64] Delucchi, M., & Lipman, T. (2010), *op. cit.,* p. 24.

[65] Khajepour, A., Fallah, S., & Goodarzi, A. (2014), *op. cit.,* p. 51.

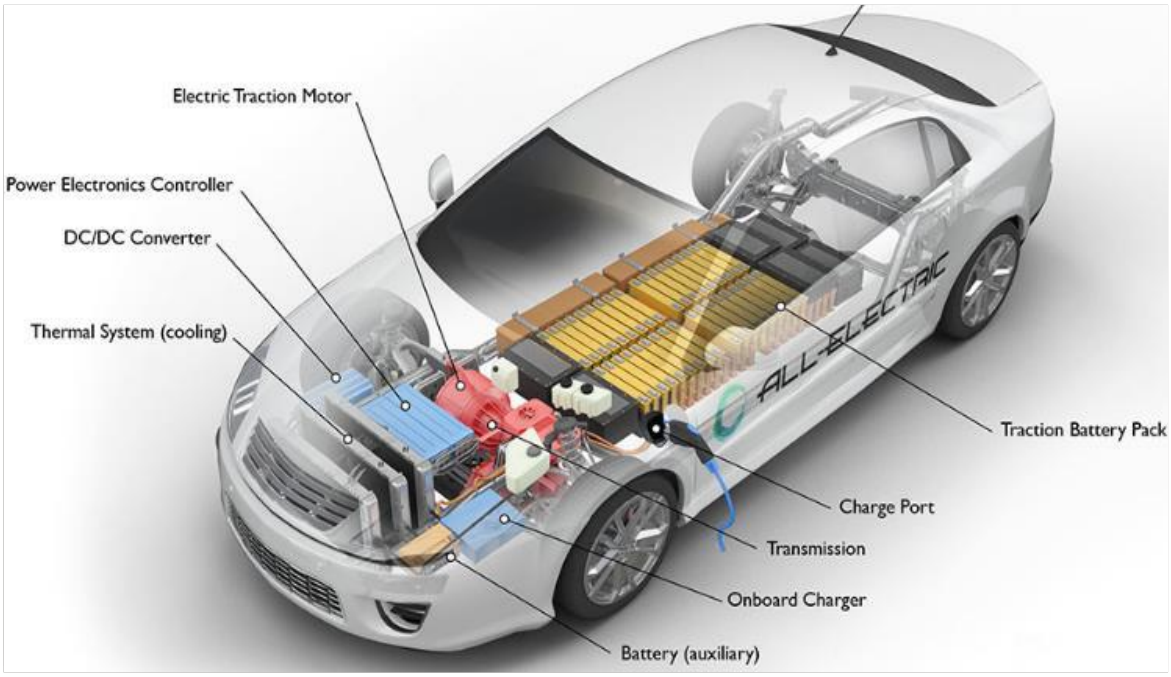

Figure 1.7: Principal elements of a battery electric vehicle.

The two types of electric powertrain systems are converted and dedicated. In converted systems, an electric motor and batteries replace the ICE and fuel tank, while other components remain the same. Dedicated electric powertrains are integrated into vehicles where the body and chassis design are optimized for BEVs, taking advantage of the flexibility that electric propulsion systems can guarantee. Dedicated systems include different configurations: out-wheel where the electric motors are mounted on vehicle chassis and provide the traction forces to the driving wheels directly or through gearboxes; in-wheel where electric motors are located inside the driving wheels. In-wheel technology can minimize the mechanical components but requires motors resistant against lateral and longitudinal loads and water intrusion. Both in-wheel and out-wheel can be converted to an all-wheel drive powertrain (fig. 1.8).[66] On the road, an electric car is able to proceed totally silently: to avoid problems and hazardous situations for citizens and drivers, all these vehicles must be equipped with a noise alarm to advice the presence of the car. To minimize the wasted energy and to increase consequently the autonomy range of BEV, two mechanisms are used: stopping the engine when it is stationary (idle-off condition) and recharging the battery during braking (regenerative braking system) or while traveling downhill (exploiting the potential energy).

[66] Un-Noor, F., *et al*. (2017, August), *op. cit.*, pp. 10-12.

Figure 1.8: In-wheel motor all-wheel drive on an electric powertrain (EM = electric motor).[67]

1.2.3 Fuel-cell electric vehicles

«Using batteries as the only energy source in BEVs is limiting in a number of ways. Most importantly, this reliance on batteries results in limited driving ranges and extended recharging times. Recently, the application of fuel-cells as and energy source in electric vehicles has received great attention».[68] A fuel-cell electric vehicle (FCEV) uses fuel-cells to generate electricity from hydrogen fuel; for this reason, they are often called hydrogen fuel-cell vehicles. However, a fuel-cell is not a storage device – differently from batteries, ultracapacitors and flywheels. It is an energy source unit where generated electricity is provided to the traction motor, while excess energy is stored in the on-board energy storage system (for example, a battery or ultracapacitor) for future needs. In this way, the driving range of a fuel-cell electric vehicle is comparable to an ICE car.[69]

[67] Khajepour, A., Fallah, S., & Goodarzi, A. (2014), *op. cit.,* p. 53.

[68] *Ivi,* p. 65.

[69] Eberle, U., & von Helmolt, R. (2010), *op. cit.,* p. 237.

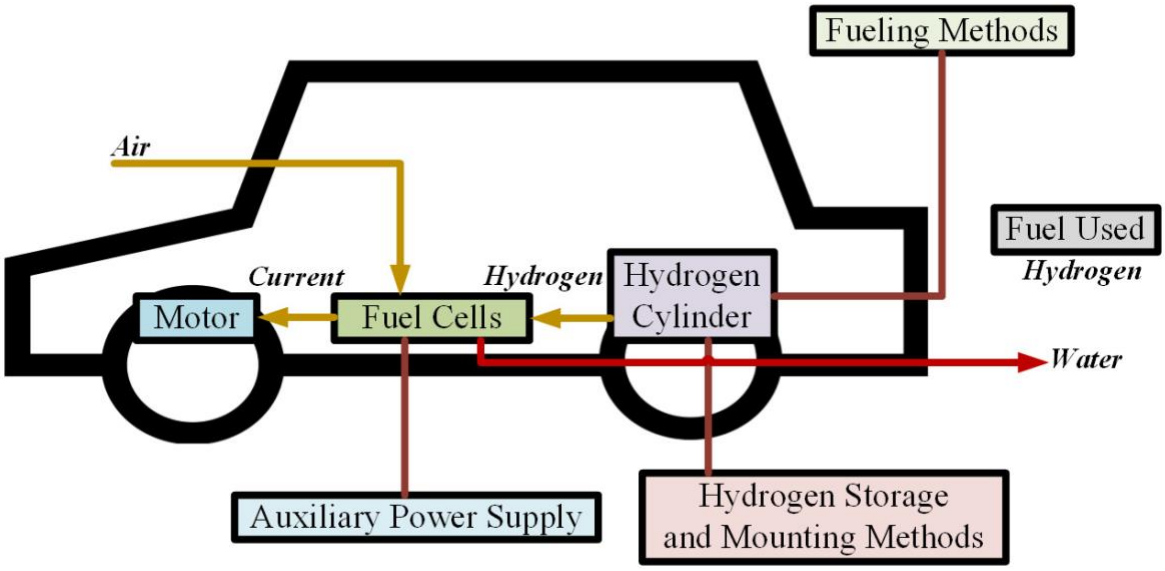

Figure 1.9: Fuel-cell hybrid-electric vehicle configuration.[70]

The electrochemical reaction converts energy stored in hydrogen to electrical energy, the efficiency of FCEVs is greater than that of internal combustion-based systems and it can reach peaks over 85%. These kinds of cars can produce their own electricity emitting no carbon and producing water as a by-product of their power generating process. The major advantage is the possibility of refilling these vehicles in the same amount of time required to fill conventional ICE vehicles.[71] The principal drawback of this solution for transportation is related to the difficulties of storing hydrogen fuels: durability, reliability, cost of implementation, storage, production and delivery of hydrogen are challenging problems for automakers. In general, to facilitate the diffusion of FCEVs, a complete hydrogen infrastructure – composed of pipeline hydrogen transport and filling stations – is needed.[72] For the production, the most common method consists of gaseous hydrogen, while the second method uses the liquid form; electrolyzing water with electricity is another solution for producing gaseous hydrogen. The method of refuelling a fuel-cell car must be safe, creating a dedicated connection between the vehicle and the station dispenser for maintaining a sealed system and avoiding hazards.[73]

[70] Un-Noor, F., *et al.* (2017, August), *op. cit.*, p. 7.

[71] *Ivi*, p. 6.

[72] Garland, N., Papageorgopoulos, D., & Stanford, J. (2012, December), *Hydrogen and fuel cell technology: Progress, challenges, and future directions*, In *Energy Procedia, 28,* p. 6.

[73] Staffell, I., *et al.* (2018, December), *The role of hydrogen and fuel cells in the global energy*, In *Energy & Environmental Science, 12(2)*, p. 5.

On the market, the first fuel-cell vehicle has been the FCX, developed by Honda in 1999, while the second generation FCX Clarity in 2007 can be considered the beginning of one of the more successful ventures in the hydrogen vehicle industry.[74] The distribution of the FCX Clarity has been limited to United States and Japan, where hydrogen refuelling stations have been opened; Honda recently estimated to start the mass production of these FCEVs in 2020. Also, Mercedes-Benz and General Motors have started developing and testing fuel-cell-based technology. «Hydrogen FCEVs combine the best features of battery electric vehicles – zero emissions, high efficiency, quiet operation, and long life – with the long range and fast refuelling time of ICE vehicles. If FCEVs can be developed economically, they will be general-purpose zero-emission vehicles (ZEVs) and will be an important component of a strategy for reducing dependence on oil, mitigating global warming, and improving urban air quality, at an acceptable cost».[75]

1.3 Hybrid-electric vehicles

In recent years hybrid-electric technology has advanced significantly: «it has now been recognized that the hybrid is the ideal transition phase between the traditional all-petroleum-fueled vehicles and the all-electric vehicles of the future. In popular concepts, a hybrid-electric vehicle (HEV) has been thought of as a combination of an internal combustion engine (ICE) and an electric motor».[76] The hybrid-electric vehicle is clearly the optimal solution to reduce the problems related to ICE and air pollution, but also to overcome the limitations of the electric car, from the autonomy to the lack of widespread systems and infrastructures of recharging stations. Hybrid-electric vehicle combines the electric motor and typically high-voltage battery – or other energy storage systems as ultra-capacitors or flywheels – of a purely electric car with the ICE of a conventional gasoline-based system. «HEVs are primarily ICE driven cars that use an electrical drivetrain to improve mileage or for performance enhancement».[77] The electric motor, in fact, allows to use the heat engine in a more efficient way and allows also to recover energy during braking and to use it for

[74] Khajepour, A., Fallah, S., & Goodarzi, A. (2014), *op. cit.,* p. 66.

[75] Delucchi, M., & Lipman, T. (2010), *op. cit.,* p. 45.

[76] Wei, L. (2017*), op. cit.*, p. 1.

[77] Un-Noor, F., *et al*. (2017, August), *op. cit.*, p. 5.

recharging the battery. Moreover, the electric motor is able to supply additional power for traction requirements.[78]

A further consideration is related to the operational mode of the electric machines: they are able to work essentially in two conditions – as generator or motor – and they can rotate in the inverse direction without any additional transmission systems. This advantage can be exploited in hybrid systems for implementing the reverse gear in a simplified way, removing all the traditional mechanical elements, reducing the weight and lowering the losses. The electric motor can be responsible for this function, optimizing the use of the ICE. Also, the generator operating mode is fundamental to recharge the energy sources through regenerative braking systems and downhill driving. Several solutions have been proposed on the market for the combination of the electric motor with the already existing ICE. Hybrid-electric vehicles became popular and widely available with the release of Toyota Prius in 1997 and Honda Insight in 1999; from the late 2000s – due to the increase of the price of petroleum, to the deterioration of air quality and to pollution thematic – HEVs have been seeing as a fundamental element in the automotive industry. It is possible to classify the vehicles depending on the typology of powertrain and on the level of hybridization.

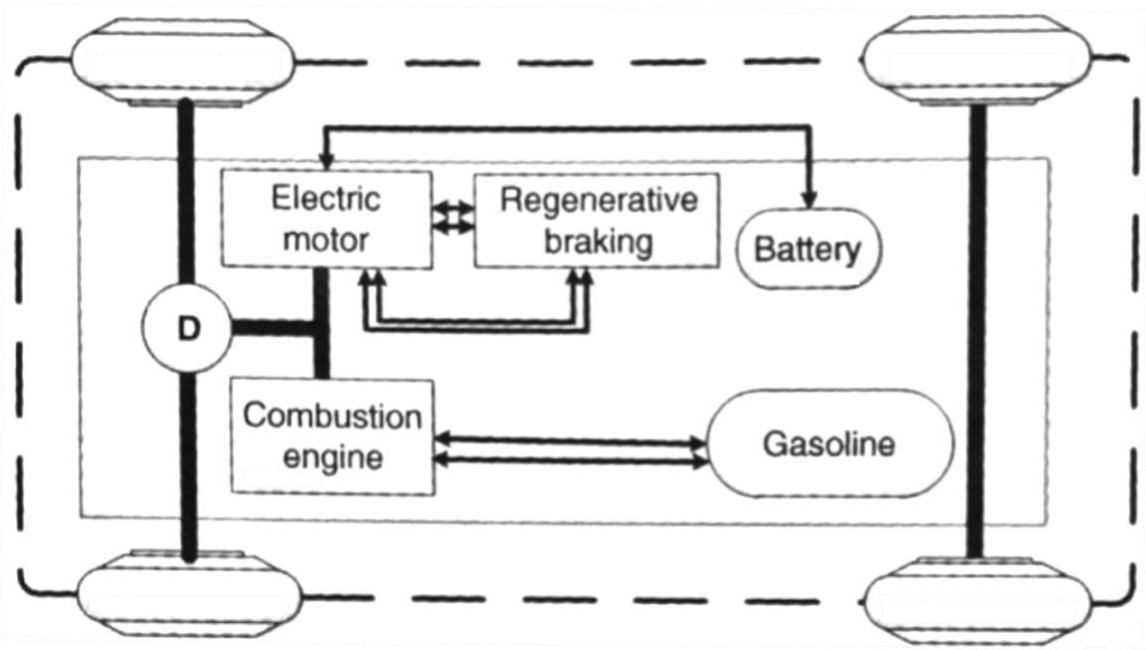

Figure 1.10: Hybrid-electric vehicle powertrain.[79]

[78] Khajepour, A., Fallah, S., & Goodarzi, A. (2014), *op. cit.,* pp. 71-72.

[79] *Ivi,* p. 72.

1.3.1 Classification of the powertrains

«The main issue for HEV is controlling the energy transfer from sources to the loads with the minimum loss of energy which depends on driving cycles».[80] For classifying the powertrains, it is fundamental to notice that the flow of mechanical and electric power can be managed in various ways, for this reason there isn't a single available configuration. The essential elements that compose the hybrid-electric system of a hybrid-electric vehicle are:

- internal combustion engine;
- inverter;
- electric engine;
- electric generator;
- batteries;
- battery management system for monitoring the battery pack;
- power split device for managing the power flow and for combining the heat engine and the electric motor;
- control system.

By changing the interconnections between these components in the design phase, many types of hybrid configurations can be proposed. Automakers, in fact, have developed different architectures for this kind of vehicles; consequently, the electric motor and the internal combustion engine can cohabit in distinct operating modes, i.e. they can be mechanically or electrically coupled. The main configurations are essentially three: series hybrid, parallel hybrid and the combination of the previous two architectures – the so-called series-parallel hybrid.

1.3.1.1 Series hybrid

The series configuration is the simplest one for developing a hybrid-electric vehicle. The electric motor is connected to the wheels, while the small engine is exploited to run a generator which provides the electrical power directly for supplying the electric drivetrain or for recharging the batteries.[81] This system is based on an electric coupling and it can be described as an extended range electric vehicle, assisted by an ICE. Moreover, the heat

[80] Bayindir, K., Gözüküçük, M., & Teke, A. (2011, February), *op. cit.,* p. 1306.

[81] Un-Noor, F., *et al*. (2017, August), *op. cit.*, p. 14.

engine can operate at its most efficient range – regardless of the vehicle load and speed – due to the decoupling between this component and the driving wheels.[82] Consequently, the fuel consumption is reduced, and the carbon emissions are lower than the other configurations, because this vehicle can be run in pure electric mode – as a zero-emission system. The regenerative braking and the down slope driving supply a substantial amount of energy. The ICE is turned on when the battery energy is reduced: if the power demand of electric motor is less than output power of generator, the remaining power is used to charge the battery pack – and the ultracapacitor, if present; if the power demand is higher, the required energy is supplied by the battery pack.[83] The heat engine operates at its optimum settings for all the time. In this case the electric motor must be significantly more powerful than the corresponding one in a parallel hybrid-electric vehicle.

One fundamental advantage of series architecture is the absence of the conventional transmission system for connecting the drivetrain to the driving wheels. In fact, the electric motor is capable to provide high torque over a wide speed range with no stepped gear, differently from the ICE that requires a complete transmission system for adapting the angular velocity of the engine to the vehicle speed. The mechanical losses due to friction in all the rotating elements are removed.[84] Furthermore, the drive line is optimized, and the control strategy is simple if compared to other configurations.[85] Also, the lifetime of this kind of vehicle is efficiently extended. On the other hand, some disadvantages are unavoidably related to series hybrid-electric architecture. First, the presence of the generator adds weight and increases the cost. Second, the energy conversion causes not negligible power losses, together with inefficiencies of generator and traction motor.[86] For all these features, series configuration is more efficient for start-stop and city driving conditions.

[82] Khajepour, A., Fallah, S., & Goodarzi, A. (2014), *op. cit.,* p. 80.

[83] Bayindir, K., Gözüküçük, M., & Teke, A. (2011, February), *op. cit.,* p. 1307.

[84] Ehsani, M., Gao, Y., & Emadi, A. (2010), *op. cit.,* p. 129.

[85] Wei, L. (2017*), op. cit.*, p. 5.

[86] Khajepour, A., Fallah, S., & Goodarzi, A. (2014), *op. cit.,* p. 80.

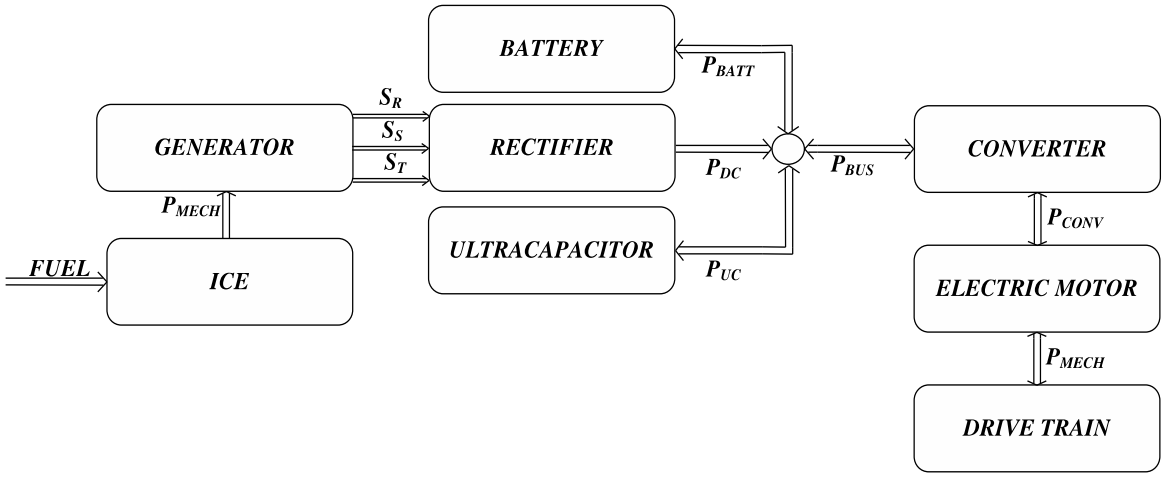

Figure 1.11: Power flow of series HEV powertrain.[87]

1.3.1.2 Parallel hybrid

In parallel hybrid-electric vehicles, the mechanical power output and the electrical power output are connected in parallel for driving the transmission. The ICE and the electric motor are mechanically combined using torque-couplers or speed-couplers, and they can operate together or individually; in fact, this system is able to work in a zero-emission configuration, by shutting off the ICE. In the most common strategy, the heat engine always works as in conventional gasoline-based vehicles, while the electric drivetrain assists the traction generation. If the power requested from the transmission is higher than the actual output power of the internal combustion engine, the electric motor starts running and supplying the additional needed power. If the power requested is less than the output power of the ICE, the remaining power is used for refilling the battery packs.[88] Moreover, regenerative braking and down slope driving are also used to recharge the energy source.

With respect to series configuration, the traction motor is smaller, and the generator is no more needed; in this way, the system is more compact, and the size of the powertrain is decreased. The batteries can also be smaller if compared to series hybrid, because the contribution of the electric motor is reduced. The major advantage is related to the mitigation of losses because no energy conversion occurs between the engines.[89] The disadvantages are the cost of the system, the complexity of the design, control and packaging, the need of high

[87] Bayindir, K., Gözüküçük, M., & Teke, A. (2011, February), *op. cit.,* p. 1307.

[88] Un-Noor, F., *et al*. (2017, August), *op. cit.*, p. 15.

[89] Ehsani, M., Gao, Y., & Emadi, A. (2010), *op. cit.,* p. 131.

voltages for efficiency and obviously the presence of the transmission system that increases the losses due to friction among mechanical elements. Consequently, the parallel hybrid-electric architecture provides better performance in highway driving.[90]

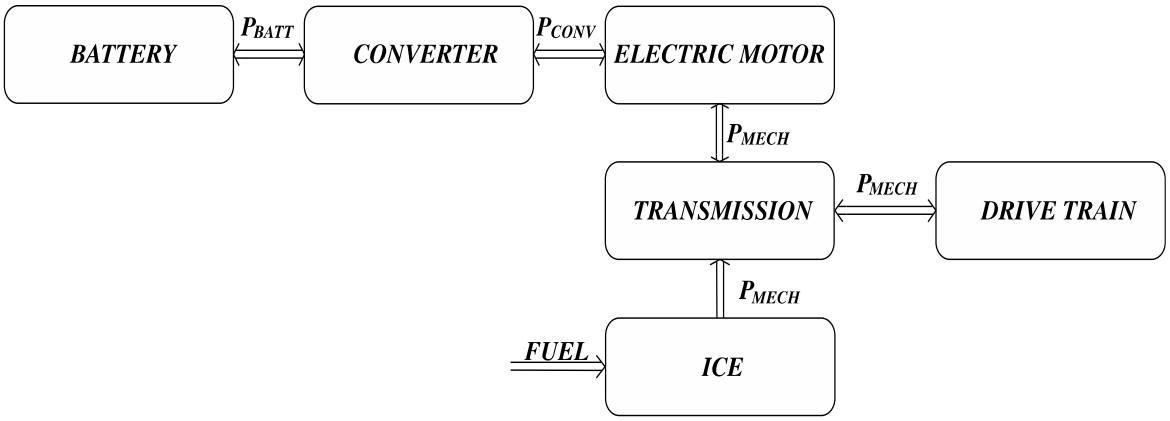

Figure 1.12: Power flow of parallel HEV powertrain.[91]

1.3.1.3 Series-parallel hybrid

The series-parallel hybrid-electric architecture incorporates the advantages of both series and parallel configurations; this combination is quickly becoming the standard in passenger cars. The electric motor, the electric generator, the internal combustion engine and the wheels of the vehicle are linked together through a planetary gear set[92] – or alternatively a floating-stator electric machine called transmotor.[93] Series-parallel configuration appears more similar to the parallel one, including a generator connected to the heat engine. With respect to series hybrid, there is a mechanical link for connecting the heat engine and the driving wheels.

This system splits the power from the engine between two paths: series and parallel. In the series path, the mechanical power of the heat engine is converted to electrical power through the generator for recharging the energy source or for supplying entirely the wheels via the electric drivetrain. In the parallel path, the ICE is connected to a conventional gearbox and transmission system; the mechanical power is transmitted to the wheels and the

90 Khajepour, A., Fallah, S., & Goodarzi, A. (2014), *op. cit.,* p. 75.

91 Bayindir, K., Gözüküçük, M., & Teke, A. (2011, February), *op. cit.,* p. 1307.

92 Wei, L. (2017*), op. cit.*, p. 6.

93 Un-Noor, F., *et al*. (2017, August), *op. cit.*, p. 15.

exceeding power is converted to electrical power through the electric motor to recharge the battery. If the mechanical power is not sufficient to satisfy the demand, the electric motor supplies additional torque.[94] This means that the electric motor and the combustion engine can work independently or in synergy for optimizing the efficiency. The architecture combines the independence of the engine operation from the driving conditions of series configuration, to the efficient mechanical transmission of the parallel one.[95] On the other hand, the series-parallel configuration requires complicated design and control and the cost for its realization is obviously elevated.

An evolution of the previous architecture is the complex hybrid-electric vehicles, called also compound hybrid. The main difference relies on the bidirectional functionality of the generator in a compound powertrain, while in the standard series-parallel the it works only in a unidirectional way. The second electric machine, in fact, is able to act both as generator and as traction motor, providing a bidirectional power flow and an additional torque. In this way, more operation modes can be exploited, for example in a three-propulsion power condition the heat engine and the two traction electric motors work together.[96] «High complexity and cost are drawbacks of this system, but it is adopted by some vehicles to use dual-axle propulsion».[97]

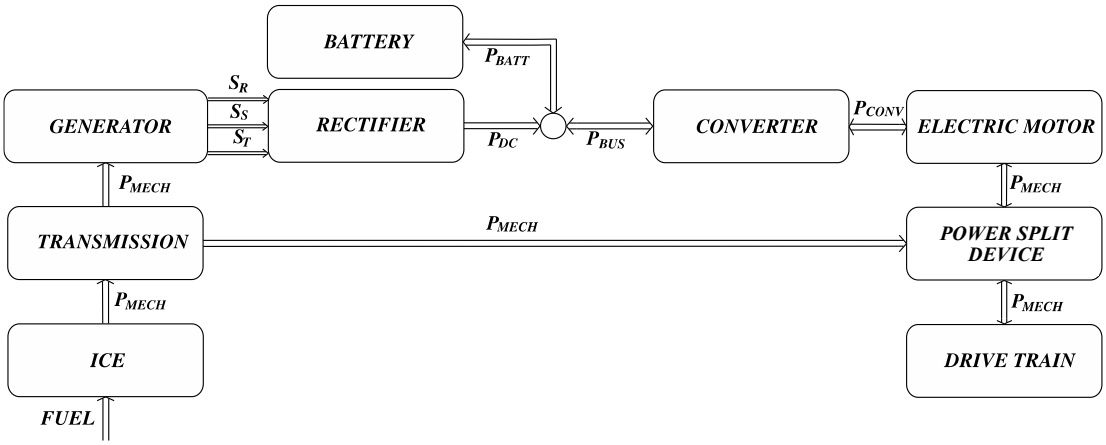

Figure 1.13: Power flow of series-parallel HEV powertrain.[98]

[94] Wei, L. (2017*), op. cit.*, pp. 6-7.

[95] *Ivi*, p. 7.

[96] Khajepour, A., Fallah, S., & Goodarzi, A. (2014), *op. cit.,* p. 84.

[97] Un-Noor, F., *et al*. (2017, August), *op. cit.*, p. 17.

[98] Bayindir, K., Gözüküçük, M., & Teke, A. (2011, February), *op. cit.,* p. 1308.

1.3.2 Levels of hybridization

During the development of hybrid-electric vehicles, different models have been proposed, considering the contribution of the electric motor as a simple support to the internal combustion engine or as a full operating powertrain. The degree of hybridization of a car is the ratio between the power of the heat engine and the power of the electric motor;[99] the three main categories are micro hybrid, mild hybrid and full hybrid. For these solutions, the charge port is not present, because the batteries are recharged using regenerative braking system and not connecting the vehicle to an external electric power socket.

1.3.2.1 Micro hybrid

In micro hybrid-electric vehicles, the electric motor capability is often under 5 kW, due to the low operational voltage – between 12 V and 48 V. For this reason, the electric machine works mainly in applications related to start-stop, when the internal combustion engine is automatically shut down under braking and idling conditions; or regenerative braking system; consequently, the fuel economy can be improved by 5-10% in city driving conditions.[100] Electric motor is used also for regenerative braking and for supplying electrically driven accessories, like air-conditioning. In many cases, the alternator-starter system is improved for realizing the micro hybrid system. Recently, carmakers have adopted this technology as hybrid solutions for their models to mitigate the emission and the fuel consumption. BMW 1 series and Smart Fortwo, manufactured by Mercedes-Benz, are two examples of commercialized successful micro hybrid vehicles.

1.3.2.2 Mild hybrid

Mild hybrid-electric vehicles normally have an independent electric drivetrain providing 5-20 kW of electric propulsion power; the electric motor is able to provide up to 10% of the maximum engine power in the form of additional torque to assist the internal

[99] Orecchini, F., & Santiangeli, A. (2010), *Automakers' Powertrain Options for Hybrid and Electric Vehicles.* In G. Pistoia, *Electric and Hybrid Vehicles. Power Source, Models, Sustainability, Infrastructure and the Market (pp. 579-636),* Amsterdam, The Netherlands: Elseiver, p. 582.

[100] Wei, L. (2017*), op. cit.*, p. 2.

combustion engine when the vehicle is accelerating. Mild hybrid systems have the capability of optimizing performance and saving fuels in the range of 15-20%.[101] ICE consumes more fuel and emits more emissions when coasting, braking or idling. Conventional mild hybrid technology uses an oversize starter motor to turn off the heat engine in these situations and to restart it quickly and safely.

This kind of vehicles cannot be driven in an exclusive electric-only propulsion mode, because the batteries are smaller, and the motor is weaker than electric machine used for full hybrid applications. For replenishing the batteries, a low level of energy recuperation systems is integrated, like regenerative braking functionality. The BMW 7 series ActiveHybrid, the Mercedes S-Class and Honda Insight are examples of mild hybrid systems; GM has used this technology for developing the Chevrolet Malibu Hybrid and the Saturn Ayra Green Line.[102]

1.3.2.3 Full hybrid

A full hybrid electric vehicle is able to run only on an internal combustion engine, on an electric motor or on a combination of the two drivetrains; in other words, in addition to the functions of micro and mild hybrids, a full hybrid car allows driving with the electric powertrain alone. In this system, the electric motor typically provides at least 40% of the maximum engine power as additional torque to increase the performance and the efficiency of the vehicle. The further functionalities require bigger and more performing batteries, together with a more powerful electric motor. Obviously, the all-electric range (ZEV functionality) is limited and these improvements have a relevant impact on the total cost of the vehicle, if compared to conventional ICE-based solutions for transportation. On the market, the first successful full-hybrid system was the Toyota Prius: the Toyota's Hybrid Sinergy Drive technology is actually the most relevant and the most widespread full hybrid solution on the market. Other automakers are actually proposing alternatives: the Ford Escape Hybrid and the Ford Fusion Hybrid, the BMW X6 ActiveHybrid, the Mercedes M-Class Hybrid, the Porsche Cayenne Hybrid, the Citroën C4 Hybride and the Volkswagen full hybrid system applied on Tuareg V6 TSI Hybrid.[103]

[101] Wei, L. (2017*), op. cit.*, p. 3.

[102] Khajepour, A., Fallah, S., & Goodarzi, A. (2014), *op. cit.,* p. 74.

[103] Orecchini, F., & Santiangeli, A. (2010), *op. cit.,* pp. 590-600.

1.4 Plug-in hybrid-electric vehicles

A plug-in hybrid-electric vehicle (PHEV) combines the characteristics of full hybrid-electric and all-electric vehicles with the capability of recharging the energy source through an external power source. In this system, the batteries are not only internally recharged using the heat engine, the downhill driving and the regenerative braking, but they can be restored to full charge by connecting a plug to the electric grid. The electric powertrain normally has an 80-150 kW electrical power capability that allows the vehicle to operate in zero-emission mode with an electric range of around 30-90 km.[104] Differently from hybrid-electric car, where the ICE is the primary propulsion system, in plug-in systems the electric drivetrain is the main driving force and the heat engine may be used as secondary power source. The conventional engine is used here to extend the range of the vehicle. Obviously, a higher battery capacity is required for supporting the primary action of the electric motor,[105] but this causes an increase of the weight and the cost. With respect to battery electric vehicles, a PHEV reduces the dependence on recharging infrastructure; on the other hand, a complex control algorithm is needed for optimizing the powertrain efficiency and reducing the energy losses.

«PHEVs have attracted the interest of researchers and policy makers because they can reduce consumption of petroleum, emissions of greenhouse gases, and emissions of urban air pollutants. PHEVs are likely to cost more than conventional ICE gasoline vehicles, primarily because of the relatively high cost of batteries, but also may have lower energy-use costs».[106] Actually, the principal solutions on the market are the best-selling plug-in hybrid car is the Chevrolet Volt, followed by the Mitsubishi Outlander P-HEV and the Toyota Prius Plug-in Hybrid.

[104] Wei, L. (2017*), op. cit.*, p. 4.

[105] Un-Noor, F., *et al*. (2017, August), *op. cit.*, p. 6.

[106] Delucchi, M., & Lipman, T. (2010), *op. cit.,* p. 31.

EV Type	Driving Component	Energy Source	Features	Problems
BEV	• Electric motor	• Battery • Ultracapacitor	• No emission • Not dependent on oil • Range depends largely on the type of battery used • Available commercially	• Battery price and capacity • Range • Charging time • Availability of charging stations • High price
HEV	• Electric motor • ICE	• Battery • Ultracapacitor • ICE	• Very little emission • Long range • Can get power from both electric supply and fuel • Complex structure having both electrical and mechanical drivetrains • Available commercially	• Management of the energy sources • Battery and engine size optimization
FCEV	• Electric motor	• Fuel cell	• Very little or no emission • High efficiency • Not dependent on supply of electricity • High price • Available commercially	• Cost of fuel cell • Feasible way to produce fuel • Availability of fueling facilities

Table 1.1: Comparison of different vehicle types.[107]

1.5 Controller area network (CAN) protocol

The CAN bus is a serial robust standard developed for allowing the communication among the microcontrollers and the devices inside a vehicle, without a host computer that manages this interaction. This protocol is based on messages, specific for multiplex electrical wiring; it is dedicated to distributed systems where different control units – the so-called nodes – need to send data, status information and to receive the proper parameters for working correctly. The initial version of CAN protocol was designed in 1983 at Robert Bosch GmbH and released in 1986 at the Society of Automotive Engineers, while the first controller chips were produced in 1987 by Intel and Philips; the initial CAN-based vehicle was the Mercedes-Benz W140 in 1991. Different versions of the CAN standard have been published by Bosch and the most adopted one is CAN 2.0 – standard and extended – for automotive applications. Actually, this protocol is used in other sectors, like industrial automation, aerospace, security systems and biomedical engineering. A recent evolution is the CAN FD – CAN with flexible data-rate – which is based on a different frame format and allows a faster bit rate. This standard is completely compatible with CAN 2.0 networks for improving its diffusion.

[107] Un-Noor, F., *et al*. (2017, August), *op. cit.*, p. 9.

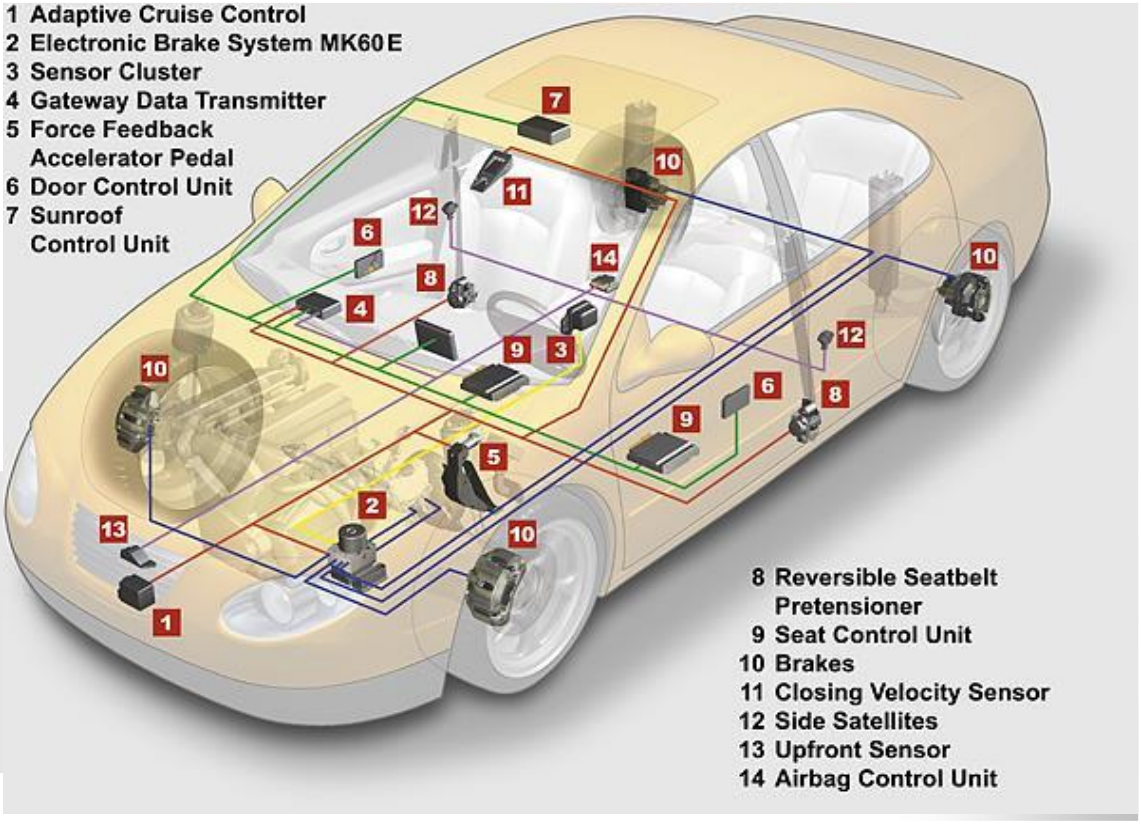

Figure 1.14: Automotive distributed system.

CAN communication is based on the differential voltage between two wires – CANH and CANL – that are terminated at both ends by 120 Ω resistors, as required for this standard. Both wires are biased to the same level of 2.5 V, equal to the supply voltage divided by two for 5 V supplied CAN controllers and transceivers. The data is sent one bit a time and each bit can be classified as dominant or recessive. The dominant state corresponds to a difference higher than 2 V between CANH and CANL, generating a dominant bit 0; the recessive state corresponds to a differential voltage lower than 0.5 V, so both wires remain at 2.5 V, generating a recessive bit 1. In fact, in CAN bus protocol the logic 0 is dominant with respect to a logic 1 - this is fundamental for arbitration policy.[108] In case of 3.3 V supplied and 5 V supplied controllers and transceivers in the same network, the protocol is designed for avoiding any problems. The generated differential voltages between CANH and CANL of these two kinds of transceivers is almost the same, thanks to the addition of a specific bias

[108] Corrigan, S. (2016, May), Texas Instruments, Retrieved from *Introduction to the Controller Area Network (CAN)*: http://www.ti.com/lit/an/sloa101b/sloa101b.pdf, pp. 7-8.

voltage for the 3.3 V devices.[109] Moreover, using a voltage difference between two wires, the electromagnetic disturbances are negligible.

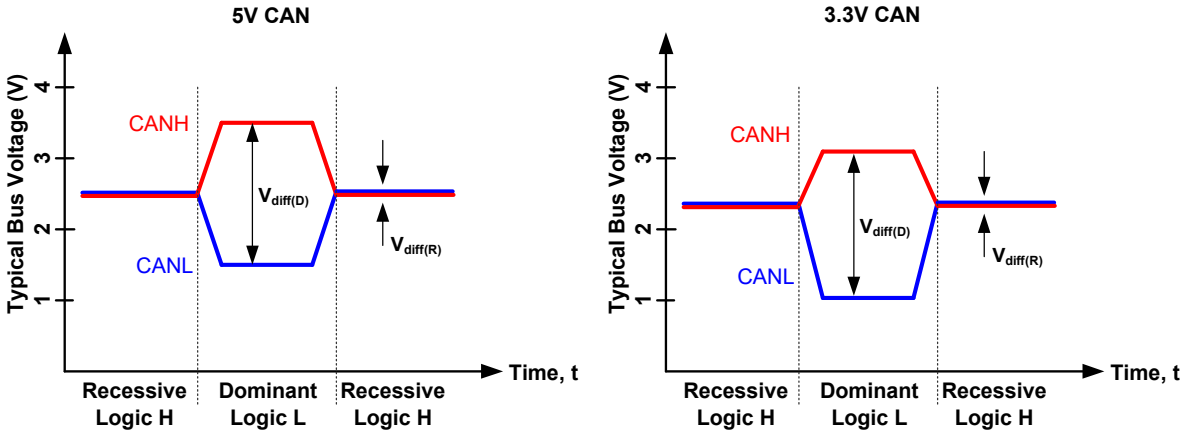

Figure 1.15: CAN bus levels for 5 V and 3.3 V transceivers.[110]

The different control units are able to filter the network to identify the useful frames for them and to avoid the risk of a too busy node. The transmitter has no identifier and it doesn't specify the receiver, because the latter is only able to identify the content of a message through a dedicated field. Messages can be standard or extended – depending on the length of their identifier – and contain many fields, like data, error and acknowledgment bits. The following figures (fig. 1.17 and fig. 1.18) show the position of each bit fields, highlighting also the differences between standard and extended CAN frames.

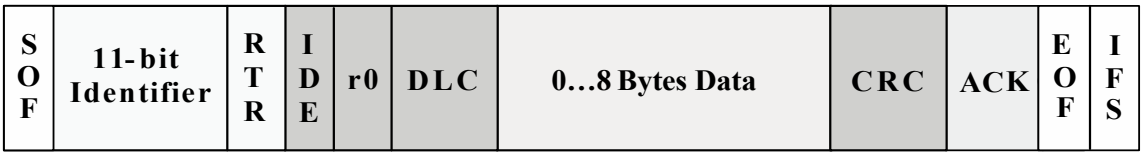

Figure 1.16: Standard CAN frame.[111]

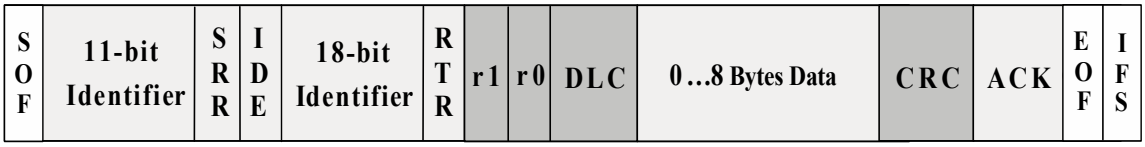

Figure 1.17: Extended CAN frame.[112]

[109] Blackman, J., & Monroe, S. (2013, January), Texas Instruments, Retrieved from *Overview of 3.3V CAN (Controller Area Network) Transceivers*: http://www.ti.com/lit/an/slla337/slla337.pdf, pp. 2-3.

[110] *Ivi*, p. 3.

[111] Corrigan, S. (2016, May), Texas Instruments, *op. cit.*, p. 3.

[112] *Ivi*, p. 4.

- SOF – start of frame, used for synchronizing the nodes on a bus;
- Identifier – 11 bits in a standard CAN frame, 29 bits in an extended CAN frame: for the arbitration, the lower is the binary value, the higher is the priority;
- RTR – remote transmission request, dominant bit in case of data frame, recessive in a remote frame;
- IDE – identifier extension, dominant in standard frame, recessive in extended frame: this means that standard messages prevail on extended ones;
- SRR – substitute remote request, in the extended format it replaces the RTR bit;
- r0, r1 – reserved bits;
- DLC – data length code, it is 4-bit field which indicates the number of bytes of the data;
- Data – in CAN protocol, data is composed up to 64 bits (64 bytes for CAN FD);
- CRC – cyclic redundancy check, used for error detection;
- ACK – acknowledgment bit, for verifying the integrity of a message: every node receiving an accurate frame overwrites this recessive bit in the original frame with a dominant bit;
- EOF – end of frame, used also for disabling bit stuffing;
- IFS – 7-bit interframe space, it contains the time required by the controller to move a correctly received frame to its proper position in the buffer area.

Depending on the used fields and the bits values, the frame of this protocol can assume different interpretations. The four message types that can be transmitted on a CAN bus are:[113]

- the data frame, that is the most common type and comprises the arbitration field, the data field, the CRC field and the acknowledgment field;
- the remote frame, similar to the previous one, except for the recessive RTR bit in the arbitration field and there is no data here. It is used for soliciting the transmission of data from another frame;
- the error frame, a special message transmitted when a node detects an error in a message, and it causes all other nodes in the network to send an error frame too. Then the original transmitter retransmits the message;
- the overload frame, similar to error frame with regard to the format in case of a too busy node.

[113] Corrigan, S. (2016, May), Texas Instruments, *op. cit.*, p. 6.

An essential characteristics of CAN protocol is the possibility of arbitrating the access to the bus, without the insertion of any additional controllers. Every time the bus is free, all the units can start transmitting the message and the dominant node is detected according to the non-destructive bitwise operation. The smallest numeric value wins the competition and uses the bus; in other words, due to the fact that the bit 0 is dominant and the bit 1 is recessive, a message with a lower identifier has a higher priority. Because a single node continuously monitors its own transmission, it can detect if its recessive bit is overwritten by a higher priority bit: the node understands that the bus state does not match with the bit transmitted by the node. Consequently, the node stops transmitting while the dominant one continues on with its message. The recessive node waits for the CAN bus to be free again. It is worth noting that a precise synchronization among the control units within the same network is required: the nodes must transmit the messages using the same clock frequency, otherwise the arbitration cannot operate correctly.

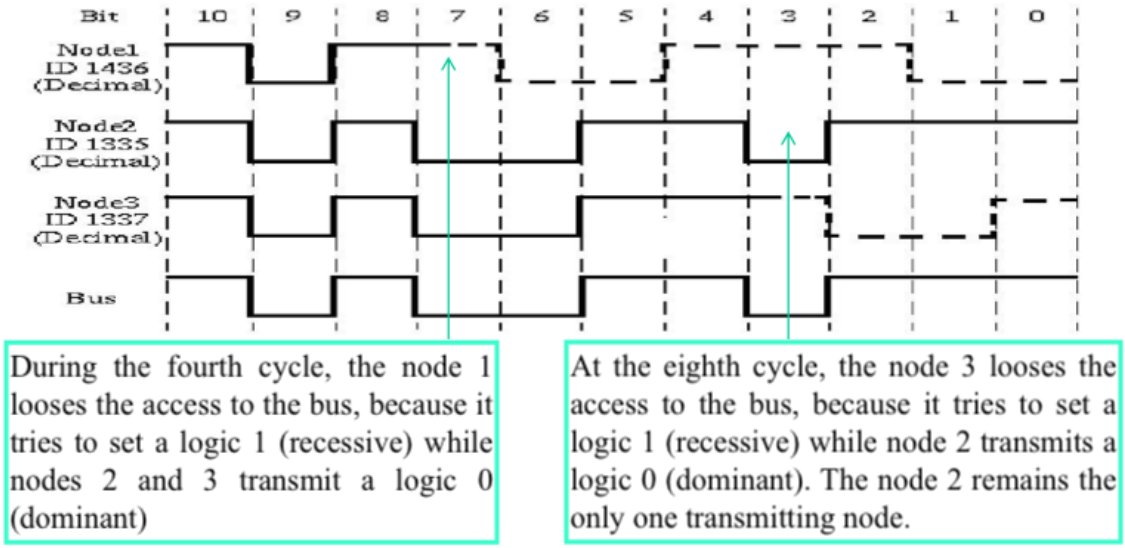

Figure 1.18: Example of arbitration between three nodes.

Depending on the transmission speed, in the automotive sector the CAN networks can be classified as A-CAN, B-CAN and C-CAN. The first one arrives up to 10 kbps, but it is no more adopted. B-CAN nodes operate between 50 kbps and 125 kbps, for non-time critical applications, like air conditioning or navigator. C-CAN arrives up to 1 Mbps and it is related to all real-time time critical applications, such as the exchange of messages related to braking system, engine, ABS, ESP, etc. Another important aspect is the presence of many kinds of error in order to identify an incorrect transmission or reception. Checksum error, frame error, acknowledgment error and bit error are examples of errors are related to the bits

that compose the fields of a certain frame, while the bit stuffing error is notified from a receiver node if it receives more than five bits with the same polarity through the network.

Inside the vehicle CAN bus, a master is responsible for administrating the communication channel and the slave nodes. This role is assigned to the body computer module (BCM), an electronic control unit – such as the other nodes of the system. Various functionalities are assigned to this device: diagnostic, breakdown individuation and tracking, notification to the user about vehicle conditions, conversion of logic bits to power value using relay, memorization of useful information. Another fundamental task is to filter messages from one network to another, allowing the communication between boards based on different hardware. This gateway operational mode is used for interfacing the medium-speed network with the high-speed network within the same vehicle, so a B-CAN node can communicate with a C-CAN one without timing problems.

Many advantages are associated to CAN network: first of all, it is a simple and flexible multi-master serial bus, and typically a twisted pair cabling is use for wiring the devices in order to reduce the electromagnetic disturbances. The nodes have no identifier, so any control units can be added to the network or removed from it without reconfiguring the complete bus: when a new device is introduced, it is connected to the lines and it can start working, sending and receiving messages. If an already present controller recognizes the identifier associated to a message that comes from the new unit, it is able to decode that frame – using the information contained in the network database. Another benefit is related to the reliability of the system: if a message stops to be sent cyclically on the bus, the node responsible for forwarding that frame is considered in breakdown, but the complete network – the other nodes and the master – continues working without drawbacks. As described before, the master takes care of notifying the problem to the user and it can sometimes compensate the absence of the message. Every node contains two counters – initially reset at zero – that grows in case of reception or transmission error: receive error counter and transmit error counter. The control unit is able to work correctly or break away from the CAN bus, depending on the counter values. This is an auto-diagnostic mechanism, for auto-isolating a broken node.

The recent evolution of the CAN bus – CAN FD – guarantees more accurate and faster (higher than 1 Mbps) communication: it has been created as answer for the increase in bandwidth requirements within an automotive network. The new protocol is closer to real-time thanks to the minimization of delays in data transferring; moreover, it allows also to send larger CAN frame, passing from the maximum of 8 bytes for the data field, to maximum of 64 bytes. The basic idea is to increase the bit rate when just one node is transmitting,

because there is no need for synchronization or arbitration mechanism. CAN and CAN FD protocol are able to work also in extreme conditions, for example if a node controller is connected to the supply or it is short-circuited. This technology is totally reliable, safety, easily available on the market, tested and well documented for automotive – and other – applications.

Chapter II:
Electric AC machines

SUMMARY: 2.1 Introduction to electric machines – 2.2 Rotating magnetic field – 2.3 Asynchronous motor – 2.4 Synchronous motor – 2.4.1 Permanent magnet synchronous motor (PMSM) – 2.4.1.1 Surface-mounted magnets and interior magnets – 2.4.1.2 Dynamic equations of the PMSM.

2.1 Introduction to electric machines

An electric machine is an electromechanical energy converter: an electric motor transforms the electricity to mechanical power, while the electric generator is responsible for converting the mechanical power into electricity. The main elements of an electric machine are the rotor – the moving part which turns the shaft to deliver mechanical power – and the stator – stationary part of the system that surrounds the rotor. Moreover, the moving part can be rotating or linear. Both electric generators and motors can be classified in direct current (DC) or alternating current (AC) machines, depending on the current's behaviour. AC motors are powered from alternating current, while the DC machines need a direct current. Their torque-speed characteristics is characterized by two regions: constant torque region and constant power region. Through the union of both of them, the range of operating speeds can be enlarged, improving performances and the possible applications.

- in the first part, for low velocity levels, the torque is maintained constant; also, the flux doesn't change and remains equal to the nominal value λ_N – this condition can be obtained with a constant excitation current or using permanent magnets. In this region the speed is proportional to the supply voltage: by increasing the voltage, the angular velocity of the rotor and the delivered power increase. When the supply

voltage results equal to the nominal – or rated – value V_N, the motor reaches the nominal – or rated or base – speed ω_N and this regulation technique can no longer be adopted;

- for exploiting the full range of motor velocities, the fundamental idea is to weaken the magnetic air-gap flux through the reduction of the excitation current – if the excitation circuit is present – or through a negative *d*-axis stator current – in case of permanent magnets. In the FOC strategy, applied to an AC machine with PMs mounted on the rotor, the stator current is decomposed in direct and quadrature contributions: a demagnetizing magnetomotive force is induced by the stator current, through the direct-axis component, to counteract the MMF due the permanent magnets flux. In this high-speed region, the voltage is maintained equal to its rated value, while the speed is increased by reducing the electromechanical torque in an inversely proportional manner. The output mechanical power remains constant, because the product between torque and speed doesn't vary. In this way, the maximum speed could be reached, but it is essential to remember that the operating speed of the motor is dependent on the load characteristics.[114]

DC motor were the first typology of electric motor widely diffused. It is a mechanically commutated system: a set of coils is responsible for generating a static electromagnetic field, through a direct excitation current running inside it. The armature – the rotating part – is mounted on bearings and turns inside the magnetic field. When an electric current pass through a coil in a magnetic field, the magnetic force produces a torque which turns the rotor. There are brushes between the static and the rotating elements of the system and these elements make contact with a commutator to realize the connection. The commutator acts as a switch to supply voltage to the revolving armature from the stationary brushes, making it turning to provide the desired mechanical power.[115] By varying the armature voltage in the constant torque region, the speed of a DC machine ca be regulated, depending obviously also on the connected load.

[114] Boglietti, A. (1995), *Concetti di base sulla macchina in corrente continua (Electrical Machines),* Biella, Italy: Politecnico di Torino, pp. 14-16.

[115] Khajepour, A., Fallah, S., & Goodarzi, A. (2014), *op. cit.,* pp. 54-55.

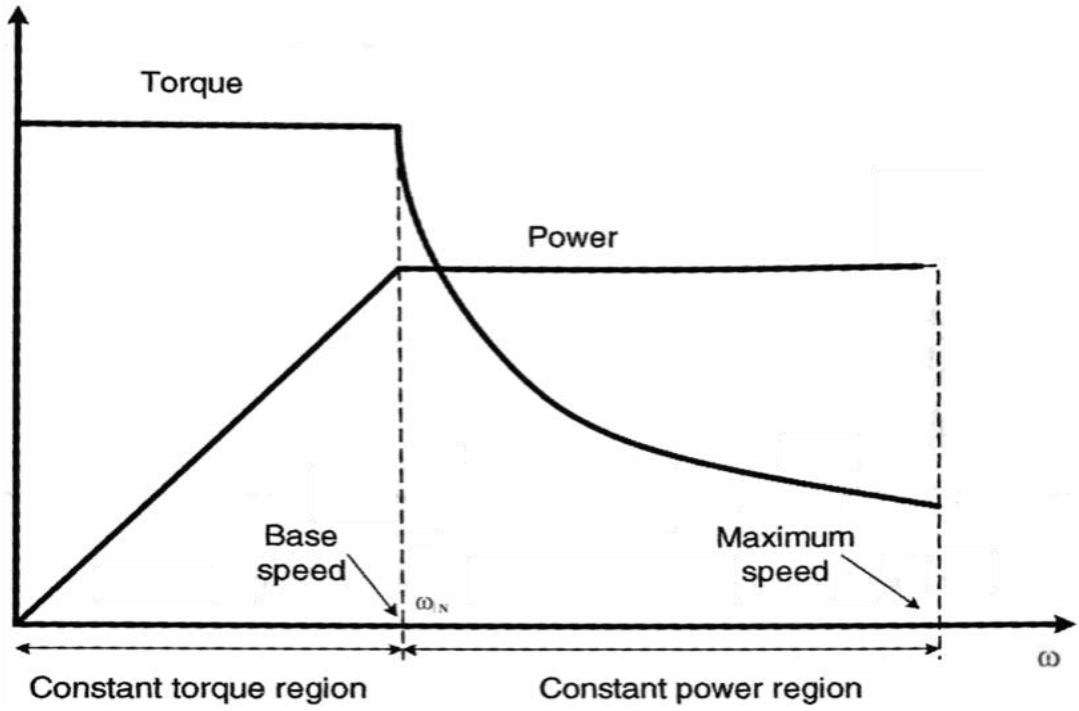

Figure 2.1: Typical traction electric motor characteristics.[116]

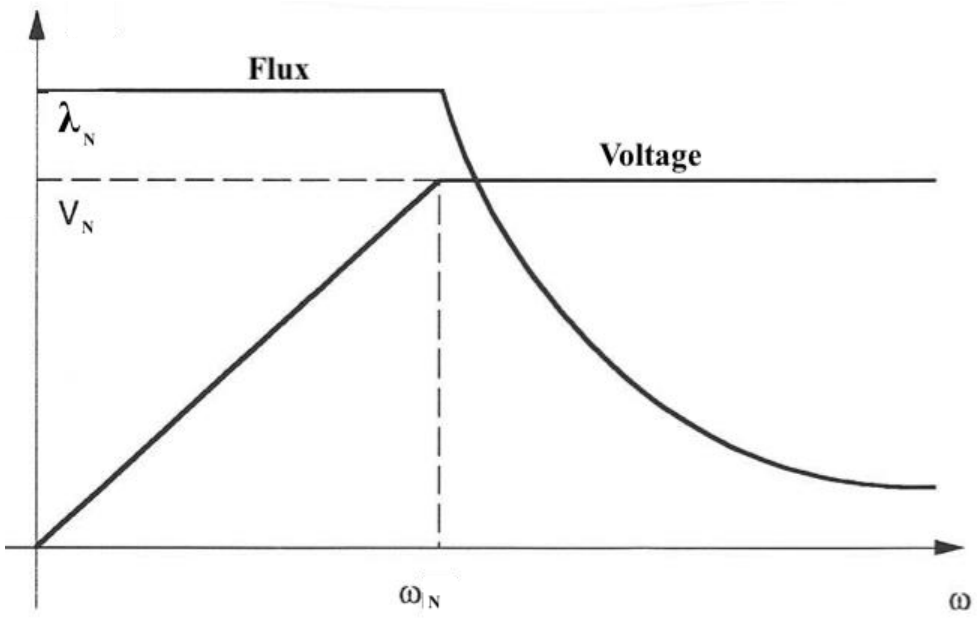

Figure 2.2: Voltage-speed and flux-speed characteristics of a generic electric motor.[117]

116 Khajepour, A., Fallah, S., & Goodarzi, A. (2014), *op. cit.,* p. 54.

117 Boglietti, A. (1995), *op. cit.,* p. 15.

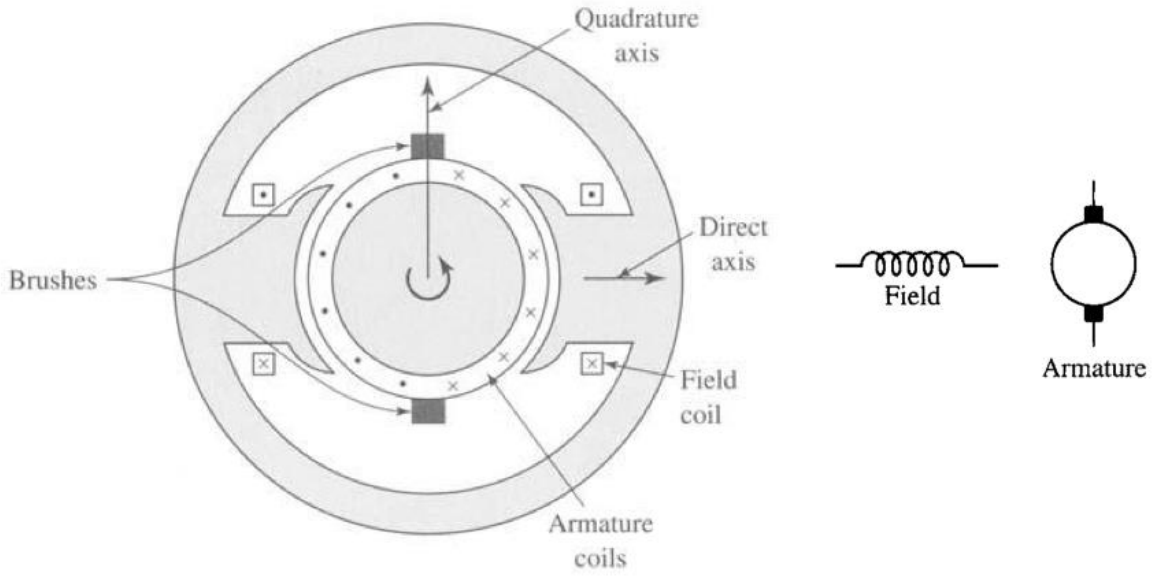

Figure 2.3: Schematic representation of a DC machine.[118]

Depending on the interconnection between the excitation circuit and the armature, DC machines can be classified in different ways:

- separated excitation, the excitation circuit is supplied in a separate way with respect to the armature;
- series excitation, the excitation circuit is connected in series to the machine, so the excitation current is also the armature current;
- parallel or shunt excitation, the excitation circuit is connected in parallel to the machine and it is supplied by the same armature voltage;
- compound DC motor, this configuration merges the series and shunt configurations with a series field winding connected in series with the armature and a shunt field winding in parallel to the armature;
- permanent magnet configuration, the flux is obtained through the use of permanent magnets, with no excitation circuit.[119]

DC motors provide excellent and simple speed control for acceleration and deceleration. In the simplest separate excitation configuration, thanks to the decoupling between armature current and excitation circuits, the excitation current is responsible for the flux generation – passing through a set of coils – while the torque is nearly proportional to that of the armature. In permanent magnet DC machine too, the torque is proportional to the

[118] Fitzgerald, A., Kingsley, C., & Umans, S. (2003), *Electric Machinery (Sixth Edition),* New York, New York, United States: McGraw-Hill, p. 358.

[119] *Ivi*, pp. 361-364.

armature current, through the torque constant – a factor that is function of motor geometries and magnetic properties.[120] This advantage, derived from this physical decoupling, is exploited also for the field-oriented control of alternating current motors. By mathematically transforming the three-phase into a two-phase system through Clarke-Park transformation, the control algorithm can be optimized and simplified, guaranteeing at the same time excellent dynamic performance.

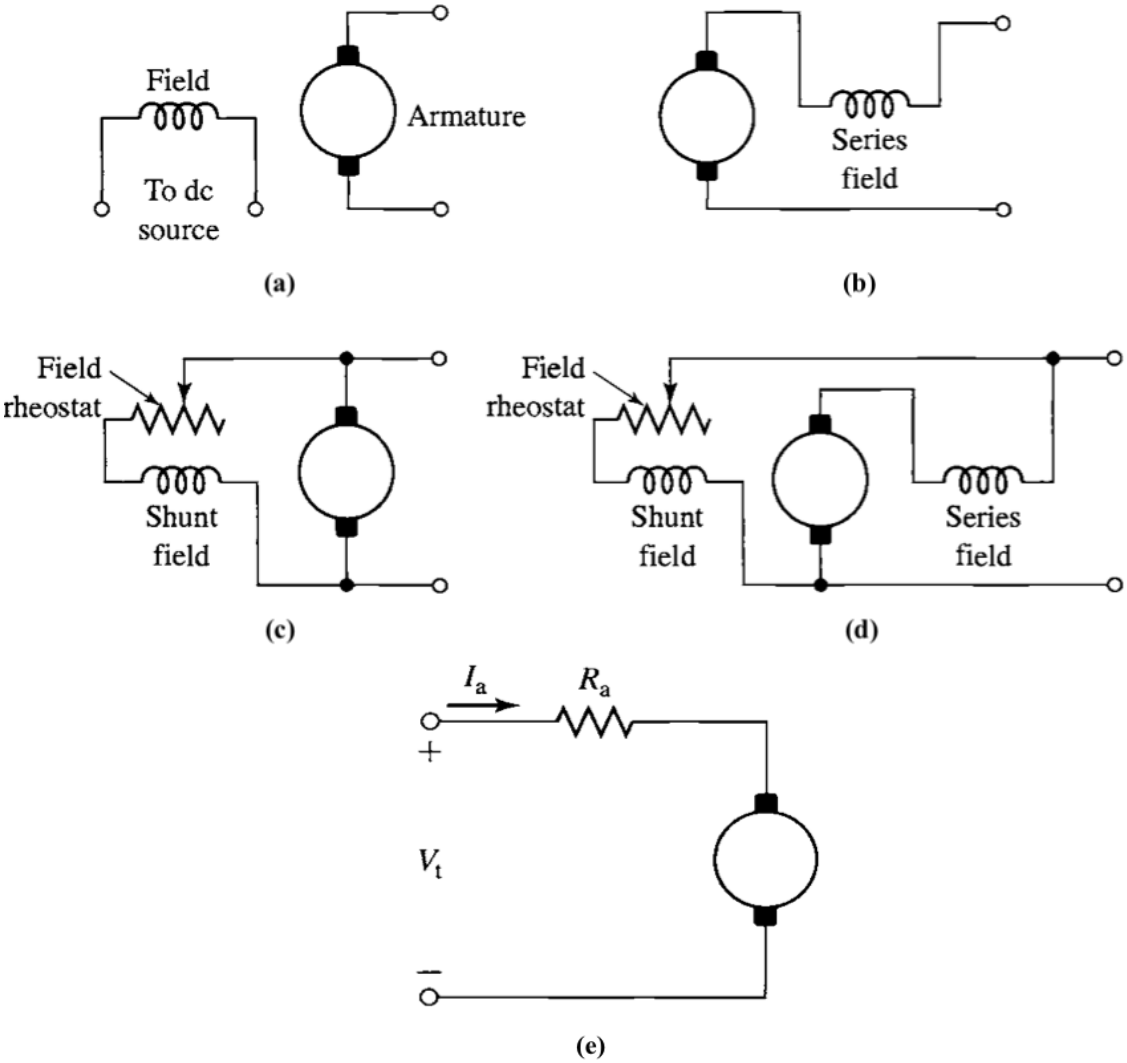

Figure 2.4: Different connections for DC machines: (a) separate excitation, (b) series, (c) shunt, (d) compound, (e) permanent magnets.[121]

Moreover, the design is simple, and the cost is not elevated, if compared to AC machines. On the other hand, this system is heavy, it has low efficiency and low reliability,

[120] Fitzgerald, A., Kingsley, C., & Umans, S. (2003), *op. cit.,* p. 389.

[121] *Ivi,* pp. 361, 389.

it requires high maintenance and it is subject to wear and tear due to the presence of the brush contacts – a periodic brush replacement is needed for this motor. The presence of brushes is a cause of torque ripple, so the automotive industry cannot adopt DC motors also for comfort reasons. Thanks to their versatility, they are still used as series motors where a high starting torque is required or as shunt motors (for centrifugal pumps, lifts, spinning machines); moreover, as compound motors they are essential for industrial mechanisms, like presses, conveyors and shears.

It is worth noting that for powertrain applications in the automotive industry, the AC motor guarantees better performances in terms of reduction of power losses, reliability, limitation of ripple and efficiency with respect to direct current motor. Similar to DC motor, the AC machine have a set of coils and a rotor, but armature windings are located on the stator. In this case there is no need for a commutator and brushes, due to the nature of the alternating current: consequently, the wear problems are eliminated, the efficiency is improved, the weight is reduced and there is no need for maintenance cost. Moreover, the power density is higher in AC motors with respect to DC configurations. The main drawback of these motors is the cost – and obviously the weight – of the power electronics needed to convert the DC from the battery into AC.[122] The basic principle of AC machines is the rotating magnetic field (RMF), generated by three equally spaced currents in the phase plane.

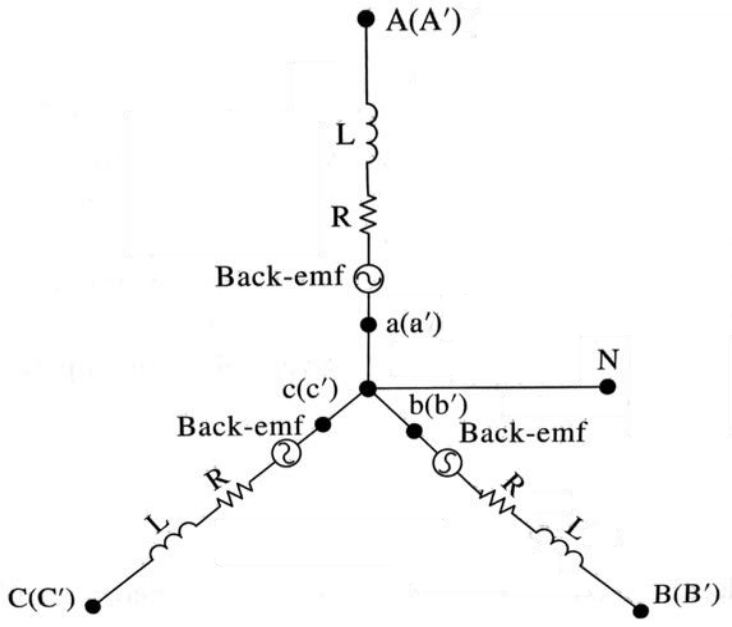

Figure 2.5: Electrical diagram of a three-phase stator.[123]

[122] Khajepour, A., Fallah, S., & Goodarzi, A. (2014), *op. cit.,* p. 55.

[123] Wei, L. (2017*), op. cit.,* p. 142.

Depending on the stator and rotor structures, on the winding distributions and the mutual inductances, a classification of these machines can be proposed. For electric powertrains, the principal solutions are induction (or asynchronous) motors, synchronous motors, switched reluctance motors. IMs are adopted for large vehicles; SMs – in the permanent magnet configuration – are suitable for passenger cars; SRMs are widely considered to have significant potential for BEV applications due to their outstanding torque-speed characteristics.[124] The switched reluctance motor is a type of stepper motor which runs on reluctance torque: power is delivered to windings in the stator rather than the rotor, so the mechanical part is simplified, but the electrical design needs a complex switching system. However, for automotive uses, they are still not feasible at this time – due to the high torque ripple, caused by the harmonic content, and difficulties in high-speed control.

Another solution for electric powertrain is based on brushless DC motor (BLDC): despite its name, it is an AC machine where permanent magnets are mounted on the rotor, while the stator is supplied by a three-phase current system. It is driven by an inverter, responsible for converting the direct current into alternating current. A BLDC motor has the same torque and speed characteristics curve of a brushed DC machine, but it doesn't use any brushes for commutation – reducing the wear, the need of maintenance and increasing the efficiency.[125] This kind of motor is conceptually identical to a permanent magnet synchronous machine, but it differs in the flux distributions and back-EMF profiles. The name DC is related to the applied control strategy – known as trapezoidal control. The motor is fed with direct currents and only two phases are active at same time. Each current has 120 degrees of phase difference with respect to the others, as usual; changes in the state of the currents happen every 60 degrees. The generated back electromotive forces present a trapezoidal behaviour – differently from the sinusoidal back-EMFs of PMSM. The rotational direction of the BLDC can be easily controlled by changing the switching sequence of the switches, depending on Hall sensor values. For the control of this motor, it is fundamental to know the exact angular position of the rotor.[126] With respect to a PMSM – where the stator flux position varies continuously – in a brushless DC motor the stator flux position

[124] Khajepour, A., Fallah, S., & Goodarzi, A. (2014), *op. cit.,* p. 56.

[125] Wei, L. (2017*), op. cit.,* p. 141.

[126] Krishnan, R. (2010), *Permanent Magnet Synchronous and Brushless DC Motor Drives,* Boca Raton, Florida, United States: CRC Press, p 50.

commutates each 60 degrees.[127] Recently, BLDC finds application in automotive because it guarantees a high power to weight ratio, high speed, elevate reliability and simple control strategy; moreover, the switching losses are reduced with respect to PMSM control. On the other hand, it presents torque ripple at commutations and not negligible core losses due to harmonic content; the regulation of torque and speed in HEV/EVs is challenging for this kind of motors.[128]

The DC machines are not considered in this discussion because they have been replaced in many applications by the AC ones. In the next paragraph, the fundamental aspects of the AC machine will be presented, focusing the attention on asynchronous motors and in particular on synchronous motor. For the latter, the permanent magnet configuration is explained, and its dynamic equations are discussed to introduce the control algorithm adopted for the project.

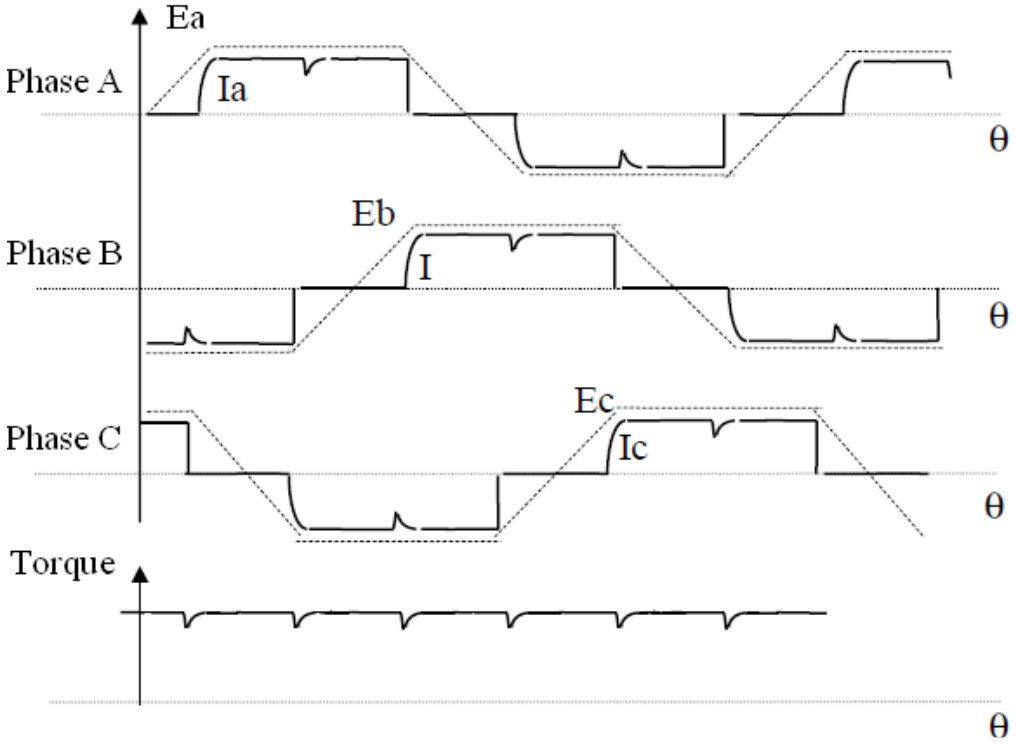

Figure 2.6: BLDC electric waveforms and torque ripple with trapezoidal control strategy.[129]

[127] Akin, B., Bhardwaj, M., & Warriner, J. (2011, April), Texas Instruments, Retrieved from *Trapezoidal Control of BLDC Motors Using Hall Effect Sensors*: http://www.ti.com/lit/an/sprabz4/sprabz4.pdf, pp. 2-3.

[128] Wei, L. (2017*), op. cit.,* p. 144.

[129] Akin, B., Bhardwaj, M., & Warriner, J. (2011, April), Texas Instruments, *op. cit.*, p. 5.

2.2 Rotating magnetic field

The basis of the AC machines is the rotating magnetic field, generated by a three-phase windings system, such that of the stator of induction and synchronous motors. According to Galileo Ferraris' theorem, three coils *a, b, c* with the same number of windings N, evenly spaced by 120 electrical degrees and drained by three balanced currents 120° evenly phased in the time with electrical frequency ω_e produce a constant-magnitude rotating magnetic field at a synchronous speed ω_S. The term "balanced" is related to the fact that at each instant the sum of the currents in a three-phase system is null. The three sinusoidal currents are expressed by:

$$\begin{cases} i_a = I\cos(\omega_e t) \\ i_b = I\cos(\omega_e t - 120°) \\ i_c = I\cos(\omega_e t + 120°) \end{cases}$$

where ω_e is the electrical pulsation, expressed in $\mathrm{rad/s}$, and I is the maximum value of the current. When this AC flows through the coil, it produces a pulsating magnetic field whose amplitude and direction are related to the instantaneous value of the flowing current. As a consequence, each phase winding produces a similar magnetic field displaced by 120 degrees in space from each other.

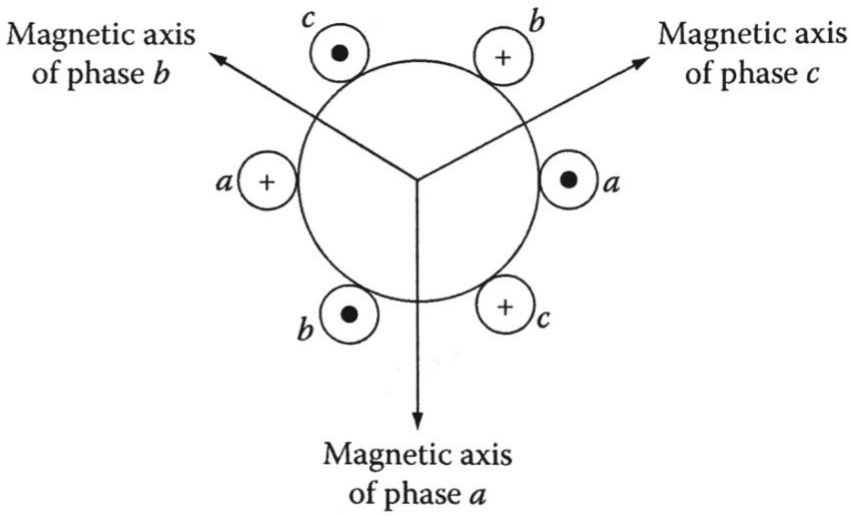

Figure 2.7: Distribution of three-phase magnetic axes.[130]

For each phase, it can be demonstrated that two counter-rotating magnetomotive forces are generated, due to the sinusoidal current. The air-gap MMF of a single-winding

130 Krishnan, R. (2010), *op. cit.,* p. 70.

excited by a source of AC can be resolved into counter-rotating waves, one moving with opposite direction – and equal angular speed – with respect to the other.[131] In this case the terms $\mathrm{MMF_a}$ expresses the space-fundamental component of the effective MMF, produced by phase a – a distributed winding system produces a closer approximation to a sinusoidal MMF than the concentrated coil:[132]

$$MMF_a = MMF_a^+ + MMF_a^-$$

where:

$$MMF_a^+ = \frac{1}{2} MMF_{max} \cos(\theta_{ae} - \omega_e t)$$

$$MMF_a^- = \frac{1}{2} MMF_{max} \cos(\theta_{ae} + \omega_e t)$$

and:

$$MMF_{max} = \frac{4}{\pi}\left(\frac{k_w N_{ph}}{poles}\right) I$$

- the first term $\frac{4}{\pi}$ is related to the Fourier-series analysis of the original rectangular MMF wave, in order to extract the fundamental harmonic;
- $k_w N_{ph}$ is the effective series turns per phase of the fundamental MMF;
- $poles$ are the number of poles, equal to $\frac{P}{2}$;
- I is the maximum value of the current;
- θ_{ae} is the electrical space angle;

In polyphase AC machines, windings are displaced in space phase and similarly currents are displaced in time phase, consequently the negative-traveling flux waves of the various windings sum to zero while the positive-traveling flux waves reinforce. The result is a single positive-traveling flux wave. For phase b and c, the resulting MMFs are similar, but axes are displaced by 120° and -120° respectively. The total MMF is the sum of the contributions from each of the three phases:[133]

$$MMF_{TOT} = MMF_a + MMF_b + MMF_c$$

[131] The demonstration for the single-phase case and the analysis of the Fourier series are omitted; only the equations and the essential results related to a three-phase system are reported in this section. For a deeper explanation of the produced magnetomotive force of a single-phase winding by a sinusoidal current: Fitzgerald, A., Kingsley, C., & Umans, S. (2003), *op. cit.,* pp. 187-203.

[132] Fitzgerald, A., Kingsley, C., & Umans, S. (2003), *op. cit.,* p. 204.

[133] *Ivi,* pp. 205-206.

The negative wave sums to zero, due to the balanced system:

$$MMF_{TOT}^{-} = 0$$

while the positive wave:

$$MMF_{TOT}^{+} = \frac{3}{2} MMF_{max} \cos(\theta_{ae} - \omega_e t)$$

and the resulting MMF is a single positive-traveling wave, with an amplitude equal to 1.5 times the amplitude of the air-gap MMF produced by the individual phase alone:

$$MMF_{TOT} = MMF_{TOT}^{+} = \frac{3}{2} MMF_{max} \cos(\theta_{ae} - \omega_e t)$$

$$MMF_{TOT} = \frac{3}{2} MMF_{max} \cos(P\theta_a - \omega_e t)$$

where θ_a is the space angle. Consequently, the value of the synchronous speed ω_S of the resulting MMF depends on the angular frequency ω_e of the electrical excitation and on the number of pole pairs pp of the system:

$$\omega_S = \frac{\omega_e}{pp}$$

For passing from the magnetomotive force to the magnetic field intensity[134] H, the length of the air-gap (l_t) is used as proportionality factor:

$$H = \frac{MMF}{l_t}$$

For a generic polyphase machine, with m phases and pp pole pairs, the equation of the resulting MMF is:

$$MMF_{TOT} = \frac{m}{2} MMF_{max} \cos(pp\theta_a - \omega_e t)$$

The rotating magnetomotive force and corresponding the rotating magnetic flux are the key to the operation of polyphase rotating electrical AC machinery. The interaction of this RMF with that of the rotor is responsible for producing the torque.

134 The relation between the magnetic field intensity H and the magnetic flux density B is: $B = \mu H$, where μ is the magnetic permeability of the material, crossed by the field.

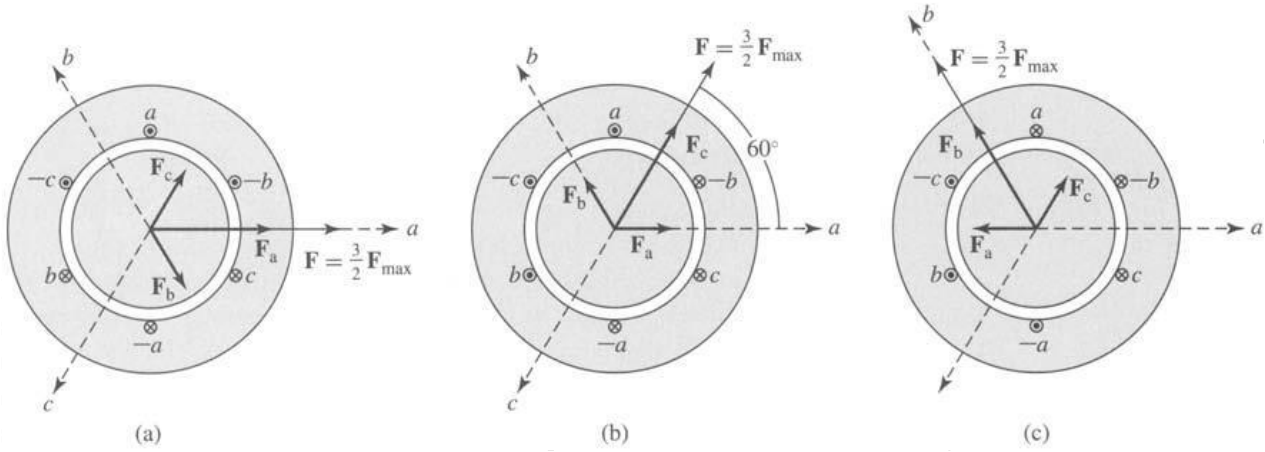

Figure 2.8: Schematic of the production of the rotating magnetic field by three-phase currents.[135]

2.3 Asynchronous motor

The asynchronous motor, known also as induction motor, consists of three-phase windings distributed in the stator slots, out of phase of 120° in the space from each other. The following discussion explains the working principles of this kind of motors – the generator functionality is not considered – without analysing the equivalent circuit and the losses. Then, the main control strategies are briefly described. In motor operating mode, the constant rotating magnetic field is produced by the three-phase sinusoidal currents and it is characterized by a synchronous speed ω_S. This value, through the number of pole pairs pp created by the stator windings, is linked to the angular frequency ω_e of the three-phase voltage applied to the stator, as described before.

The rotor in automotive applications is typically a squirrel cage rotor (fig. 2.10), composed of a series of conductive bars that are welded together at either end, forming the short-circuited windings. In order to have torque, it is necessary that rotor speed ω_R is different from the rotating magnetic field's synchronous speed ω_S; in fact, in case of perfect synchronism, a null torque is generated by the motor. The working principle is the following: the RMF cuts the rotor conductors at this speed difference, known as slip speed ω_{slip}, inducing a corresponding EMF which causes current to flow in the short-circuited windings of the rotor; consequently, another flux will get generated by the induced current in the rotor.[136] This phenomena is described by the Lenz's law of electromagnetic induction: the

[135] Fitzgerald, A., Kingsley, C., & Umans, S. (2003), *op. cit.,* p. 208.

[136] Wei, L. (2017*), op. cit.,* p. 152.

direction of the current induced in a conductor by a changing magnetic field – in this case it rotates, maintaining always the same amplitude – is such that the magnetic field created by the induced current opposes the initial RMF which produced it.

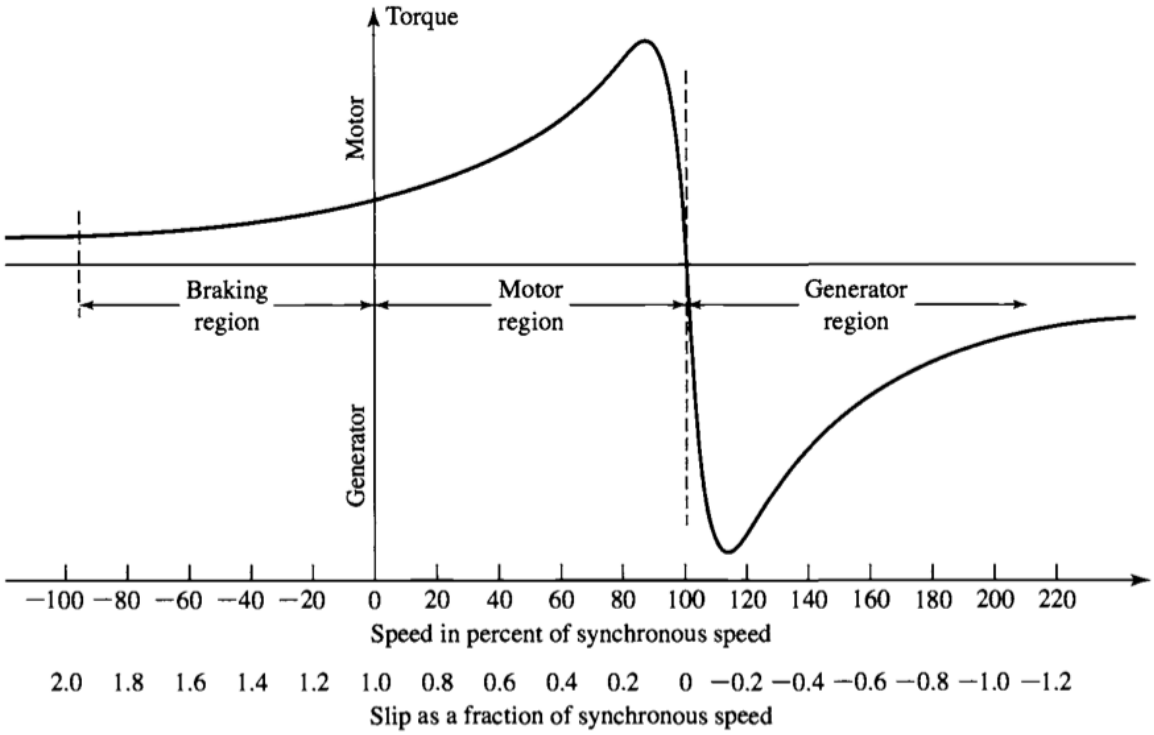

Figure 2.9: Torque-slip characteristic of an induction machine, showing braking, motor and generator regions.[137]

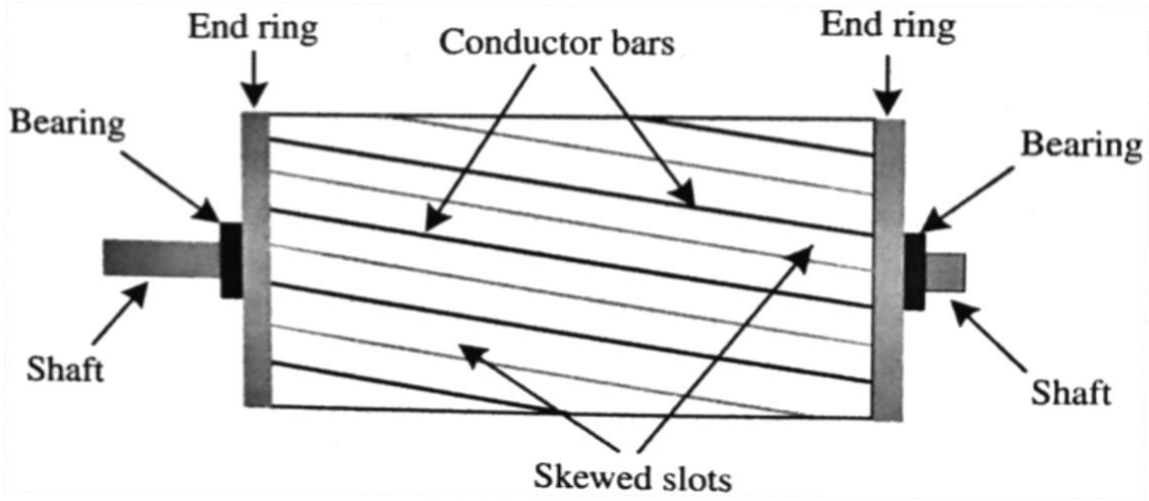

Figure 2.10: Structure of a squirrel cage rotor for an AC induction machine.[138]

137 Fitzgerald, A., Kingsley, C., & Umans, S. (2003), *op. cit.,* p. 324.

138 Wei, L. (2017*), op. cit.,* p. 152.

There are two fluxes, one due to the stator and the other one (that is lagging with respect to the first) due to the rotor. The opposing force of the two magnetic fields create a torque that pulls the rotor in the same direction of the stator's RMF, according to the Lorentz force law. When current flows in a conductor – in this case the rotor windings – immersed in a magnetic field, a force is generated:[139]

$$F = lI \times B = lIB$$

where l is the length of the wire surrounded by the magnetic flux density B, while I flows in the conductor (perpendicularly to B). The short-circuited rotor follows the rotating magnetic field of the multicoiled stator: the induced rotor eddy currents in the rotating field – produced by the stator – cause the turning of the rotor itself by Lorentz force. In fact, considering that in IMs the current-carrying wires are closed, this force acts on both side of the rotor winding, in opposite directions, producing the electromagnetic torque that turns the shaft. Electric energy is converted into mechanical energy in this process. In other words, the squirrel cage rotor turns because it tries to reach the synchronous speed for opposing to the variation of the magnetic field, although it cannot reach a synchronization in induction motors.

Differently from a synchronous machine, the rotor of an induction machine does not itself rotate synchronously; it is the "slipping" of the rotor with respect to the synchronous armature flux that gives rise to the induced rotor currents and hence the torque.[140] Induction motors operate at speeds less than the synchronous mechanical speed. The slip speed ω_{slip} is usually expressed in relation to ω_S through the following equation – where the quantity s is called slip:[141]

$$s = \frac{\omega_{slip}}{\omega_S} = \frac{\omega_S - \omega_R}{\omega_S}$$

For a squirrel cage induction motor, the principal control strategies are three:[142]

- change the number of poles, since the synchronous speed of the rotating magnetic field depends on the pole pairs of an induction motor;

139 Fitzgerald, A., Kingsley, C., & Umans, S. (2003), *op. cit.,* pp. 113-114.

140 *Ivi,* p. 184.

141 Ferraris, L. (1999), *Macchine Elettriche,* Turin, Italy: CLUT, pp. 300-302.

142 Wei, L. (2017*), op. cit.,* p. 156.

- change the magnitude of the supplied voltage – scalar control – because the developed torque and the motor speed decrease if the supplied voltage is reduced;
- combine torque and speed regulation by adjusting the supply voltage and frequency, using the vector control – or field-oriented control, analysed in chapter III for PMSM applications. This strategy provides independent control of air-gap flux and torque, thank to Clarke-Park transformations, so the IM is driven like a separate excitation DC motor.

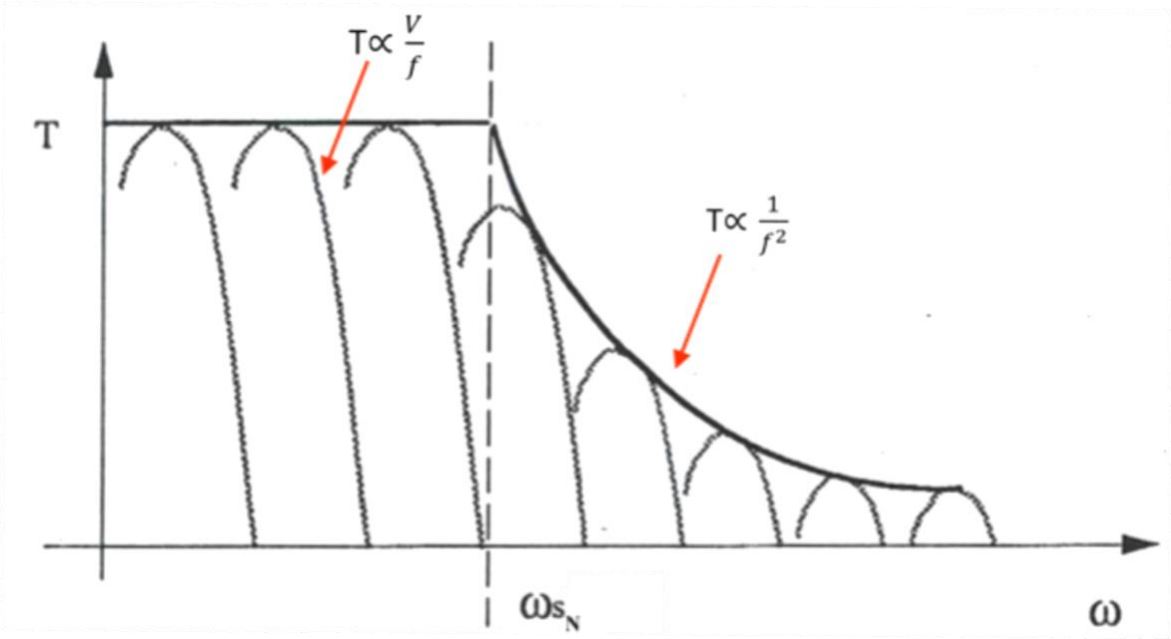

Figure 2.11: Torque-speed characteristics of an IM.[143]

2.4 Synchronous motor

The synchronous machine is composed by a moving part (rotor) – that is fed by a DC excitation – and by a stationary part (stator) – where the alternating current flows, through the armature three-phase windings. Alternatively, permanent magnets can be mounted on the rotor for producing the magnetic field – this configuration is analysed in detail in next section. A brief introduction to SMs is reported here, analysing the working principles and motivating their use as generators and motors. This kind of machines is used in the parallel configuration as alternators (they are called in this way when they work as generators), for

[143] In constant torque region, the different curves correspond to different voltage-frequency couples, in order to maintain constant their ratio (typical of scalar control, chapter III). In constant power region, the motor torque decreases in an inversely proportional manner with respect to the square of the frequency.

producing almost the total energy of the electric grid. The use as motor was not diffused, due to the lack of starting torque. Actually, the PMSM guarantees optimal performance and, for this reason, it is implemented in recent automotive EV/HEV applications. Synchronous machines – as the name suggests – are able to work only at the synchronous speed, so the rotor angular velocity is equal to the RMF's speed.

Different rotors can be used in synchronous machine, providing difference performances in term of power, torque and losses. The principal classification is DC excited and non-excited motors. The first configuration requires a direct current supply for the rotor, that presents a winding; depending on the generator or motor operational mode, the responsible for the generation of the magnetic field in the rotor is this excitation current. This kind of SM is larger in size and has more losses, due to the presence of this additional direct current. In non-excited motors, the rotor is made of steel and presents no windings around it; consequently, the Joule losses are reduced. At synchronous speed, these motors are able to rotate in synchronism with the RMF of the stator, because the field magnetizes the rotor inducing the magnetic poles to turn the shaft. A high-retentivity steel is used for the rotors – like cobalt steel; the three possible designs for non-excited motors are:

- reluctance motor consists of a rotor composed by a soft magnetic material, such as laminated silicon steel. No windings are mounted on the rotor, while the stator presents the usual three-phase configuration. Construction and production processes of these motors are similar to all the asynchronous motors, but in this case the rotor is anisotropic (not symmetrical). With respect to an IM, there is no rotor slip and there are no rotor losses – no current flows in the rotor, so efficiency grows; moreover, this system requires easy maintenance if compared to permanent magnet motors. The working principle of this kind of machine is the presence of saliency, due to the magnetic material's multiple projections which act as salient magnetic poles. The rotor's poles are typically fewer than those of the stator in order to minimize the torque ripple. Consequently, a reluctance torque is generated thanks to the variation of the reluctance with the rotor angular position because the air-gap is not constant, due to the shape of the rotor;
- hysteresis synchronous motor has cylindrical rotor and produces torque due to hysteresis and eddy currents induced in the rotor. The latter is composed of a high coercivity magnetic material – usually hardened cobalt steel – that has a wide hysteresis loop, so when it is magnetized in a direction, it requires a large reverse magnetic field for reversing the magnetization. This motor presents a uniform air-

gap and can operate in both three-phase or single-phase supply – in single-phase configuration, an auxiliary winding is added to the stator for starting the machine;

- permanent magnet synchronous motors (PMSM) present permanent magnets embedded in the steel rotor to create a constant magnetic field. The stator is connected to an AC supply, producing the RMF; at synchronous speed the rotor poles lock to the rotating magnetic field. For motor starting, a variable-frequency power source is required due to the absence of induction windings in the rotor. The desirable properties of the materials used for these motors are high flux density and high coercivity. Depending on rotor shape and permanent magnets' position, the reluctance may vary with the angular position and a reluctance torque could be added for increasing the maximum deliverable torque – as it happens in interior magnet configuration. PMSMs are typically used for high-performance and high-efficiency motor drives, where fast acceleration and deceleration, full torque control, and excellent dynamics are required – like in EV/HEV automotive applications.[144]

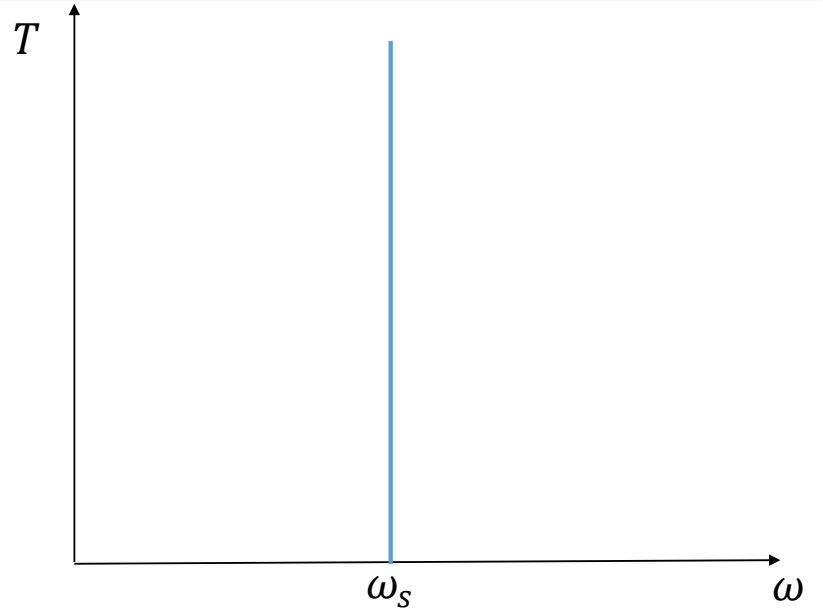

Figure 2.12: Torque-speed characteristics of a SM.

[144] NXP Freescale Semiconductor (2012), Retrieved from *Permanent Magnet Synchronous Motor Control*: https://www.nxp.com/docs/en/brochure/BBPRMMAGSYNART.pdf, p. 1.

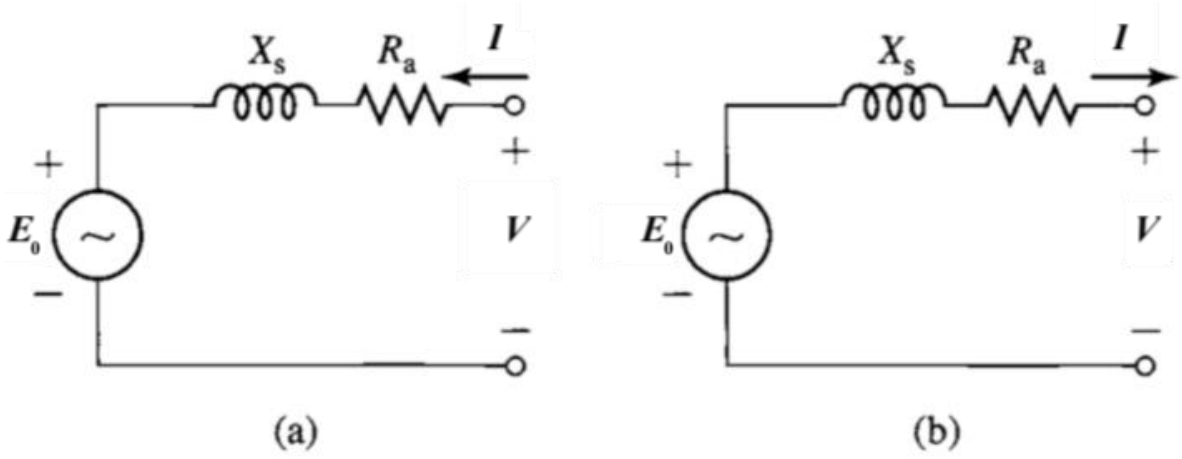

Figure 2.13: SM equivalent circuits: (a) motor reference direction and (b) generator reference direction.[145]

From the equivalent circuit of the generic synchronous machine, the following equations can be obtained for power and torque. The approach is based on vector diagram, neglecting any saturation effects and approximating the results just to motivate the main working principles; concerning the parameters, the most important is the synchronous reactance X_s, obtained by the sum of the equivalent stator and rotor reactance. From Kirchhoff law, applied to fig. 2.13 (according to generator reference direction):

$$V = E_0 - (R_a + jX_s)\, I$$

where the contribution due to the armature resistance is usually negligible with respect to the other one – in fact it is not considered for the vector representation of figure 2.14. By studying the following diagram for an isotropic machine and considering the parameters:[146]

- δ load angle, important for defining the operating mode of a SM;
- φ phase angle, between the load voltage and the corresponding current;
- β current angle.

$$\overline{CB} = X_s\, I \cos(\varphi)$$

$$\overline{CB} = E_0 \sin(\delta)$$

$$X_s\, I \cos(\varphi) = E_0 \sin(\delta)$$

In this condition, the generated active electric power is:

$$P_e = 3\, V\, I \cos(\varphi) = \frac{3VE_0}{X_s} \sin(\delta)$$

[145] Fitzgerald, A., Kingsley, C., & Umans, S. (2003), *op. cit.,* p. 253.

[146] Ferraris, L. (1999), *op. cit.*, pp. 256.

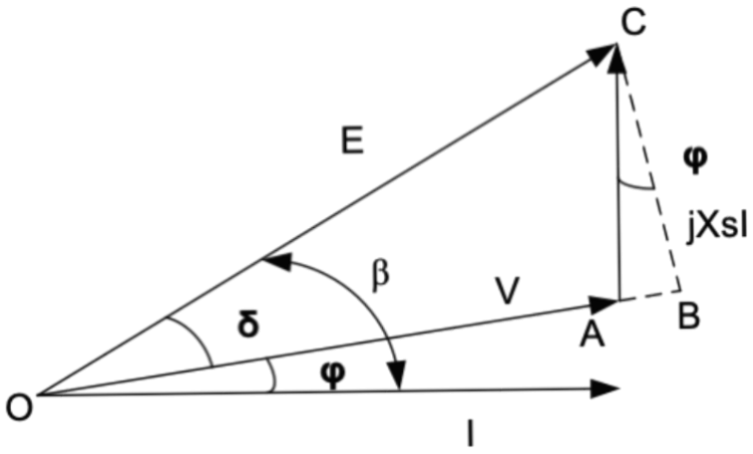

Figure 2.14: SM vector diagram representation.

The term 3 at the beginning is due to the three-phase nature of the system, while $\cos(\varphi)$ is known as power factor – which represents the ratio between the real power and the apparent power flowing in the circuit. The corresponding motor torque is obtained by equalizing the mechanical and electric power. For simplicity, the efficiency of the machine is assumed to be one – ideal conditions.

$$P_e = P_m = T\omega_m$$

$$T = \frac{3VE_0}{\omega_m X_s}\sin(\delta)$$

Remembering the relationship between the mechanical speed ω_m and the pulsation of the electric quantities ω_e, through the number of pole pairs pp ($\omega_e = pp\ \omega_m$):[147]

$$T = pp\frac{3VE_0}{\omega_e X_s}\sin(\delta)$$

When the machine works as generator, it converts the mechanical power due to the rotor angular movement into electric power. In other words, the rotating permanent magnet that constitutes the non-excited rotor in a PMSM, or the equivalent excitation DC flowing in the rotor winding, produce a rotating magnetic field which induces currents in the three-phase windings of the stator. Depending on the load angle, the machine can pass from generator to motor behaviour. Furthermore, by zooming the diagram of figure 2.15, it can be shown that alternator can work in stable or unstable conditions (fig. 2.16): a stable area means that an increase of load angle is followed by an increase of the torque.

147 Ferraris, L. (1999), *op. cit.*, pp. 255-258.

ltant air-gap flux per pole
f of the dc field winding
trical phase angle between magnetic axes of Φ_R a

Figure 2.15: Synchronous machine torque - load angle characteristic.[148]

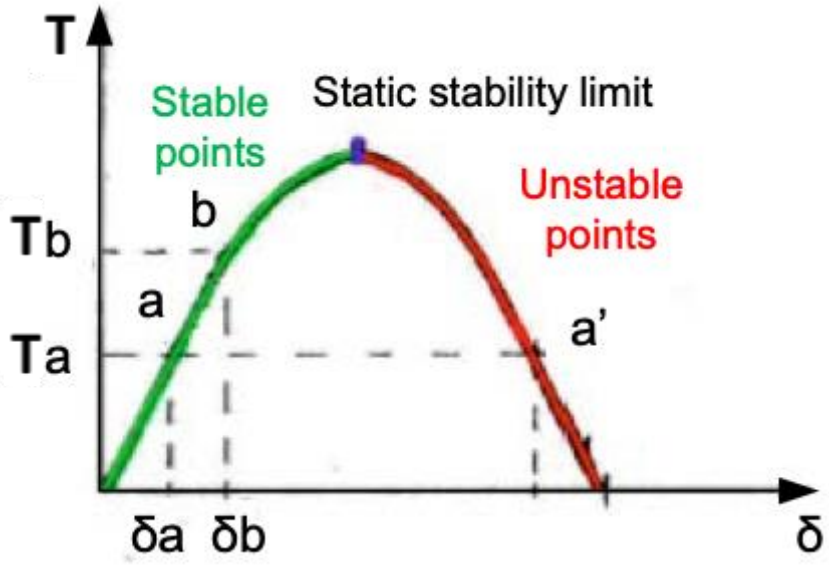

Figure 2.16: Synchronous machine torque - load angle characteristic, zoom on the generator region for showing stable and unstable working points.

Concerning the motor operational mode, its behaviour is similar to an induction motor: the three-phase sinusoidal currents flow in the stator winding and generate the rotating magnetic field; the rotor as a result – both in excited and non-excited cases – starts rotating at the same rate, providing the second synchronized RMF. For an anisotropic machine, an additional term depending on $\sin(2\delta)$ represents the reluctance torque. As

[148] Fitzgerald, A., Kingsley, C., & Umans, S. (2003), *op. cit.,* p. 247.

result, the maximum motor torque is incremented, but the stable area is reduced – because the additional torque has a doubled pulsation, as shown in next figure for the generator working region; consequently, also the power grows:

$$T = pp\frac{3VE_0}{\omega_e X_s}\sin(\delta) + 3pp\frac{V^2}{2\omega_e}\left(\frac{1}{X_q} - \frac{1}{X_d}\right)\sin(2\delta)$$

where X_q and X_d are the equivalent quadrature and direct reactance respectively, expressed in the two-phase rotating reference frame synchronized with the rotor (obtained from the Clarke-Park transformations).

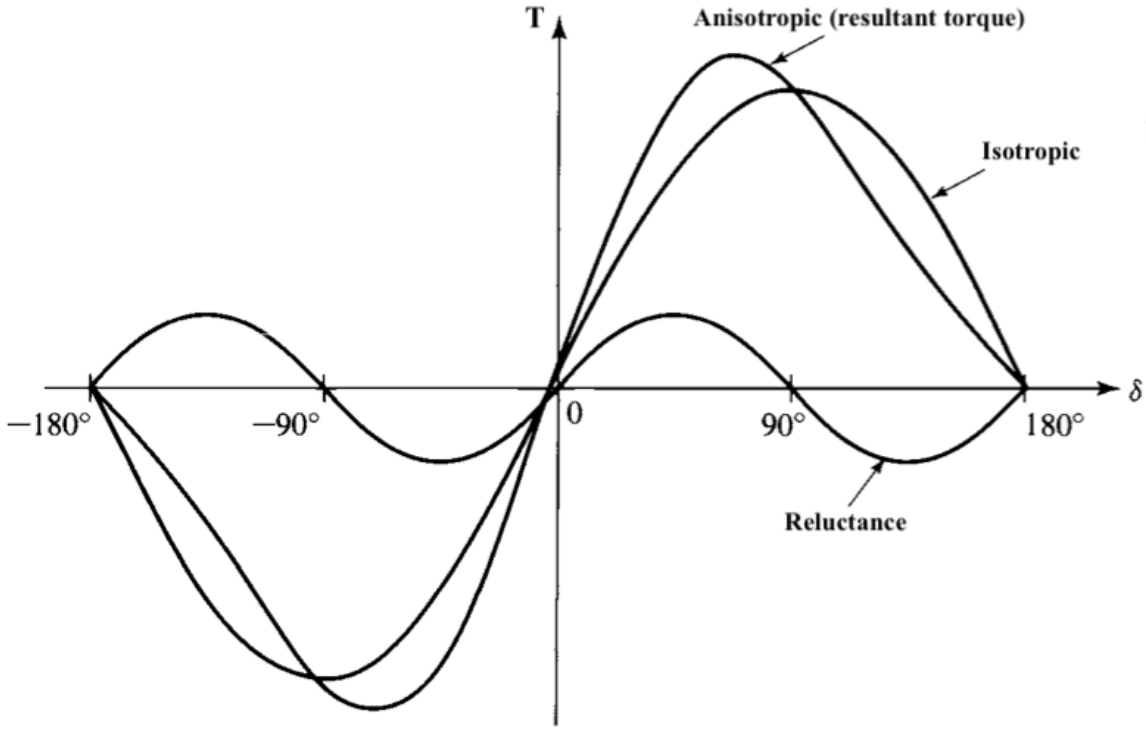

Figure 2.17: Synchronous machine torque - load angle characteristic, highlighting the different contributions (anisotropic, isotropic and reluctance torque).[149]

From the theoretical analysis of a generic DC-excited synchronous motor, it can be demonstrated that the resulting magnetic flux linkages with the armature phases *abc* and field winding *f* are expressed in terms of the self and mutual inductances and four currents:[150]

[149] Fitzgerald, A., Kingsley, C., & Umans, S. (2003), *op. cit.,* p. 290.

[150] *Ivi*, p. 250.

$$\begin{cases} \lambda_a = L_a i_a + M_{ab} i_b + M_{ac} i_c + M_{af} i_f \\ \lambda_b = M_{ba} i_a + L_b i_b + M_{bc} i_c + M_{bf} i_f \\ \lambda_c = M_{ca} i_a + M_{cb} i_b + L_c i_c + M_{cf} i_f \\ \lambda_f = M_{fa} i_a + M_{fb} i_b + M_{fc} i_c + L_f i_f \end{cases}$$

where:

- λ_i is the magnetic flux linkage with the *i*-winding;
- i_i is the current flowing in the *i*-winding of the stator or in the excitation circuit (i_f represents the current in the field coil of the rotor);
- L_i is the self-inductance of the *i*-winding;
- M_{ij} is the mutual inductance between two different windings; it is evaluated between two different phases of the stator or between one stator winding and the rotor field coil.

In an alternator, the relation between the terminal voltage and the current of a single phase is expressed by the following equation:[151]

$$v_a = R_a i_a + \frac{d\lambda_a}{dt}$$

where:

- v_a is the terminal voltage of *a*-phase;
- R_a is the equivalent resistance of the *a*-winding;
- i_a is the current flowing in the *a*-winding;
- $\frac{d\lambda_a}{dt}$ is the time derivative of the magnetic flux linkage with the *a*-phase. Not only the currents vary in time, but also the self and mutual inductance change depending on the actual rotor position.

By generalising this consideration for a three-phase stator and a DC-excited rotor, the complete dynamics of the synchronous machine is obtained. The main problem of this representation is that inductances are functions of rotor position, so they vary during the working time, and the analysis of voltages and currents increase in complexity. For this reason, a mathematical approach based on phase transformations is used for simplifying the equations and consequently also the control strategy. In case of PMSM, the equations are modified, due to the presence of permanent magnets.

[151] Fitzgerald, A., Kingsley, C., & Umans, S. (2003), *op. cit.,* p. 252.

2.4.1 Permanent magnet synchronous motor (PMSM)

As introduced in previous section, the PMSM is composed of a three-phase windings system in the stator and of a steel rotor where permanent magnets are inserted for producing the constant magnetic flux. In the motor operational mode, when the rotor speed is near to synchronous speed, it locks in synchronism with the RMF generated by stator current. The generator functionality of this machine is used for refilling the batteries in EV/HEV applications by exploiting the regenerative braking system or the downhill driving: the kinetic energy of the rotating shaft is converted into electric energy, so opposite-sign currents are generated in the stator and the energy source can be recharged. Most of the PMSMs rely on rare-earth elements, such as neodymium, that guarantee optimal performance and efficiency. On the other side, the use of these rare-earth metals in automotive applications has been limited, for preserving resources; consequently, the price is continuously increasing – and the vehicle cost grows at the same time. Recently, ferrite magnets have been employed in IPM and SPM motors for reducing the economic impact.[152] The most advanced ferrite magnet grade – the Lanthanum-Cobalt substituted strontium ferrite – achieves high remanence and intrinsic coercivity. Ferrite magnets have positive temperature coefficient, so the higher the temperature, the higher the intrinsic coercivity, and for this reason they are good candidate for high temperature automotive motor applications.[153]

The main features that motivate the adoption of permanent magnet synchronous motors are the elevate power to weight radio, the high torque density, the very wide speed range, little torque oscillations, the possibility of working efficiently at high torques, the reduction of maintenance and losses because there is no current in the rotor and also an excellent torque-inertia ratio. The structure is also very compact, reducing the total weight of the vehicle, while the efficiency is always high in a PMSM. With respect to other configuration, a smaller dimension motor can be realized for delivering the same power. Despite these machines are not self-starting, no starter devices are required, because the variable-frequency stator drive is sufficient to allow the motor to start running. Concerning the field weakening of a PM machine, it is implemented by using a demagnetizing stator

152 Kim, Y.-H., e*t al.* (2015), *Comparison of IPM and SPM motors using ferrite magnets for low-voltage traction systems*, Presented at *The 28th International Electric Vehicle Symposium and Exhibition*, Goyang, South Korea, p. 1

153 Zhang, S., *et al.* (2012), *Permanent Magnet Technology for Electric Motors in Automotive Applications,* Presented at *2nd International Electric Drives Production Conference (EDPC)*, Nuremberg, Germany, pp. 1-2

current, in order to weaken the magnetic flux due to rotor permanent magnets for increasing the speed over its rated value.

The principal control techniques for permanent magnet synchronous motor – and also reluctance motor – can be classified in sinusoidal and trapezoidal. The latter is mainly related to brushless DC motors, as described before, but both of them can be adopted for PMSM and BLDC control. Sinusoidal control offers more advantages in terms of reduction of the harmonic content and continuous variation of the flux; on the other hand, it is more complex, and the losses related to switching mechanism are increased. Sinusoidal control strategies are divided into scalar and vector. The first one requires a variation in the magnitude of the supply voltage – and also the frequency changes proportionally for maintaining the same torque. This regulation technique is less accurate, but simpler to be implemented; a feedback of the actual angular position or angular speed can be inserted for improving the dynamic behaviour. The vector control – called field-oriented control – is the most adopted solution: it needs a mathematical effort due to three-phase to two-phase transformation, but it offers the possibility of using PMSM for automotive application in a safe, reliable and performing manner. On the other side, trapezoidal techniques are classified as closed loop or open loop, depending on the presence or not of the feedback position and angular velocity – measured through Hall effect sensors or encoders. The essential difference between trapezoidal and sinusoidal PM motors is based on the shape of their induced EMF: sinusoidal in the PMSM, while trapezoidal in the BLDC.[154]

2.4.1.1 Surface-mounted magnets and interior magnets

During the design phase of a PMSM, two possible solutions are generally used for implementing the permanent magnets in the rotor: surface-mounted permanent magnets or interior permanent magnets. In surface-mounted configuration, the permanent magnets are mounted on the outer periphery of motor lamination: this structural arrangement causes a lower integrity and a less robust mechanical action. The principal aspect is the absence of anisotropy and the corresponding null reluctance torque. This system, in fact, can act using only the torque due to the flux linkage between the rotor permanent magnet field and the stator electro-magnetic field. This kind of machines is considered isotropic because the air-gap is uniform, so the properties of the magnetic field distribution in the air-gap are the same

[154] Krishnan, R. (2010), *op. cit.,* p. 48.

in all directions. In the maximum torque per ampere (MTPA) region – in constant torque condition – the value of the maximum deliverable torque is reduced with respect to an equivalent interior permanent magnet motor, and the *d*-axis stator current component is imposed equal to zero – its module is increased only in constant power region. Moreover, SPM motors are more efficient in low-speed range, because the absence of anisotropy and the reduced magnetic field make smaller the flux weakening area.[155] In fact, if the inductances are very low – such as in SPM servo motors – the field weakening doesn't provide substantial advantages, because the possibility of increasing the speed over than the rated value is limited. As described in next paragraph, in a SPM configuration the reluctance variation between the direct and quadrature axes inductances are is fairly small because these magnets have very low permeability and can be regarded as air in inductance calculations; the SPM motor has very low inductance saliency.[156] The control strategy for this configuration is obviously easier due to the simpler structure.

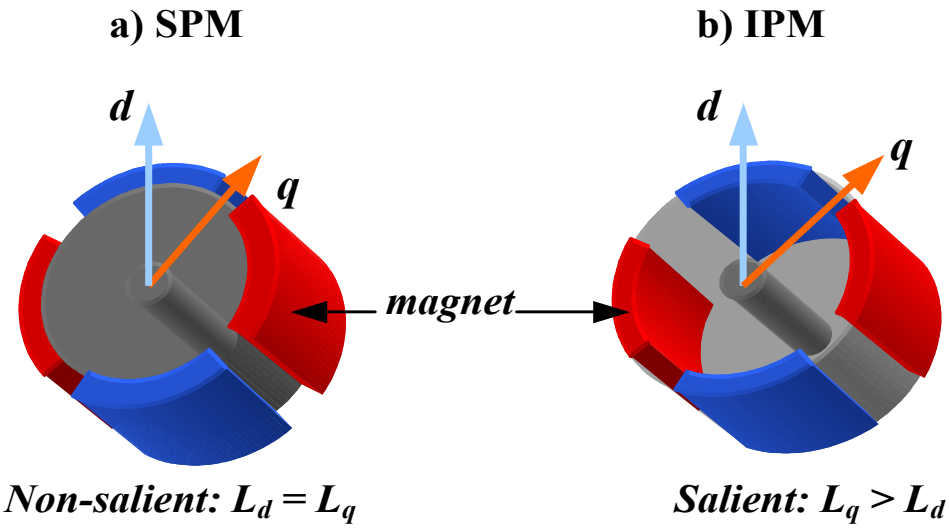

Figure 2.18: Schematic of surface-mounted (a) and interior permanent magnet (b) synchronous machine.[157]

For decades, surface-mounted PMSMs dominate the market; in recent years, due to the emerging hybrid-electric and electric vehicles, the diffusion of IPM solutions is being boosted, because they are able to guarantee better performance in terms of traction and

[155] Krishnan, R. (2010), *op. cit.,* p. 34.

[156] Ghazimoghadam, M., & Tahami, F. (2011), *Sensorless Control of Non-Salient PMSM using Asymmetric Alternating Carrier Injection,* Presented at *IEEE Symposium on Industrial Electronics and Applications*, (pp. 7-12), Langkawi, Malaysia, p. 7.

[157] Chin, Y., & Soulard, J. (2003), *A Permanent Magnet Synchronous Motor for Traction Applications of Electric Vehicles*, Presented at *IEEE Electric Machines and Drives Conference,* Madison, Wisconsin, United States, p. 1.

speed-range. Interior permanent magnet synchronous motors are more performing in terms of torque density (and consequently power density), because it exploits the anisotropic properties of the airgap. The magnets are embedded within the rotor and they produce the constant rotor magnetic field; since the magnets have lower permeability than iron, the effective air-gap in the magnetic flux path varies depending on the rotor position. The magnetic saliency results in variation of the inductance at the motor terminal with the rotor position – rotor position and measured inductance are always related. These motors have a more intensive magnetic field in the air-gap with respect to previous typology; moreover, the magnets can be thinner than those of surface-mounted PMSM for delivering the same torque. In this configuration, an identical SPM power output can be achieved with higher efficiency and smaller stator excitation.[158] In fact, the resulting torque is the addition of isotropic and anisotropic (or reluctance) torque contributions, producing a higher maximum value than the corresponding value in a SPMSM.[159] In the MTPA region, in this case, also the contribution of the *d*-axis current is fundamental for producing the additional reluctance torque. Thanks to saliency and anisotropic properties, the flux weakening region can be extended and the speed-range becomes wider: this is a fundamental aspect that motivates the diffusion and adoption of IPM synchronous motors in HEV/EV applications.

2.4.1.2 Dynamic equations of the PMSM

In this paragraph, the dynamic equations of an interior permanent magnet synchronous machine are described. The IPM configuration is considered, because it is the most general one; for SPM, the necessary modifications in the equations will be motivated and explained. In the standard representation self and mutual inductances are functions of rotor position, increasing the complexity of the needed control algorithm. The Clarke-Park transforms are introduced and applied for passing from a three-phase system to an equivalent rotating two-phase system: thanks to this mathematical operation, the vector control – or field-oriented control – can be exploited for managing the PMSM in a more efficient and more performing manner. The effective FOC implementation will be discussed in next chapter.

158 Krishnan, R. (2010), *op. cit.,* p. 35.

159 Ghazimoghadam, M., & Tahami, F. (2011), *op. cit.*, p. 7.

Starting from the dynamic system of a generic DC-excited synchronous machine, the equations can be simplified removing the term of the excitation current and using the flux linkage contribution due to permanent magnets. In a PMSM, there is no i_f in the stator, so the terms $\lambda_{ra},\ \lambda_{rb},\ \lambda_{rc}$ are added – they represent the flux linkages established in the stator *abc* phase windings respectively, due to the presence of PMs on the rotor. These values change depending on the electric angle θ_e of the electric quantities. [160] Furthermore, this is a simplified mathematical model because the mutual inductances are considered symmetrical, so $M_{ij} = M_{ji}$, the core saturation and winding leakage inductance are neglected, the magnetic potential in the air-gap is considered sinusoidal, and the higher harmonic waves in the magnetic field are ignored. [161]

$$\begin{cases} \lambda_a = L_a i_a + M_{ab} i_b + M_{ac} i_c + \lambda_{ra} \\ \lambda_b = M_{ba} i_a + L_b i_b + M_{bc} i_c + \lambda_{rb} \\ \lambda_c = M_{ca} i_a + M_{cb} i_b + L_c i_c + \lambda_{rc} \end{cases}$$

where:

$$\begin{cases} \lambda_{ra} = \lambda_{PM} \cos(\theta_e) \\ \lambda_{rb} = \lambda_{PM} \cos(\theta_e - 120°) \\ \lambda_{rc} = \lambda_{PM} \cos(\theta_e + 120°) \end{cases}$$

The term λ_{PM} is the nominal flux linkage due to rotor permanent magnets. Then:

$$\begin{cases} v_a = R_a i_a + \dfrac{d\lambda_a}{dt} \\ v_b = R_b i_b + \dfrac{d\lambda_b}{dt} \\ v_c = R_c i_c + \dfrac{d\lambda_c}{dt} \end{cases}$$

Considering the generic three-phase quantities x_{abc} in the phase plane, the Clarke transform is used for passing from the fixed *abc* reference frame to an equivalent fixed two-phase *αβ* reference frame. The three-phase RF is composed of three axes, displaced each other by 120°; the *αβ* reference frame is composed of two perpendicular axes. Different transformations are proposed in literature, depending on what quantity is maintained constant during the transformation. In this project, the amplitude-invariant Clarke

[160] Ohm, D. (2000), Drivetech Inc., Retrieved from *Dynamic Model of a PM Synchronous Motor*, pp. 1-3.

[161] Amin, F., *et al*. (2017, May), *Modelling and Simulation of Field Oriented Control based Permanent Magnet Synchronous Motor Drive System,* In *Indonesian Journal of Electrical Engineering and Computer Science, 6(2)*, p. 389.

transformation is considered:[162] the magnitude of the electric quantities is conserved, but this will imply a multiplication factor $\left(\text{equal to } \frac{3}{2}\right)$ in the final torque equation.

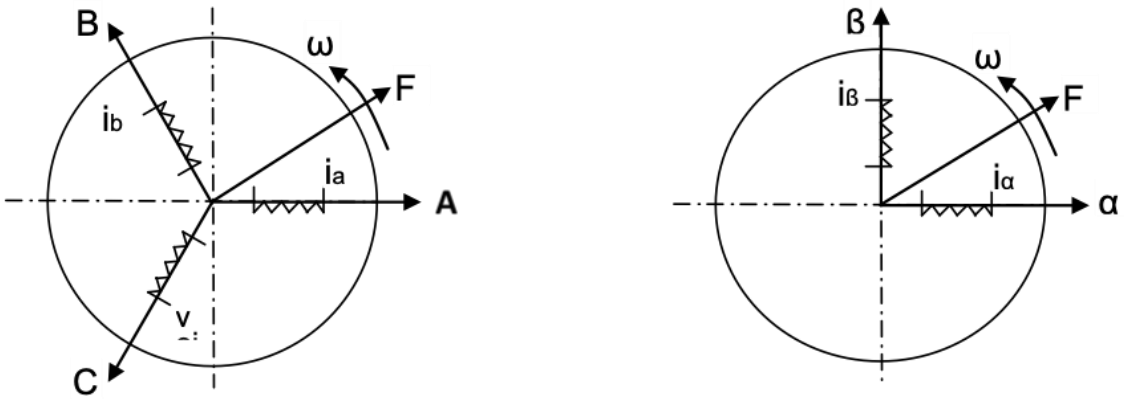

Figure 2.19: Three-phase balanced AC currents on the left, two-phase balanced AC currents on the right.[163]

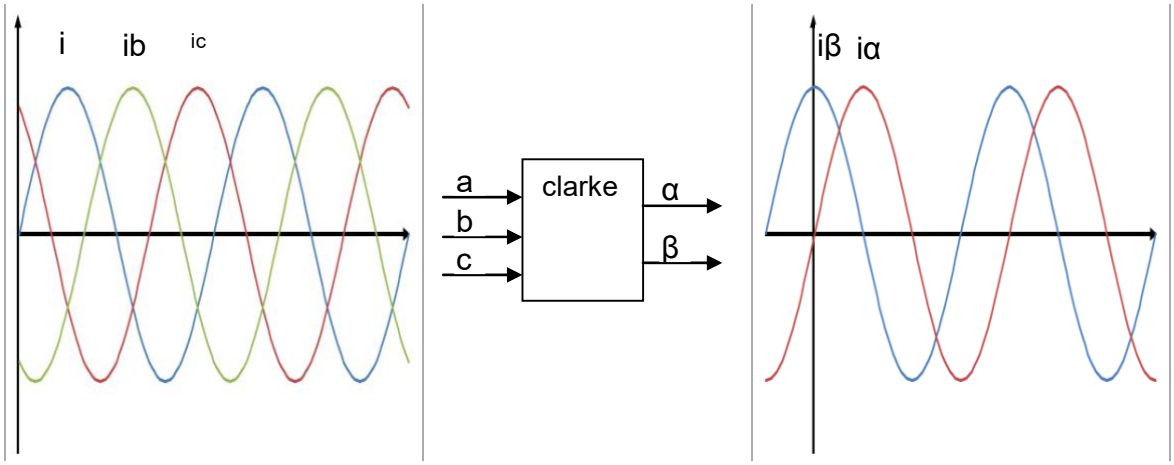

Figure 2.20: Current waveforms with Clarke transformation.[164]

$$\begin{cases} x_a = X \sin(\omega t) \\ x_b = X \sin(\omega t + 120°) \\ x_c = X \sin(\omega t - 120°) \end{cases}$$

$$\begin{cases} x_\alpha = x_a = X \sin(\omega t) \\ x_\beta = \dfrac{\sqrt{3}\, x_a}{3} + \dfrac{2\sqrt{3}\, x_b}{3} = X \sin(\omega t + 90°) \end{cases}$$

[162] Cypress Semiconductor (2017), Retrieved from *Coordinate Transform in Motor Control*: https://www.cypress.com/file/222111/download, pp. 2-4.

[163] *Ivi*, p. 2.

[164] *Ivi*, p. 4.

The homopolar axis is neglected, because a balanced three-phase machine is considered, so the sum of the three-phase currents is zero at any time.[165] This operation is completely reversible, in order to reconstruct the three-phase quantities from the equivalent two-phase representation:

$$\begin{cases} x_a = x_\alpha \\ x_b = -\frac{1}{2}x_\alpha + \frac{\sqrt{3}}{2}x_\beta \\ x_c = -\frac{1}{2}x_\alpha - \frac{\sqrt{3}}{2}x_\beta \end{cases}$$

The successive step is the Park transformation: a rotating *dq* reference system is considered for the generic quantities, with an angular velocity ω and an angular position θ. For applying this transformation, the measured angle θ of the rotating axes is required – obviously *d*-axis and *q*-axis remain perpendicular during their rotation.[166] It is fundamental to notice that the resulting values x_d, x_d are DC quantities (fig. 2.22) with respect to the rotating *dq*-axes, because the electric variables and the axes have the same pulsation – they are no more sinusoidal values, such as in the fixed RFs. This benefit is exploited for decoupling the stator current components in a PMSM – like in separated excitation DC motors – and for regulating the motor in a more efficient manner through the FOC.

$$\begin{cases} x_d = x_\alpha \cos(\theta) + x_\beta \sin(\theta) \\ x_q = -x_\alpha \sin(\theta) + x_\beta \cos(\theta) \end{cases}$$

As usual, also the Park inverse transformation is considered for reconstructing the three-phase quantities:

$$\begin{cases} x_\alpha = x_d \cos(\theta) - x_q \sin(\theta) \\ x_\beta = x_d \sin(\theta) + x_q \cos(\theta) \end{cases}$$

[165] The equations for computing the electric quantities expressed with respect to the homopolar axis are not inserted. For a deeper analysis: Krishnan, R. (2010), *op. cit.,* pp. 239.

[166] Cypress Semiconductor (2017), *op. cit.*, pp. 6-8.

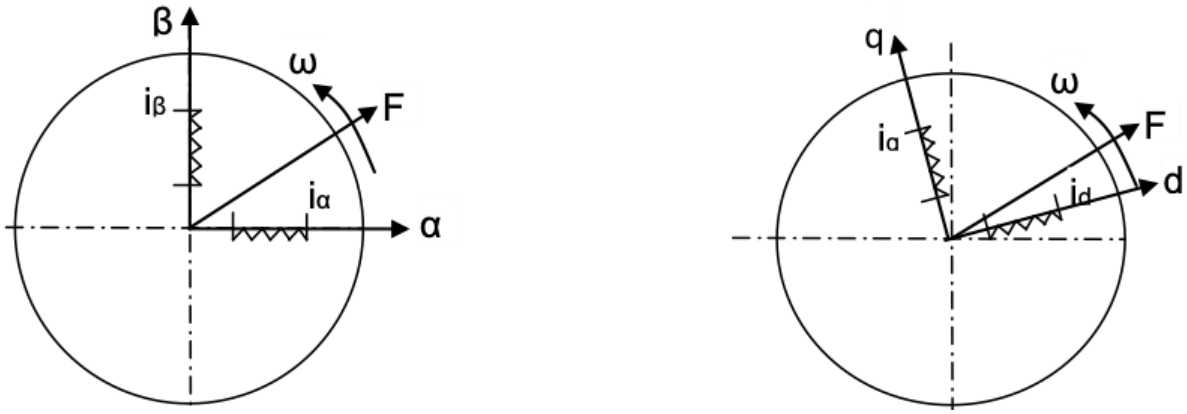

Figure 2.21: Currents in αβ reference frame on the left, current in rotating dq reference frame on the right.[167]

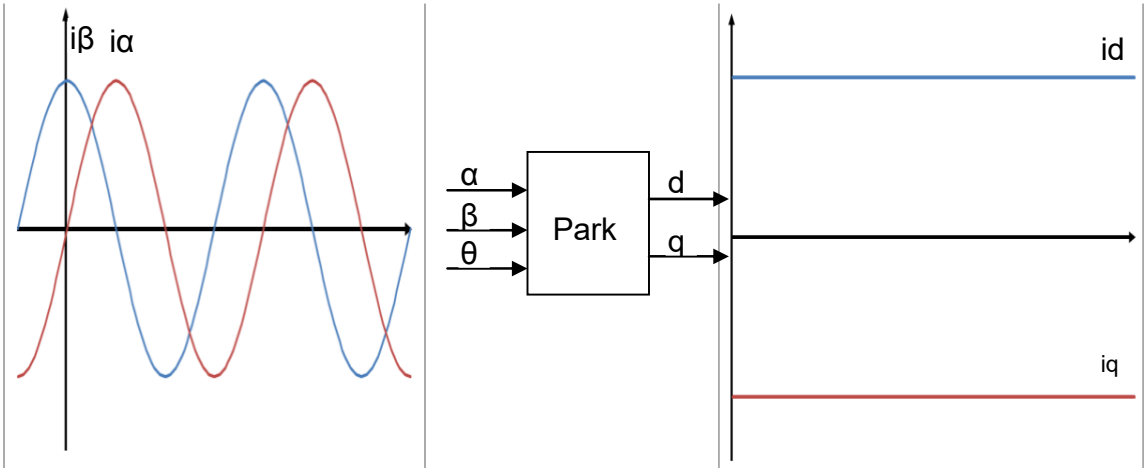

Figure 2.22: Current waveforms with Park transformation.[168]

For the PMSM, the used angular position for the mathematical operation is the electrical angle θ_e because in the AC machine's stator there are electric quantities. In fact, Clarke-Park transforms are used for obtaining the representations of stator currents, termination voltages and flux linkages in the rotor *dq* reference frame. From the field-oriented control block scheme of successive chapter it is possible to see that sensors are used for measuring the rotor mechanical position; this value is then multiplied for the number of pole pairs in order to obtain the rotor electrical angle. In a similar manner, the corresponding electrical speed is computed from the measured mechanical velocity of the rotor. With this approach, the Clarke-Park direct and invers transformations are correctly implemented, and stator voltages and currents maintain the correct pulsation. By using this strategy for

167 Cypress Semiconductor (2017), *op. cit.*, p. 6.

168 *Ivi*, p. 7.

simplifying the analysis and the control of a PMSM, the obtained stator quantities in the rotor *dq*-axes are the following ones. All the values are referred to the rotor RF, so the apex *r* is omitted. In the chosen configuration, the rotor *d*-axis is aligned along the PMs' magnetic flux direction.

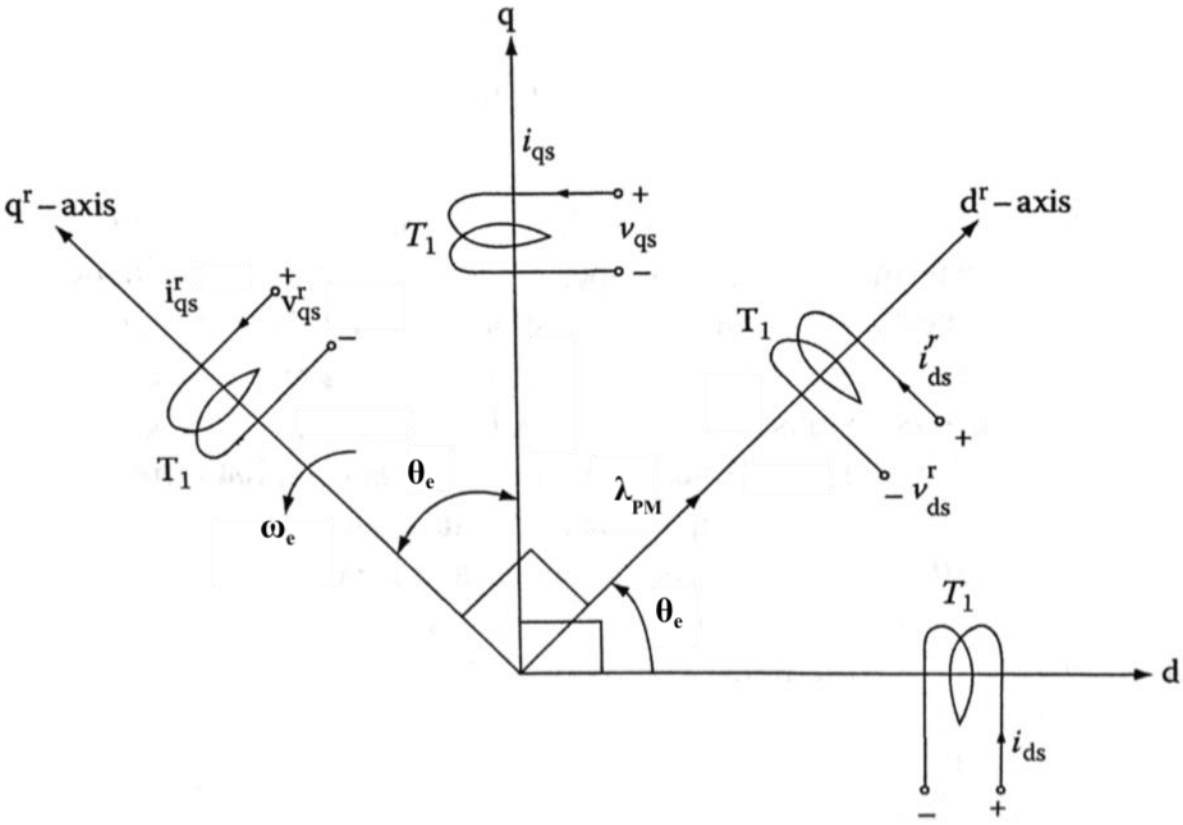

Figure 2.23: Stationary and rotor dq reference frames.[169]

The variables that appear in the equations are:

- λ_d, λ_q stator magnetic flux linkages in the rotor *dq* reference frame;
- λ_{PM} armature flux linkage due to rotor permanent magnets;
- i_d, i_q stator currents expressed in the rotor *dq* RF;
- v_d, v_q stator voltages expressed in the rotor *dq* RF;
- L_d, L_q direct and quadrature axes stator inductances in the rotor *dq* RF, with $L_q > L_q$;
- R_s stator resistance, because the windings are balanced and therefore the *d*-axis and the *q*-axis and so $R_s = R_{s,d} = R_{s,q}$;
- ω_e rotor electrical speed;

169 Krishnan, R. (2010), *op. cit.,* p. 232.

- ω_m rotor mechanical speed;
- pp number of pole pairs;
- T_{em} electromagnetic torque (motor torque), composed of a synchronous contribution $T_{em,syn}$ and a reluctance contribution $T_{em,rel}$ in a generic IPMSM;
- T_r resistance torque;
- J motor moment of inertia;
- k_T torque constant.

$$\begin{cases} \lambda_d = L_d i_d + \lambda_{PM} \\ \lambda_q = L_q i_q \end{cases}$$

consequently:[170]

$$\begin{cases} v_d = R_s i_d + \dfrac{d\lambda_d}{dt} - \omega_e \lambda_q = R_s i_d + L_d \dfrac{di_d}{dt} - \omega_e L_q i_q \\ v_q = R_s i_q + \dfrac{d\lambda_q}{dt} + \omega_e \lambda_d = R_s i_q + L_q \dfrac{di_q}{dt} + \omega_e L_d i_d + \omega_e \lambda_{PM} \end{cases}$$

The equation of the electromagnetic torque T_{em} can be obtained by equalizing the input electric power and the output mechanical power. In a generic interior magnet synchronous motor (where the saliency of the rotor can be exploited for generating additional torque) T_{em} contains a term that is related to q-axis current only – and it is called synchronous torque $T_{em,syn}$ – and another term $T_{em,rel}$ – reluctance torque – which depends on the difference between the equivalent d-axis and q-axis stator inductances. This reluctance torque is added to the other value in order to increase the torque and power density of these motors, with respect to surface-mounted PMSMs:[171]

$$T_{em} = \frac{3}{2} pp\ i_q \left[\lambda_{PM} + \left(L_d - L_q\right) i_d\right] = T_{em,syn} + T_{em,rel}$$

$$T_{em,syn} = \frac{3}{2}\ pp\ \lambda_{PM} i_q$$

$$T_{em,rel} = \frac{3}{2}\ pp\ \left(L_d - L_q\right)\ i_d i_q$$

while the mechanical dynamic equation for taking into account the delivered motor torque T_{em}, the moment of inertia J of the motor, the mechanical speed ω_m of the rotor and the resistance (or load) torque T_r and is:

170 Krishnan, R. (2010), *op. cit.,* p. 233.

171 *Ivi*, pp. 244-245.

$$T_{em} = T_r + J\dot{\omega}_m$$

typically, the load torque can be decomposed in a fixed contribution and a varying term[172] – which is proportional to the mechanical speed through an ideal constant factor called γ (a damping factor) in the LabVIEW project:

$$T_r = T_{r,const} + \gamma\omega_m$$

In FOC strategy, the motor is driven by voltages, while the stator currents are extrapolated from the PMSM in order to regulate the speed and the torque. Consequently, the equations have to be expressed highlighting the current contributions for computing i_q and i_d from the stator command voltages (expressed in the rotor *dq*-axes reference frame), as it happens in the LabVIEW project for the plant:

$$\begin{cases} i_d = \dfrac{1}{L_d}\displaystyle\int \left(v_d - R_s i_d + \omega_e L_q i_q\right) dt \\ i_q = \dfrac{1}{L_q}\displaystyle\int \left(v_q - R_s i_q - \omega_e L_d i_d - \omega_e \lambda_{PM}\right) dt \end{cases}$$

These quantities are then transformed into the three-phase measured current i_a, i_b, i_c and provided as output from the motor. At the same time, the mechanical speed is necessary to be obtained in the model, because with this value the electrical angular speed and the electrical angle can be obtained – and used in the Clarke-Park transformation and antitranformation blocks. For this purpose, the mechanical equation is integrated in order to obtain ω_m; by integration θ_m and consequent θ_e are computed:

$$\begin{cases} \omega_m = \dfrac{1}{J}\displaystyle\int (T_{em} - T_r)\, dt \\ \theta_m = \displaystyle\int \omega_m\, dt \\ \theta_e = pp\ \theta_m \end{cases}$$

In a SPMSM, the equivalent stator *d*-axis and *q*-axis reluctance are considered equal and constant. Consequently, the motor torque is expressed only as function of i_q, so the synchronous torque contributes singularly. This relationship depends on motor parameters (pp and λ_{PM}) and usually the torque constant k_T is used for linking torque and current:[173]

[172] Kulkarni, S. S., & Thosar, A. G. (2013, June), *Mathematical Modeling and Simulation of Permanent Magnet Synchronous Machine*, In *International Journal of Electronics and Electrical Engineering, 1*(2), p. 68.

[173] Krishnan, R. (2010), *op. cit.,* p. 282.

$$k_T = \frac{3}{2}\,\lambda_{PM}\,pp$$

$$T_{em} = T_{em,syn} = k_T\,i_q$$

Concerning the constant torque region, for realizing the MTPA condition, the reference stator direct contribution is kept null, because there is no anisotropy to be exploited. The quantity i_d is used only for the flux weakening area, where the magnetic flux produced by rotor PMs is weakened by this magnetizing *d*-axis current. As described before, the SPM structure has relatively small inductances and the speed cannot be increase too much over its rated value. In IPMSMs, the use both direct and quadrature contributions is fundamental for maximizing the delivered torque in MTPA area – the algorithm used to realize the optimization of the electromagnetic torque is described in chapter V. Then, the reluctance of this kind of motors is used for increasing the speed in the constant power region: the magnitude of i_d (which is always negative) is increased with respect to the quadrature one – producing a rotation of the current vector – for demagnetizing the PM flux in the machine. In FW condition, the torque is reduced in an inversely proportional way respect to the speed, for keeping constant the delivered power.

Chapter III:
Control applications for PMSMs

SUMMARY: 3.1 Inverter – 3.1.1 Voltage source and current source inverters – 3.1.2 Modulation strategies for three-phase inverters – 3.1.2.1 Six-step modulation – 3.1.2.2 Pulse-Width Modulation (PWM) – 3.1.2.3 Space Vector Pulse-Width Modulation (SVPWM) – 3.2 Scalar control (V/f) – 3.3 Vector control (Field-Oriented Control).

3.1 Inverter

An inverter is a semiconductor-based power converter, used for application where an alternating sinusoidal voltage – whose amplitude and frequency are controllable – is required; this device is mainly used for driving AC motors, as shown in figure 3.1. The inverter converts a direct voltage (and current) into an alternating voltage (and current), and for this reason it is called DC/AC converter. In general, the term inverter can be referred to the complete feeding scheme of an AC machine, including the AC/DC converter and the DC/AC inverter.[174] For conventional applications, the AC electricity is supplied at various frequencies and voltages. For efficiently driving a motor, the main supply is converted into the optimal frequency and voltage through the converters.

174 Mohan, N., Undeland, T., & Robbins, W. (2003), *Elettronica di Potenza. Convertitori e Applicazioni (Terza Edizione),* Milano, Italy: Hoepli, p. 223.

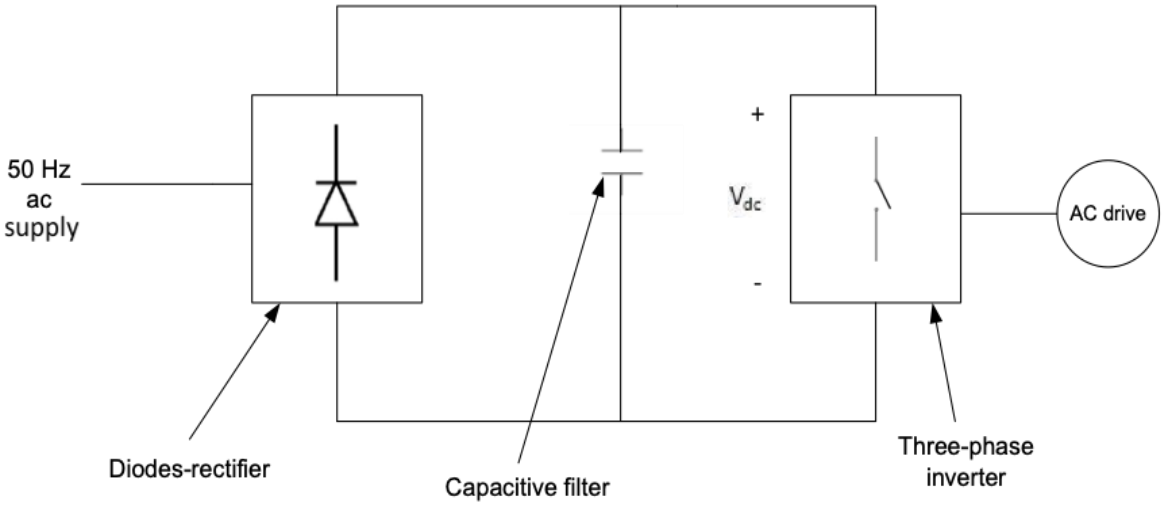

Figure 3.1: Feeding scheme for an AC motor, from the AC electric grid supply.[175]

The electrical grid supplies a nominally 230 V, 50 Hz AC voltage: in order to connect the inverter to a DC bus voltage, the AC/DC converter is inserted inside the chain. If a DC power supply is directly available, this conversion is no more necessary. A diodes rectifier (such as a Graetz bridge of figure 3.2) is adopted to rectify the sinusoidal wave, combined with a large-value capacitor – for voltage source inverters – that filters and eliminates the ripple. Obviously, some little oscillations remain in the output voltage, due to the discharging of the capacitor: the low pass filter behaviour of the driven motor will overcome this problem, reducing also the distortion caused by the high-frequency harmonics – this aspect is essential for modulation strategies. For hybrid-electric and electric automotive applications, the energy source – typically a battery in recent vehicles – acts as power supply for the system, providing the necessary DC voltage to the inverter. During the recharging phase, the battery pack is connected to the external electric grid through a charger system in case of plug-in cars: the charger acts as an AC/DC converter for using the AC external electric grid in order to feed the batteries. Alternatively, the regenerative braking is exploited for refilling the onboard energy source.

175 Mohan, N., Undeland, T., & Robbins, W. (2003), *op. cit.*, p. 224.

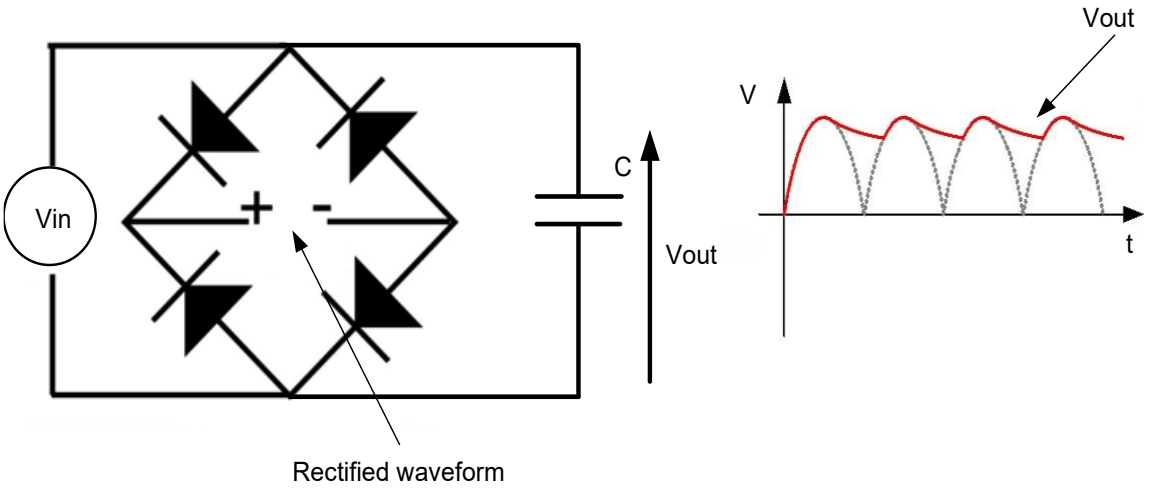

Figure 3.2: Graetz bridge configuration for rectifying the AC supply voltage.

For induction and synchronous machines control applications, a three-phase system is required for providing the desired three sinusoidal voltages v_a, v_b and v_c. Each waveform has a phase difference equal to 120 degrees with respect to the others. The three-phase inverters are composed of three legs – or branches – with two switches in each one; the upper and lower switches are turned on and off properly for modulating the output phase and concatenated voltages.[176] The need of an inverter for control applications is related to the motor velocity: for controlling the rotational speed of a three-phase AC machine, the following relation expresses the proportionality between frequency and motor speed and inverse proportionality between the latter and the number of pole pairs:[177]

$$n = \frac{60 \cdot f}{pp}$$

- n is the number of revolutions per minute (RPM), that represents the motor rotational velocity;
- f is the frequency of the voltage waveforms v_a, v_b and v_c;
- pp is the number of pole pairs of the motor.

[176] Mohan, N., Undeland, T., & Robbins, W. (2003), *op. cit.*, p. 253.

[177] Toshiba Electronic Devices & Storage Corporation (2018), Retrieved from *DC-AC Inverter Circuit*: https://toshiba.semicon-storage.com/info/docget.jsp?did=61546&prodName=GT30J341, p. 4.

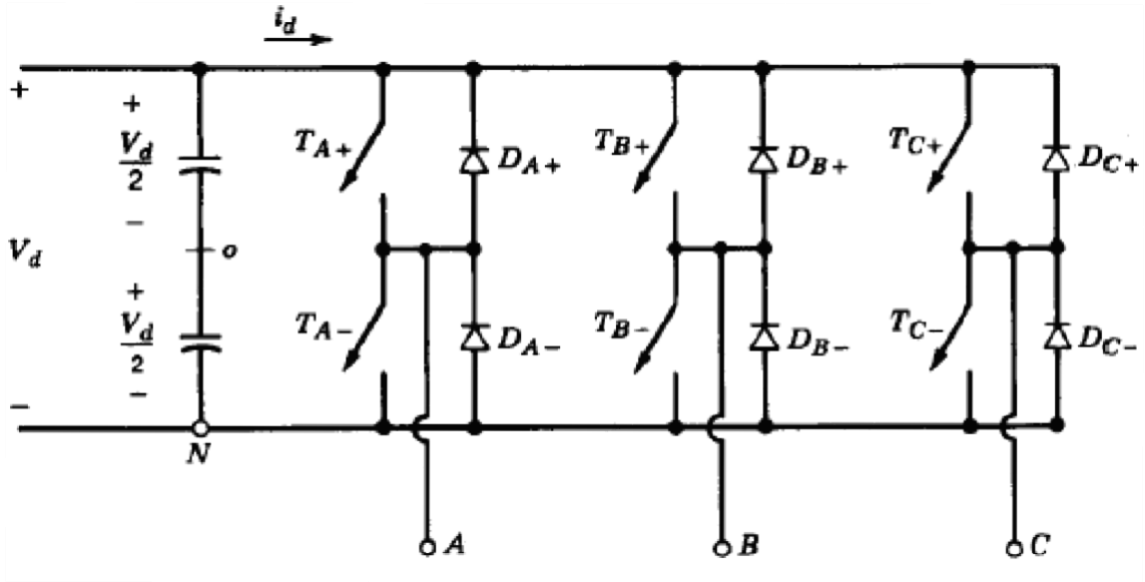

Figure 3.3: Three-phase inverter.[178]

3.1.1 Voltage source and current source inverters

Voltage source inverters (VSIs) – or, alternatively, voltage fed inverters – control the output voltage and require a constant DC bus voltage. A large-value capacitor is placed in parallel on the input DC line of the inverter. In case of low impedance load, series reactors are needed for each phase; for AC machine applications the leakage reactance of the motor acts as reactor. As switches, reverse-conducting semiconductor are used;[179] in this configuration, the diodes are connected in parallel to the switches.

In current source inverters (CSIs) – called also current fed inverters – a large-value inductor is placed in the input DC line of the inverter in series and the input current is kept constant. In this configuration, the inverter works as a current source and the output current is independent of load – while the output voltage depends on it. Moreover, the commutation circuit is simple because it contains only capacitors, useful for reducing the motor ripple current;[180] CSI doesn't require any feedback diode. On the other hand, BJT, MOSFET and IGBT can be used only for voltage source inverters, because these devices don't require any reverse-blocking diodes. Reverse-blocking devices such as thyristors are required as

178 Mohan, N., Undeland, T., & Robbins, W. (2003), *op. cit.,* p. 254.

179 Toshiba Electronic Devices & Storage Corporation (2018), *op. cit.*, p. 6.

180 *Ibidem*.

switching devices for CSI, because they must withstand large reverse voltages; in case of IGBTs and so on, series diodes are needed in each branch of current fed inverters.

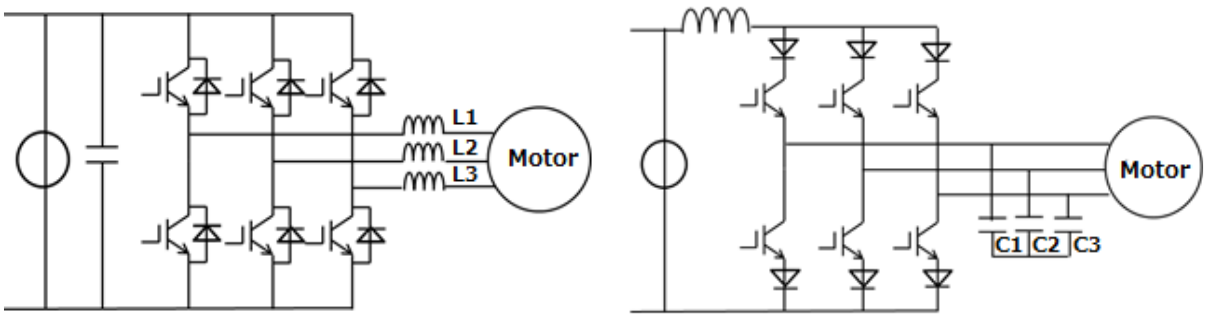

Figure 3.4: Voltage source inverter on the left, current source configuration on the right.[181]

Voltage fed type are the most adopted solution for all home appliance and industrial power applications, thanks to their reduced voltage drop, faster response to system dynamics and easier controllability. In fact, it is easier to obtain a regulated voltage than a regulated current. Generally, a CSI is preferred only where there is a changing input DC voltage source; in some applications like high-voltage direct current transmission – where a DC current travels a long distance – the current fed type inverter is still used. Furthermore, VSI structure is more compact because the reactor is not needed on the DC side. Concerning the modulation strategies, the pulse-width modulation is more efficient and easier to be applied to a VSI. For this reason, in next paragraphs the methods for controlling only voltage source inverters are described.

3.1.2 Modulation strategies for three-phase inverters

In a voltage source three-phase inverter, the six switches are controlled to provide the desired output voltage; in fact, the inverter is commanded in order to regulate magnitude, phase and frequency of the resultant waveforms.[182] There are various types of inverter systems which adopt different control, commutation and modulation methods. Depending on the required efficiency level and also on the characteristics of the motor, different strategies are adopted. The output of each branch of the inverter is related to the DC bus voltage and the status of the switches; the voltage doesn't depend on the load current because

[181] Toshiba Electronic Devices & Storage Corporation (2018), *op. cit.*, p. 6.

[182] Krishnan, R. (2010), *op. cit.*, pp. 162-163.

the switches are never all opened at the same instant. As simplification, these components are assumed to be ideal, without considering losses or voltage drops. The three most adopted techniques are described in this chapter: six-step modulation, pulse-width modulation and space vector pulse-width modulation.

3.1.2.1 Six-step modulation

The six-step modulation strategy is the simplest one, but obviously this method is used for applications that don't require high efficiency and precision; it usually causes a huge acoustic noise. For the three-phase inverter – composed of six switching devices – the idea is to connect each command voltage to the power source V_{DC} for 180 electrical degrees by closing the upper switch (S_1 for command A of figure 3.5) and opening the lower corresponding switch (S_4 for A). Then the command is inverted for other 180 electrical degrees (S_1 open and S_4 closed for A). It is necessary to insert a delay of at least 1 µs between the commutations of the switches in the same leg to avoid the hazardous short-circuit situation. At any time, the electric current is conducted through two resistive components, because two command voltages are active.

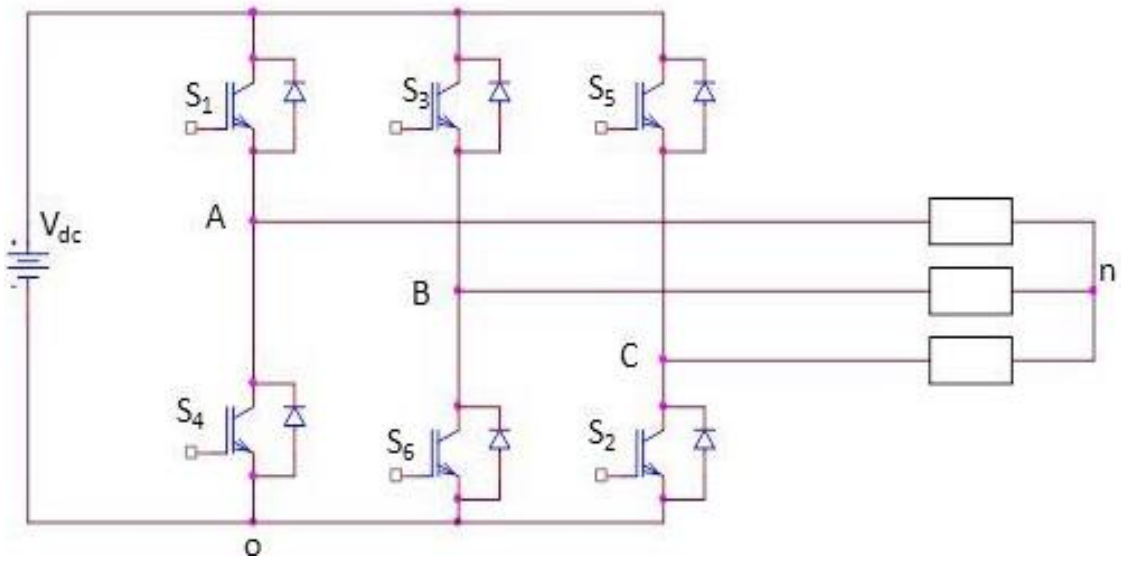

Figure 3.5: Three-phase inverter connected to the load (AC motor), used for six-step modulation.

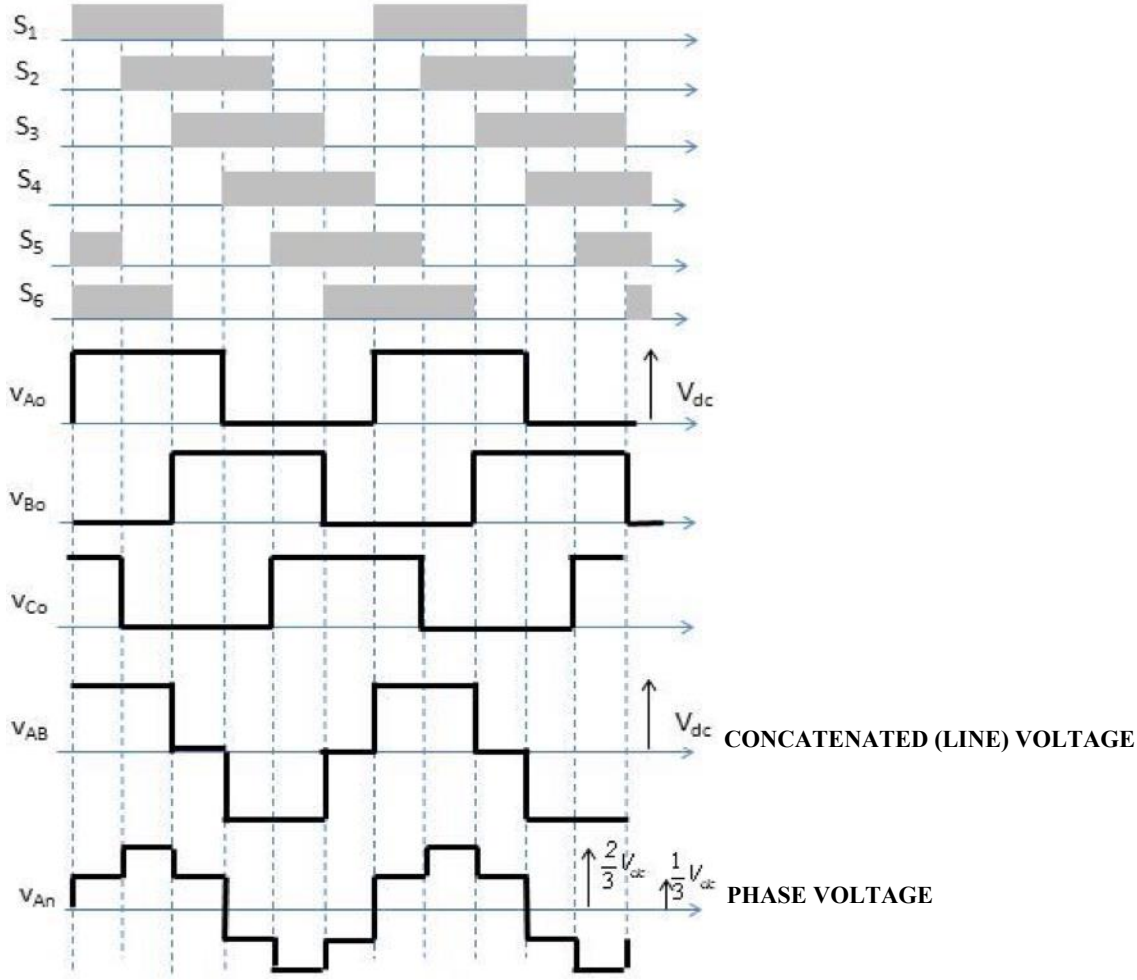

Figure 3.6: Six-step modulation switching strategy and output phase and line voltages.

In this way – considering that each command (A, B, C) is shifted of 120° with respect to the others for realizing a three-phase system – the concatenated voltages can be approximated as alternating waves for driving the electric motor. Moreover, the phase voltages on the load present a six-step behaviour, as shown in fig. 3.6 – the strategy is called six-step for this reason. From the inverter, a sinusoidal output is not directly available: a Fourier series is used for obtaining the first harmonic and the superior harmonics. The fundamental of the series related to the resultant waveform is sinusoidal and its contribution is the largest one for motor control; the low pass filter behaviour of the driven machine is able to reduce the distortion due to higher frequencies disturbances only, but with this method the other harmonics are not deleted or moved. Consequently, the ripple due to harmonics at relatively low frequencies is not negligible for current and torque waveforms – causing noise and reducing the efficiency.

The amplitude of the produced voltage by the inverter is depending on the DC bus voltage. The main problem of this strategy is that the frequency of the output wave can be changed, but its magnitude depends on V_{DC}. According to the theory of scalar control (paragraph 3.2) applied to induction and synchronous machines, if the frequency varies, also the DC voltage must be changed in order to have the same flux. In fact, these two quantities are proportional in the constant torque region, as represented in the following figure 3.14 referred to V/f regulation strategy. For managing the frequency, the DC/AC inverter is the dedicated device; for the V_{DC} variation, the AC/DC power converter is inserted in the system.

3.1.2.2 Pulse-Width Modulation (PWM)

The pulse-width modulation is the most adopted technique for driving a voltage source inverter. It is superior with respect to six-step commutation in terms of precision, efficiency and acoustic noise rejection: the superior harmonics are moved to higher frequency thank to this modulation, so the motor can easily filter them. On the other hand, it requires an increase of hardware and software complexity and extra costs, but the continuous technological evolution has boosted the diffusion of PWM method for all the industrial – and in particular automotive – applications. The principle is to use three control signals and compare them at each instant with a carrier triangular wave with a frequency at least 10 times greater. The control inputs – called reference or modulating signals – are sinusoidal waves out of phase of 120° with respect to each other: if the instantaneous value of the carrier wave is less than that of the sine wave, the PWM output signal is in high level; if the carrier is higher than the modulating wave, the PWM output is in low level.[183]

From this comparison between each command voltage and the carrier triangular wave, different duty cycles are obtained for phase *a*, *b* and *c*. «Sinusoidal PWM techniques are characterized by constant amplitude pulses with different duty cycles for each period. The widths of these pulses are modulated to obtain inverter output voltage control and to reduce its harmonic content».[184] The phase *a* generates a duty cycle coming from the reference signal *a* and this will drive the upper switch of the first leg, called S_1 in previous

[183] Bird, B., King, K., & Pedder, D. (1993), *An Introduction to Power Electronics (Second Edition).* Chichester, West Sussex, United Kingdom: Wiley.

[184] Raju, N., Islam, M., & Uddin, A. (2013, January), *Sinusoidal PWM Signal Generation Technique for Three Phase Voltage Source Inverter with Analog Circuit & Simulation of PWM Inverter for Standalone Load & Micro-grid System*, In *International Journal of Renewable Energy Research, 3*(3), p. 649.

figure 3.5; the corresponding negated signal will drive the lower switch, called S_4. Again, a small delay must be introduced between the commutations to avoid short-circuit situations – two switches of the same branch cannot be switched off simultaneously.

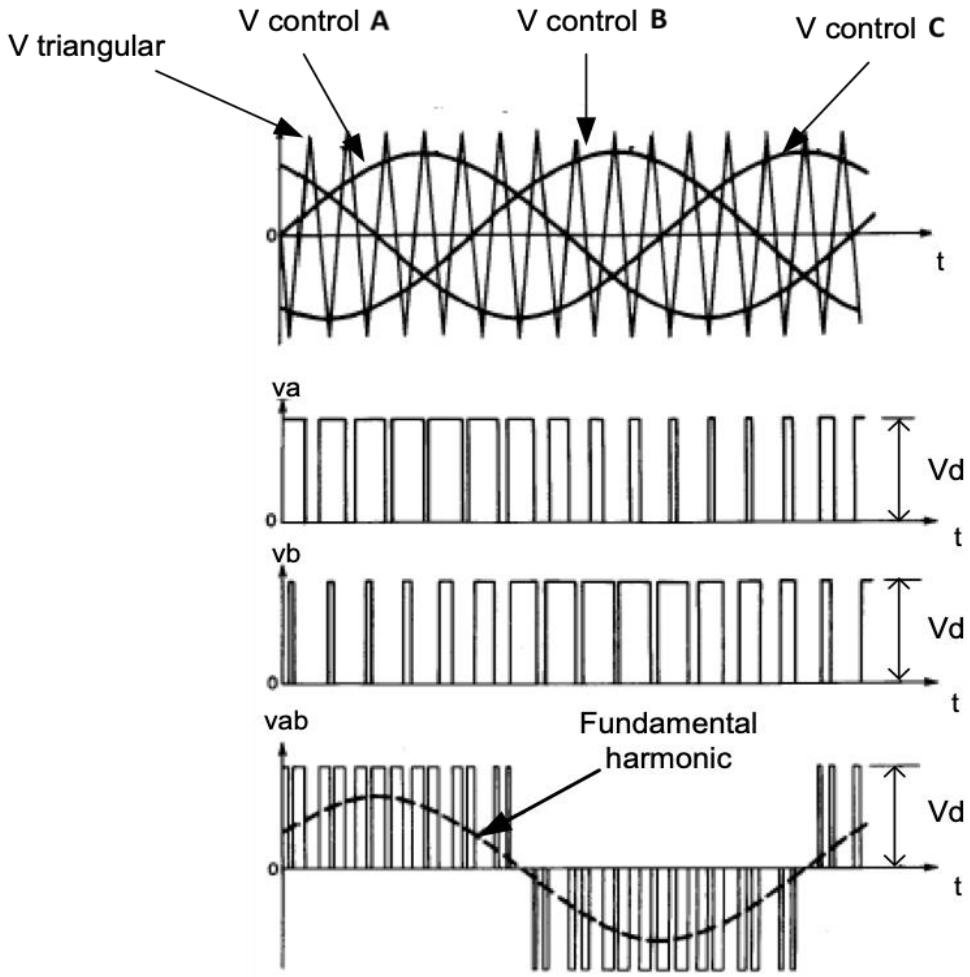

Figure 3.7: Pulse-width modulation command waveforms (modulating sine waves and triangular carrier) and output voltage signals.[185]

The desired sinusoidal concatenated voltage output is given by the fundamental harmonic (fig. 3.7) of the PWM output signal and it has the same frequency of the modulating signals; in this way by choosing the desired value for the sinusoidal references, the resulting output will have that imposed frequency. The superior harmonics are shifted to frequencies that are multiple of the one of the carrier signal: considering the fact that the triangular wave has a frequency at least 10 times greater than that of command sinusoidal waves, the distortion caused by higher harmonics is reduced because the motor easily filters

[185] Mohan, N., Undeland, T., & Robbins, W. (2003), *op. cit.*, p. 255.

the high frequency components – consequently the torque and current ripples are reduced. An important parameter for this technique is the modulation index m:

$$m = \frac{V_m}{V_c}$$

where V_m is the peak value of the modulating signal and V_c is the peak value of the carrier signal. By changing m, it is possible to modify the amplitude of the fundamental harmonic of the PWM output signal – without considering the DC bus voltage – in order to obtain the desired amplitude value for driving the motor.[186] In fact, another important advantage of the pulse-width modulation is the possibility of leaving always the V_{DC} constant: there is no need of varying the DC bus voltage of the inverter for modulating the sinusoidal output voltage.

An example of PWM algorithm implementation on LabVIEW is reported here: the modulating 5 Hz sinusoidal signals are three-phase voltages – with a difference of 120° with respect to each other – while the carrier signal is a 1 kHz sawtooth wave – its frequency is the same of the timed loop. By using the sawtooth instead of the triangular carrier, the results are not compromised. The amplitude is equal to 100 V for all the waveforms, so the modulation ratio is unitary. The switching mechanism is obtained through the comparison between the modulating waves and the carrier: if the sawtooth wave is less than the sine, the corresponding switch is on (high level); if the sawtooth wave is higher than the sine, the corresponding switch is off (low level). In this way, different duty cycles are generated for the three switches. Then, for reconstructing the first fundamental the low pass filter of the motor is simulated, using a simple RC structure. Knowing that the frequency of the fundamental is the same of the modulating, while the other harmonics are shifted at multiple frequencies of the carrier, a cut frequency equal to 7 Hz is used for the filter. In order to realize it the following values are chosen:

$$f_{cut} = \frac{1}{2\pi RC} = 7 \text{ Hz}$$

$$C = 1\ \mu F$$

$$R = \frac{1}{2\pi f_{cut} C} = 22.736 \text{ k}\Omega$$

[186] Nagarajan, R., *et al*. (2016, September), *Implementation of SPWM Technique for Inverter*, In *International Journal of Advanced Research in Biology, Engineering, Science and Technology (IJARBEST), 2*(9), p. 11.

For the simulation, a discrete time interval equal to 1 ms is considered, and the analysis lasts 3000 ms. As shown in figure 3.10, the resultant waveform V_a (such as V_b and V_c) is in delay with respect the modulating wave and it is affected by ripple: this degrading effect can be reduced by increasing the carrier frequency, by making a more accurate filter or by using the space vector approach. The used waves (modulating and carrier) are only positive; for a more generic situation, an offset can be inserted for equalizing to zero the mean value of the waveforms. Moreover, the negate waves – for the lower switches in the three legs of the inverter – are not considered in this example.

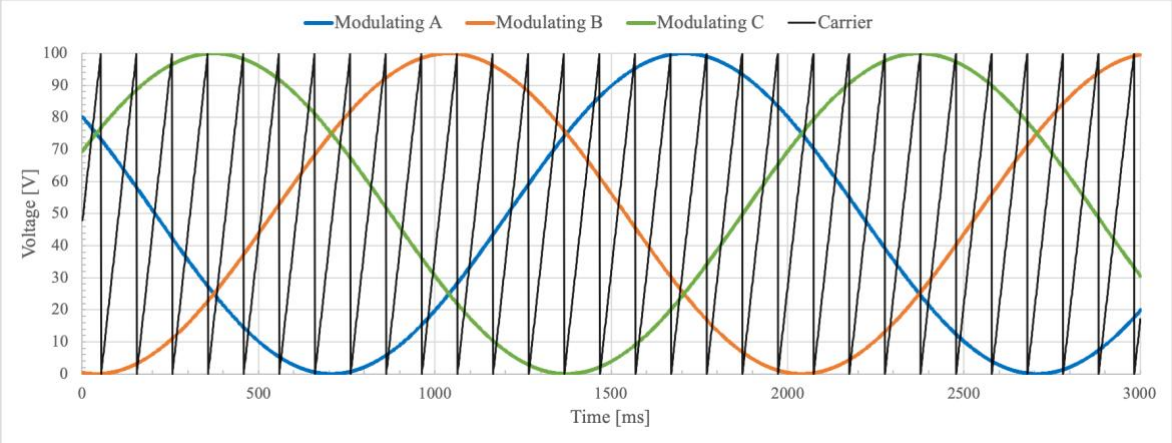

Figure 3.8: PWM three-phase modulating waves and carrier sawtooth wave.

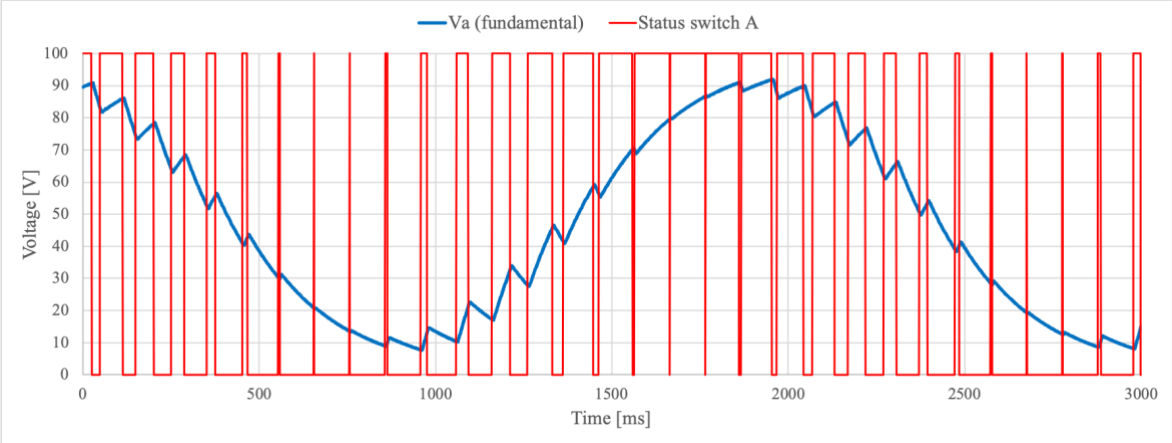

Figure 3.9: Duty cycle of switch A, with the resultant voltage waveform V_a.

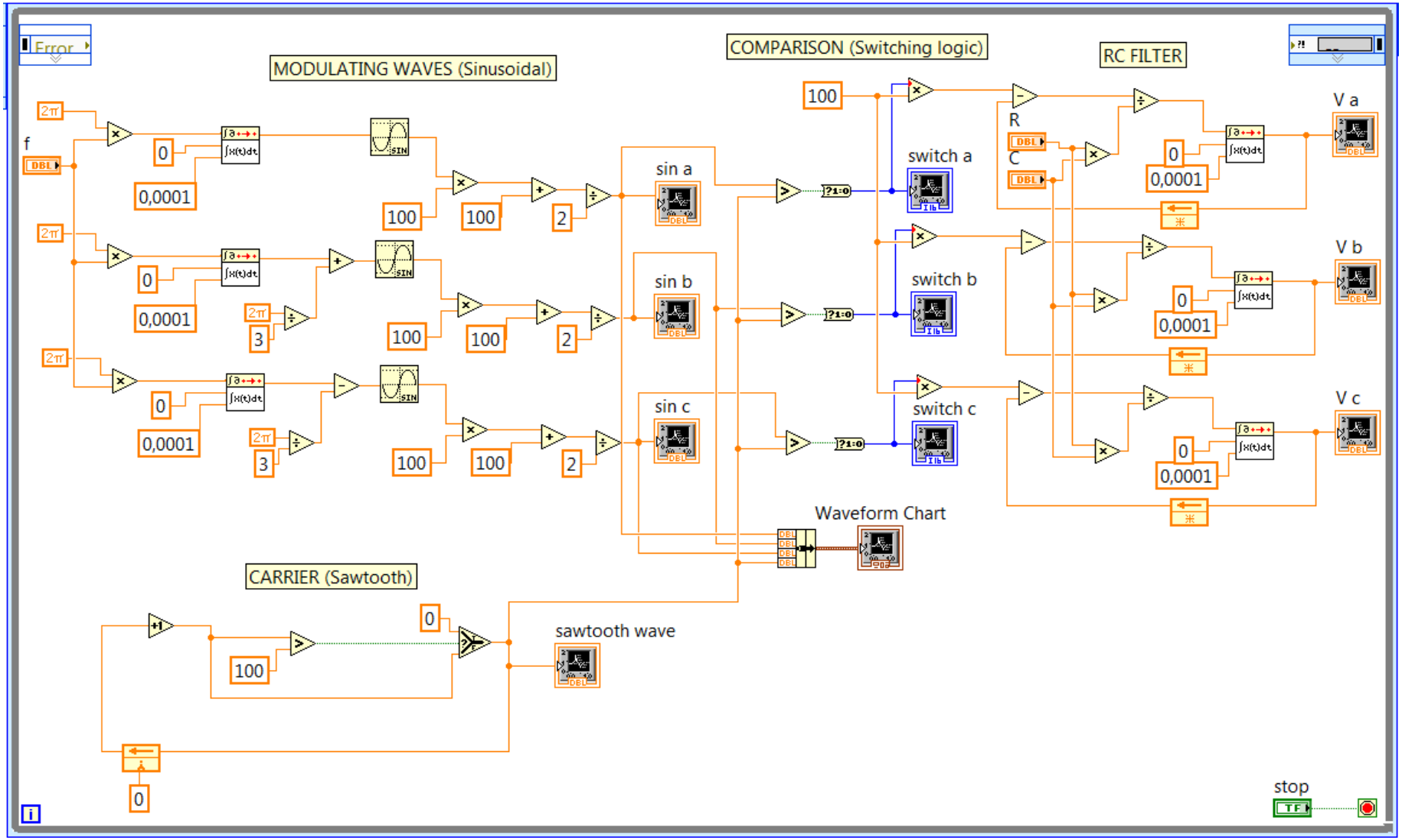

Figure 3.10: PWM implementation in LabVIEW.

3.1.2.3 Space Vector Pulse-Width Modulation (SVPWM)

Space vector pulse-width modulation is an advanced control algorithm, applied to induction motors and PMSMs where the field-oriented control technique is typically adopted. SVPWM is used as final step of FOC, for modulating the inverter output waveforms.[187] For this strategy, the basic elements are the voltages in the $\alpha\beta$ plane, obtained through the Park inverse transform from v_d and v_q or from v_a, v_b and v_c using Clarke transformation (three-phase to two-phase). Voltage is delivered to the motor by the three-phase inverter with six transistors; each of the three outputs can have the top transistor closed and the bottom one open, or vice versa. The total number of possible states is eight.

A single output configuration is called base vector and the union of all of them composes a hexagonal star diagram. Each vector (from V_0 to V_7) is a spoke of the star in $\alpha\beta$ plane, with 60° of phase difference between adjacent vectors. The two vectors V_0 and V_7 are plotted at the centre of the star as null vectors, and they contain output values that are either all plus or all minus. The three-phase inverter may supply a maximum amplitude equal to $\frac{V_{DC}}{2}$ from the DC source, so using the transformation from three-phase to two-phase the base vectors have a magnitude equal to $\frac{2V_{DC}}{3}$ in the $\alpha\beta$ reference plane.[188]

The SV-based modulation is a digital technique in which the objective is to generate PWM load line voltages that are on average equal to given line voltages: in other words, the desired voltage vector V_{OUT} is obtained by producing – during the PWM period T_{PWM} – a mean vector equal to the desired one. The vector V_{OUT} lays in a sector limited by two base vectors: these two constraint vectors, together with one of the null vectors, are used for obtaining the desired voltage. Considering the following example, for a specified time T_1 the V_1 is applied, then for another specified time T_3 the V_3 is applied to provide the required V_{OUT}; during the remaining time $T_{PWM} - T_1 - T_3$ one of the two null vectors V_0 or V_7 is applied:

$$V_{OUT} = \frac{V_1 T_1 + V_3 T_3}{T_{PWM}}$$

[187] Kumar, K., Michael, P., John, J., & Kumar, S. (2010, July), *Simulation and comparison of SPWM and SVPWM control for three phase inverter*, In *ARPN Journal of Engineering and Applied Sciences, 5*(7), p. 62.

[188] Prasad, E., Suresh, B., & Raghuveer, K. (2012), *Field Oriented Control of PMSM Using SVPWM Technique*, In *Global Journal of Advanced Engineering Technologies, 1*(2), p. 41.

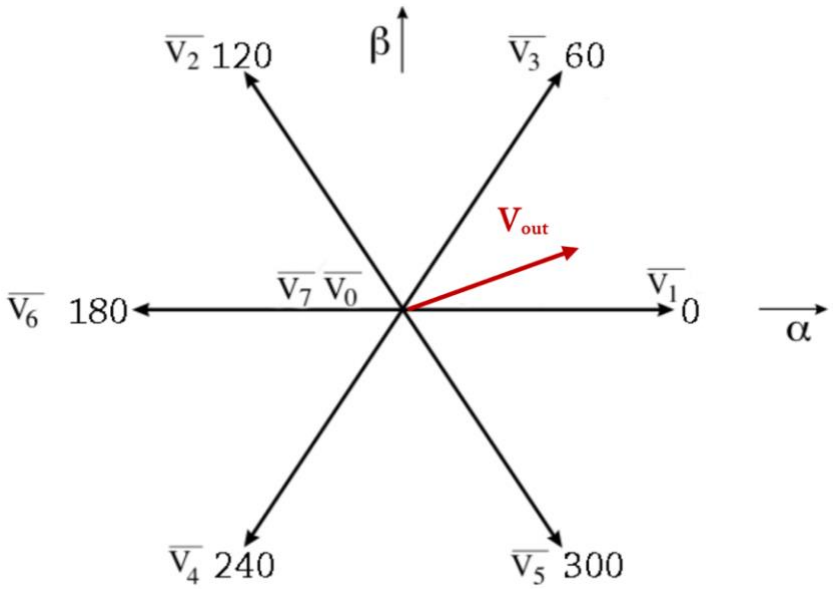

Figure 3.11: Hexagonal star diagram of the base and null vectors, with the desired output voltage vector.

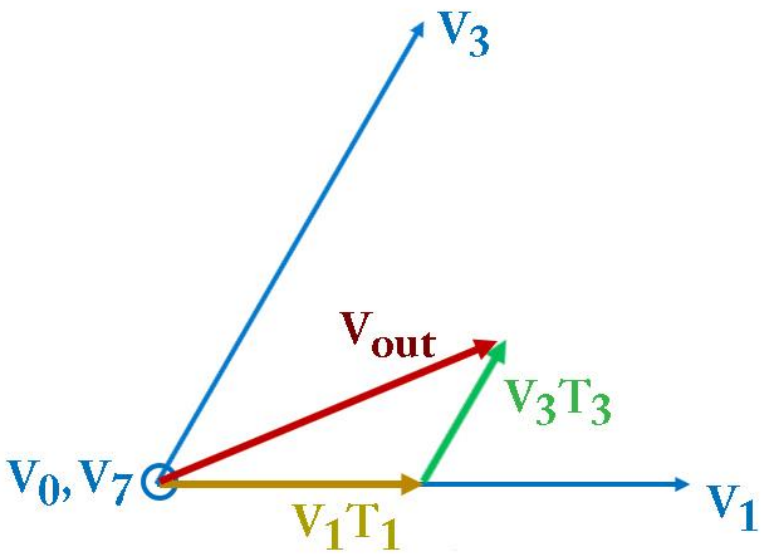

Figure 3.12: Space vector pulse-width modulation strategy for obtaining the desired output vector V_{OUT} during the PWM period, using V_1 and V_3.

The main advantages of space vector PWM are the increase of efficiency of the DC bus voltage use, the limitation of harmonic distortion with respect to standard PWM, the improvement of power factor and the reduction of torque ripple. The switches commutation is done taking into account the minimum losses: the more is the modulation frequency, the less will be the ripple. Consequently, this technique is becoming the most popular and

important modulation strategy for three phase voltage source inverters for the control of AC induction, brushless DC, switched reluctance and permanent magnet synchronous motors.[189]

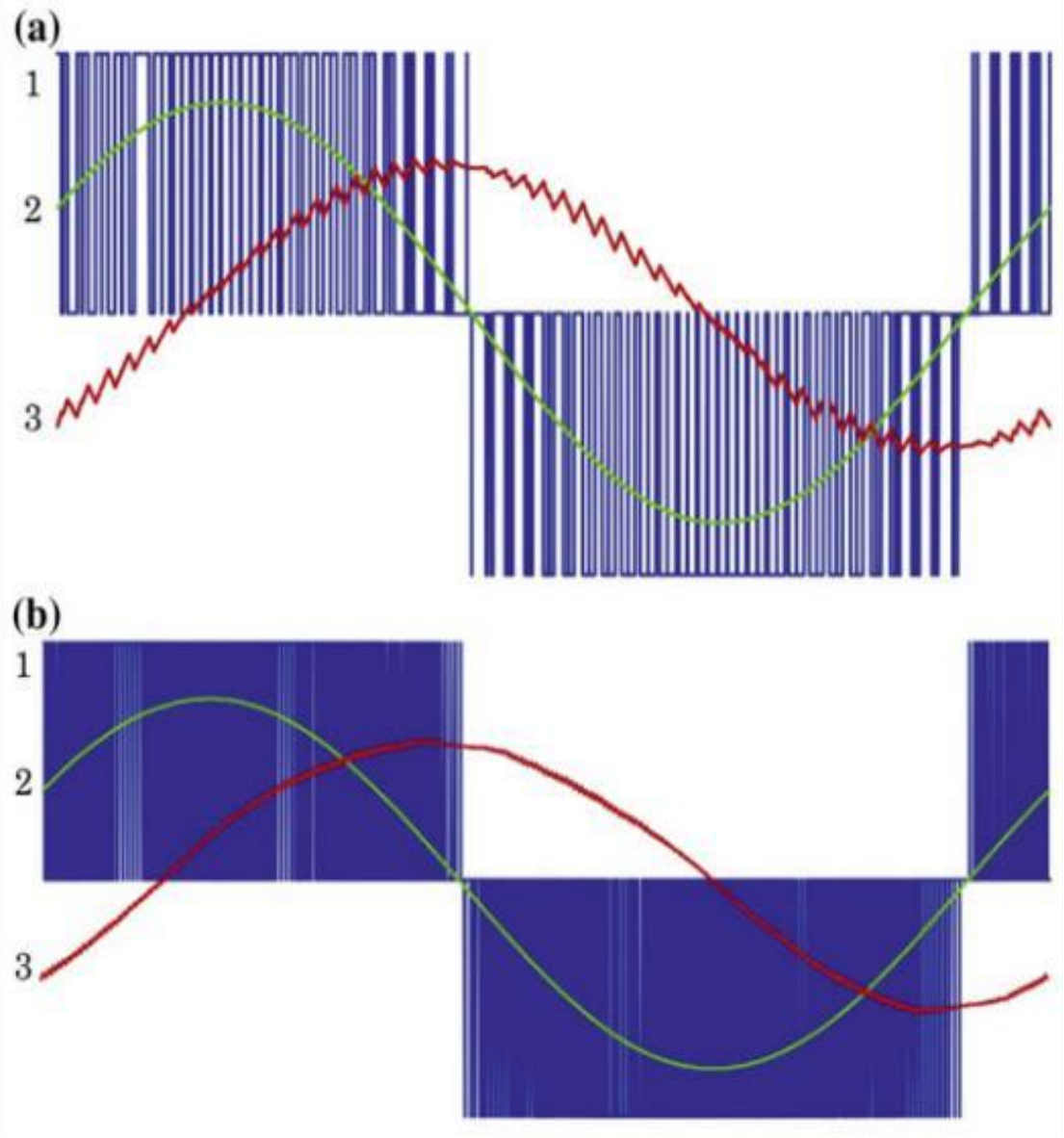

Figure 3.13: SVPWM output waveforms: 1 is the inverter output voltage, 2 is the fundamental harmonic, 3 is the current wave. In (b) a higher commutation frequency is used, reducing the ripple with respect to the other case (a).

[189] Kumar, K., Michael, P., John, J., & Kumar, S. (2010, July), *Simulation and comparison of SPWM and SVPWM control for three phase inverter*, In *ARPN Journal of Engineering and Applied Sciences, 5*(7), p. 74.

3.2 Scalar control (V/f)

Many typical applications require the motor speed to be changed, while the torque has to remain constant. The velocity of an AC motor can be changed in different ways: changing the number of pole pairs, varying the magnitude of the supplying voltage or varying the frequency of the same voltage. Depending on the electric machine, different control strategies can be applied.[190] Typically, constant volts-per-Hertz control in open loop is used for induction motor applications with squirrel cage rotor. In this paragraph, the scalar control of a permanent magnet synchronous motor is analysed, according to the principal argument of the thesis.

In various industrial application the scalar control strategy, called also constant voltage/frequency control or constant volts-per-Hertz control, is used for variable speed AC drives, where is no need for high dynamical performance; generally, this control can be applied is reduced speed-range application. This method is the simplest one to control a PMSM and it is realized by varying only magnitudes: the relationship between voltage (or current) and frequency is kept constant within the motor speed range.[191] There is no control over angles in this strategy for driving the motor. The required computational power of the hardware is low if compared to vector control, and its simplicity is the major advantage. Moreover, this technique offers benefits in terms of sensorless control, because the loop remains open and there is no feedback of the actual values of current or voltage. In the following figure 3.14 the structure of the scalar control is represented; the principal blocks are:

1. the first block is used for passing from the desired speed – so from the desired frequency – to the desired voltage magnitude, using the constant factor between ω_e and $|V_s|$. It is possible to notice that the ratio between these two variables is constant only in the constant torque region; then, the magnitude of the voltage remains equal to the rated value in the constant power region. Consequently, for this reason the operating range of the scalar regulation is restricted;
2. the integrator for computing the reference electrical angle from the reference electrical speed;

190 Kohlrusz, G., & Fodor, D. (2011), *Comparison of scalar and vector control strategies of induction motors*, In *Hungarian journal of industrial chemistry Veszprém, 39(2),* p. 265.

191 Parmar, Y., *et al*. (2016, December), *Scalar control of Permanent Magnet Synchronous motor*, In *International Research Journal of Engineering and Technology (IRJET), 3*(12), p. 364.

3. the conversion block for calculating the three-phase reference v^*_{abc} from the desired magnitude of the voltage and the reference electrical angular position;
4. the inverter for driving the motor;
5. the permanent magnet synchronous motor.

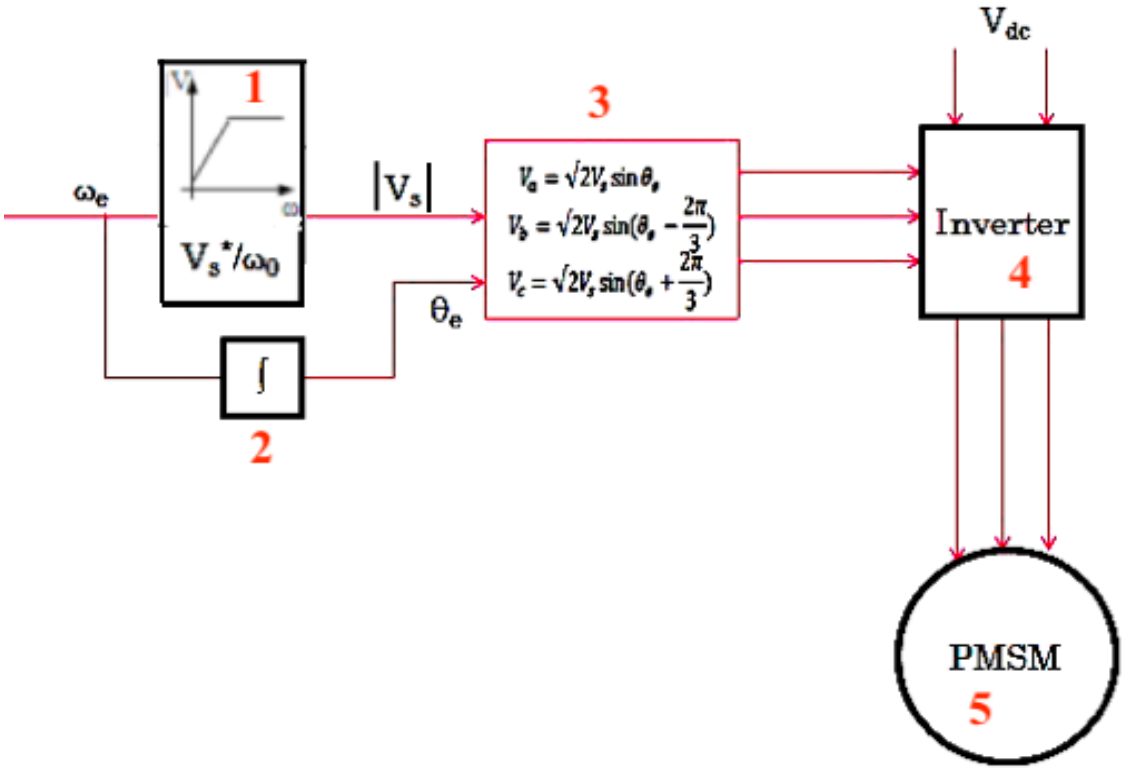

Figure 3.14: Scalar control open loop scheme for a PMSM.[192]

On the other side, the principal disadvantages are related to the instability and the dependence on motor parameters and on load. After exceeding a certain frequency range, the control stops to work properly; to overcome the problem, the rotor must be constructed with damper windings – with magnets located on the inside of the damper bars – for always guaranteeing the synchronization of the rotor to the electrical frequency. The major part of permanent magnet synchronous machine is not built with damper windings, limiting the choice of suitable motors for traditional scalar control. The lack of feedback obviously is a substantial drawback for the dynamic performance range, limiting the safe applications of this method.

For obtaining more information in order to increase the accuracy of voltage/frequency control, the angular speed can be estimated indirectly from the frequency of the motor supplying voltage. As improvement to guarantee the synchronization between

[192] Parmar, Y., *et al*. (2016, December), *op. cit.,* p. 364.

rotor and field, the rotor position can be used in feedback loop. Substantially, the method is based on keeping the stator flux constant at the nominal value for developing the rated torque/ampere ratio over entire speed range. For rising the amplitude of the fundamental voltage, a sinusoidal voltage PWM algorithm is implemented.[193] The possibility of controlling only the magnitudes and not the angles, combined with the poor dynamic performance and high overshoot, limits the possible applications of this algorithm. For the previous reasons, the vector control is a more efficient and more performing solution for regulating the behaviour of permanent magnet synchronous motors.

3.3 Vector control (Field-Oriented Control)

Vector control strategy can be applied to induction and synchronous machine: in this section, the field-oriented control related to a PMSM is analysed. In the final chapter, the implementation of this technique and the obtained results will be described, for evaluating the performance of both surface-mounted and interior permanent magnet synchronous motors. The previously analysed dynamic equations of this kind of motor are useful for implementing the FOC algorithm: thanks to the possibility of mathematically decoupling the stator current along *d* and *q* axes, the motor torque can be directly controlled.

This strategy is based on the control principle of a separate excitation DC motor; in that case, the armature current directly control the torque, while the excitation current is responsible for the magnetizing flux generation. For that kind of DC motor, the two currents are independently accessible and the armature magnetomotive force is orthogonal with respect to rotor flux, through mechanical commutation system such as brushes and commutators.[194] In case of AC motors (synchronous or induction), the spatial angle between rotating stator field and rotor flux changes depending on the load characteristics. Field-oriented control emulates the DC conditions in AC motor structure, by monitoring the rotor field position and orienting the stator field so that the angle between both fields is maintained at 90 degrees.[195] Consequently, the maximum torque condition can be achieved, and the rotor speed can be controlled independently.

193 Parmar, Y., *et al*. (2016, December), *op. cit.,* p. 365.

194 Wei, L. (2017*), op. cit.,* p. 160.

195 Amin, F., *et al*. (2017, May), *op. cit.,* p. 387.

FOC requires a position sensor, such as a Hall effect sensor, for constantly monitoring the rotor position, in order to use this value for decoupling the stator current in i_d and i_q. The Hall effect sensor is a device that measures the magnitude of a magnetic field: the output voltage is directly proportional to the magnetic field density around the sensor. This device is made with a thin piece of semiconductor material passing a continuous current through itself; the external magnetic flux exerts a force on this material, deflecting the charge carriers (electrons and holes) to either side of the slab. As a consequence, a measurable voltage is generated.

Alternatively, an encoder can be used for analysing directly the rotor angular position or for obtaining it by integration of the measured angular velocity – the actual rotor speed is measured also for realizing the speed control loop, instead of the torque-based one. Encoders are useful device for measuring angular and linear velocity, through the relationship between the encoder's pulse frequency and its rotational speed. The incremental encoder is able to report immediate changes in position: it uses two output square waves in quadrature A-B and – depending on the phase difference between them – it can determine the direction of rotation. The frequency of the two pulses A or B is directly proportional to the encoder's – and consequently the motor's – velocity. As drawback, the incremental encoder doesn't keep track of the absolute position when the mechanism starts: for a correct measurement, this type of encoder must be moved to a reference fixed point to align it with the magnetic field generated by the permanent magnets present in the rotor.

The absolute encoder is a device that doesn't require any initialization because it maintains position information when power is removed from the system. During the assembly phase, the relationship between the encoder value and the corresponding physical position is established: the multiple rings of the device represent various binary weightings and the combination of them provide the binary data that represents an absolute position. By increasing the number of rings, the accuracy of the measurement can be improved. Moreover, the speed can be obtained by counting the number of complete revolutions.

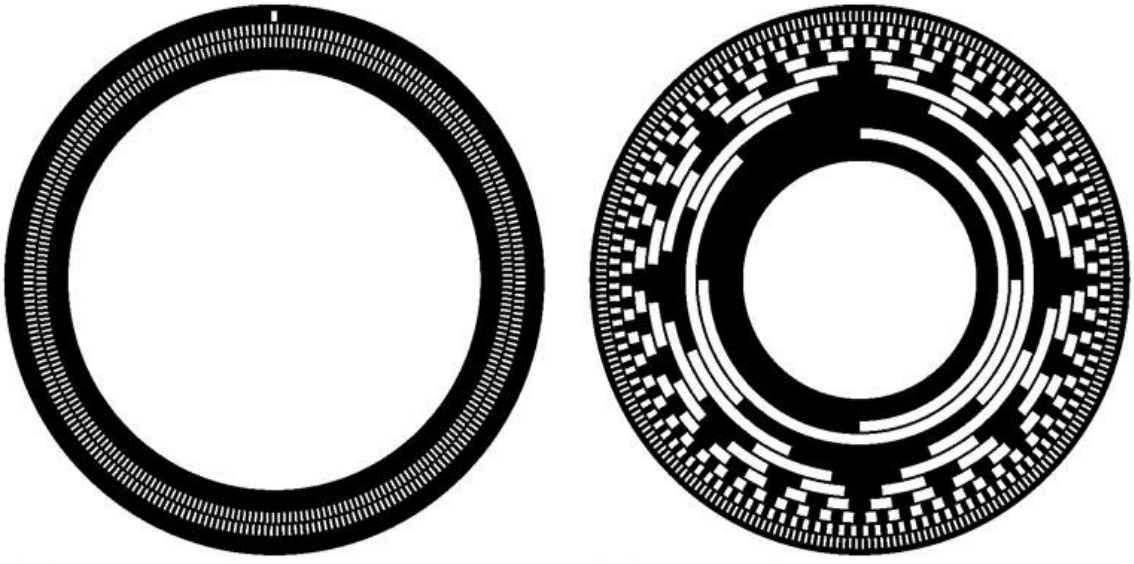

Figure 3.15: Incremental encoder on the left, absolute encoder on the right.

As practical example, the speed-loop FOC structure of a surface-mounted PMSM is shown in figure 3.16. This scheme doesn't include blocks that are essential for a real-time application of the system, such as the saturations, the proportional integral (PI) controller for managing the battery pack and inverter DC and the PI for regulating the direct current in the constant power region – flux weakening area. In chapter V, the effective block schemes are provided, together with the obtained output results for both IPM and SPM synchronous motors; in that case, all the previous elements are inserted for realizing a more accurate and more reliable vector control implementation. In figure 3.16 the represented elements are:

1. the SPMSM;
2. the inverter for driving the motor;
3. a sensor for measuring the actual rotor mechanical angular position $\theta_r = \theta_m$ and a derivative block for obtaining the actual angular speed ω_r. The electrical angle θ_e is obtained from θ_r by multiplying it for the number of pole pairs pp;
4. the Clarke-Park transformations for computing the direct-quadrature stator current from the three-phase current in *abc* reference frame. For this mathematical block, the measurement of the actual electric angle is needed – the value θ_e is obtained from θ_r. Thanks to this decoupling action, the feedback stator currents i_d and i_q are controlled as DC quantities and are compared with the reference values i_d^* and i_d^* through subtractors;
5. the PI regulator is used for obtaining the reference quadrature stator current i_q^* from the rotor speed error. Alternatively, from the speed error the reference motor torque

T^* can be obtained and then this value is converted into i_q^*. As described in previous chapter, a SPM synchronous machine, there is a proportional dependence between torque and quadrature current in the constant torque region, through the torque constant k_T;

6. the reference direct stator current i_d^* is always equal to zero in this simple example, because the flux-weakening region is not considered for extending the range of rotor speed values;
7. the PI controllers are used for estimating the reference *dq* voltage values from the direct and quadrature current errors;
8. the Clarke-Park inverse transform blocks are then used for computing the three-phase reference voltage v_{abc}^* from the direct-quadrature values v_d^* and v_q^*;
9. finally, a PWM (or alternatively a SVPWM) technique is implemented based on the three-phase reference voltages, and the outputs of this block are sent to the inverter.

As simplification for the vector control used for the thesis project, the three-phase reference waveforms v_a^*, v_b^* and v_c^* are used for directly driving the synchronous motor, without inserting the inverter. In fact, within the LabVIEW development environment ideal configurations are considered for the PMSM and the applied control strategy.

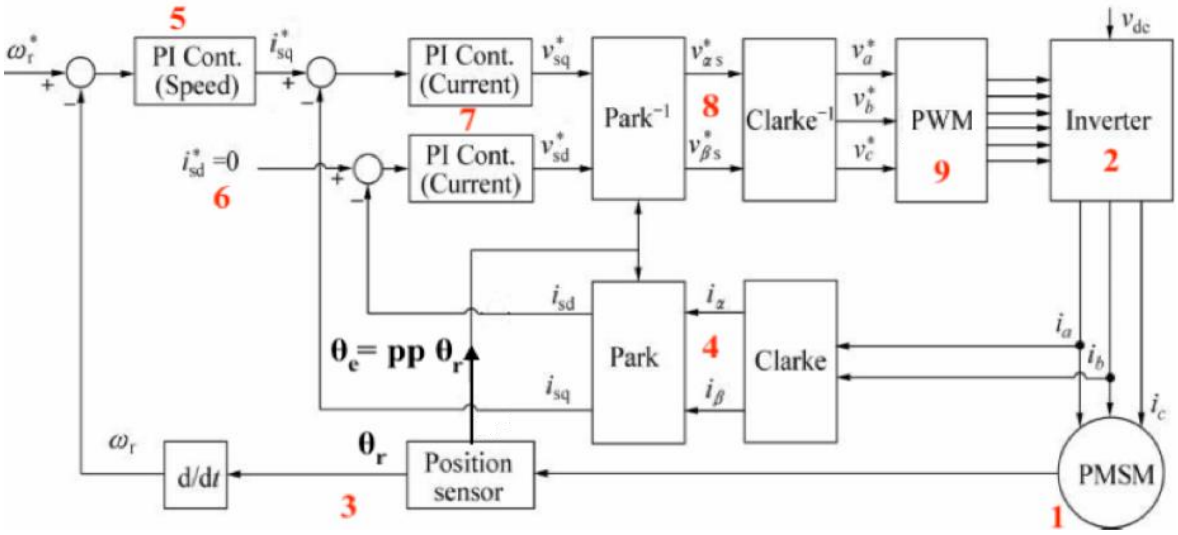

Figure 3.16: Speed-based field-oriented control scheme for a PMSM.[196]

Thanks to its feedback structure, the field-oriented control algorithm guarantees optimal dynamic performance and fast response, such as rapid acceleration and deceleration.

196 Rusu, C., Birou, I., Radulescu, M., & Bara, A. (2014), *Developing Embedded Control System Platform for Testing PMSM Drives*, Presented at *International Conference and Exposition on Electrical and Power Engineering (pp. 677-682),* Iasi, Romania, p. 679.

Using the PI regulators, a certain amount of overshoot is associated to reference input variation; by modifying the parameters of the controllers, the output result can be improved. Nowadays, in induction and synchronous AC machines drive this method has displaced the scalar volts-per-Hertz control, because of its accuracy and reliability; for the same reasons, in industrial applications FOC offers safer real-time performance. The continuous and fast evolution of microcontrollers – in terms of computational capability and reduction of power consumption – is boosting the adoption of vector control technique also for lower level motor drives.

Chapter IV:
Development environment

SUMMARY: 4.1 LabVIEW – 4.1.1 LabVIEW FPGA – 4.1.2 LabVIEW Real-Time – 4.1.3 Example: blinking red LED – 4.2 Hardware platform: SPARK control prototyping unit – 4.2.1 Field programmable gate array (FPGA).

4.1 LabVIEW[197]

LabVIEW is a system-design platform and development environment for a visual programming language, from National Instruments. LabVIEW integrates programs-subroutines (called virtual instruments, VIs) that are composed of three elements: a front panel, a block diagram and a connector pane. The first one is built with controls – for the inputs of the VI – and indicators – to display the outputs corresponding to the given controls; this panel is used for the user interaction with the running program. The second one contains all the objects that are placed in the front panel and the functions and blocks that are used for developing a certain algorithm. The third is useful to insert the VI in other virtual instrument schemes, because with the connector pane it is possible to define the inputs and outputs of that block, in order to link it as a subsystem (called SubVI).

197 National Instruments, Retrieved from *LabVIEW Environment Basics*: http://www.ni.com/getting-started/labview-basics/environment.

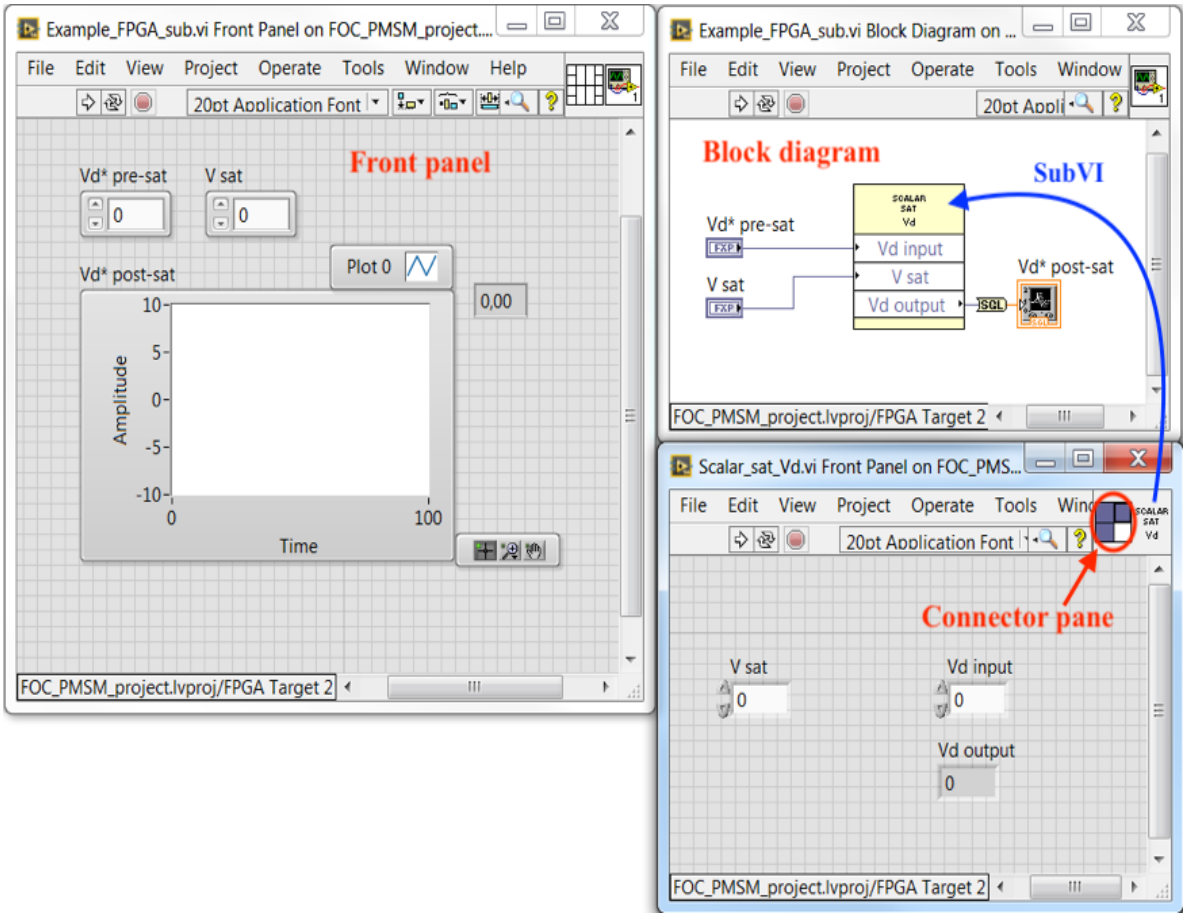

Figure 4.1: VI Components: front panel on the left, block diagram on the top right, connector pane (highlighted on the bottom right) for creating and using a SubVI inside another VI.

The used graphical language is called "G", and the development approach is very intuitive because it enables nonprogrammers to build programs by dragging and dropping virtual representations of laboratory equipment. In this way, users can be more familiar with the design and with the basic blocks used in the VI. LabVIEW allows interfacing with different devices, instruments for measurement, vision systems, etc. User can communicate with the hardware by writing direct bus commands or using high-level device-specific drivers that recall the native functions for correctly controlling the connected board. A compiler – included in LabVIEW – provides the latter functionality: the executable machine code is generated in this way, translating the graphical code according to hardware native functions.

The presence of many different and large libraries permits to manage a huge number of functions for signal generation or acquisition, mathematics, statistics, signal conditioning, filtering and other specialized abilities. Another fundamental aspect is the possibility to program multiple tasks that are performed in parallel, for example using two while loops –

one for the plant and the other one for the control algorithm. Some critical aspects are related to the use of LabVIEW for programming: first, only small applications can start in the run-time environment, due to its slowness; second, the G language is non-textual, needing specific additional tools for making comparison or merging code.

For the project in the laboratory of Teoresi Group S.p.A., the adopted versions are LabVIEW 2014, LabVIEW FPGA Module 2014 and LabVIEW Real-Time Module 2014. Concerning the drivers, on the host the following drivers have been installed: NI CompactRIO 14.5, NI-RIO 14.5, NI FPGA Compile Farm 2014, NI LabVIEW FPGA Xilinx Vivado 2013.4 Tools, NI MAX 18.5, NI-Embedded CAN for RIO Real Time 15.0, NI-XNET 17.5 and NI-VISA 14.0.1. For the compilation of the VIs on the FPGA integrated circuit of SPARK engine control unit and for the automatic generation of the HDL files, the version 2013.4 of Xilinx Vivado has been used.

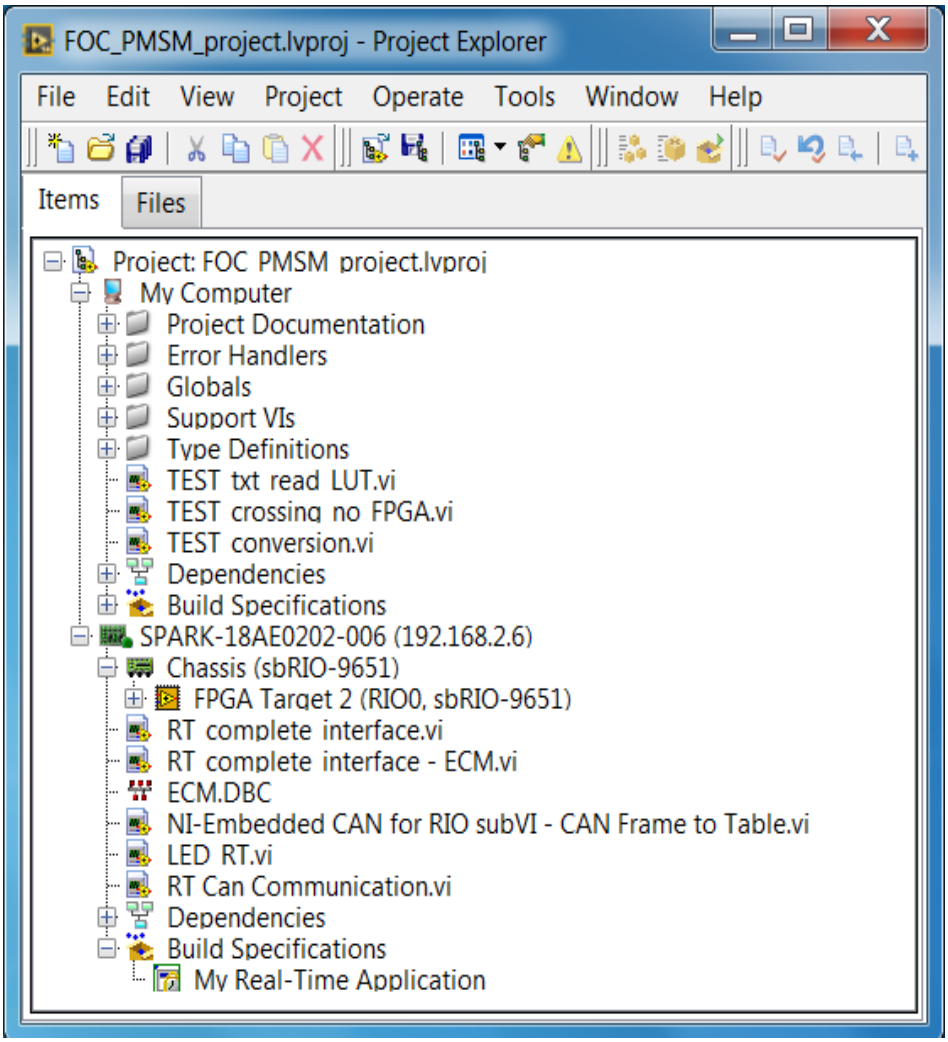

Figure 4.2: The LabVIEW project tree.

4.1.1 LabVIEW FPGA[198]

Regarding LabVIEW FPGA Module, it is used for developing and debugging custom hardware logic that are compiled and then deployed on the NI FPGA hardware. This is a software add-on for LabVIEW that can be used for designing efficiently FPGA-based systems in an integrated development environment, that includes IP libraries, simulator and debugging features. In this way, FPGA VIs can be created for combining the user-defined applications with the board used for running and testing the project.

The principal uses of this module are related to digital protocol communication and to rapid control prototyping hardware-in-the-loop (HIL) validation – the two functionalities have been exploited for developing and then debugging the project. Concerning the HIL, it is a technique used to test complex real-time embedded systems. The effective computing platform – the Alma Automotive SPARK board, used in Teoresi laboratory – runs the controller and it is tested by adding the complexity of the plant, i.e. the mathematical representation of the dynamic system under control – in this case the model of the electric motor is deployed together with the control algorithm on the same hardware. By the combination of the LabVIEW FPGA Module with Xilinx Vivado compiler, from the selected virtual instrument the corresponding hardware description language (HDL) programming file is generated; the latter is then used in the real-time user interface for running the program on the target board – in this case the SPARK engine control unit.

One of the major advantages of this module is the possibility of optimizing the use of the resources that are present in the hardware: the high throughput mathematical blocks allow selecting the width of each fixed-point value. Once defined the number of bits associated to a certain word, it is possible to choose how many bits are reserved to the integer part, in order to determine the maximum range and the delta of a certain number – the delta, called also resolution, is the minimum interval between two consecutive values. Moreover, the fixed-point number can be defined as signed or unsigned.

198 National Instruments, Retrieved from *What Is the LabVIEW FPGA Module*?: http://www.ni.com/en-gb/shop/electronic-test-instrumentation/add-ons-for-electronic-test-and-instrumentation/what-is-labview-fpga-module.html.

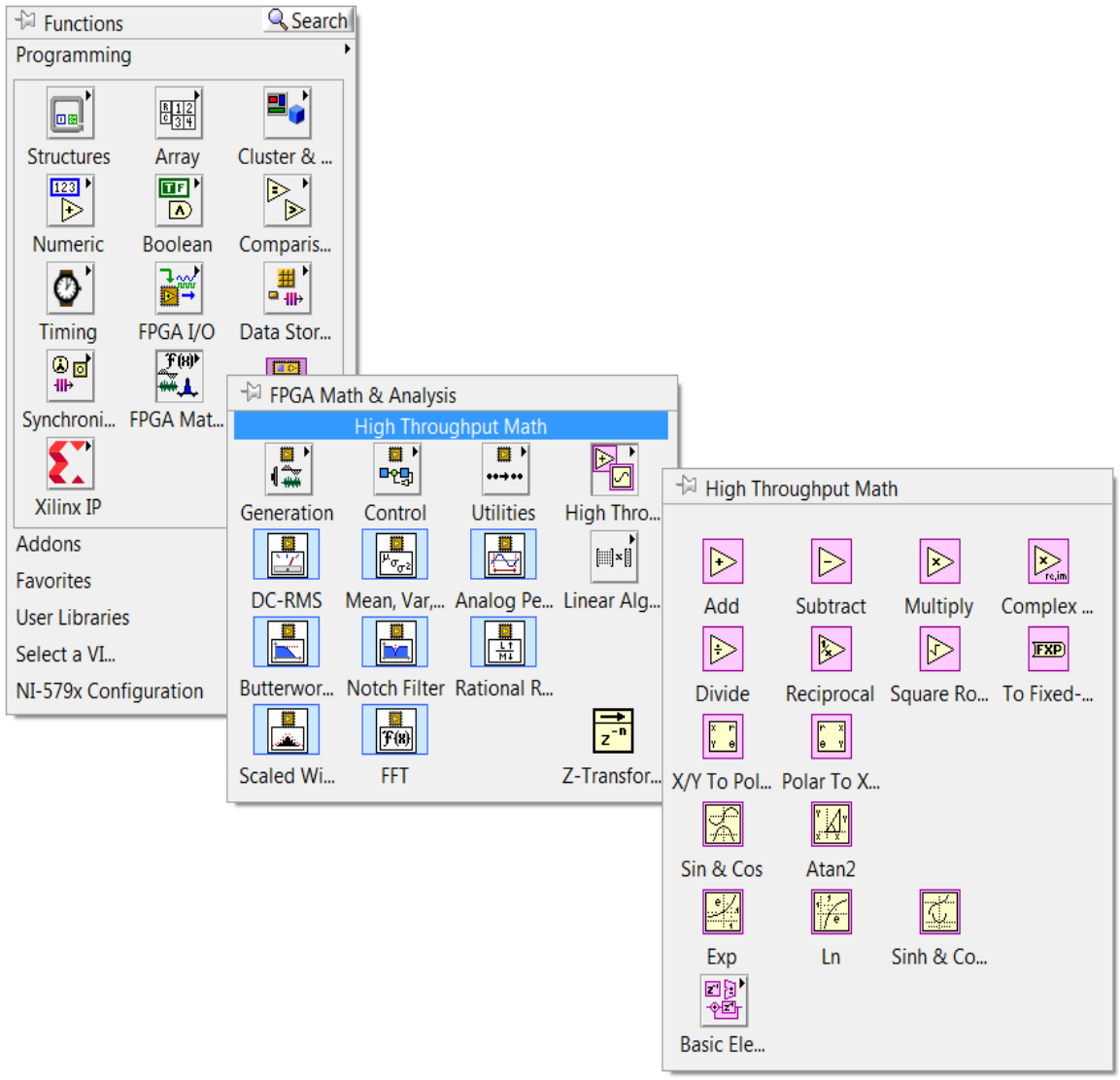

Figure 4.3: High throughput mathematical blocks.

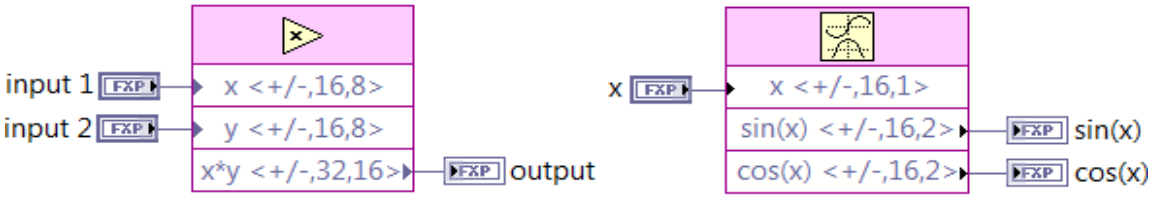

Figure 4.4: Example of FPGA VI, with controllers and indicators connected to high throughput blocks.

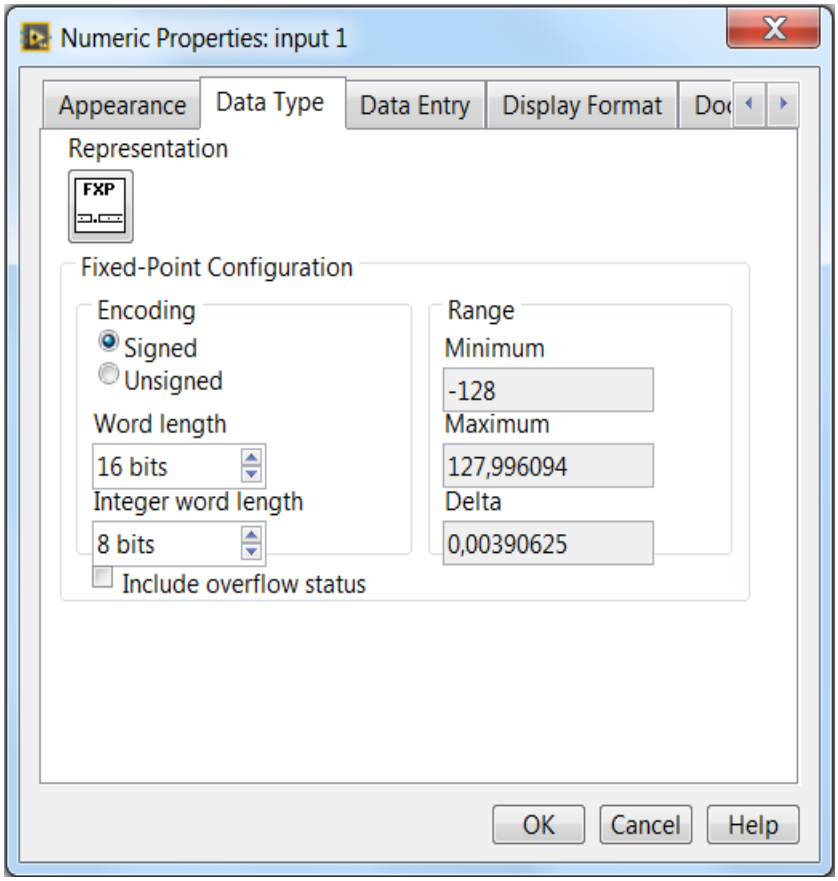

Figure 4.5: Numeric properties of the controller input 1 of previous figure 4.4; here it is possible to choose the word length and the integer word length for establishing the range and the delta.

The first step of the design process is to define the width of each input parameter – fixed or controllable – of the FPGA VI; afterwards, the values are wired to the high throughput mathematical blocks, where for all the operations – addition, subtraction, multiplication, division, reciprocal, square root, sine and cosine, exponential and natural logarithm, etc. – the output number of bits can be manually set or automatically established. Consequently, by deciding the maximum range and the adequate resolution for each parameter inside the models of controller and plant, it is possible to reduce the amount of unnecessary bits and to optimize the use of the FPGA integrated circuit resources.

Alternatively, the different fixed-step parameters are connected to blocks that are already present in standard LabVIEW environment, to filters, to discrete nonlinear blocks – hysteresis, saturation, signal analysis and processing (as Boolean crossing or zero crossing), trigger, etc. – to other predefined discrete linear systems – discrete normalized integrator, unit delay, discrete transfer function, etc. – or to SubVIs, where all the previous elements can be inserted to process the data.

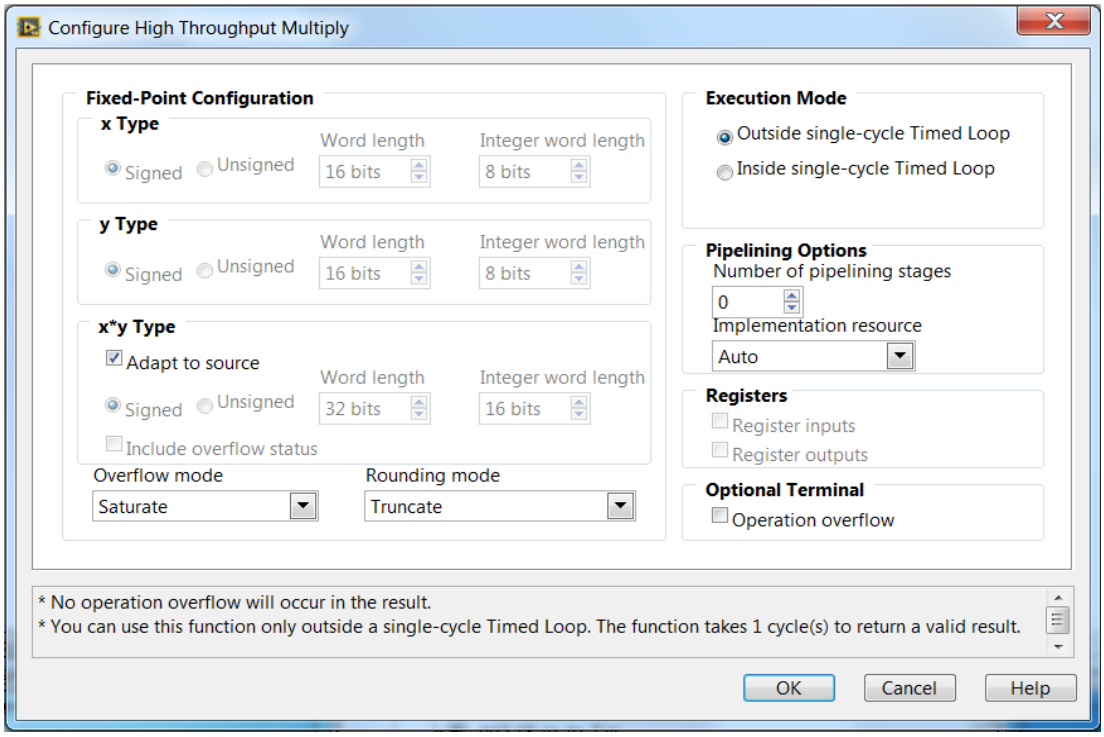

Figure 4.6: Configuration of the multiplier high throughput block, where the word length and the integer word length can be modified or adapted to the source signals.

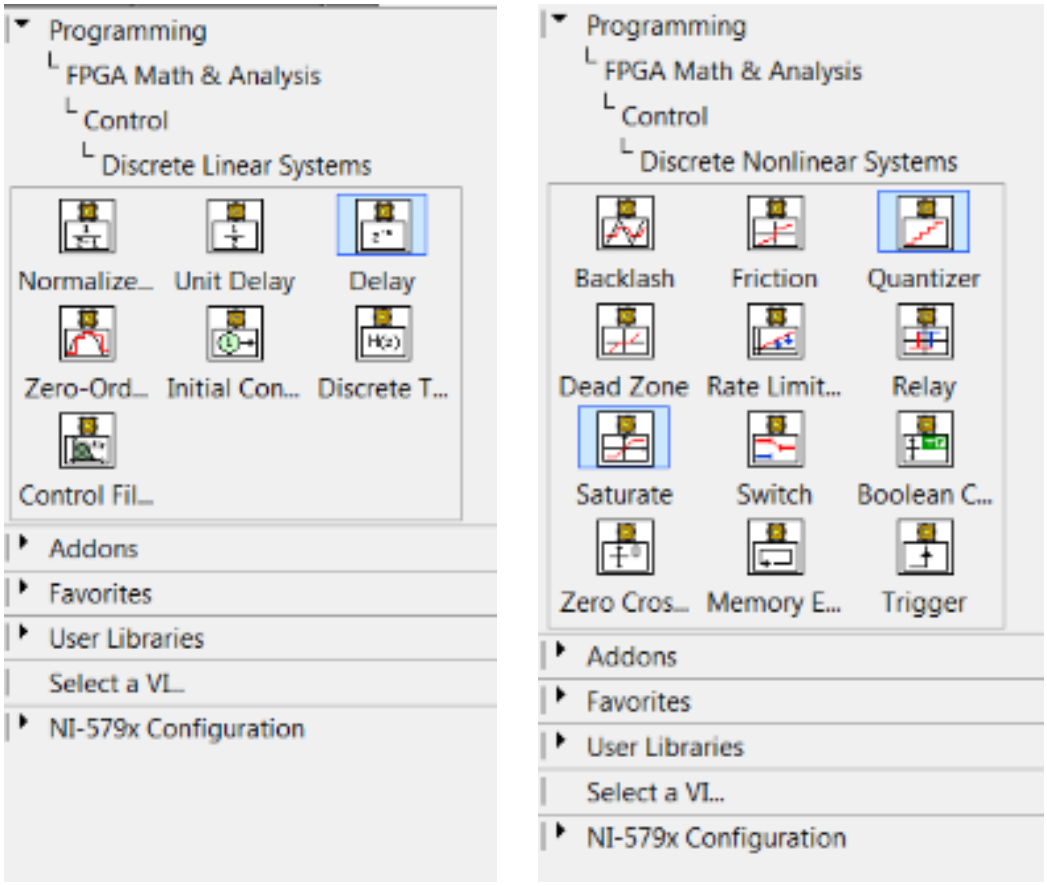

Figure 4.7: Discrete linear and nonlinear systems used in LabVIEW FPGA.

4.1.2 LabVIEW Real-Time[199]

LabVIEW Real-Time Module is a software add-on for LabVIEW, used for creating and deploying real-time applications and for testing, monitoring and controlling them, ensuring reliability and precise timing. In fact, the principal aspect for generating and using programs is the determinism: an application (or critical piece of an application) that runs on a hard-real-time operating system is referred to as deterministic if its timing can be guaranteed within a certain margin of error. The Real-Time Module is implemented for developing reliable projects, and many libraries have been introduced to interface with different boards: NI Real-Time hardware and software work together to run applications securely and deterministically on CompactRIO systems, on embedded PXI controllers and Industrial controllers. Thanks to this module, LabVIEW delivers deterministic real-time performance for data acquisition and control systems. On a desktop machine, the real-time user interface is realized, in order to set all the parameters used in the FPGA VI and to run the selected VI on the hardware. The LabVIEW Real-Time control application is first developed, then downloaded on an independent board through the Ethernet serial communication and finally executed. Moreover, using this module it is possible to set the desired FPGA VI as startup real-time application, so the board automatically runs the code when it is powered on.

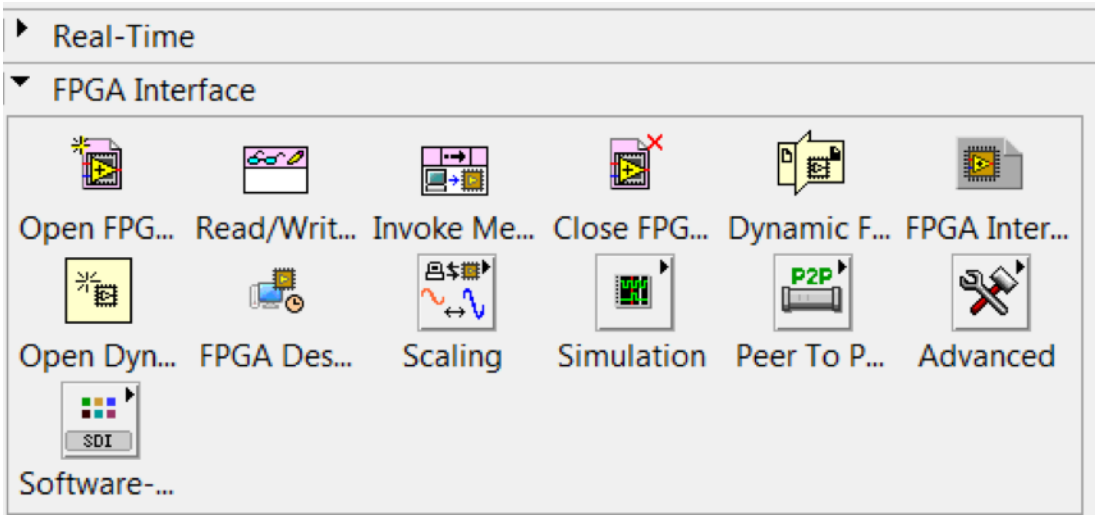

Figure 4.8: FPGA interface blocks for connecting the FPGA VI with the real-time user interface.

199 National Instruments, Retrieved from *What Is the LabVIEW Real-Time Module?*: https://www.ni.com/en-gb/shop/data-acquisition-and-control/add-ons-for-data-acquisition-and-control/what-is-labview-real-time-module.html.

The NI-Embedded CAN for RIO Real-Time driver allows to implement the CAN protocol inside the real-time user interface, for the used sbRIO-9651 board. The blocks present in the industrial communication library – figure 4.9 – are placed inside the scheme for creating, configuring and starting the CAN communication. Moreover, it is possible to filter the bus in order to select the messages that the engine control unit can visualize and read: this operation is fundamental in order to reduce the traffic of incoming signals and to improve the timing performance. The CANRead and CANWrite VIs are used to read and write respectively on the network. At the end of the execution, the communication is stopped, and the interface is closed. The CAN bus is used for interfacing the board – that runs controller and plant models – with the simulated battery management system (BMS) and dashboard.

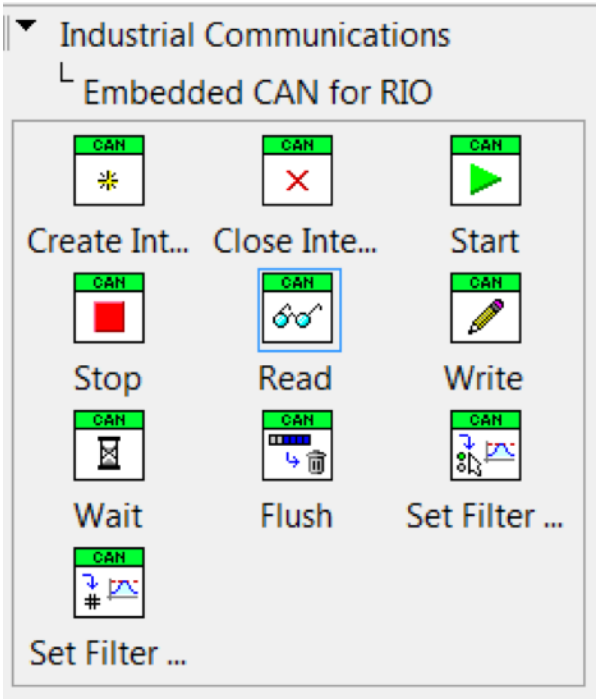

Figure 4.9: Embedded CAN for RIO blocks.

4.1.3 Example: blinking red LED

To present the possible LabVIEW applications and to show the interconnection between the real-time part and the FPGA VI, the following example is reported. This is a simple project for periodically blinking a red LED on the Alma Automotive SPARK engine control unit (ECU), with a period of 500 ms. Concerning the FPGA, the I/O FPGA Node is used for choosing the desired input/output among the possible nodes of the sbRIO-9651

Socket – called SPARK V1b. The latter file is used for mapping the various I/O pins present in the hardware and for assigning a specific name to each of them.

As initialization, the *LED_R_enable* value is set to true for enabling the possibility of using that LED. Then a while loop is created for modifying the status of the LED, through a Boolean controller variable – called *R LED status* – connected to the node *LED_R_out*. The configuration of the hardware requires a true value (logic 1) for LED on and a false value (logic 0) for LED off. In this VI, the output signal is not varied, and the LED does not blink on the board: the FPGA VI is used only for create the necessary controllers and nodes, but they will be used in the real-time interface for switching on and off the light.

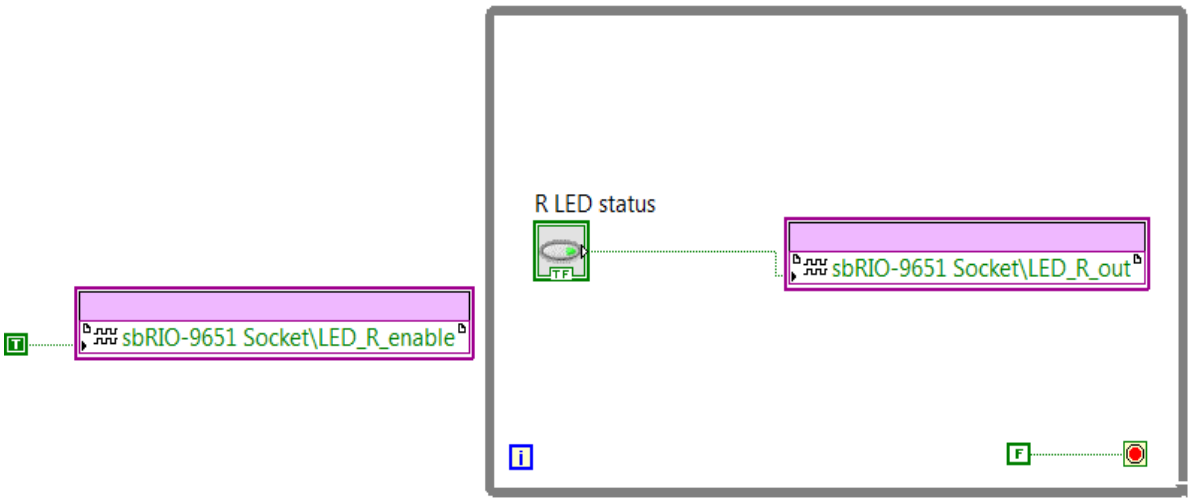

Figure 4.10: FPGA VI of the blinking red LED example.

The FPGA VI is compiled and deployed on the SPARK ECU; then the real-time interface is used for controlling the hardware. First, through the Open FPGA VI Reference block, the compiled VI is chosen; as second step, it is reset, and it starts running continuously. The yellow error wire connects all the blocks in a consecutive way to report the presence of malfunctions. The timed while loop is created by selecting a timing source of 1 kHz and a period equal to 1 ms. Inside this loop, the control algorithm is developed: the Read/Write control block reports all the input and output variables of the FPGA VI – in this case just the Boolean controller *R LED status*. The initial value is true, so LED on. By connecting the number of iterations to a Quotient & Reminder block, the blinking period is set to 500 ms; every time the reminder is equal to 499, the value of the controller variable is toggled through the Not logic gate. A shift register is used for memorizing the *LED status* value at each iteration and for using it as input for the successive cycle. The loop continues

until the stop button is pressed; when this happens, the Abort block stops the FPGA execution, and then the FPGA reference is closed.

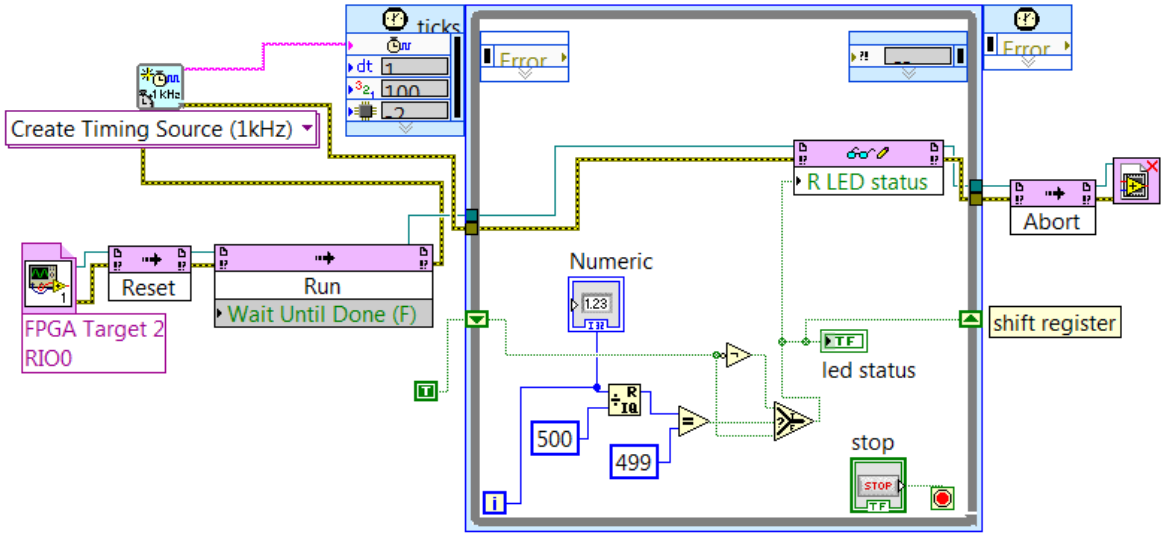

Figure 4.11: Real-time interface of the blinking red LED example, connected to the previous FPGA VI through the FPGA interface blocks.

4.2 Hardware platform: SPARK control prototyping unit[200]

Alma Automotive SPARK engine control system is a fully programmable control prototyping unit based on National Instruments System-On-Module sbRIO-9651. This system is actually used for many motorsport applications thanks to its flexibility, efficiency and accuracy and to the possibility of developing successfully every control strategy. Previously developed basic operations concern gasoline and diesel engines, from control functionalities, torque structure-based control, electronic throttle control, lambda control, speed limiter, gear cut for sequential gear box, fuel cut off, traction control, launch control, turbo boost control, knock control. For this project – in the Teoresi laboratory in Turin – the ECU is used for the control and the simulation of an electric permanent magnet synchronous motor (interior or surface-mounted structure).

200 Alma Automotive S.r.l., Retrieved from *SPARK - The open source ECU project*: https://www.alma-automotive.it/public/sitemin/SPARK.pdf.

Figure 4.12: The Alma Automotive SPARK engine control unit.[201]

The main advantage of this system is the presence of Artix-7 FPGA processor and real-rime module in the same system: on the FPGA the models of controller and plant are flashed in order to use the high clock frequency of 40 MHz – obviously reduced by a proper factor, due to the complexity of the algorithm – while the user interface is implemented in the real-time part. Another advantage of the subdivision is the possibility of selecting all the parameters, exploiting the functionalities of the real-time module: in this way, the basic settings of the PMSM and of the regulators can be changed and different kind of plant can be considered. This versatility is a fundamental feature of the project, because by simply varying the values in the user interface the behaviour of both interior permanent magnet and surface-mounted permanent magnet machines can be analysed, without recompiling the models in the FPGA integrated circuit. The ECU software, both real-time and FPGA, are completely accessible and open, so the user can read, edit or even replace everything he wants.

Regarding the communication tools, Ethernet is used for connecting the engine control unit to the computer for flashing the models and for creating the interface; CAN protocol is used for the final part of the project, for the graphic visualization of the results –

201 Alma Automotive S.r.l., *op. cit.*

like rotor speed or engine torque – on the simulated dashboard and for passing values to the control algorithm – i.e. the actual limits for charging and discharging DC. Using the software of National Instruments Measurement & Automation Explorer – the so-called NI MAX – the installed software and the functionalities of the board are examined. Through the Web Configuration tool, it is possible to deploy on the hardware the text files containing the look-up tables (LUTs), used for the control algorithm – in particular for the maximum torque per ampere (MTPA) region in the constant torque operation mode of the IPM synchronous motor. Concerning the CAN communication, the program XNET Database Management is used for uploading the database – created ad hoc and called *ECM* for this project – used to identify the exchanged messages. Using the real-time interface and the blocks of the NI-Embedded CAN for RIO library, the communication between the board and other nodes is implemented. For the project, the SPARK ECU is responsible for sending the following messages:

- the torque request from the driver;
- the actual engine torque – which is usually communicated to the transmission control unit in a hybrid-electric vehicle;
- the effective engine speed to the dashboard, for graphically visualizing it;
- the main close request for reporting that the contactors are closed, so the motor can operate safely, and the control algorithm can start working;
- the signal engine on and key on to activate the dashboard.

The control algorithm uses two parameters that arrive from the battery management system, through a dedicated message. These values are the maximum discharging current of the batteries and the maximum charging current level. Moreover, also the charging and discharging power limit values can be sent inside the same message from the BMS to the engine control unit. The last consideration concerns the possibility of using the real-time module for deploying a startup VI on the SPARK control prototyping system. Using LabVIEW, in fact, it is possible to select one specific FPGA VI and to use it as startup application; using the build specifications for the sbRIO-9651 board, the selected VI – in this case, the one containing the models of plant and controller – is deployed on the hardware and it is set as startup. When the engine control unit is powered on, it automatically starts working. The corresponding drivers that are installed on Alma Automotive SPARK ECU are the following: LabVIEW Real-Time 14.0.1, NI Scan Engine 4.3, NI Web-based Configuration and Monitoring 15.0.0, NI-Embedded CAN for RIO 15.0.0, NI-RIO 15.0, NI-RIO IO Scan 15.0, NI-VISA 15.0.1 and NI-XNET 15.5.0.

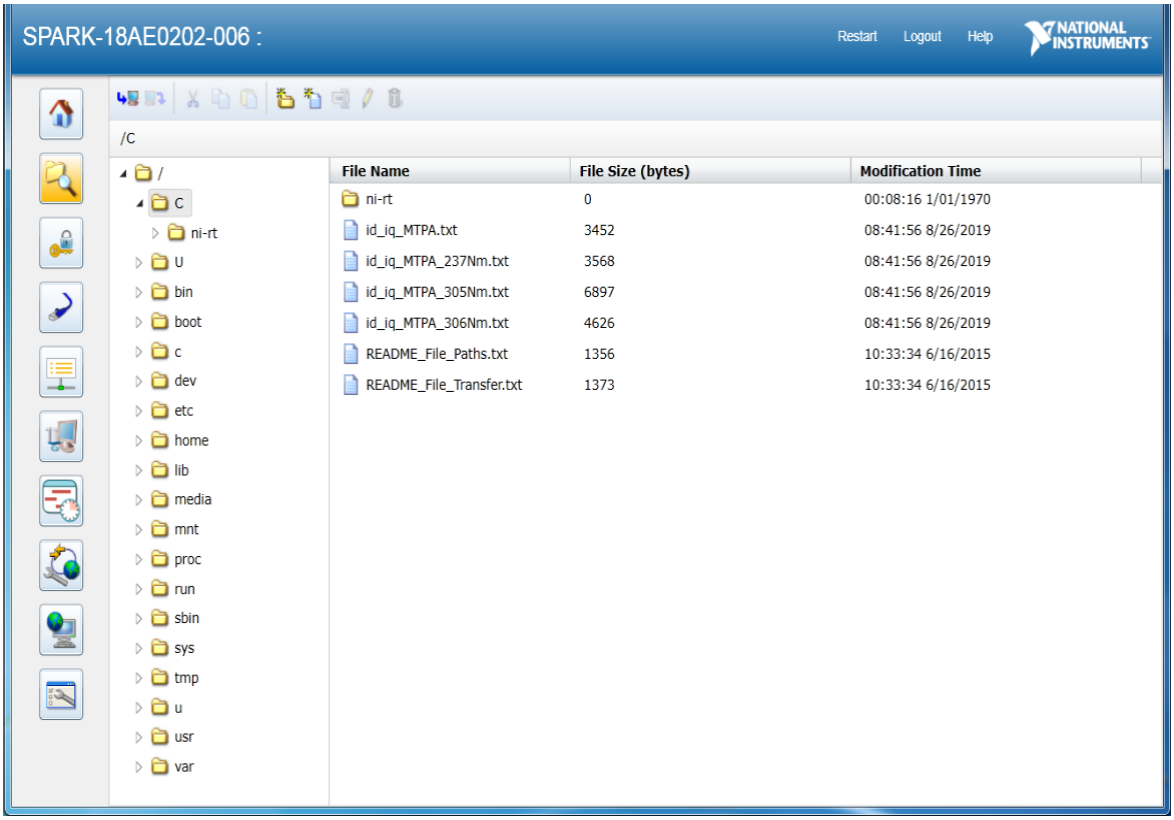

Figure 4.13: Web configuration of the SPARK board for uploading the needed text files for the control algorithm (in particular for the LUTs).

4.2.1 Field programmable gate array (FPGA)

In order to completely describe the mechanism for flashing the models – implemented with LabVIEW FPGA module – on the SPARK engine control unit, a brief description of the field programmable gate array is reported in this paragraph. FPGA is a semiconductor integrated circuit designed to be configured by a customer after manufacturing; its structure is generally specified using a hardware description language (HDL), that in this case is automatically generated when the realized VIs with LabVIEW FPGA are compiled. The languages such as VHDL and Verilog are used in order to write the code for FPGA programming. FPGAs contain a matrix of configurable logic blocks and a hierarchy of reconfigurable interconnects to link the different blocks: in this way the logic gates can be inter-wired in many possible ways. Logic blocks can be configured to perform elementary logic operations or complicated combinational functions. Moreover, in most of these integrated circuits memories are present, from simple flip-flops to complete blocks.

Benefits of this integrated circuit are essentially related to the possibility of reprogramming the device and reusing it any number of times: in fact, a field programmable gate array is flexible, but at the same time can be used for generating complex operations and has reduced cost with respect to an application-specific integrated circuit (ASIC). In FPGA design, software takes care of routing, placement and timing, requiring less manual intervention for timing analysis and floor planning operations; the implementation process consists of translating the input netlists to the logic design file, then mapping the circuit into sub-blocks for fitting it into the FPGA logic blocks, placing the sub-blocks – obtained from the mapping process – into the logic blocks according to physical constraints and finally connecting them. The possibility of programming the device at logic level assures faster and parallel signal processing.[202] Obviously, some disadvantages are related to the use of a FPGA: power optimization is difficult to be managed by the user if compared to ASIC systems, a field programmable gate array has limited resources and it is clearly more useful for prototyping applications, testing and low quantity production with respect to dedicated circuits. FPGA is principally used for high customizable system-on-a-chip, for powerPC or ARM based CPU, for signal and image processing due to the high number of multipliers and internal memory that are present within the integrated circuit. Moreover, recent applications concern machine learning and computer vision, image recognition and compression, security systems, by exploiting FPGAs as processor accelerators. Another fundamental use regards the emulation and simulation of an ASIC in loop testing, like for this project.

The architecture of a field programmable gate array can be essentially divided in three parts: logic blocks, hard blocks and clocking. Logic blocks usually consist in a few logical cells, composed typically of a 4-input LUT, a full adder and a D-type flip-flop; common FPGA architecture consists of an array of logic blocks, input/output pads and routing channels, but obviously an application circuit must be mapped into an integrated circuit with adequate resources. Modern FPGA families include higher level functionality fixed in silicon, so hard blocks are introduced: in this way, common functions are embedded in the circuit – like multipliers, generic DSP (digital signal processing), processors, embedded memories – reducing the required area and increasing the speed with respect to building the blocks from logical primitives. Higher level FPGAs can contain transceivers, Ethernet medium access control units and external memory controllers. Finally, most of the circuitry built inside the FPGA is synchronous and requires a clock signal: for this reason,

[202] Xilinx Inc., Retrieved from *Field Programmable Gate Array (FPGA)*: http://www.xilinx.com/products/silicon-devices/fpga/what-is-an-fpga.html.

these devices contain dedicated global and regional routing networks for clock and reset, reducing the skew. Moreover, complex designs can use multiple clocks with different frequency, generated by an oscillator or recovered by high speed serial data stream. Basic process technology involves SRAM – static memory, but an external boot device is required – which are based on CMOS. Flash memory or EEPROM devices often load contents into internal SRAM that controls routing and logic. Previous FPGA were based on fuse and antifuse, then on programmable read-only memory (PROM) and erasable programmable read-only memory (EPROM): all these techniques are actually obsolete. Electrically erasable programmable read-only memory (EEPROM) and flash technology are used, because both of them can be erased and some of them can be in-system programmed too. To shrink the size and power consumption of these integrated circuits, 3D or stacked architectures have been introduced, using several (three or four) levels of active FPGAs.

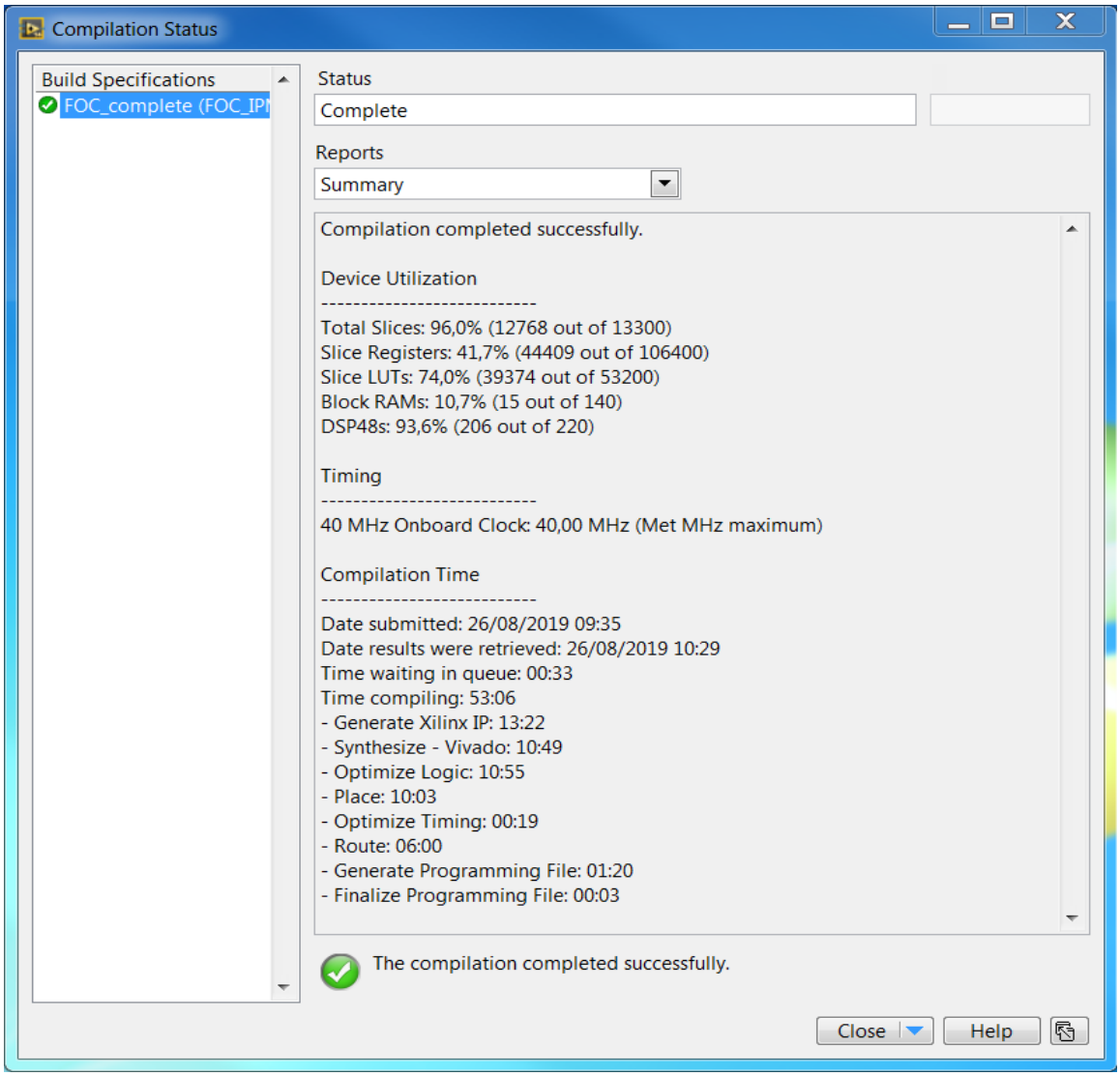

Figure 4.14: Compilation status summary of the FPGA VI on the SPARK ECU.

Chapter V:
Project of the FOC algorithm for a PMSM

SUMMARY: 5.1 Presentation of the system – 5.2 FOC strategy for an IPM synchronous motor – 5.2.1 Clarke-Park transformations – 5.2.2. Plant implementation – 5.2.3 PI regulators, saturation blocks and anti-windup – 5.2.4 Torque control loop and MTPA region – 5.2.5 Speed control loop – 5.2.6 Flux-weakening for an IPMSM – 5.2.7 Battery pack direct current regulation – 5.2.8 Real-time interface and results – 5.2.8.1 First case: torque loop – 5.2.8.2 Second case: speed loop and regenerative braking – 5.2.8.3 Third case: battery DC limitation in torque loop – 5.3 FOC strategy for a SPM synchronous motor – 5.3.1 Differences with respect to IPM control algorithm – 5.3.1.1 Decoupling – 5.3.1.2 MTPA region – 5.3.1.3 Flux-weakening for a SPMSM – 5.3.2 Real-time interface and results – 5.4 BMS and dashboard simulation using CAN protocol.

5.1 Presentation of the system

In this chapter, the design procedure of the field-oriented control strategy, the implementation of the algorithm on the Alma Automotive SPARK engine control unit and the results – obtained in the Teoresi laboratory in Turin – are discussed. The controller and plant models are both flashed on the same hardware, while the real-time user interface is exploited for setting the parameters and for plotting the output signals and waveforms. Moreover, in the final part of the project the CAN communication is implemented: the battery management system is simulated for sending the direct current limits, due to battery overcharges or malfunctions – this approach is used to consider a realistic application of the control algorithm in a battery electric vehicle, where the BMS manages the battery pack. The behaviour of a dashboard is reproduced too, for showing the output values of the system, like the angular speed in RPM or the motor torque. For a more generic approach, an interior PMSM and a surface-mounted PMSM are evaluated, showing the differences in the plant

equations and in the control strategy. In fact, two examples of permanent magnet synchronous motors – one for each typology – are inserted in this chapter. The inverter is not included, because the output voltage waveforms pass directly from the controller to the plant. The control method is designed in an ideal condition where no switching mechanism, no losses and no eddy currents are considered. The rotor electrical speed and electrical angular position are passed to the controller by using local variables in LabVIEW environment – so also the encoder and Hall effect sensor are neglected in this situation.

In the first part, the IPM is analysed, because in this case the FOC is more complex and contains more blocks – such as the regulator for the direct current of the simulated battery pack and inverter, the speed control loop and the realization of the CAN bus. Initially, the schematics of the controller and plant are presented, showing their general structures. Then, the blocks are analysed individually, describing the main features and the adopted solutions for their realization. The different PI regulators, the maximum torque per ampere area and the flux-weakening region are described, highlighting the optimization tools for increasing the dynamic performance and the maximum deliverable torque. For the IPMSM, the torque control loop is combined with a speed control loop: the two regulation algorithms can be switched during standard operations, where no current limitations are observed. In figure 5.1, an equivalent complete block diagram – in order to realize a more readable structure – is shown. It is useful for visualising the inputs and the outputs for each element, the exchanged values between the controller and the interior permanent magnet synchronous motor and the status variables.

Regarding the SPMSM, the control strategy is simplified, because the MTPA in constant torque region consists of a null *d*-axis component of the stator current, while the flux-weakening is very limited due to the little saliency, with respect to IPMSM. For this structure, just the torque control loop is implemented. On the other hand, a decoupling block is designed for isolating and removing the direct axis and quadrature axis voltage and current contributions on the opposite axis. Finally, the implementation – just for the IPM configuration – of CAN communication on LabVIEW Real-Time module is described, showing parts of the schematic and of the frame characteristics and then the graphical results. An ad-hoc database – called *ECM* – has been created for this purpose using the software CANalyzer from Vector Informatik. Through the same program, a graphic panel is realized for visualizing the output values, while the exchanged messages among the three nodes (engine control unit, simulated battery management system, simulated dashboard) are analysed with their periodicity.

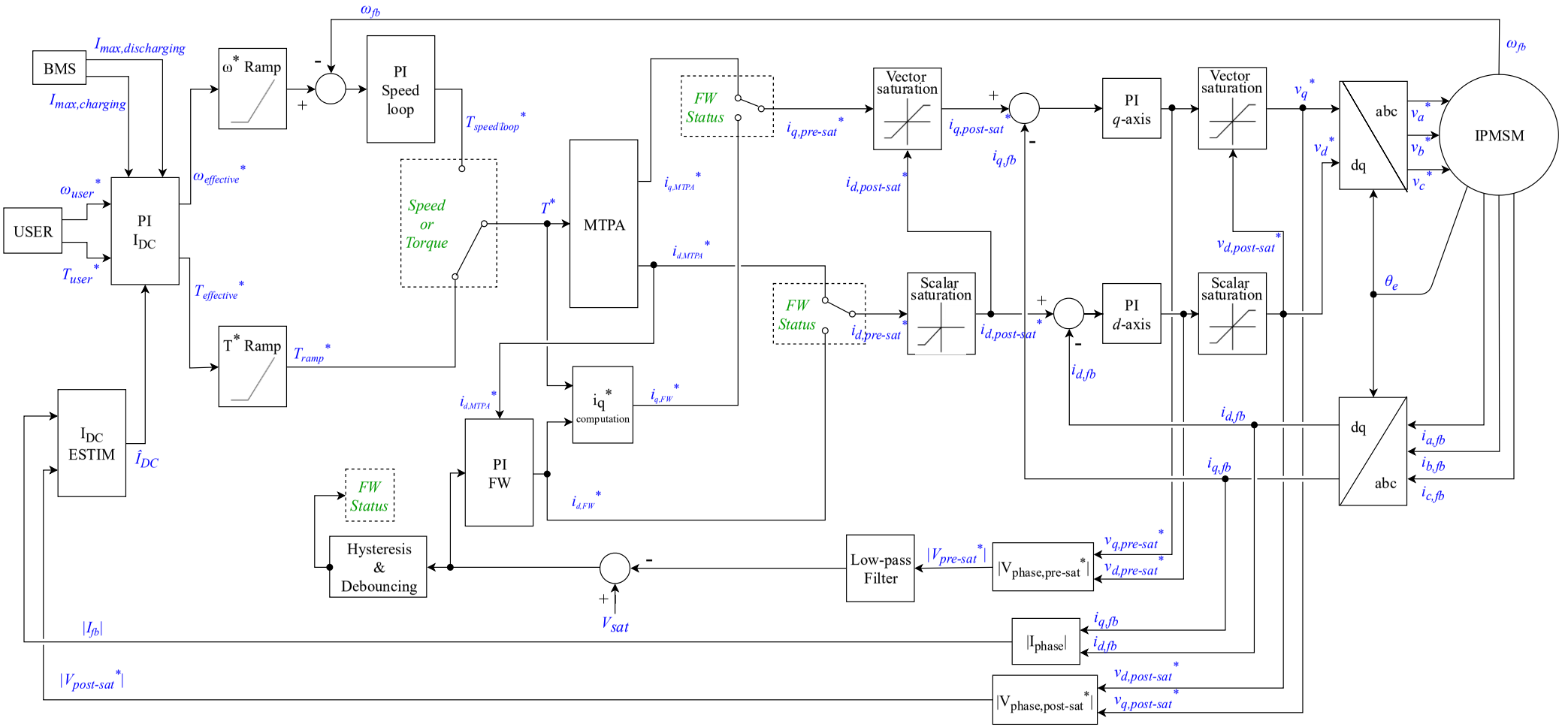

Figure 5.1: Block scheme of IPMSM control algorithm.

5.2 FOC strategy for an IPM synchronous motor

The interior permanent magnet synchronous motor is able to guarantee a larger power density and a higher maximum torque with respect to a SPMSM in the same operating condition: this advantage is related to the presence of saliency in the air-gap. In fact, the equivalent direct axis and quadrature axis stator inductance – respectively L_d and L_q – are different (in detail, $L_q > L_d$ because the *d*-axis is aligned along the magnetic flux direction), so the additional reluctance torque can be exploited. In the design process, first of all the model of the plant is developed, by using the generic PMSM mathematical model (analysed in chapter II). The block scheme in the FPGA VI is realized considering the three-phase voltage commands as input for the motor, while the three-phase stator currents, the electrical speed and electrical angle are the outputs. Using the dynamic equations, the delivered electromagnetic torque can be computed, considering also resistance and damping effects. The model of the motor is inserted in a while loop and it uses a different discrete time interval for the integrators with respect to that of the controller. The LabVIEW occurrence block is used for running one loop at a time.

Concerning the field-oriented control, initially the Clarke-Park transformation blocks are created, for verifying the correct conversion from the three-phase stationary reference frame to the two-phase rotating axes. For increasing the accuracy and reducing the loss of precision, a proper number of bits must be used for the resolution; obviously, this requires more FPGA resources. In the following paragraph, the graphic representation of the converted quantities is included too. Then, the proportional integral regulators are analysed and designed, removing all the possible problems related to saturation and windup. Two kinds of saturation blocks are used, in order to give priority to the direct axis with respect to the quadrature – this is an essential feature for efficiently reducing the flux. Once established the core of the FOC, the reference values of the currents are obtained through the MTPA block. For this purpose, look-up tables are generated in MATLAB and are copied in the directory of the SPARK ECU with NI-MAX. As alternative control, the speed loop is implemented, so the user can directly set a desired rotor angular velocity. For obtaining more performing dynamic performances and for reducing the ripple, the torque and speed reference values are converted from step inputs into ramp signals. The two most challenging problems of the project are the flux-weakening region and the regulation of direct current. The first one is faced analysing both feedforward and feedback techniques: the second one is chosen in the final configuration, including PI to limit the user torque or speed request,

according to the actual I_{DC} and to the constraints related to battery maximum charging and discharging rates. These values are set by the user in the real-time interface as first approach; afterwards the CAN communication is implemented for passing the limiting values through a simulated battery management system. For the simulation, the IPM synchronous motor parameters are reported in the following table 5.1. A star-connection (fig. 5.2) has been considered for the three-phase stator, so the relations between phase and line quantities are:

$$V_{line} = \sqrt{3}\, V_{phase}$$

$$I_{line} = I_{phase}$$

$$P_e = 3\, V_{phase}\, I_{phase} \cos(\varphi)$$

where $\cos(\varphi)$ is called power factor and it represents the angle between current and voltage phasors, while P_e is the total active electric power of the system – obtained through the sum of the three individual contributions (one for each phase).

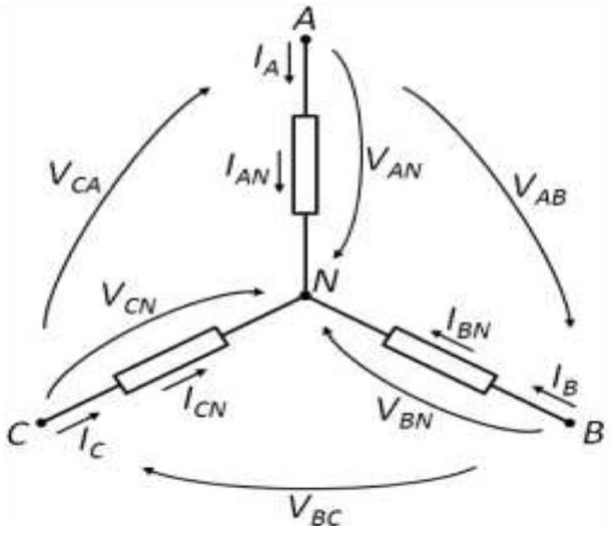

Figure 5.2: Star-connected three-phase stator windings.[203]

[203] Ferreira, F., Ge, B., Quispe, E., & De Almeida, A. (2014), *Star- and Delta-Connected Windings Tolerance to Voltage Unbalance in Induction Motors*, Presented at *International Conference on Electrical Machines (ICEM),* Berlin, Germany, p. 2.

PPMSM Parameter	Symbols	Values
Nominal speed	n_N	4800 RPM
Nominal torque	T_N	145 Nm
Maximum speed	n_{max}	15000 RPM
Maximum torque	T_{max}	237 Nm
DC voltage	V_{DC}	400 V
Saturation phase voltage	$V_{sat,phase}$	325 V
Saturation phase current	$I_{sat,phase}$	485 A
Pole pairs	pp	5
Power factor	$\cos(\varphi)$	0.94
d-axis Inductance	L_d	215 µH
q-axis Inductance	L_q	86 µH
PM flux	λ_{PM}	0.044 Vs
Stator resistance	R_s	8.5 mΩ
Moment of inertia	J	650.2 kg cm^2

Table 5.1: Parameters of the simulated IPMSM.

5.2.1 Clarke-Park transformations

The first step is the implementation of Clarke-Park direct and inverse transformations inside the FPGA VI. Particular attention must be dedicated to the dimensioning of the different parameters: considering the electric quantities' range, their minimum, maximum and delta values are chosen in order to obtain accurate results, but at the same time to reduce the amount of unnecessary bits – and consequently to decrease the needed resources. FOC loop and plant loop work by using dq-axes quantities, but their inputs and outputs are three-phase: for this reason, in the complete VI, one direct transformation and one inverse transformation blocks are present in each part – one couple for control that receives currents and provides voltages, the other couple for the plant which receives voltages and provides

current. It is possible to notice that the instantaneous electrical angular position is needed for Park transformation and antitransformation: this value is extracted from the motor loop by using a simple local variable. Furthermore, the electrical angle must be normalised with respect to π, because the high throughput sine & cosine requires this operation. The input angular position for Clarke-Park SubVIs is already normalised in the plant loop. Starting from the controller:

- the first block (fig. 5.3) is used for converting the input three-phase stator currents – passed from the motor through local variables – into *dq*-axes contributions, which are used as feedback values for the regulators. Knowing that in the considered IPMSM the saturation value for phase and line stator current is equal to 485 A, for the controllers $i_{a,FB}$, $i_{b,FB}$ and $i_{c,FB}$ the word length is equal to 29 bits, while 11 bits are reserved to the integer part – these values arrive from the motor, so a better resolution is adopted. This consideration is valid also for the output values $i_{d,FB}$ and $i_{q,FB}$ of this block. The size of these values and, in particular, their resolutions are chosen using a trial and error approach, for finding the optimal compromise between performance and required resources. For the constant parameters, a smaller delta is used, for increasing the accuracy of the transformations. The normalized electrical angle must be precise too, and its range is [0,2], consequently it is a 28-bit fixed-point variable, where just 3 bits are dedicated to the integer part;
- the output block is used for converting the *dq* command voltages v_d^* and v_q^* into the corresponding three-phase stator quantities. The saturation value for line stator voltage is equal to $V_{DC} = 400$ V, so for the phase voltage:

$$V_{phase,sat} = \frac{V_{line,sat}}{\sqrt{3}} = 231\ V$$

  For the inputs – because they are in the FOC loop – 26 bits are used for the complete word and 11 bits for the integer. The outputs are sent to the plant, so they contain three additional bits. Again, the constant values and the normalized electrical angle have a more accurate resolution.

For the two blocks of the motor:

- inside the first block of the scheme, the Clarke-Park inverse transformation is realized. It is used for converting the input three-phase voltage commands – passed from the control loop through local variables – into *dq*-axes contributions. Then, the dynamic equations of the PMSM are implemented through mathematical blocks. The saturation value for the phase voltage is 231 V and the motor loop is considered, so

29 bits are used for the fixed-point inputs and outputs' length, while 11 bits are reserved to the integer part;

- the output block is used for converting the *dq* actual currents into the corresponding. In the analysed IPMSM, they are saturated at 485 V: 29 bits are used for the complete word, while 11 bits are sufficient for the integer.

The multiplier, adder, sine & cosine and other high throughput blocks require a certain number of resources when they are compiled and flashed on the FPGA – in particular, slices, slice registers, slice LUTs, RAMs, DSPs are present in the device. For optimization reasons and for respecting the limited available hardware elements, the range of each controller, constant and indicator – as well as the output of the mathematical blocks – is carefully selected. Moreover, because both controller and plant run on the same FPGA, this operation requires a huge effort: as general consideration, for motor parameters a better resolution is adopted, in order to obtain a more accurate simulation of the real PMSM's behaviour. Concerning the FOC algorithm, the delta is bigger with respect to motor values, because the resultant controller is made up of discrete elements. In fact, in automotive applications the engine control unit runs just the control part, using sensors for measuring stator currents and rotor speed and wires for passing the command voltages to the inverter. An example of Clarke-Park transformations is reported in this paragraph, considering different reference torques in succession – one positive, one null and one negative (with the same magnitude of the first): the corresponding current waveforms are obtained using the motor parameters of the previous table (tab. 5.1). For completeness, also the rotor electrical angular position is displayed, showing how the sawtooth waveform is inverted when the reference torque changes its sign.

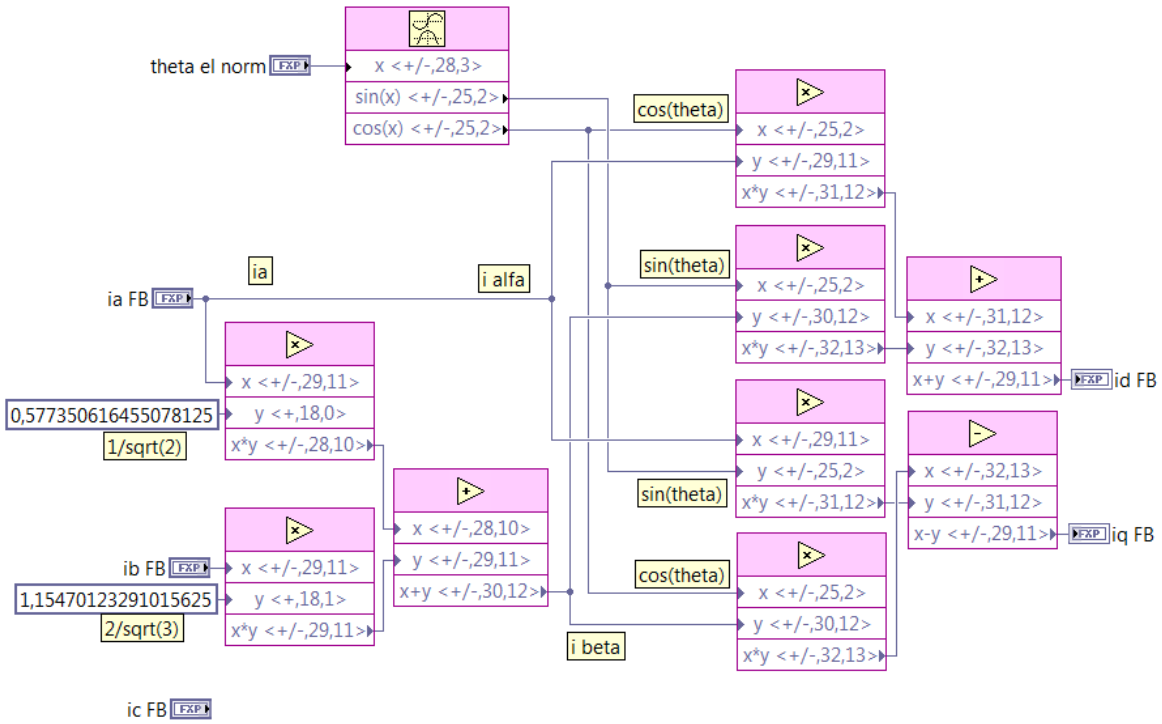

Figure 5.3: Clarke-Park transformations SubVI for three-phase feedback currents.

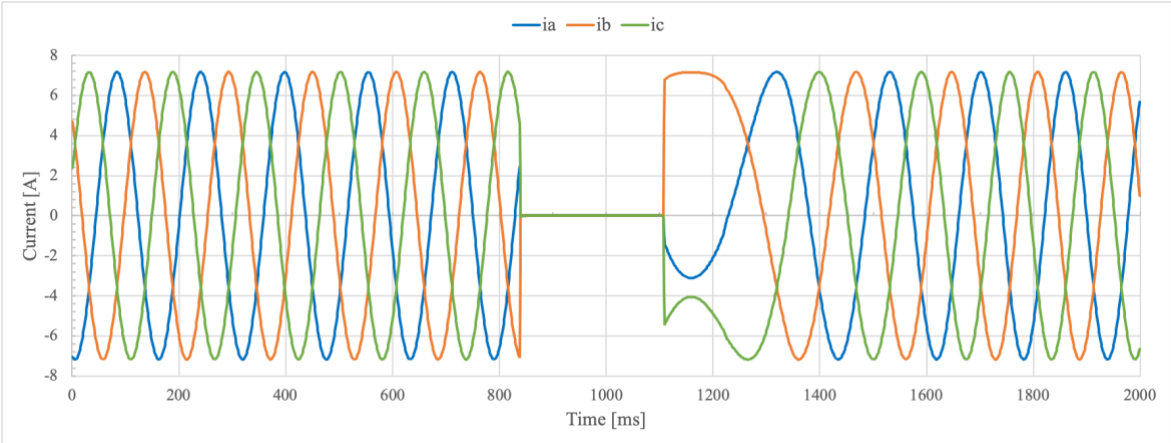

Figure 5.4: Three-phase currents in fixed abc reference frame.

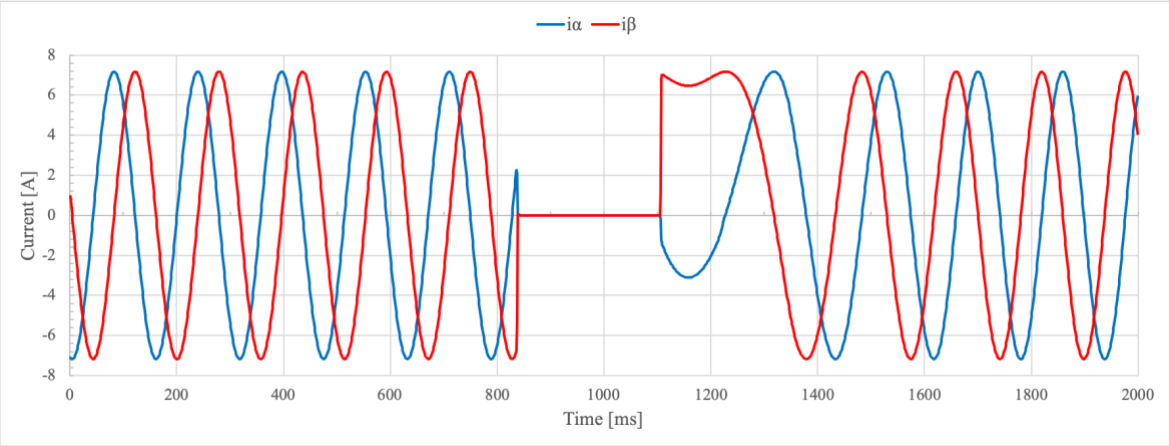

Figure 5.5: Three-phase currents in fixed αβ reference frame.

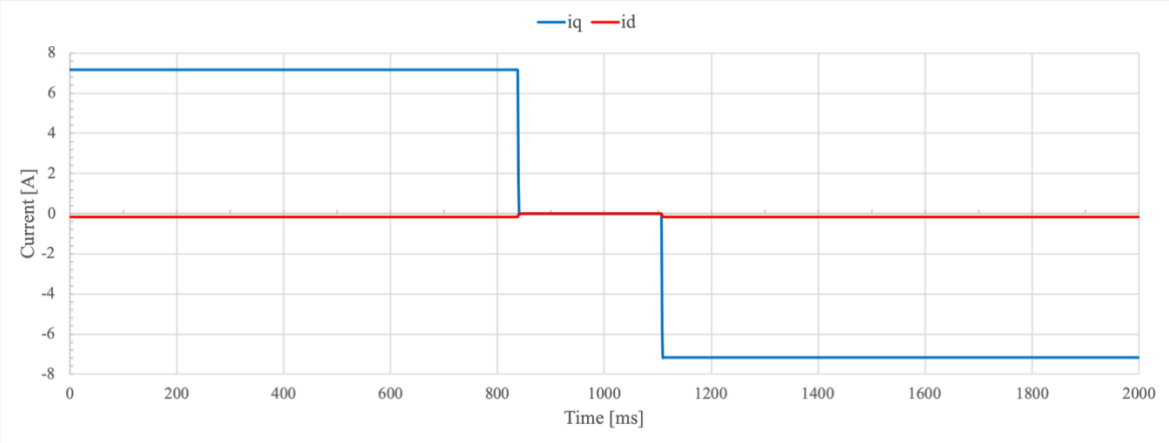

Figure 5.6: Three-phase currents in rotating dq reference frame.

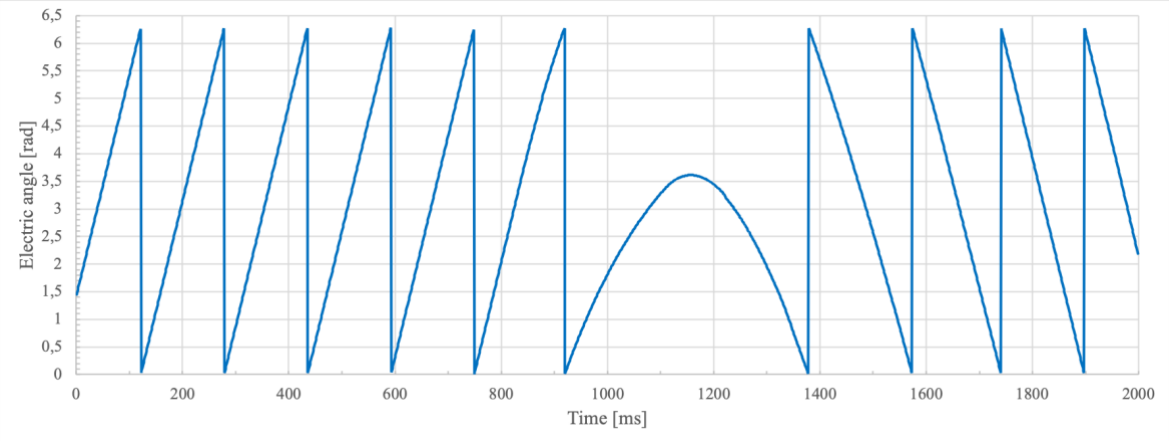

Figure 5.7: Electric angular position.

5.2.2 Plant implementation

For realizing the plant through the high throughput mathematical blocks, the starting point is the dynamic model of the IPMSM, analysed in the second chapter. The command variables of the motor are the three-phase stator voltages, which are transformed in the corresponding *d*- and *q*-axis values and then used for computing the direct and quadrature components of stator current. In this operation, the values of stator resistance R_s, direct and quadrature inductances L_d and L_q, permanent magnet flux linkage λ_{PM} and rotor electrical speed ω_e appear. The integration is realized through a discrete normalized integrator: this block requires the discrete time interval to be directly multiplied to the value that has to be integrated – there is no additional input for establishing the integration step. Moreover, it acts as an adder, which continuously increases or decreases its value – this feature could create the windup degrading condition, in case of saturation (such as in the controller structure). Once obtained the actual i_d and i_q, these quantities are transformed into the corresponding i_a, i_b and i_c through the inverse Clarke-Park transformations and passed to the controller. From *d*-axis and *q*-axis contributions of stator current, the mechanical equation of the IPMSM is implemented for computing the motor torque. By subtracting from T_{em} the constant resistance torque and the variable term – depending on the actual mechanical speed and on the damping factor γ – the mechanical angular acceleration is calculated. In the successive step, for simplicity, the integrator output is the electrical speed, obtained by multiplying the inverse dynamic equation for the pole pairs:

$$\begin{cases} \omega_e = \dfrac{pp}{J}\displaystyle\int \left(T_{em} - T_{r,const} - \gamma\omega_m\right) dt \\ \omega_m = \dfrac{\omega_e}{pp} \end{cases}$$

Finally, in the last section of the loop the electric angle is obtained by integration. This diagram can be also exploited for SPM structure, because once imposed $L_d = L_q$ the corresponding reluctance contribution disappears from the resultant electromagnetic torque. The plant loop is consequently used for both IPM and SPM field-oriented control algorithm without any substantial modifications. The dynamic equations are transformed into diagrams for computing all the motor variables, i.e. three-phase stator currents, motor torque, mechanical and electrical speed and angle. The corresponding LabVIEW blocks for i_d calculation are shown in figure 5.8. For i_q the mechanism is similar, but obviously with the opposite axis quantities. In the IPMSM loop, a better precision is used, in order to simulate

a realistic application, where the motor is physically connected to the engine control unit. In detail, 29-bit signed fixed-point words – with 11 bits for integer part – are used for the currents. It is worth noting that the discrete time normalized integrator increases the length of the input value of 16 bits, entirely dedicated to the integer section. A conversion FXP block in inserted on its output wire in order to reduce the word size, obtaining the desired 26-bit fixed-point. This changeover is applied on each integrator in the VI, for managing smaller quantities and for reducing the hardware resource consumption.

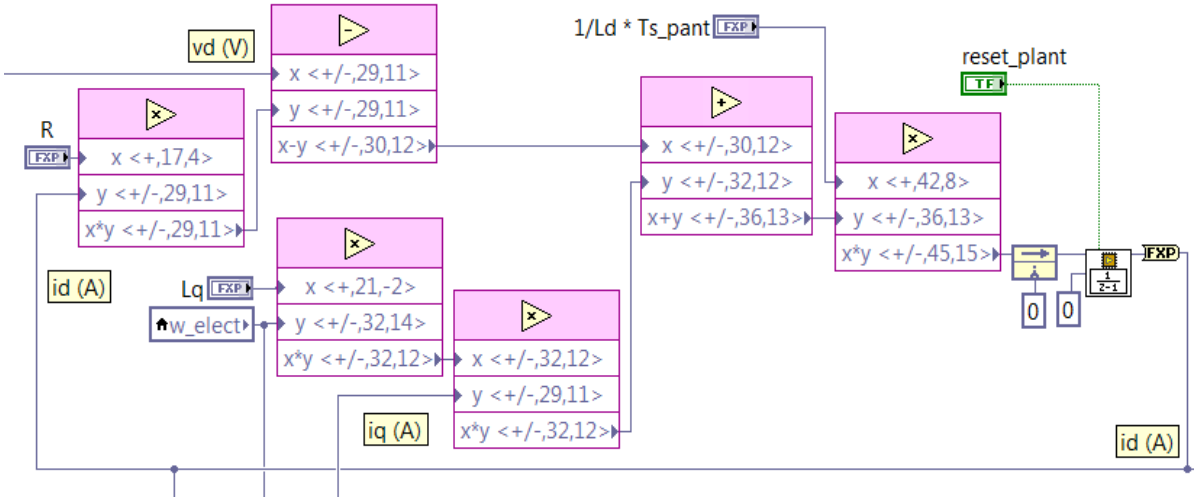

Figure 5.8: Block scheme for computing i_d.

The implementation in the FPGA VI of the mechanical equation is shown (fig. 5.9), for displaying how the rotor mechanical and electrical speeds are obtained from the motor and resistance torques, considering the moment of inertia of the machine. As introduced before, the integrator output is the quantity ω_e, because the number of pole pairs is multiplied for the discrete time interval of the plant loop. For the torque 30 bits are reserved (11-bit integer) for both motor and control schemes. For the angular velocities, in order to obtain accurate results and precise transformations, the word size is 32 bits (14-bit integer). The resistance torque and the damping value γ can be freely chosen. The constant terms and the motor parameters are directly passed from the real-time VI. To reduce the computational complexity, the combined values $\left(L_d - L_q,\ \frac{3}{2}\ pp,\ \frac{pp\ T_{s,plant}}{J}\right)$ are computed in the user interface. In the last sector of the plant loop – figure 5.10 – the electrical angle is estimated. The integrator is the most critical element: the reset is exploited for obtaining as output an angle in the range $[0,2\pi]$. In particular, when the output value is over 2π (or below zero), the integrator is reset and the difference between the output and 2π (or between output and zero) is added to the initial condition. In this way, the electric angle is confined in the desired

range. This quantity is normalized with respect to π, as the high throughput sine & cosine element requires. For the angular position 30 bits are reserved, with 7 bits for the integer part, while the 28-bit signed normalized value has just 3 bits for the integer. This elevated accuracy is fundamental for obtaining precise transformations in motor and FOC loops.

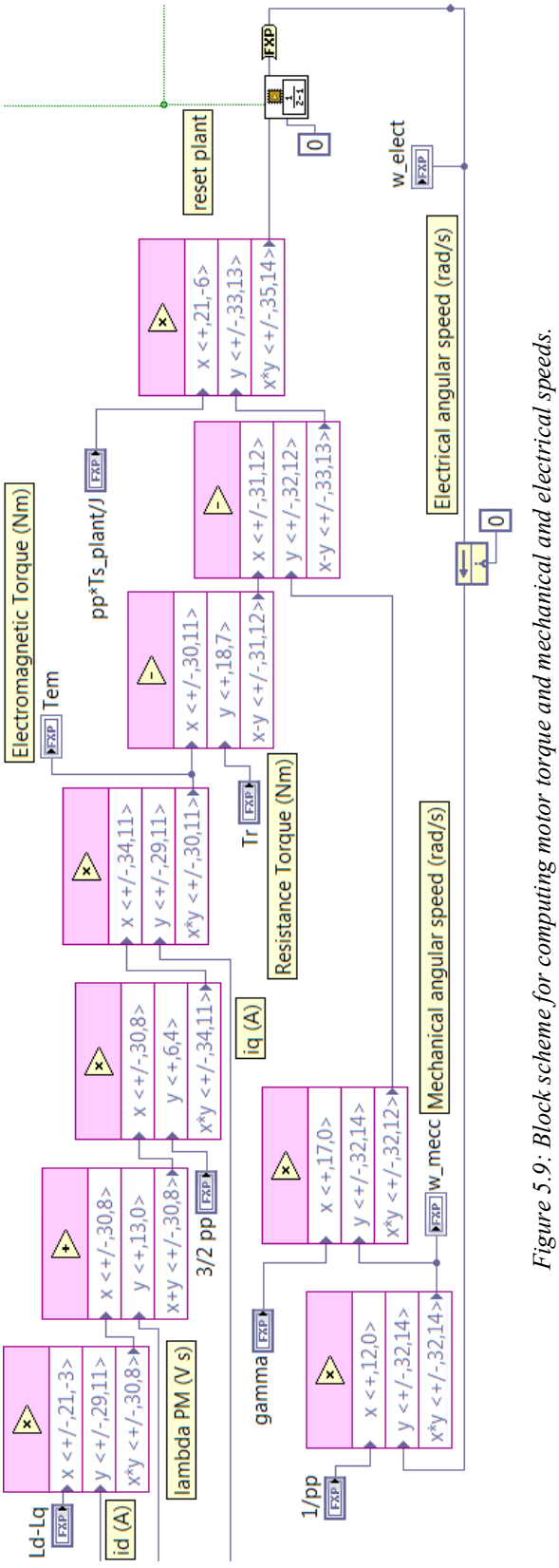

Figure 5.9: Block scheme for computing motor torque and mechanical and electrical speeds.

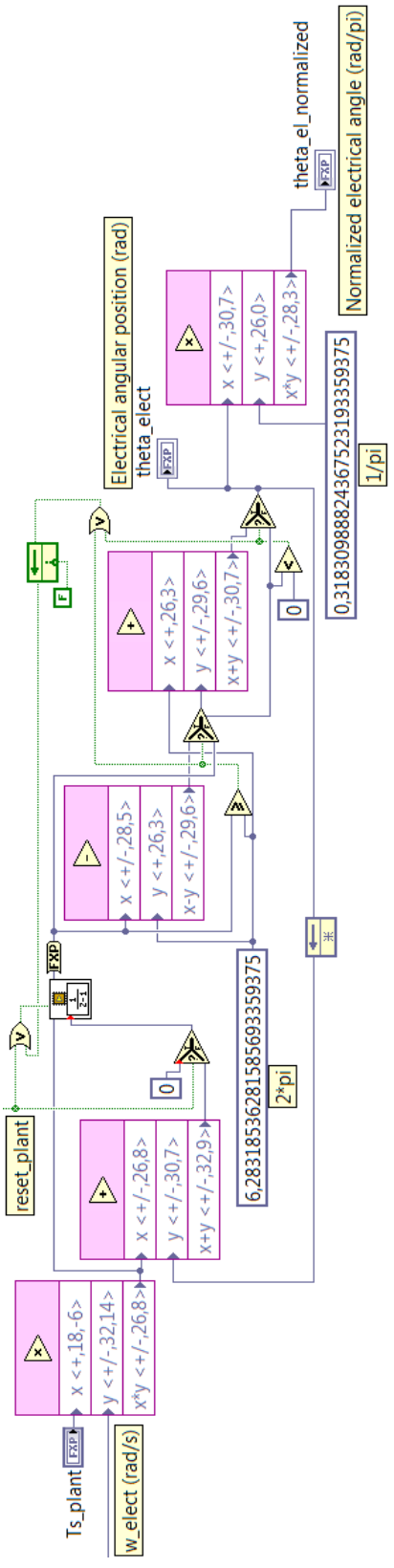

Figure 5.10: Block scheme for computing the electrical angular position and the normalized angle.

5.2.3 PI regulators, saturation blocks and anti-windup

The first application of the proportional integral regulators is to obtain the direct and quadrature contributions of the command voltages – which are then transformed in the corresponding three-phase quantities. The standard configuration requires, for computing as example v_q^*:

- a subtractor for evaluating the error, by comparing the reference quadrature current and the feedback value;
- a proportional branch, where the error is multiplied for the factor $K_{p,quadrature}$;
- an integrative branch, where the error is multiplied for $K_{i,quadrature}$ and for the sampling time of the control loop, and then it is passed to the normalized discrete integrator;
- finally, the two contributions are summed, and the command quadrature voltage is obtained.

For choosing the two multiplicative constants of each regulator, the strategy is the classic trial and error: once realized the control algorithm, in the real-time user interface the parameters are set for obtaining the best compromise in terms of dynamic performance, quickness, overshoot and ripple.

This mechanism can work correctly only if no saturation blocks are present. The discrete integrator works as an adder, so at each cycle it increases (or decreases) its value. However, if the output reaches the saturation value, the integrator keeps working, generating the hazardous windup problem. In other words, the integrator continues to accumulate, while the saturation block limits the output value. Consequently, when the reference signal magnitude decreases (i.e. the input error changes its sign), the output cannot vary immediately because the integrator must dispose of the stored error before providing the right result. This situation is evident analysing the following motor torque waveform (fig. 5.11) where different references are set, and the windup delay is shown.

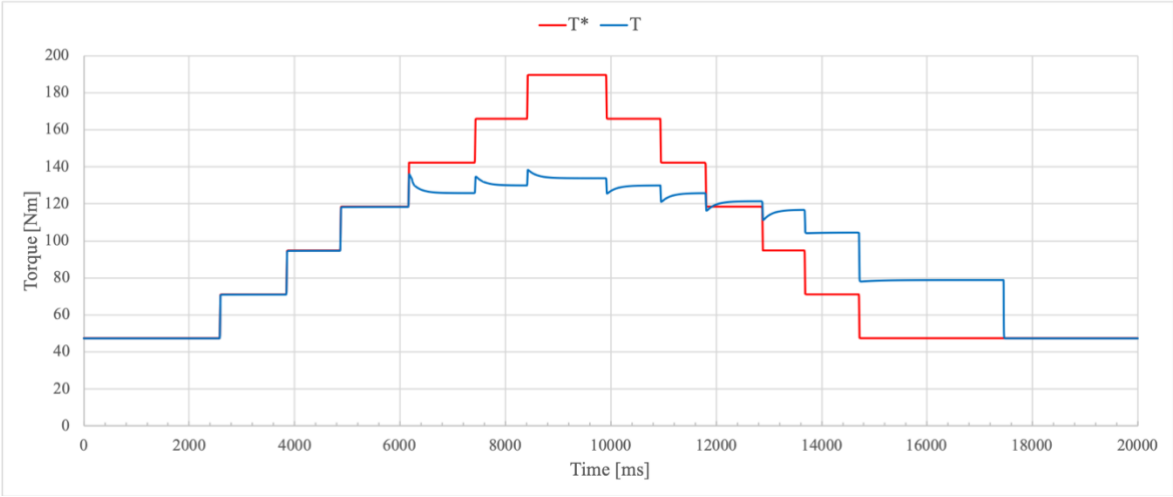

Figure 5.11: Delay in motor torque waveform (with respect to the reference value), due to windup problem.

Different techniques are adopted for solving the problem: in this project, the integral term is corrected by subtracting a value equal to the difference between the pre-saturation output and the saturated value. This contribution allows maintaining a fixed value on the integral branch, eliminating the delay. The torque waveform (fig. 5.12) is no more affected by any deteriorating effects. A similar anti-windup mechanism is used also for the PI that manages the speed request for computing the corresponding reference torque. In the other proportional integral regulators – used for flux-weakening and limitation of battery pack DC – a different strategy is implemented. In those cases, the saturation is present within the PI block, in order to limit the integral action based on the actual proportional contribution. The mechanism will be discussed in the successive sections.

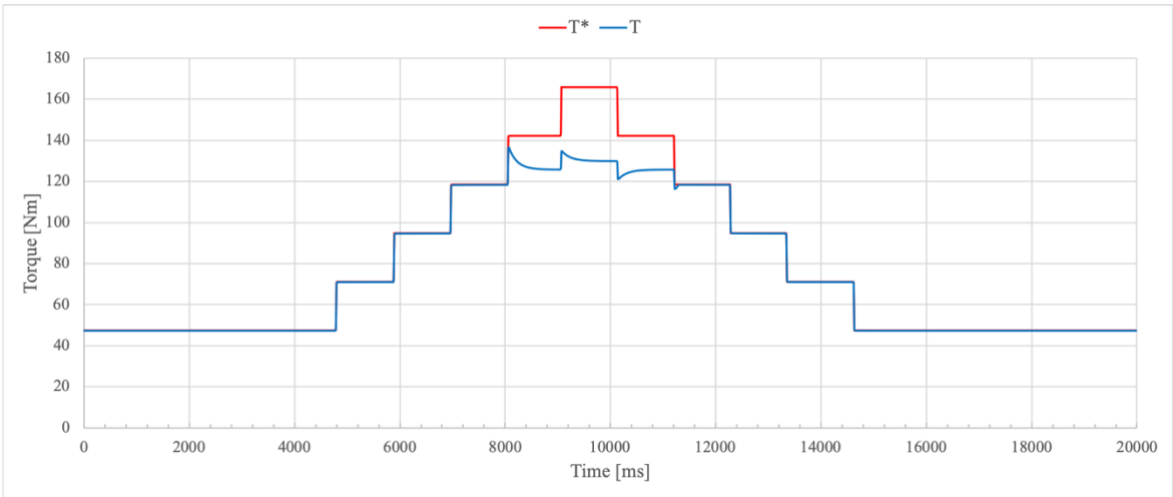

Figure 5.12: Anti-windup action, with different reference torques.

Analysing in the details the saturation blocks, two different structures are present in the model, one for the direct axis, the other for the quadrature one. In the first case, the saturation values for both i_d^*, v_d^* are fixed and they depend on the previously set maximum phase current and maximum phase voltage. For what concerns the quadrature axis, a dynamic vector saturation is considered in order to give priority to the direct contribution. This condition is essential for exploiting the flux-weakening region, because – as analysed before – by increasing the *d*-axis stator current magnitude, the flux in the air-gap can be reduced and the rotor is able to reach a mechanical speed higher than the nominal value. Otherwise, the quadrature axis quantity would stop the rotation of the current vector – this aspect is analysed in detail in the section dedicated to FW implementation. The complete PI for generating the reference v_q^* is displayed in figure 5.15, while the interconnection between saturation blocks and regulators in shown in the successive scheme (fig. 5.16).

$$\begin{cases} -I_{sat,phase} \leq i_d^* \leq 0 \\ -\sqrt{I_{sat,phase}^2 - {i_d^*}^2} \leq i_q^* \leq \sqrt{I_{sat,phase}^2 - {i_d^*}^2} \end{cases}$$

$$\begin{cases} -V_{sat,phase} \leq v_d^* \leq V_{sat,phase} \\ -\sqrt{V_{sat,phase}^2 - {v_d^*}^2} \leq v_q^* \leq \sqrt{V_{sat,phase}^2 - {v_d^*}^2} \end{cases}$$

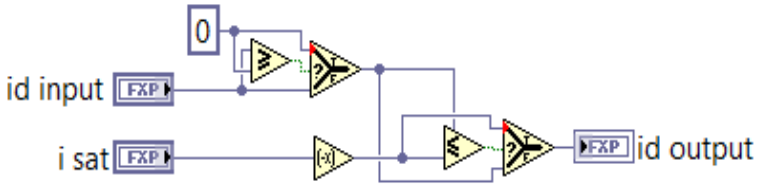

Figure 5.13: Scalar saturation of i_d^*.

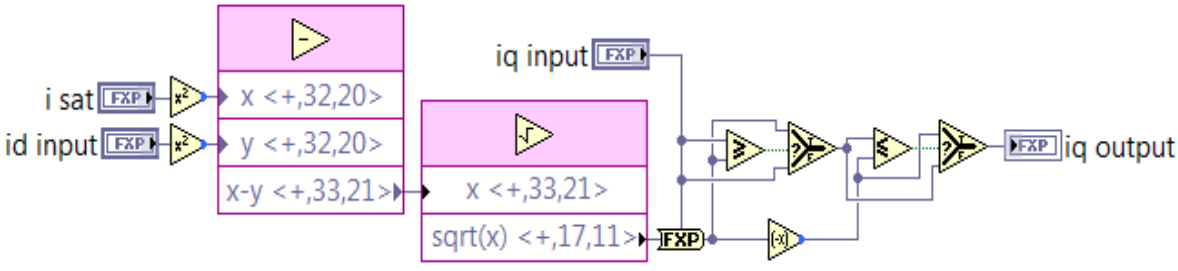

Figure 5.14: Vector saturation of i_q^*.

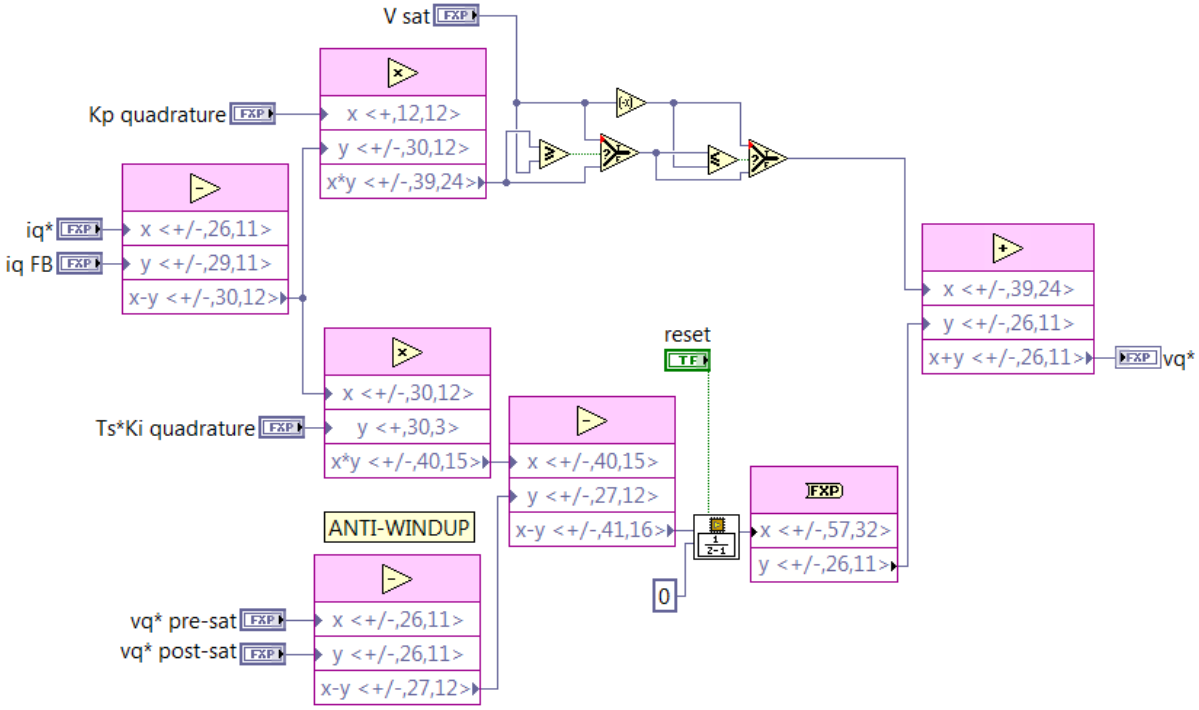

Figure 5.15: Reference quadrature voltage complete PI regulator.

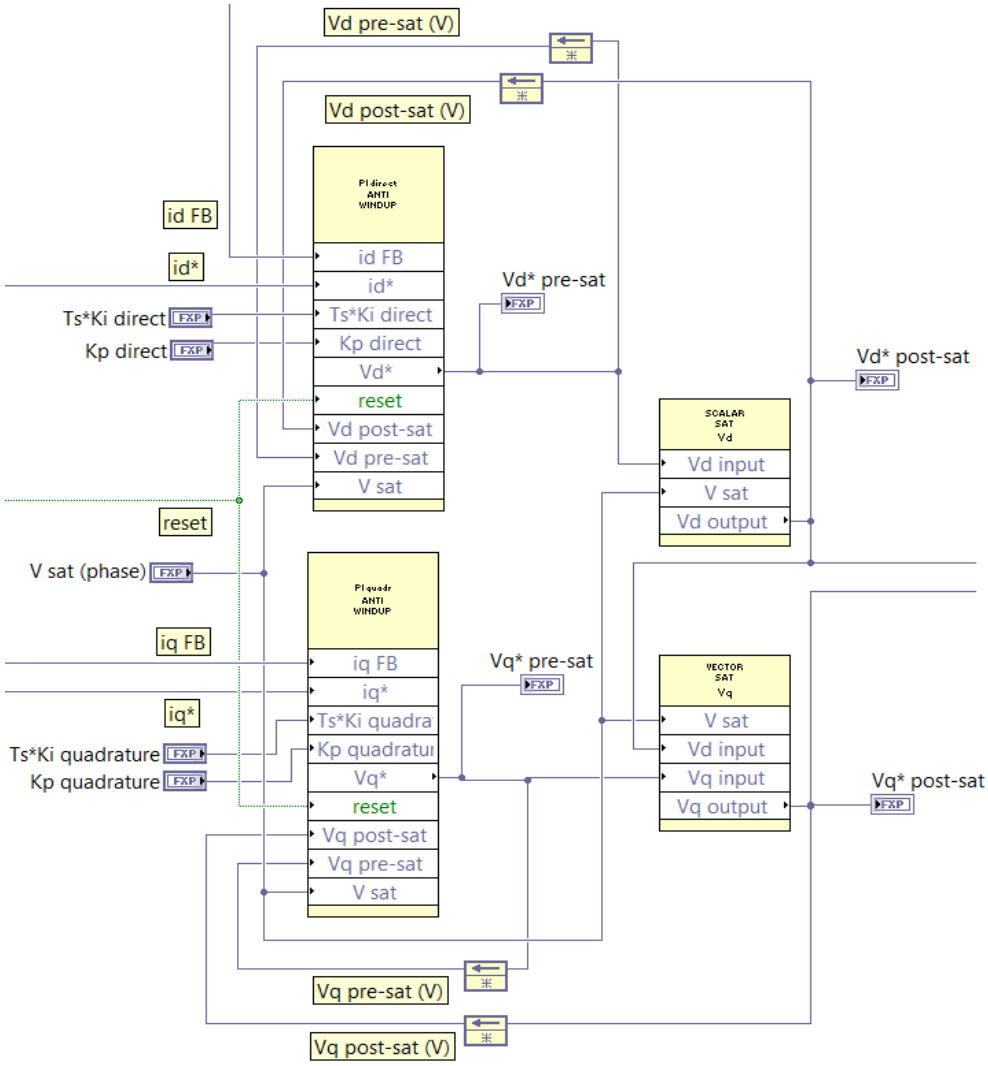

Figure 5.16: Connection between the PI regulators and the saturations for avoiding the windup condition.

5.2.4 Torque control loop and MTPA region

The first control loop implemented in the system is the torque-based one: the user can directly impose a torque demand that is then converted in reference stator direct and quadrature currents. Inside the vehicles, the user torque request is expressed as percentage of the maximum motor torque and it is obtained by mapping the accelerator and brake pedals. Through the real-time interface a certain percentage of the maximum torque can be set. In an IPM configuration, the direct contribution is fundamental for generating the additional reluctance torque for increasing the torque and power density of the machine. This condition is obtained in the maximum torque per ampere (MTPA) region. A deeper analysis of the PMSM mathematical model is required:

$$T_{em} = \frac{3}{2} pp\, i_q \left[\lambda_{PM} + \left(L_d - L_q\right) i_d\right]$$

considering that:

$$\begin{cases} i_d = -I \sin(\beta) \\ i_q = I \cos(\beta) \end{cases}$$

where I is the magnitude of the stator current vector and β is the so-called MTPA angle. Consequently, the previous equation becomes:

$$T_{em} = \frac{3}{2} pp \left[\lambda_{PM}\, I \cos(\beta) - \left(L_d - L_q\right) I^2 \frac{\sin(2\beta)}{2}\right]$$

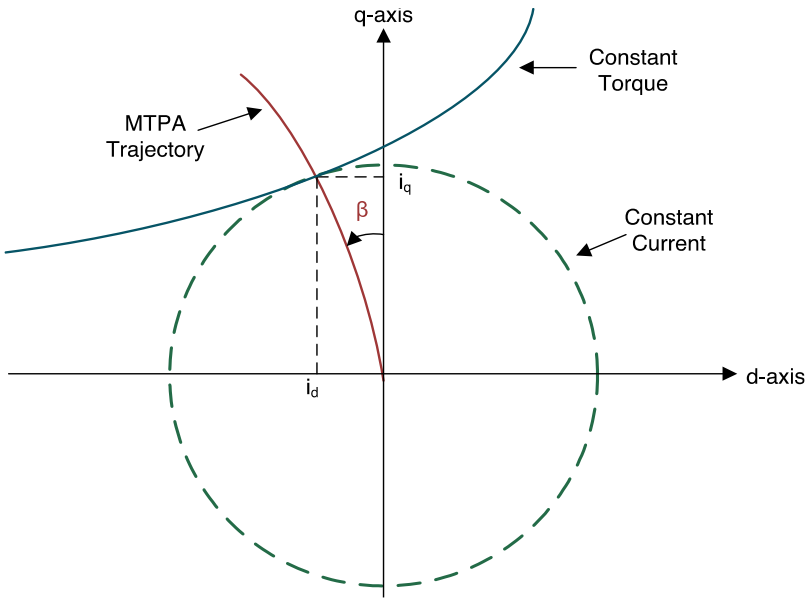

Figure 5.17: Maximum torque per ampere trajectory.[204]

[204] Lim, S. (2018, April), Texas Instruments, Retrieved from *Sensorless-FOC With Flux-Weakening and MTPA for IPMSM Motor Drives*: http://www.ti.com/lit/an/spracf3/spracf3.pdf, p. 4.

Now it is possible to optimize the system and to compute the angle which guarantees the maximum torque for different amplitude values of the stator current. A simple code is implemented in MATLAB for computing the direct and quadrature contributions in correspondence of the torque request:

```
%% Motor parameters
lambdaPM=0.044; %Vs, PM magnetic flux
Ld=0.000086;    %H, direct axis inductance
Lq=0.000215;    %H, quadrature axis inductance
pp=5;            %# pole pairs
Tmax=237;       %Nm, maximum torque

%% MTPA
T=[0:1.5:Tmax];
beta=[0:(pi/2/3000):pi/2]; %angle from positive q-axis to negative d-axis
for i=1:size(T,2)
    for j=2:size(beta,2)
        a=3/2*pp*(Lq-Ld)*sin(2*beta(j))/2;
        b=3/2*pp*lambdaPM*cos(beta(j));
        c=-T(i);
        delta=b^2-4*a*c;
        I1(j-1)=(-b+sqrt(b^2-4*a*c))/(2*a);  %positive value (used)
        I2(j-1)=(-b-sqrt(b^2-4*a*c))/(2*a);  %negative value (neglected)
    end
    [a b]=min(I1);
    Imtpa(i)=a;
    theta_mtpa(i)=beta(b(1));
end

%% OUTPUT LUTs
LUT_id=(-Imtpa.*sin(theta_mtpa))';
LUT_iq=(Imtpa.*cos(theta_mtpa))';
```

In the upper part, the motor parameters are set. Then, for each torque value in the range $[0,T_{max}]$, with a delta equal to 1.5 Nm, the amplitude of the stator current is computed in a for loop, where the MTPA angle varies. A 90° rotation is considered for β (from the positive part of q-axis towards the negative part of d-axis), with an accurate resolution to obtain an efficient algorithm. An array of possible magnitude I is obtained by inverting the previous equation for fixed torque and angle:

$$\frac{3}{2}pp\left(L_q - L_d\right)\frac{\sin(2\beta)}{2}I^2 + \frac{3}{2}pp\,\lambda_{PM}\cos(\beta)\,I - T_{em} = 0$$

Because it is a quadratic equation, two solutions are obtained: one of them is always negative, so it cannot be accepted for a magnitude quantity. In the resulting vector, corresponding to a specific torque value, the minimum is chosen, and it is assigned to a different array. Finally, using the angle β corresponding to that minimum magnitude, the direct and quadrature contributions are evaluated. Then, for the successive torque request

the loop is repeated and another array of possible magnitude I is established: through the minimization function, the optimal stator current is obtained and the new MTPA angle is used for computing i_d and i_q. In this way the look-up tables can be generated for both direct and quadrature stator currents. The number of elements in each array is 159, due to the maximum torque and the delta. The i_d sign should always be negative, while i_q depends on the torque sign. In fact, in this project also the negative request T^* is analysed and managed, realizing a simple reverse gear system (with a negative speed). Moreover, a negative torque is present in regenerative braking conditions, as it will be shown in the real-time results section. It is worth noting that the MTPA angle is different for each current amplitude: this means that the resulting curve in dq reference frame is not linear (fig. 5.17). In the constant torque region, for any possible request a different couple of values i_d, i_q is obtained.

Once realized the LUTs, in the real-time interface the mechanism for reading them is implemented: the arrays are then passed to the FPGA VI, where an interpolation strategy is used for evaluating the direct and quadrature reference currents from the torque request. The interpolation is fundamental, because due to hardware limitation, the dimension of the two arrays is restricted (159 elements for each of them) and a high delta (1.5 Nm) – and consequently low resolution – is used in the MATLAB code between two successive torque values. The algorithm is the following: the torque request magnitude is firstly compared with the minimum and maximum – reduced by the same delta used in the code – allowable values; then, a multiplication for the reciprocal of the torque is executed and the so-called x_{in} is obtained. This strategy allows simplifying the system, because the array index is directly extracted: from the range $[0{,}237]$ Nm the values are passed to the range $[0{,}158]$. The indexes for i_d and i_q are computed by using a floor operator to evaluate the next lowest integer (x_1) and an increment block for the next highest integer (x_2). The upper (y_2) and lower (y_1) values – with respect to the reference ones – of both direct and quadrature currents are pulled out from the arrays. The interpolation is realized through a simple linear approach:

$$y_{out} = y_1 + \frac{(y_2 - y_1)}{(x_2 - x_1)}(x_{in} - x_1) = y_1 + (y_2 - y_1)\,(x_{in} - x_1)$$

In fact, thanks to the multiplication of the torque for the reciprocal of the delta, the value $x_2 - x_1$ is constantly equal to one; so, the computation of the output reference i_d^* and i_q^* is facilitated. To manage also the negative request, a selector is used for switching from i_q^* to $-i_q^*$. A negative torque corresponds to a negative quadrature contribution, while the direct value remains unchanged and negative. The complete MTPA block is shown in figure 5.18.

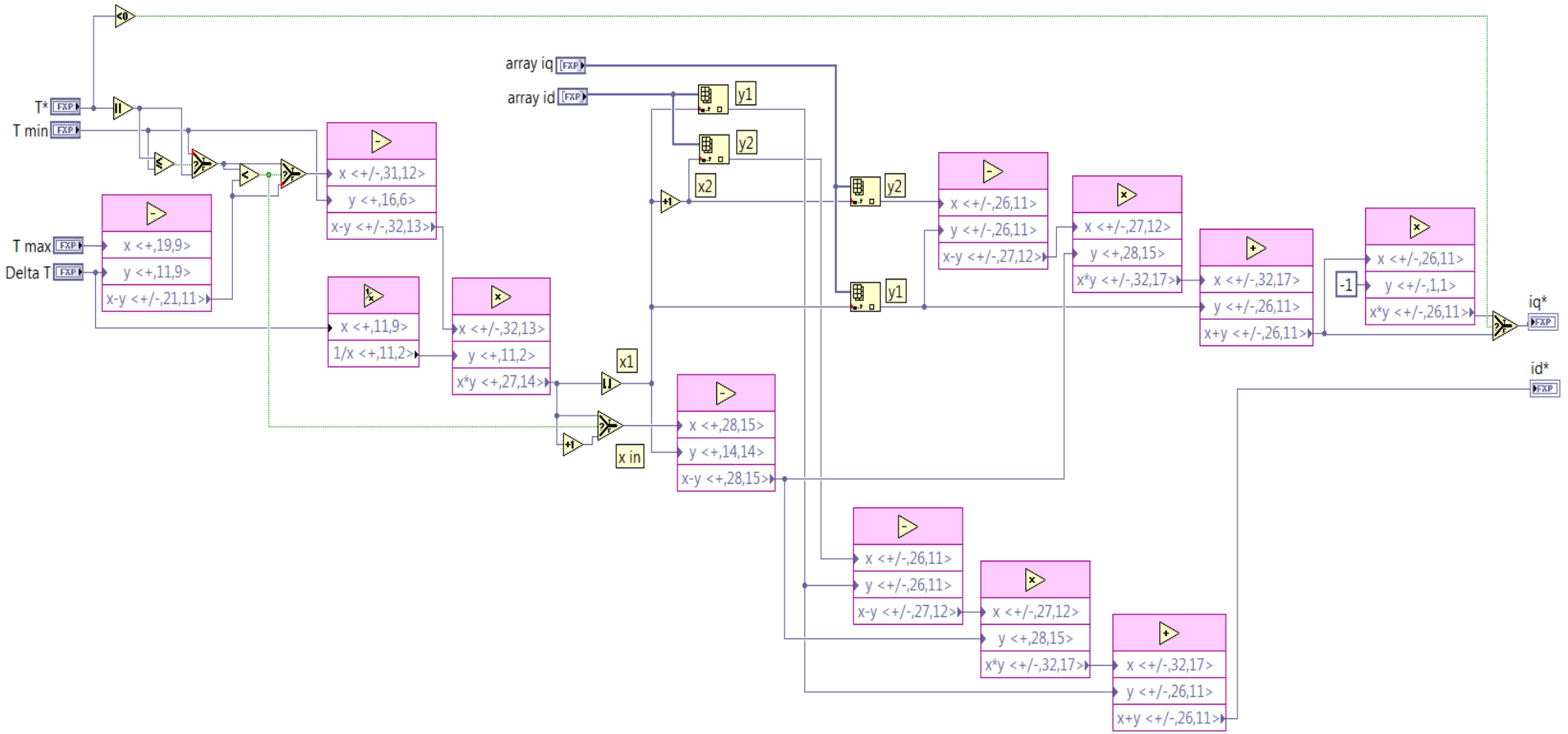

Figure 5.18: MTPA interpolation block diagram.

The previous analysis is valid just for the constant torque region. In flux-weakening condition (constant power) the MTPA block stops working, because the PI regulator is responsible for establishing the value i_d^*. In other words, the last MTPA *d*-axis current is used as initial condition for computing the value in correspondence to the request – arrived directly by the user or filtered by the I_{DC} regulator. The reference quadrature contribution is obtained by inverting the torque equation, knowing i_d^* and T^*:

$$i_q^* = \frac{T^*}{\frac{3}{2} pp \left[\lambda_{PM} + \left(L_d - L_q\right) i_d^*\right]}$$

Then, saturation blocks are used in order to give priority to the direct axis and to limit the quadrature value, depending on the maximum amplitude of the phase current and on the actual direct reference i_d^*. The working principle of the flux-weakening PI regulator will be analysed in successive sections.

By implementing this mechanism in real-time, many overshoots, ripples and hazardous peaks are detected. The step variation of the user request, in fact, is responsible for deteriorating the dynamic performance of the control system. For counterbalancing this problem, an improvement is inserted in the chain: the torque and speed references are converted into ramp signals through dedicated blocks. Consequently, the velocity of the response is reduced, but the stability is increased. For realizing the mechanism, the impulsive demand is constantly compared with the output value of the block at the previous cycle – a feedback node is used for this purpose. If the reference step is positive, the feedback quantity is constantly increased by the chosen slope multiplied for the discrete time interval of the control loop – control and plant loops have different integration steps in order to reflect their different dynamic behaviours. In case of a reduction of the torque (or speed) request, the output value of the block is decreased by again the multiplication of the slope for the controller discrete integration step. Once the block output has reached the reference value, the selectors are managed to maintain a fixed value, until a different request arrives. For torque quantities, in order to obtain accurate results, 30-bit fixed-point words are used, with 11 bits for the integer part – to completely cover, with an adequate resolution, the maximum range ($T_{max} = 237$ Nm). Furthermore, in the final configuration of the control system the user request, if necessary, is filtered and limited by the PI that manages the actual DC of simulated battery pack and inverter, depending on the maximum and minimum limits – which arrive through the CAN bus. Because the regulator is at the beginning of the chain, for the other blocks – i.e. the regulators, the transformations, the MTPA block – the working principle remains unchanged.

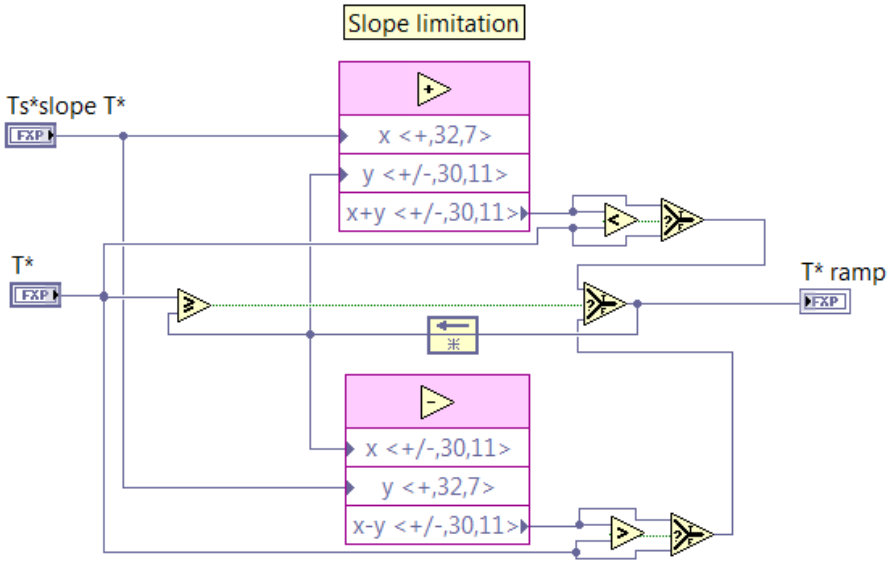

Figure 5.19: SubVI for converting the step torque request into a ramp reference signal T^*.

5.2.5 Speed control loop

As additional feature, for stopping completely the motor or for implementing the cruise control strategy, the speed control scheme is realized in the while loop. A proportional integral regulator is adopted for computing the reference torque from the speed error. In this block, the speed request arrives directly from the user or it is limited by the direct current PI; then, the feedback electric angular velocity is passed through a local variable from the motor loop, in order to compare it with the reference value and to evaluate the input error for the integral and the proportional branches. The output is the corresponding reference torque: in this way, the other elements of the scheme remain unchanged, because T^* is then passed to the MTPA block and so on. Because there is a saturation in the PI, the accumulation problem is present due to the fact that the output value is limited between the minimum and maximum admissible torques for the configured motor. To overcome this hazardous condition, the anti-windup strategy in inserted: the integral term is reduced by a quantity equal to the difference between the saturated output signal and the pre-saturation value. A further optimization requires the limitation of the proportional branch value, just to reduce the anti-windup action on the integrator and to increase the performance.

For the electrical speed reference value, the same issues of the torque loop are analysed. First, the reference value is filtered by the regulator which manages the direct current of the battery pack. Based on the actual current limits, the PI could operate or not: if it is working, the user speed request is reduced, and the effective reference value is sent to

the ramp block and compared with the actual rotor electrical velocity. Otherwise, the user directly imposes the reference velocity. In the initial configuration, on the real-time interface the electrical speed was settable. For a more realistic system, it has been decided to express the request is mechanical RPM: once imposed the reference value in real-time, this quantity is converted into mechanical and then electric angular velocity (evaluated in rad/s) and passed to the FPGA VI:

$$n_{RPM} = \frac{60}{2\pi}\omega_m = \frac{60}{2\pi}\frac{\omega_e}{pp}$$

For the request – directly imposed or limited by the PI – also in this case a block is inserted for converting the step signal in a ramp. In this way, harmful glitches, overshoots and ripples are reduced, by selecting a proper slope. The mechanism is the same described for torque loop, with a feedback node for increasing the output of this block at each cycle. For electrical speed fixed-point, 31 bits are used for the signed word and 15 of them are reserved for the integer: this guarantees a large range of values, in order to exploit also the flux-weakening region for increasing the velocity – without risking any fixed-point saturations.

A practical issue is related to the switching mechanism between torque and speed loops. During the simulation, many peaks are present when the system passes from the torque-based control strategy to the other one. This problem is mainly related to the integral branch of the PI which tries to reduce as soon as possible to input error. In order to limit this drawback, two countermeasures are implemented. First, through the user interface, the integral factor $K_{i,speed}$ is regulated so that the corresponding contribution acts slowly. Then, in the FPGA VI scheme, the additional block for estimating the actual motor torque is inserted. In fact, in real applications of the engine control unit the instantaneous torque is not directly available, so it cannot be passed from the PMSM loop to the field-oriented control algorithm. Based on motor parameters (magnetic flux of permanent magnet, number of pole pairs, direct and quadrature inductances) and feedback values of stator direct and quadrature currents, the actual torque can be easily evaluated – using the same high throughput mathematical elements of the plant model. The computed value is provided as input to the PI that manages the speed request and it is used as initial value for the integrator. In practice, every time that the user activates the speed control, the integral branch of the PI is reset at its initial value. Consequently, the peaks are reduced because the output of the regulator starts from the instantaneous estimated motor torque. Integral and proportional actions are less sharp, guaranteeing better performance in the real-time simulation.

5.2.6 Flux-weakening for an IPMSM

One of the most complicated challenges of the project is the constant power region management, for increasing the speed range of the motor over the base value. From the theory, it is worth noting that the flux-weakening area starts when the phase (and consequently line) voltages – as well as the delivered power – reach the saturation condition. On the other hand, the phase currents are still free to vary, because there is a margin compared to the maximum value. For exploiting the rotation of the current phasor, a proportional integral regulator is used for rising the magnitude of *d*-axis negative contribution. In fact, the increase of $|i_d|$ – because this contribution remains always negative – causes a weakening of the air-gap magnetic flux. A demagnetizing magnetomotive force is induced by the stator current, through the direct-axis component manipulation, to counteract and to reduce the apparent MMF due the permanent magnets flux. The control mechanism can be subdivided in three successive operating modes, depending on the delivered torque and the actual mechanical angular velocity. The situation is shown in the *dq* reference frame and in motor characteristics of figure 5.20:

1. from O to A, the trajectory represents the previously described MTPA region, where the current phasor *d*- and *q*-axis components are set for guaranteeing the highest torque with the lowest possible current;
2. for increasing the speed over the base value, the motor enters the flux-weakening condition – from A to C – so the reference i_d^* is increased through the PI regulator; here, the voltage magnitude has reached the nominal value. In the first part, the constant torque curve is travelled, from A to B. Then, the delivered torque is decreased, while the power remains constant – thanks to the increasing motor speed. Consequently, the current vector rotates towards the *d*-axis, and it is saturated in order to remain in the maximum current circle;
3. finally, the maximum torque per voltage (MTPV) condition – from C to D – can be exploited for obtaining a higher maximum speed. In the project this further implementation is neglected.

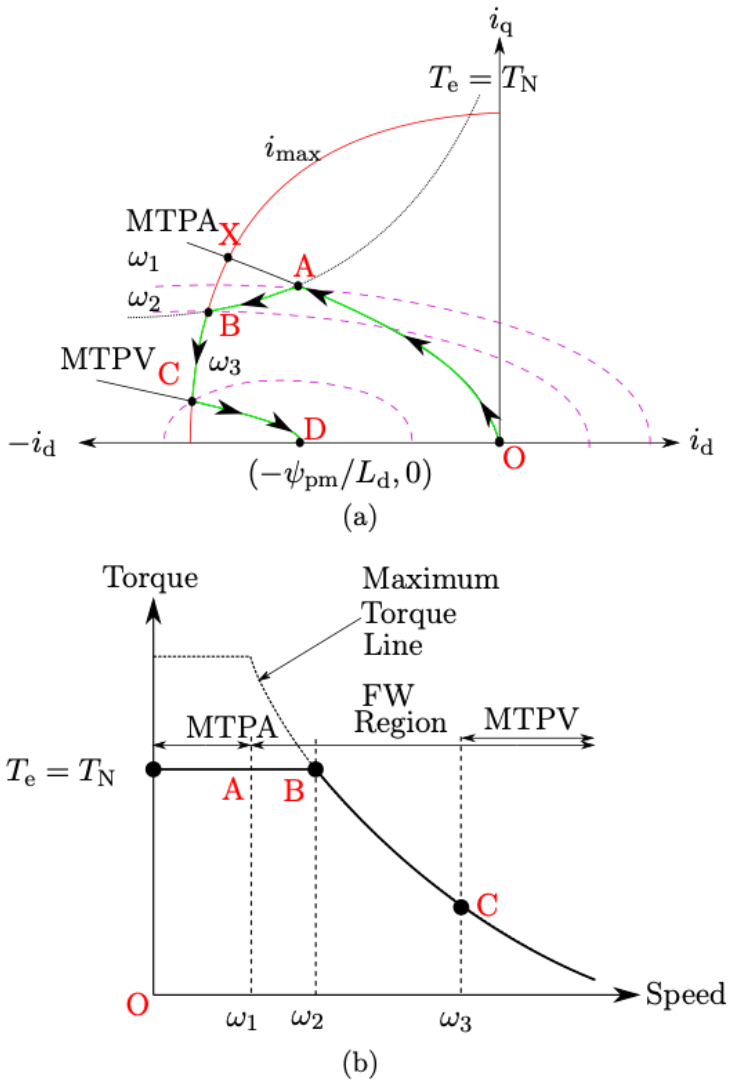

Figure 5.20: (a) Current trajectory using MTPA, FW and MTPV regions; (b) Torque - speed characteristics.[205]

The theoretical analysis is converted into block diagram by comparing the pre-saturation module of the phase voltage with the saturation value ($V_{sat,phase} = 231$ V). To realize this, the *dq* reference command voltage – so the PI regulator outputs $v^*_{d,pre-sat}$ and $v^*_{q,pre-sat}$ – are vectorially summed, for obtaining $|V^*_{pre-sat}|$. A low-pass Butterworth filter is inserted in the chain in order to reduce the oscillations of the computed quantity. The filter parameters are set through the real-time interface, as usual. In the regulator, the error is computed, and the proportional and integral branches are added for providing the reference i^*_d. Any possible delay due to windup condition must be avoided inside the system: because

[205] Khan, W. (2016), *Torque Maximizing and Flux Weakening Control of Synchronous Machines (Thesis)*, Helsinki, Finland: Aalto University, p.18.

the direct contribution has to remain in the range $[-I_{sat,phase},0]$, the integrator risks to accumulate error when one of the two saturation values is reached. Consequently, the integral term must be reduced for maintaining a constant output. This operation is done in a different way with respect to previous PIs – which manage the direct and quadrature voltages and the speed control loop – because the priority is assigned to the proportional term. In practice, the latter is saturated in the range $[-I_{sat,phase},0]$, while the integral contribution undergoes a dynamic saturation, because its minimum value depends on the difference between the saturation phase current and the instantaneous proportional value:

$$\begin{cases} -I_{sat,phase} \leq i_{d,prop}^{*} \leq 0 \\ -(I_{sat,phase} - i_{d,prop}^{*}) \leq i_{d,int}^{*} \leq 0 \end{cases}$$

Finally, the anti-windup mechanism is completed by subtracting to the input of the integrator the difference between the pre-saturation and the post-saturation values of the integral branch. In this way the accumulation is deleted. This mechanism is not sufficient, because the output of the PI always starts from a null value when the IPMSM enters the FW zone. For overcoming the problem, the last MTPA i_d^* value – before the PI begins working – is passed to the integrator as initial condition. Consequently, the *d*-axis current is regulated from this value, instead of starting from zero, and the motor keeps track of the maximum torque per ampere region. It is worth noting that the maximum torque in constant power region decreases with respect to the corresponding motor parameter ($T_{max} = 237$ Nm). In fact, for increasing the speed the torque must decrement in an inverse proportional manner. The current phasor rotates – respecting always the limit circle – and it reaches a lower torque curve with respect to the nominal one.

The working principle in the constant power region is described in this section. First, the amplitude of the filtered pre-saturation phase voltage is compared with the maximum value $V_{sat,phase}$ through a hysteresis nonlinear block. The two different thresholds (upper and lower) are fundamental for avoiding a continuous oscillation. For practical reason and for reducing any dangerous ripple, a debouncing SubVI is designed (fig. 5.21). The first transition of the Boolean input (false/true or true/false) is reflected in the output, while the successive settlement variations are neglected for a certain configurable number of cycles.

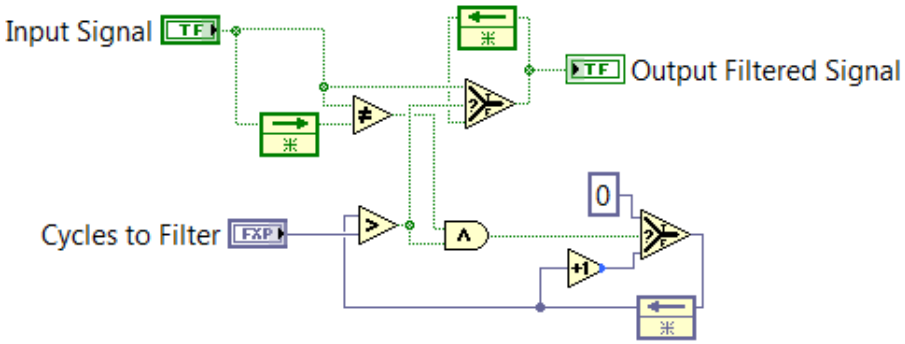

Figure 5.21: Debouncing FPGA SubVI for filter the Boolean signal oscillations.

The resulting Boolean signal is used for establishing whether the motor is in constant power region or not: true if this condition is verified, false if not; it also acts as reset of the PI which starts regulating the *d*-axis reference current from the last computed – before the signal (called *FW Status* in LabVIEW) becomes true – MTPA value i_d^*. Once computed the *d*-axis reference in flux-weakening condition, the corresponding i_q^* is evaluated by inverting the torque equation:

$$i_q^* = \frac{T^*}{\frac{3}{2} pp \left[\lambda_{PM} + \left(L_d - L_q\right) i_d^*\right]}$$

In fact, the reference torque is available because it is directly set by the user or obtained by the PI which manages the speed control loop. This request may be filtered, depending on the battery pack (and inverter) DC actual value. Referring to the diagram of figure 5.20, from point A to B the *d*- and *q*-axis contributions maintain a constant torque. Once reached the limit current circle – so the phasor current has a magnitude equal to $I_{max,phase}$ – for increasing the motor speed, the vector is rotated. The computed i_q^* is no more significant, because it would cause the overcoming of the IPMSM boundary value. The vector saturation block is used for limiting the *q*-axis reference value, depending on the actual saturated i_d^* and on the motor maximum phase current. The remaining blocks of the diagram work as in constant torque region, while the MTPA SubVI is ignored.

When the system enters in the FW region, the control algorithm acts in the previously described way. A deeper analysis is required when the motor decreases its mechanical velocity and returns in the constant torque operating mode. In fact, the integral action is not instantaneous because it depends on the chosen factor $k_{i,FW}$. On the other hand, the MTPA block acts by interpolation so it provides immediately (neglecting the required cycles for the high throughput elements) the output reference values i_q^* and i_d^*. This difference in the dynamic behaviour causes peaks when the motor leaves the FW region – when the motor

enters that region the degrading effect is not present, because it passes from a faster regulation to a slower one. In order to overcome the problem, two different mechanisms are used for passing from the flux-weakening PI action to the MTPA – one for the quadrature axis, the other for the direct one. The first one is less complicated, because its value is a consequence of the actual $\left|V^*_{pre-sat}\right|$. In fact, when the pre-saturation phase voltage magnitude falls below the lower threshold of the hysteresis, the Boolean signal *FW Status* becomes false and a selector is used for switching to the corresponding MTPA value – which depends on the torque request. Concerning the direct axis, it has the highest priority and its regulation must be more accurate: because the PI starts working from the last MTPA reference value, it has to be stopped only when it reaches again a MTPA i^*_d. The selector is managed by a signal derived from the negate *FW Status* and the comparison between the actual output of the MTPA block and the flux-weakening PI *d*-axis reference current. When the second value is smaller than the first and the voltage magnitude is below the lower threshold – so *FW Status* is false – a logic AND generates a true signal and the selector switches to the MTPA value. The remaining parts of the block scheme are unchanged. The complete PI which manages the *d*-axis current in constant power condition is shown in figure 5.22.

Another tested technique for managing the flux-weakening region is based on a feedforward strategy.[206] The method uses the reference speed and the maximum phase voltage value for computing the reference *d*-axis current:

$$i^*_d = \frac{-2L_d + \sqrt{4L_d^2 - 4(L_d^2 - L_q^2)\left(1 + L_q^2 I_{max}^2 - \frac{V_{max}^2}{\omega^2}\right)}}{2(L_d^2 - L_q^2)}$$

Then, the quadrature contribution is set at the maximum possible value:

$$i_q = \sqrt{I_{max}^2 - {i^*_d}^2}$$

The corresponding maximum electromagnetic torque T_{ef} is computed from the previously obtained *dq* quantities. This value is compared with the command torque T_{ec}: if T_{ef} is higher than T_{ec}, the request torque is equal to the lower one; if the maximum value is lower, T^* equalizes T_{ef}. Finally, the definitive quadrature reference current is obtained by inverting the IPMSM torque equation, as usual. One drawback is the substantial required

[206] Lu, D., & Kar, N. (2010), *A Review of Flux-weakening Control in Permanent Magnet Synchronous Machines*, Presented at *IEEE Vehicle Power and Propulsion Conference.* Lille, France, pp. 2-3.

computational effort, because more high throughput elements are inserted in the chain. Moreover, the absence of a feedback line causes worse dynamic performance and decreases the stability. Once inserted in the block diagram, the simulation of the control algorithm shows significant degrading results. For this reason, the feedforward technique is neglected. A possible further implementation could be a hybrid solution, where the computed i_d^* and the feedback variables are combined in order to increase the accuracy. Obviously, this analysis must take into account the load and, in particular, the resistance torque contribution. Depending on the intersection between the load torque curve and the motor torque, different speed values are reached and the IPMSM could enter the flux-weakening region or not.

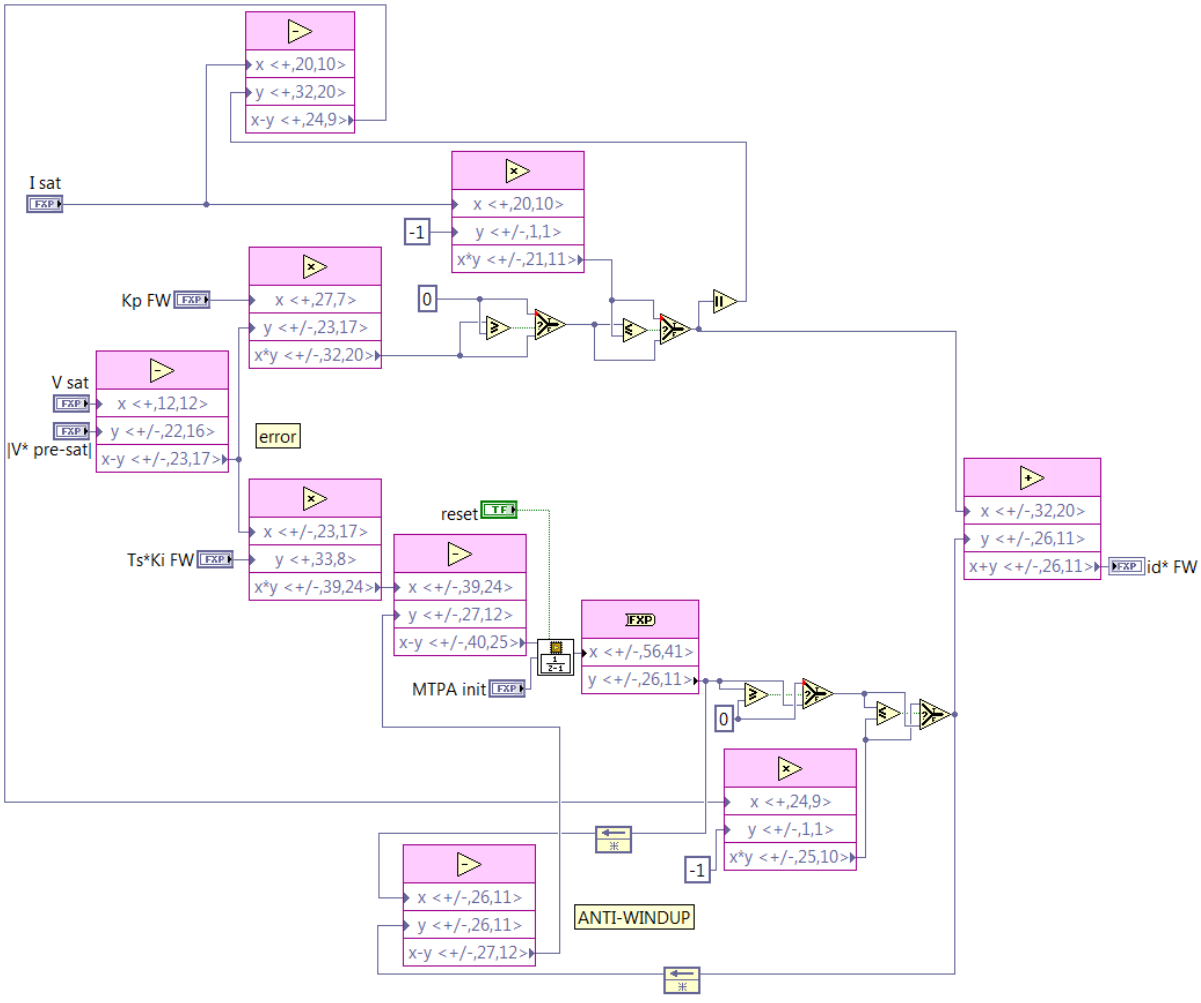

Figure 5.22: PI for regulating the d-axis reference current in flux-weakening region.

5.2.7 Battery pack direct current regulation

The project concerns a possible application of the control strategy in a battery electric vehicle. Consequently, the battery pack DC is a parameter that has to be continuously controlled and regulated, if necessary. In case of hazardous conditions for the battery, the BMS is responsible for imposing more stringent limits for the charging and discharging current rates, with respect to standard safety boundaries. The constraints influence the complete control algorithm, because they are used for filtering the external request: for this reason, the proportional integral regulator is inserted at the beginning of the chain. First of all, the actual current on the DC branch is estimated through a dedicated block. Because this electric quantity flows from the battery towards the inverter in discharging phase – and in the opposite direction during the recharge – it can be computed by using the equation of the three-phase DC/AC converter:[207]

$$\hat{I}_{DC} = 3\frac{V_{RMS,phase} I_{RMS,phase}}{V_{DC}}\cos(\varphi) = \frac{3}{2}\frac{V_{pk,phase}\, I_{pk,phase}}{V_{DC}}\cos(\varphi)$$

where:

- $\hat{I}_{DC}$ is the estimated DC;
- V_{DC} is the constant voltage on battery pack and inverter terminals;
- $\cos(\varphi)$ is the so-called power factor, i.e. the angle between the current and voltage phasors;
- $V_{RMS,phase} = \frac{V_{pk,phase}}{\sqrt{2}}$ is the root mean square value of the phase voltage, while $V_{pk,phase}$ is the corresponding amplitude (or peak value) of phase voltage;
- $I_{RMS,phase} = \frac{I_{pk,phase}}{\sqrt{2}}$ is the root mean square value of the phase current, while $I_{pk,phase}$ is the corresponding amplitude (or peak) value.

Because the direct current is assumed to be negative during the charging phase, the sign of the estimated $\hat{I}_{DC}$ is the same of the actual feedback i_q. For the evaluation of this quantity, the constant parameter $\frac{3}{2}\frac{\cos(\varphi)}{V_{DC}}$ is passed directly through the real-time interface for reducing the computational complexity of the scheme. The peak value of phase current corresponds to the magnitude of the phasor, so the feedback i_d and i_q are added vectorially in another SubVI – they are the two components of the vector in the *dq* reference frame. For the phase

[207] Mohan, N., Undeland, T., & Robbins, W. (2003), *op. cit.*, p. 263.

voltage peak, the same operation is executed, using the post-saturation direct and quadrature voltage commands in the vector sum. Once obtained all the necessary quantities, the block diagram for estimating the inverter (and battery) DC works properly.

In the PI regulator, the comparison between $\hat{I}_{DC}$ and the positive and negative limit currents happens. Depending on the sign of the estimated DC, one of the two errors is selected. Then, through the proportional and integral branches, the current contributions are computed and added. Finally, the resulting value is subtracted from the user request magnitude, in such a way to reduce the reference quantities only if the PI is effectively working – so if the estimated DC exceeds one of the limits. The user request could be either torque or speed – a selector is managed by a Boolean which sets the desired control strategy, also in presence of a negative demand. Moreover, a relay – i.e. a hysteresis – is inserted in the block diagram for establishing whether the PI has to limit the user request or not. If the magnitude of $\hat{I}_{DC}$ is below the maximum charging and discharging currents, the regulator is totally neglected, and the reference values are not filtered. On the other hand, when $\hat{I}_{DC}$ tries to overcome the discharging limit $I_{DC,pos}$ or the charging one $I_{DC,neg}$ the request is reduced and the Boolean indicator (*PI DC active* in the SubVI) is true, for indicating that the PI is operating. The hysteresis is fundamental for avoiding a hazardous ripple when the actual DC is close to the boundaries. In this block, two different couples of multiplier factors are considered, depending on the active control loop. Selectors are inserted for switching from the speed set ($K_{p,DC-\omega}$, $K_{i,DC-\omega}$) to the torque set ($K_{p,DC-T}$, $K_{i,DC-T}$), and vice versa.

A particular attention is dedicated to the saturation mechanism: in this situation, the output of the adder must never exceed the user demand. The priority, as well as the PI that manages the flux-weakening region, is given to the proportional term, which is saturated between zero – when the PI is not needed – and the actual external request. The integrator acts for compensating the other contribution and its saturation value is dynamic, because it is equal to the difference between the user request and the output of the proportional branch. Consequently, the integrator has a limited activity. For all the proportional integral regulators – where a saturation is present, like in this situation – the windup problem must be counteracted for avoiding any delaying accumulation. Similarly to the FW controller, the difference between the pre-saturation and post-saturation values of the integral branch is subtracted from the input of the discrete time integrator. Thank to this operation, the latter stops increasing its output and the windup is cancelled. When the external charging and discharging maximum DC values are very stringent, for example equal to zero in presence of a dangerous operating condition, the filtered request will be null and the saturation of the

two contributions acts in such a way that the adder output equalizes and totally counterbalances the user demand. Concerning the dimension of the variables, knowing the IPMSM parameters, 26 bits are used for the signed estimated battery and inverter DC, with 11 bits in the integer part. The charging and discharging limits can be less precise, so 19-bit words are used (with always 11-bit integer). For the signed output limited request, because it could be either torque or speed, 31 bits are reserved, with 15 bits for the integer section. At the beginning, the maximum values of charging and discharging battery pack direct current are configurable by the user in the real-time interface – this condition is useful for testing the efficiency of the PI. Then, once implemented the CAN communication, the limits are provided to the engine control unit by a simulated battery management system. Vector CANalyzer tool is used for sending the periodic message containing this information. The proportional integral block diagram is shown in figure 5.23.

Two additional issues are analysed during the real-time simulation, and the FPGA VI is modified in order to overcome the degrading effects. First, in case of loop strategy variation (from torque to speed or vice versa) in correspondence of an active PI for regulating the DC, many peaks and dangerous overshoots are generated. In order to avoid the problem, the switching mechanism is disabled when the regulator is working. By exploiting the Boolean output indicator (*PI DC active*) and by using logic gates for comparing the different signal states, the speed loop button is deactivated. The second consideration regards the limit of the negative torque. Typically, in automotive application a boundary – for example equal to 30% of the maximum – is imposed for the torque. The user cannot demand a lower value and the developed electromagnetic motor torque must stay above the constraint – for this purpose, a saturation is used in the PI used for passing from the speed error to the T^*. In other words, the torque must stay in the range $[T_{neg.limit}, T_{max}]$ where $T_{neg.limit}$ is negative. The boundary is configurable in the real-time interface through a dedicated control. In case of stringent maximum DC in charging or discharging conditions, a regulation is applied on the external request. Consequently, also the admissible lowest torque value must be reduced, otherwise in case of speed loop control strategy the direct current could exceed the limit. A proportional integral regulator is inserted in the SubVI for reducing the magnitude of $T_{neg.limit}$ similarly to the limitation of user requests. This PI operates only when a negative DC is estimated – corresponding to a negative i_q and so a negative motor torque. The implementation of this additional controller is not shown because it is identical to the previous one: the priority is given to the proportional branch and the anti-windup mechanism is internal in the SubVI.

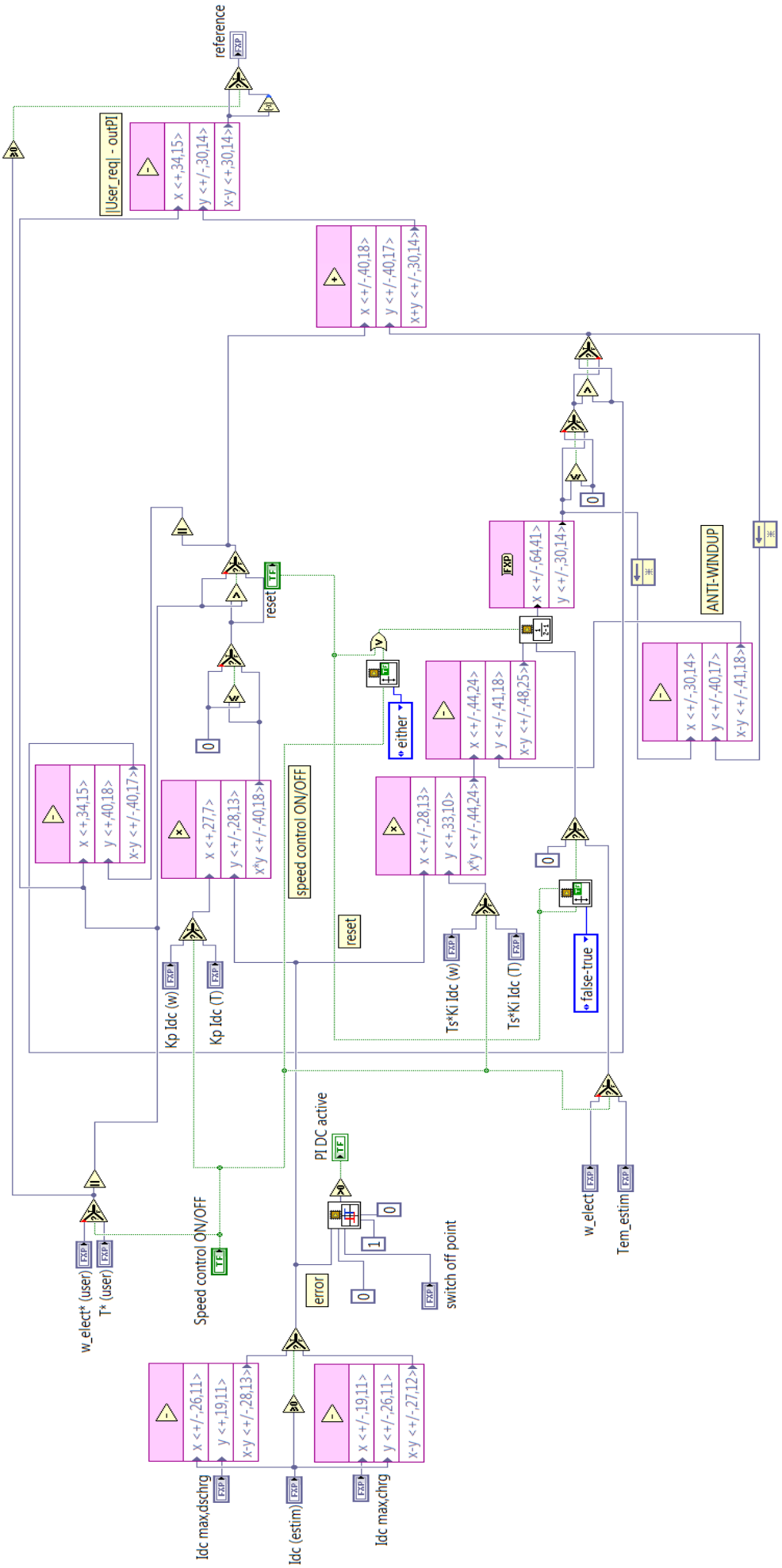

Figure 5.23: PI for regulating the battery pack (and inverter) direct current, depending on the charging and discharging constraints.

5.2.8 Real-time interface and results

Once compiled the field-oriented control and motor loops, the user interface is created by using the LabVIEW Real-Time Module on the development computer in Teoresi laboratory. A 1 kHz timed loop is used for running the FPGA VI: the block diagram contains read/write control blocks, while the front panel is used for choosing the parameters and visualizing the results. A short description of both elements is inserted to explain the design process. The first one can be subdivided in three sections, one for the initialization, the second for the execution and the last one for the stop. The Boolean signals for starting the control or for resetting are turned off, while the LUTs – which have been previously uploaded in a dedicated folder of the Alma Automotive SPARK ECU, through NI-MAX – are read and exploited to create the *dq* axes current arrays (fig. 5.24). In order to start the real-time VI, the desired FPGA reference is opened, reset and run. Moreover, the 1 kHz timing source is generated and connected to the timed while loop, with a period equal to 1 ms.

Then, the algorithm is executed, and the read/write blocks are inserted for sending the chosen parameters to the FPGA module, for selecting the discrete time intervals, for reading and displaying the resulting variables. The fixed quantities are directly computed in the loop, such as $\frac{3}{2}\frac{\cos(\varphi)}{V_{DC}}$ for the battery pack direct current estimation, in order to reduce the FPGA computational effort. Finally, once stopped the loop, the reference VI is closed. A particular attention is dedicated to the sampling times: the discrete time intervals used for control integrators is 10 µs, while for the IPMSM a smaller value 2 µs is set – the motor loop is faster because it requires less blocks. Knowing that the hardware has an internal 40 MHz clock, the ticks are counted for verifying that both FOC and plant cycles are completed with the sampling time values. A tick is obtained from the multiplication of the board clock for the selected periods. The complete motor cycle requires 80 ticks, while the control algorithm 400.

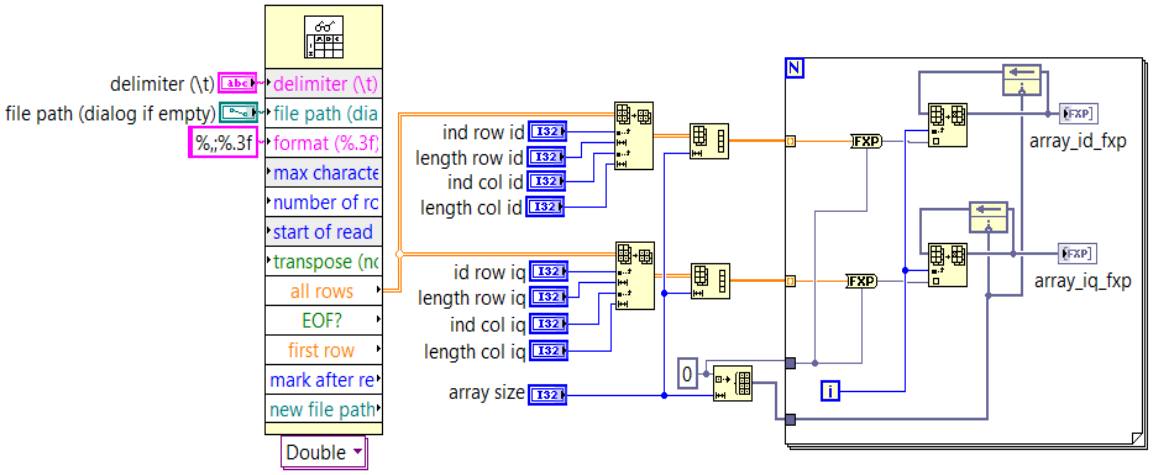

Figure 5.24: Block diagram for reading the uploaded LUTs.

Concerning the front panel, a tab control is inserted for separating the different interfaces – one for the parameters and the main diagrams, another one for the electric and control variables, the third for MTPA look-up tables analysis. When the CAN communication is added to the real-time, one section is reserved for visualizing the exchanged frames. Through the controllers, all the parameters are set for configuring the motor and for regulating the PI multiplicative factors, the reference ramp signal slope, the Butterworth cut-off frequency, the hysteresis thresholds and the number of filtered cycles for the debouncing mechanism. When the simulation starts, the user is able to activate the control algorithm, to send the request, to switch from speed to torque loop and also to establish the maximum charging and discharging current rates – the BMS is not yet simulated through the CAN bus in this phase. The waveform charts, the numeric indicators and the LEDs are inserted in the panel for reading and displaying the resulting variables, such as rotor speed, motor torque, flux-weakening and direct current PI status, etc. The simulation is classified as hardware-in-the-loop, because the SPARK board effectively runs the field-oriented control algorithm. However, the plant model is developed on the same board, so the HIL condition is not perfectly verified in prototyping phase. This aspect gives the chance for further consideration and future optimization – which will be discussed in the conclusive section. A part of the realized IPM user real-time interface for setting the parameters is shown in figure 5.25.

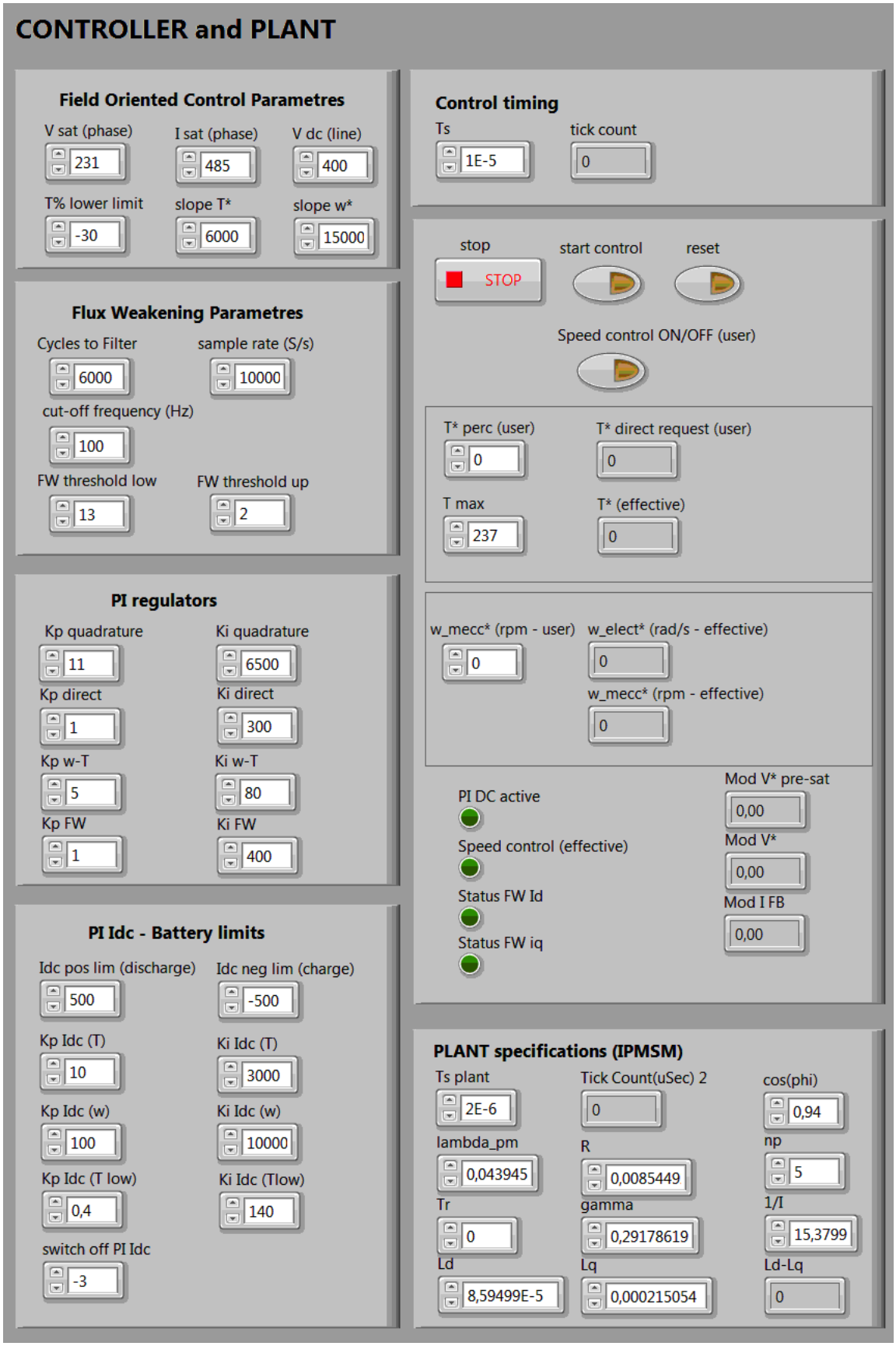

Figure 5.25: Section of the IPMSM front panel.

5.2.8.1 First case: torque loop

For the first simulation of the interior permanent configuration on the Alma Automotive SPARK hardware, the torque loop is used for regulating the motor's behaviour. In this case, the battery management system doesn't send any stringent maximum charging and discharging current rates – default values equal to ± 500 A are set, because the inverter DC never reaches the limits. The resistance torque is speed dependant, with a factor $\gamma = 0.182$ Nm s/rad in the first case and $\gamma = 0.076$ Nm s/rad in the second one. The external demand is equal to the maximum torque – 100% reference value – and the resulting waveforms are plotted is successive figures. In vehicle applications, the user torque request is traditionally obtained by mapping the position of accelerator and brake pedals. Thanks to flux-weakening algorithm, the speed is increased over the corresponding nominal parameter ($n_N = 4800\ RPM$). It is possible to verify that the instantaneous maximum electromagnetic torque is 237 Nm only in constant torque condition, because in constant power area it decreases. Finally, the different loads produce different motor outputs. When the resistance torque T_r meets the delivered T, the motor achieves the steady-state condition: for a smaller factor γ a higher speed is reached. For the reference value, a slope equal to 6000 Nm/s is chosen.

The *d*- and *q*-axis current contributions are shown in the following figure 5.26: both diagrams represent only the passage from null reference to maximum torque request. The motor starts from the MTPA condition in order to reach the constant power region, neglecting the opposite transition. The plotted waveforms are similar to the previous theoretical results.

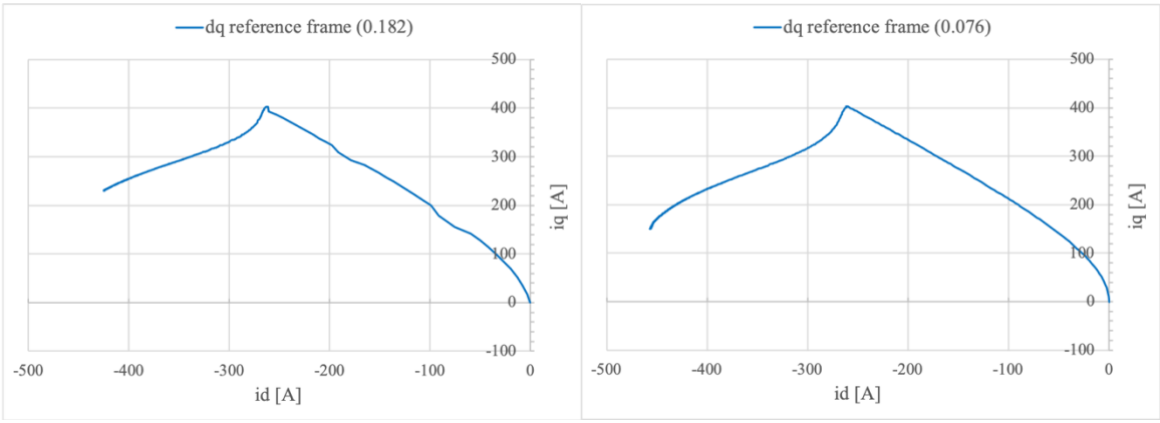

Figure 5.26: Resulting dq-axes current contributions in IPMSM simulation, with $\gamma = 0.182\ Nm\ s/rad$ on the left and $\gamma = 0.076\ Nm\ s/rad$ on the right.

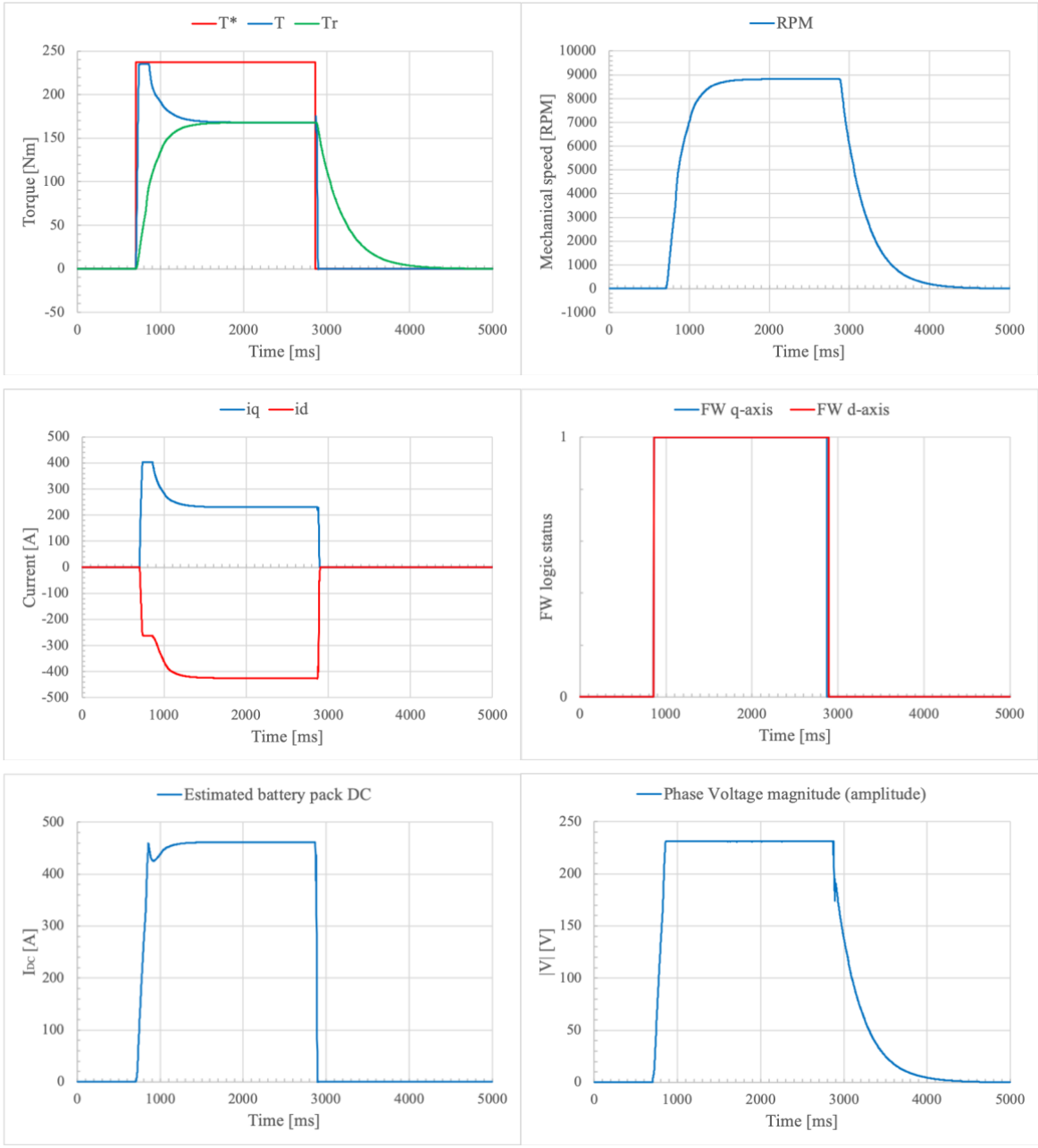

Figure 5.27: Results of IPMSM simulation, with a 100% *torque request and* $\gamma = 0.182\ Nm\ s/rad$.

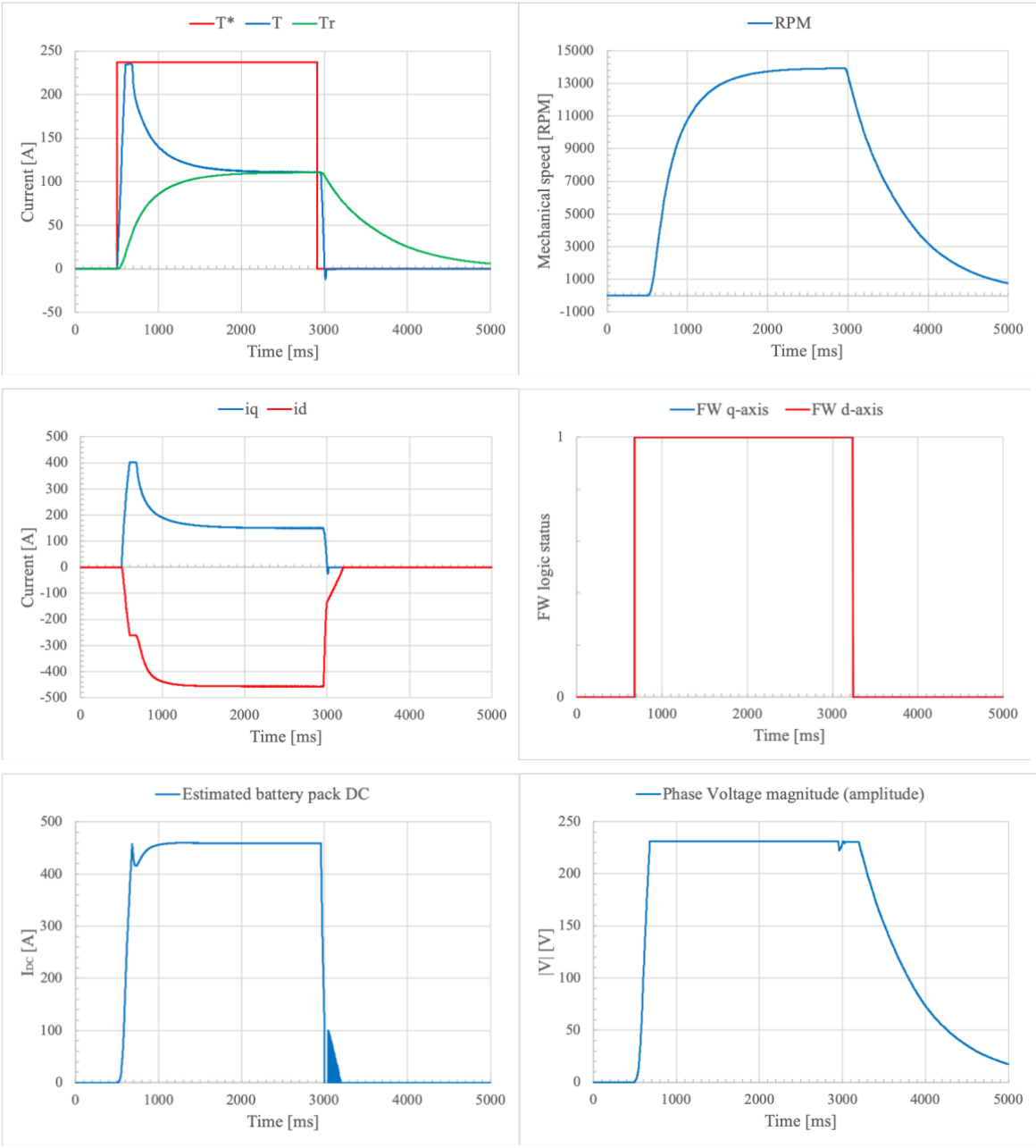

Figure 5.28: Results of IPMSM simulation, with a 100% *torque request and* $\gamma = 0.076\ Nm\ s/rad$.

5.2.8.2 Second case: speed loop and regenerative braking

The successive step is the simulation of the speed loop to verify its performance. In order to obtain comparable results, the request is close to the obtained result with a 100% torque demand and a factor γ equal to $0.182\ \mathrm{Nm\,s/rad}$. In fact, through the real-time interface, $n^*_{RPM} = 8830$ RPM is set and then transformed into the corresponding electrical angular velocity – because the controller operates using the reference ω^*_e. Also in this case,

the battery pack direct current proportional integral regulator is not working, because the estimated $\hat{I}_{DC}$ never reaches the imposed constraints: consequently, the user request is not limited. In the graphical results, the reference torque is obtained from the PI which manages the speed loop. It is possible to visualize when the motor reaches the voltage saturation condition, passing from maximum torque per ampere region to flux-weakening. The principal aspect is the regenerative braking zone when a null speed request arrives. The velocity value is always positive and tends to zero, while the quadrature current contribution becomes negative: the motor torque is negative, while the speed not, so the machine works in regenerative braking mode in forward direction (referring to figure 1.2). Consequently, the energy can be recovered because the energy source – a battery for the project – is recharged. On the other hand, for practical reason a saturation value has to be used, because the torque cannot freely change towards an excessively negative value. The lower limit is inserted in the block diagram for this purpose, and it is configurable in the interface: a value equal to -30% of the maximum torque is used ($T_{neg.limit} = -71$ Nm). For the reference value, a slope equal to 15000 rad/s is imposed.

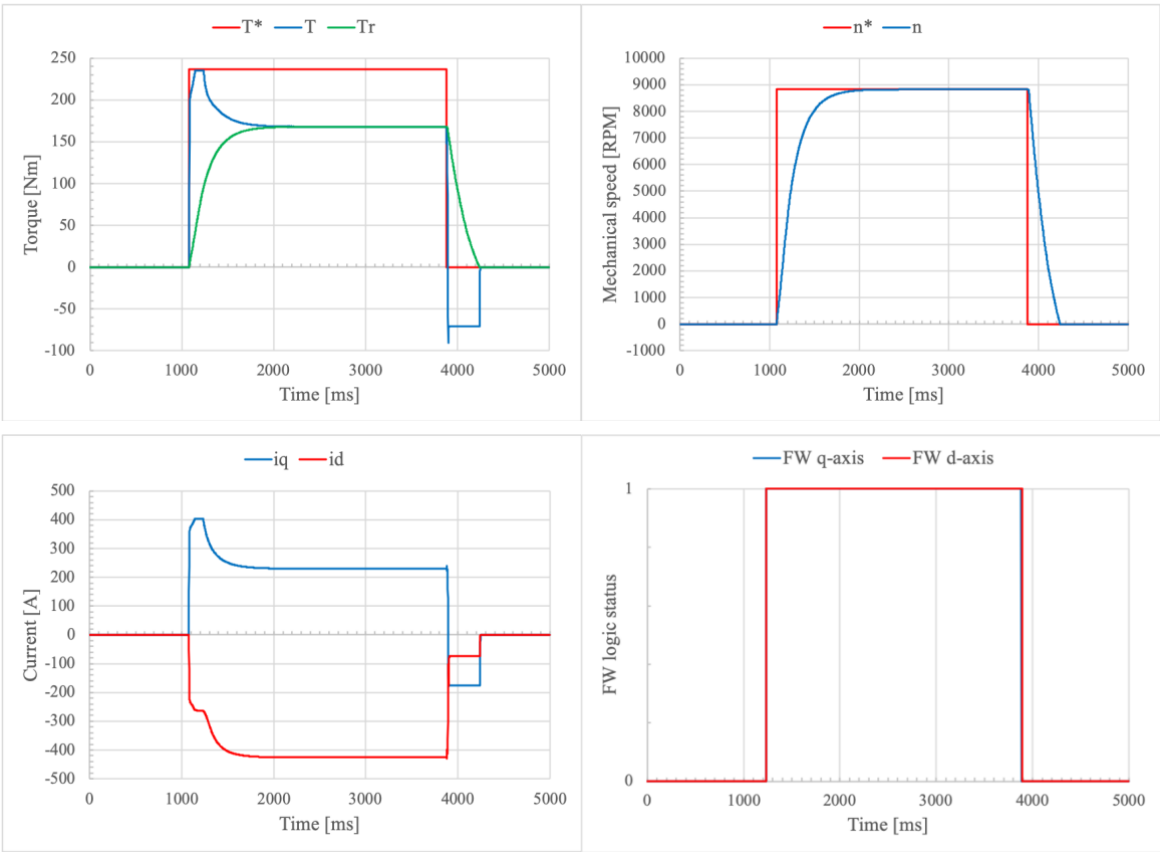

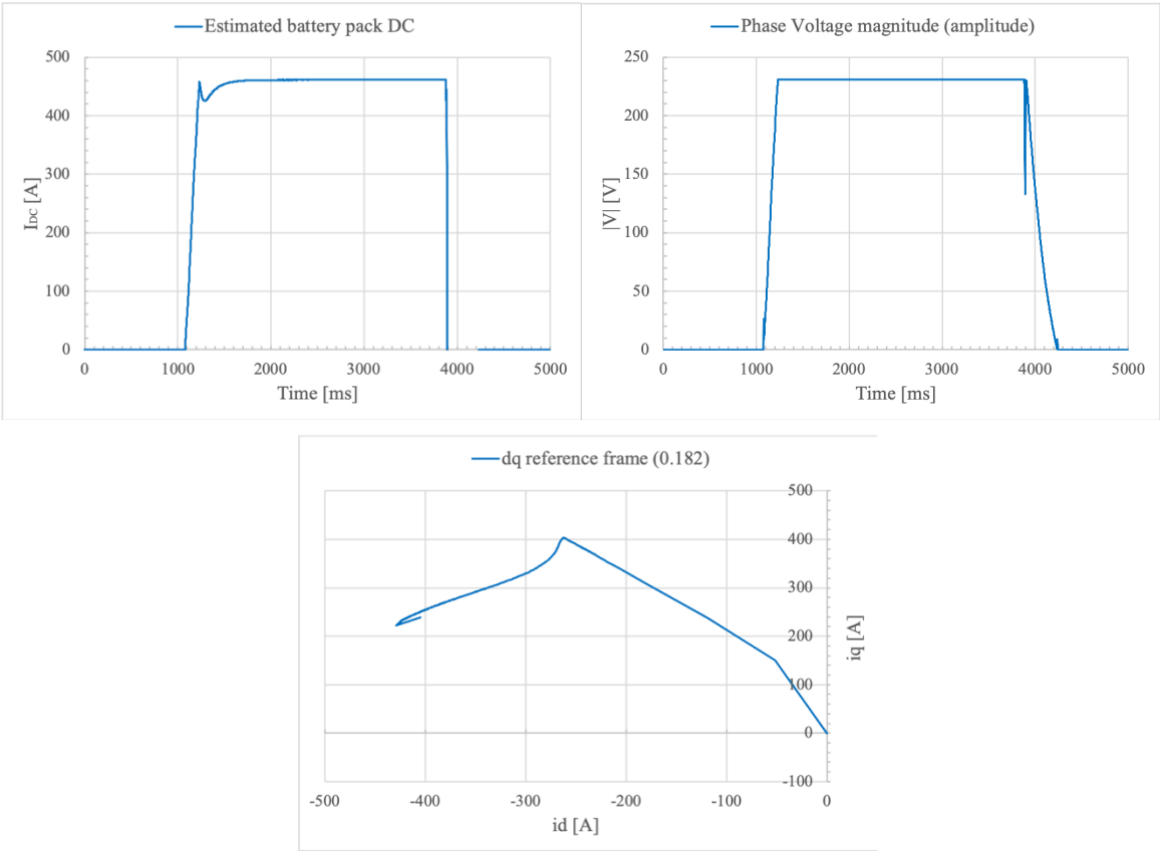

Figure 5.29: Results of IPMSM simulation, with $n^*_{RPM} = 8830\ RPM$ *request and* $\gamma = 0.182\ Nm\ s/rad$*. As well as in previous torque loop cases, the two current contributions in dq-axes represent only the passage from MTPA region to flux-weakening condition.*

5.2.8.3 Third case: battery DC limitation in torque loop

The last case in the most complete one, because it includes the action of the PI which manages the battery (and inverter) DC. It is again a torque control loop, with a 100% user request and $\gamma = 0.182$ Nm s/rad for comparing the output waveforms with the previous results. In this case, the maximum discharging current is 320 A – the negative limit is not considered for this operating condition. Consequently, when $\hat{I}_{DC}$ increases and reaches the constraint, the regulator is activated (status on) and the switching mechanism (from torque to speed control or vice versa) is disabled. The IPM synchronous motor reaches the flux-weakening condition, but obviously a smaller mechanical speed is obtained. The PI, in fact, reduces the external request: for this reason, both user direct demand and filtered torque request – the regulated output – are displayed in the charts, obtained during the prototyping phase in the Teoresi laboratory.

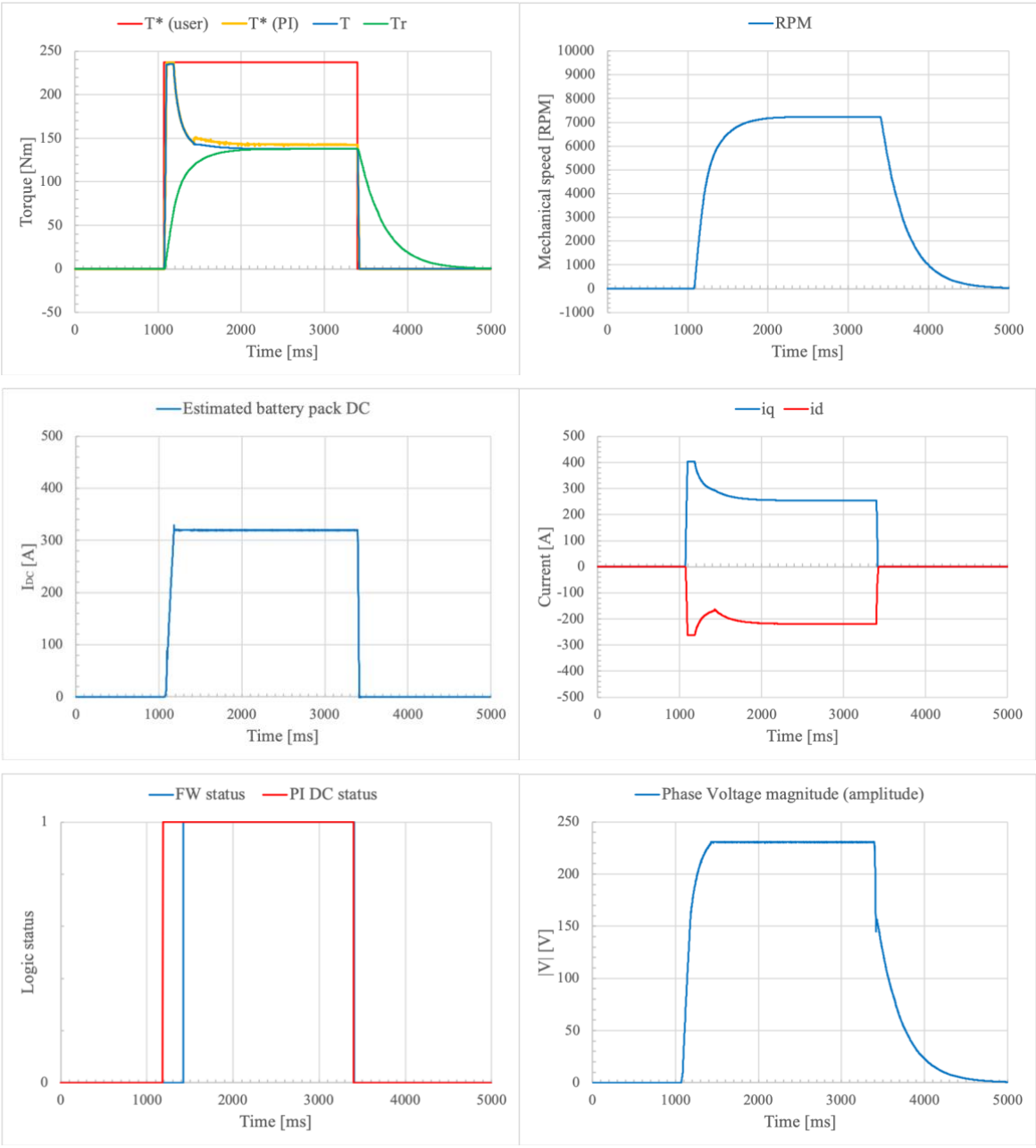

Figure 5.30: Results of IPMSM simulation, with a 100% *torque request,* $\gamma = 0.182\ Nm\ s/rad$ *and a maximum value equal to* 320 *A for the discharging current. The DC regulator limits the user demand.*

5.3 FOC strategy for a SPM synchronous motor

The field-oriented control algorithm for a surface-mounted PMSM is developed just to underline the main differences among this structure and the previous one and to explain the adopted strategies for managing the behaviour of the simulated motor. As described before, this kind of brushless synchronous machine is used for lower-speed applications,

because the absence of saliency and the reduced magnetic flux cause a limitation of the flux-weakening area. In many applications, the SPM is used just in constant torque condition, neglecting the possibility of exceeding the nominal rotor speed. For optimizing the design, an accurate analysis of the length of each controller and indicator is done in the FPGA VI. Many blocks are similar to the previous project, with – in some cases – a different bit-sizing in order to respect the new torque, current, voltage and speed limits. An additional consideration about direct and quadrature axes decoupling is discussed in the development of the FOC algorithm, and the corresponding block is added to the scheme. For the real-time interface, the graphical results obtained through the HIL simulation are displayed, while the CAN communication is neglected. The chosen motor parameters are inserted in the table 5.2 – the electric values represent the peak limits. A delta-connected (fig. 5.31) servomotor is considered, so the correlation between phase and line quantities is expressed by:

$$V_{line} = V_{phase}$$

$$I_{line} = \sqrt{3}\, I_{phase}$$

$$P_e = 3\, V_{phase}\, I_{phase} \cos(\varphi)$$

where the values have the same meaning of a star-configuration. The surface-mounted typology of AC machine is no more used in automotive applications, due to their limited torque and power density. While IPM structure – in particular with rare-earth permanent magnets – is the most used for electric vehicle traction, such as Toyota Prius and Nissan Leaf,[208] the SPM is replacing the induction motor in low-performance and low-speed industrial systems, i.e. pumps or fans. The equivalent block scheme is shown in figure 5.32.

[208] Huynh, T. A., & Hsieh, M.-F. (2018, May), *Performance Analysis of Permanent Magnet Motors for Electric Vehicles (EV) Traction Considering Driving Cycles*, In *Energies, 11*(6), p. 1.

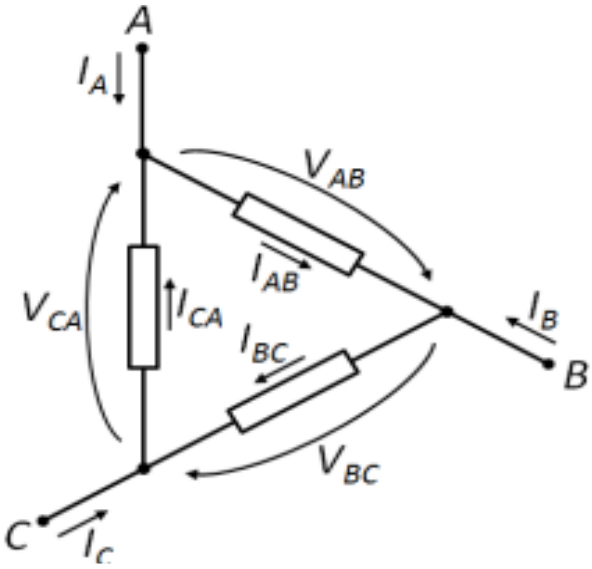

Figure 5.31: Delta-connected three-phase stator windings.[209]

SPMSM Parameter	Symbols	Values
Nominal speed	n_N	2700 RPM
Nominal torque	T_N	33 Nm
Maximum speed	n_{max}	6000 RPM
Maximum torque	T_{max}	60 Nm
Saturation phase voltage	$V_{sat,phase}$	325 V
Saturation phase current	$I_{sat,phase}$	47 A
Torque constant	k_T	1.54 Nm/A
Pole pairs	pp	4
Inductance	L	6 mH
PM flux	λ_{PM}	0.257 Vs
Stator resistance	R_s	0.28 Ω
Moment of inertia	J	48.03 kg cm^2

Table 5.2: Parameters of the simulated SPMSM.

[209] Ferreira, F., Ge, B., Quispe, E., & De Almeida, A. (2014), *op. cit.,* p.2.

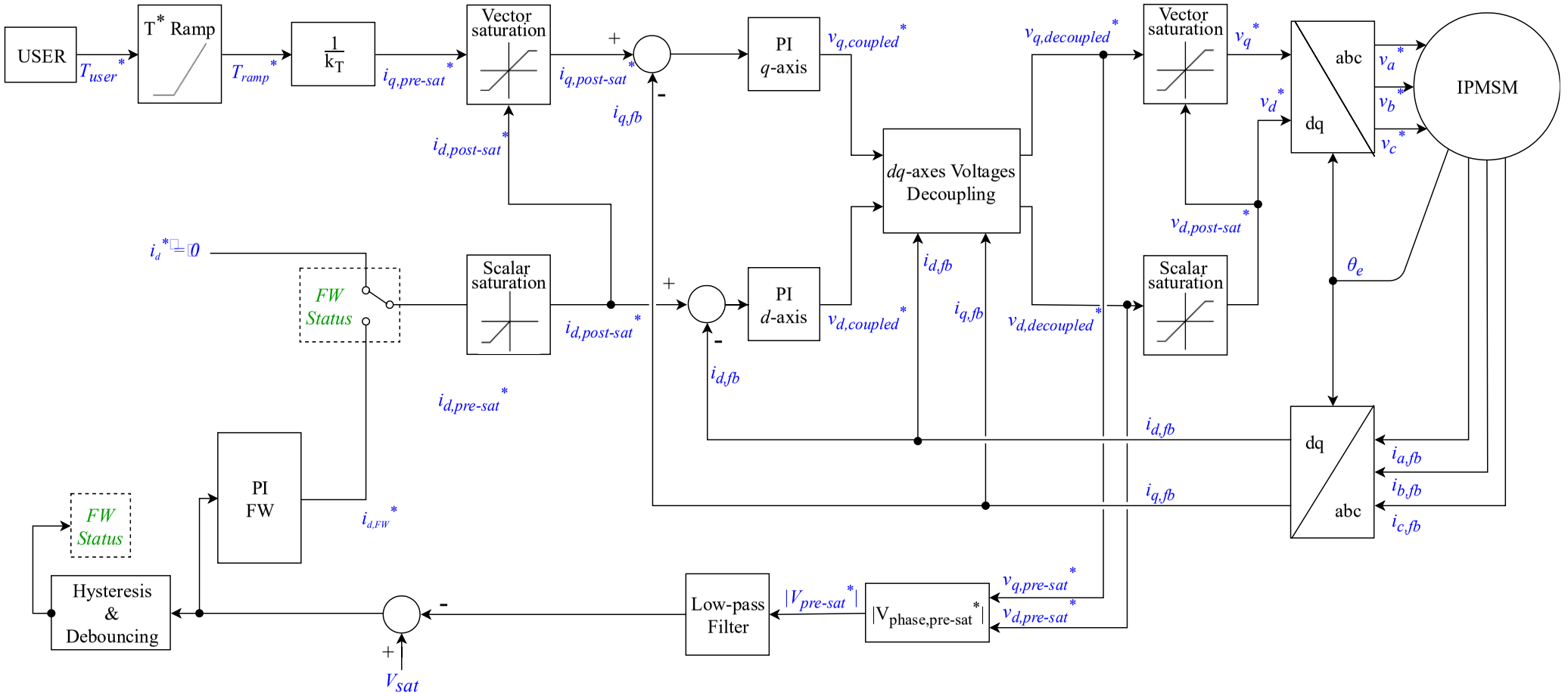

Figure 5.32: Block scheme of SPMSM control algorithm.

5.3.1 Differences with respect to IPM control algorithm

As anticipated, in the second design process there are some differences inside the block diagram, for analysing the behaviour of the SPM in a more specific way. The FPGA VI, in this case, is simplified because the direct current regulator, the estimator of actual DC and the motor speed control loop are not implemented. Moreover, the maximum torque per ampere area has a reduced complexity, because in constant torque region the contribution of the reference stator current on the *d*-axis is kept null – the motor torque is just related to i_q through a constant. An additional feature is the decoupling block, in order to eliminate the dependence of the reference command voltages v_d^* and v_q^* from the opposite axis contribution. This element can also be inserted in the FOC algorithm of the interior permanent magnet synchronous motor. However, due to hardware constraints, it is removed from the FPGA VI for leaving more resources to the implementation of other essential blocks – in particular for increasing the MTPA arrays size. The Clarke-Park direct and inverse transformations, the PI regulators for computing v_d^* and v_q^* from the current error, the saturations for phase current and phase voltage and the ramp generator for torque request are identical to the corresponding IPM control loop blocks – except for the length of the words. For this reason, the analysis is neglected. Concerning the motor scheme, i_d and i_q are obtained in the same way, as well as the mechanical equation for evaluating rotor mechanical and electrical speed and angular position. The only difference in the motor loop is the independence of the electromagnetic torque from the *d*-axis current, because through the mathematical high throughput blocks the SPMSM already discussed equation is realized:

$$T_{em} = \frac{3}{2}\,\lambda_{PM}\,pp\,i_q = k_T\,i_q$$

where only the synchronous term contributes to torque generation. The principal variations with respect to previous project are discussed in the following sections.

5.3.1.1 Decoupling

The most innovative element is the block responsible for eliminating the coupling terms from the direct and quadrature command voltages – they are inserted between the PI regulators and the saturations. A case structure is implemented in the FPGA VI for choosing

whether to activate the mechanism or not and for comparing the different performances. From the PMSM dynamic model in *dq* reference frame, the resulting equations are:

$$\begin{cases} v_d = R_s i_d + L_d \dfrac{di_d}{dt} - \omega_e L_q i_q \\ v_q = R_s i_q + L_q \dfrac{di_q}{dt} + \omega_e (L_d i_d + \lambda_{PM}) \end{cases}$$

It is possible to visualize the link between v_d and the q-axis current, through the quadrature inductance and the electrical speed, and the dependence of v_q on d-axis current and inductance and on magnetic flux of the permanent magnets, through again the electrical velocity. For obtaining the decoupling of the reference voltage terms, a simple mathematical operation is realized with the high throughput elements:

$$\begin{cases} v^*_{d,decoupled} = v^*_d + \omega_e L_q i_q \\ v^*_{q,decoupled} = v^*_q - \omega_e (L_d i_d + \lambda_{PM}) \end{cases}$$

where $v^*_{d,decoupled}$ and $v^*_{q,decoupled}$ are the outputs – which are sent to the saturators – while v^*_d and v^*_q are the reference quantities managed by the PI regulators; i_d and i_d are feedback quantities, obtained from the Clarke-Park transformations of the three-phase stator currents (passed from the motor loop through local variables). For the indicators of this SubVI, the same fixed-point dimension of the input voltages is used. In detail, 34 bits are reserved to the signed words and 11 of them are dedicated to the integer part. The block diagram is shown in figure 5.33.

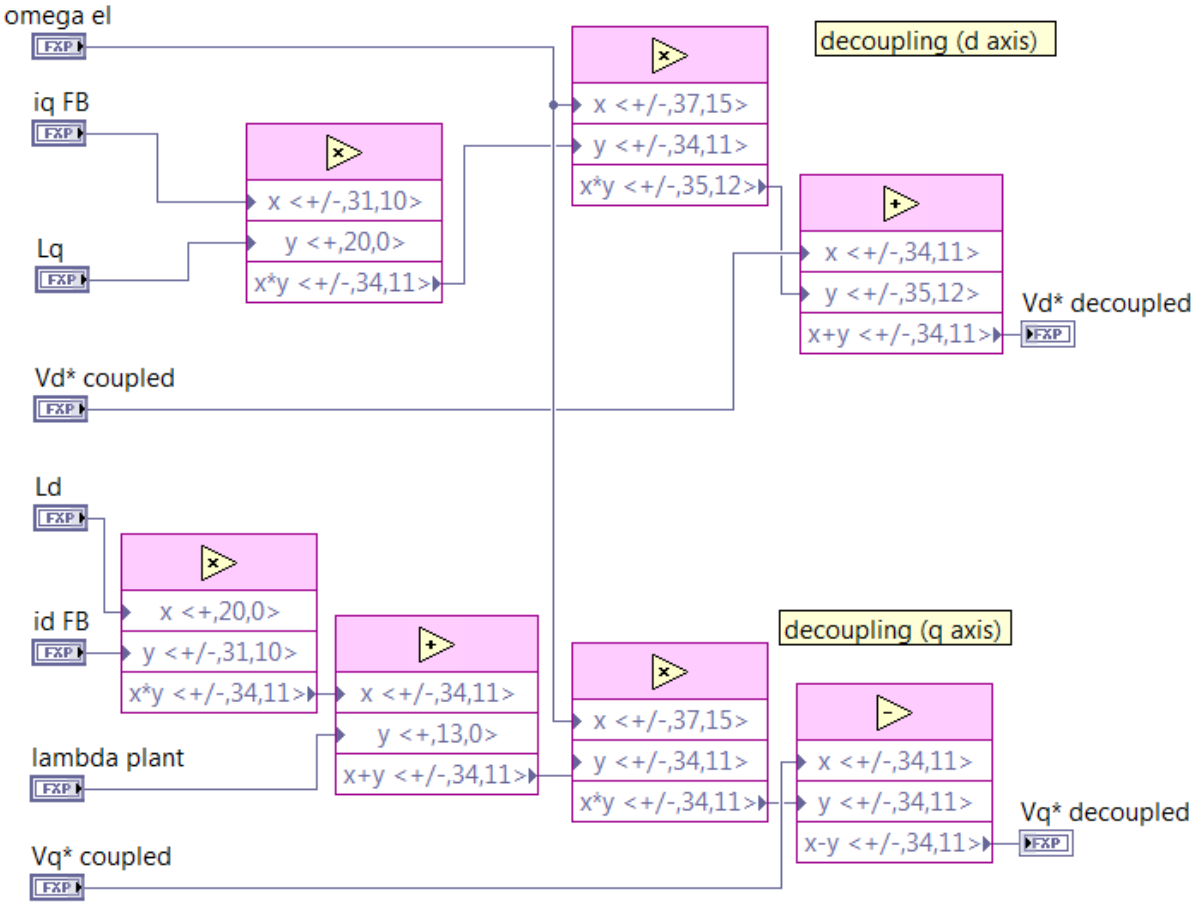

Figure 5.33: Decoupling SubVI.

5.3.1.2 MTPA region

In the SPM field-oriented control loop there is no dedicated block for realizing the MTPA interpolation: as described before, in constant torque region the *d*-axis reference value of the stator current is kept null, because the direct and quadrature inductances are equal and consequently the motor torque contains just the synchronous contribution: in other words, no reluctance term is added. A switching mechanism is implemented for selecting the reference i_d^*:

- a null value in constant torque region;
- a negative value obtained from the PI regulator that manages the FW in constant power region.

As a consequence, the representation of the current vector in the *dq* reference frame is aligned to the vertical quadrature axis for speed values below the nominal one. In the constant torque region, instead of the previous MTPA SubVI – used for applying the

interpolation to the LUTs, computed on MATLAB – a block scheme is implemented for realizing the inverse equation of the electromagnetic torque:

$$i_q^* = \frac{T^*}{k_T} = \frac{T^*}{\frac{3}{2}\,\lambda_{PM}\,pp}$$

T^* is the requested torque from the user – no PI regulator filters the reference value in this case – while i_q^* is the corresponding reference quadrature contribution, used in the field-oriented control algorithm. The value $k_T = \frac{3}{2}\lambda_{PM}pp$ is the torque constant and it depends on motor parameters: for reducing the computational complexity, this quantity is directly passed from the real-time interface to the FPGA VI when the model runs on the SPARK engine control unit. Concerning the flux-weakening – described in next paragraph – the phasor rotation happens, as well as in the IPM synchronous motor, with an increase of the direct contribution, and the saturation blocks are inserted in order to respect the phase current limit.

5.3.1.3 Flux-weakening for a SPMSM

The flux-weakening condition is implemented in the SPM project just for completeness, because in real applications this kind of motor doesn't guarantee any substantial advantages in terms of increasing mechanical velocity. In fact, the absence of saliency – the direct and quadrature inductances are equal – and the relatively small permanent magnet flux limit the constant power region. As described, the surface-mounted motors are applied in lower speed applications and are actually abandoned by the automotive industry. The working principle of the SubVI is similar to the previous one, inserted in the IPMSM control algorithm. The mathematical blocks are identical, and the only difference is related to the initial condition of the integrator. In the interior permanent magnet configuration, the *d*-axis reference current is a negative value different from zero in the MTPA region, in order to exploit the additional reluctance torque; that quantity is used as initial condition when the motor enters the FW zone. In SPM case, i_d^* is constantly null in in the lower speed region, so the PI regulator starts working from zero in order to manage the negative reference *d*-axis contribution for weakening the motor flux.

The other parts of the algorithm are copied from the IPMSM control project. In particular, the pre-saturation phase voltage module is computed from the command *dq* contributions and compared to the maximum value; again, a Butterworth filter is inserted for reducing the oscillations. Then, a relay block is used for generating a Boolean signal which

is true in FW region, false in MTPA. The PI starts working by comparing the filtered pre-saturation magnitude with the motor $V_{sat,phase}$, in order to regulate the reference d-axis current. A selector is managed by the Boolean indicator in order to set i_d^* equal either to zero or to the PI output, depending on the motor status. As usual, the direct axis is affected by a scalar saturation, for giving priority to the phasor rotation in constant power region. The other reference quantity i_q^* is obtained directly from the user request through the torque constant, but it is vectorially saturated in order to respect the phase current limit – depending on the actual regulated i_d^* – before being passed to the quadrature PI. When this kind of synchronous motor leaves the FW zone, the algorithm is simplified because the output of the proportional integral block is not compared to any quantities. There is no need for a MTPA interpolation here: when the phase voltage module falls below the lower threshold, the selector switches to $i_d^* = 0$ A. The PI regulator output can assume at maximum a null value, consequently in case of a voltage magnitude smaller than $V_{sat,phase}$ it is automatically set equal to zero. Finally, also the anti-windup mechanism is identical to the IPMSM scheme, where the priority is given to the proportional branch, while the integral term is affected by a dynamic saturation.

5.3.2 Real-time interface and results

For the SPM synchronous motor, the user interface is implemented on the Alma Automotive board in a very similar manner to the previous project. Through the block diagram and the front panel, the parameters are set, and the resulting waveforms are graphically displayed. The real-time VI is simplified now, because no look-up tables are used in the algorithm and only the torque loop is present. For this reason, only one simulated case is shown for the surface-mounted permanent magnet configuration. A 100% torque request is imposed by the user, in order to exploit the flux-weakening region – it is worth remembering that in this kind of motors the constant power region is reduced, due to the absence of saliency. The user demand is applied to the motor, with a slope equal to $2000\ \mathrm{Nm/s}$, with an active decoupling block. The PI parameters are properly regulated in order to guarantee an optimal dynamic behaviour. The decoupling mechanism is activated, and a speed dependant resistance torque is used (with $\gamma = 0.076\ \mathrm{Nm\,s/rad}$). The flux-weakening condition is achieved with the chosen reference signal. It is demonstrated that in

this simple situation, the resulting voltage waveforms in decoupling condition are close to the corresponding curves obtained when the dedicated SubVI is deactivated.

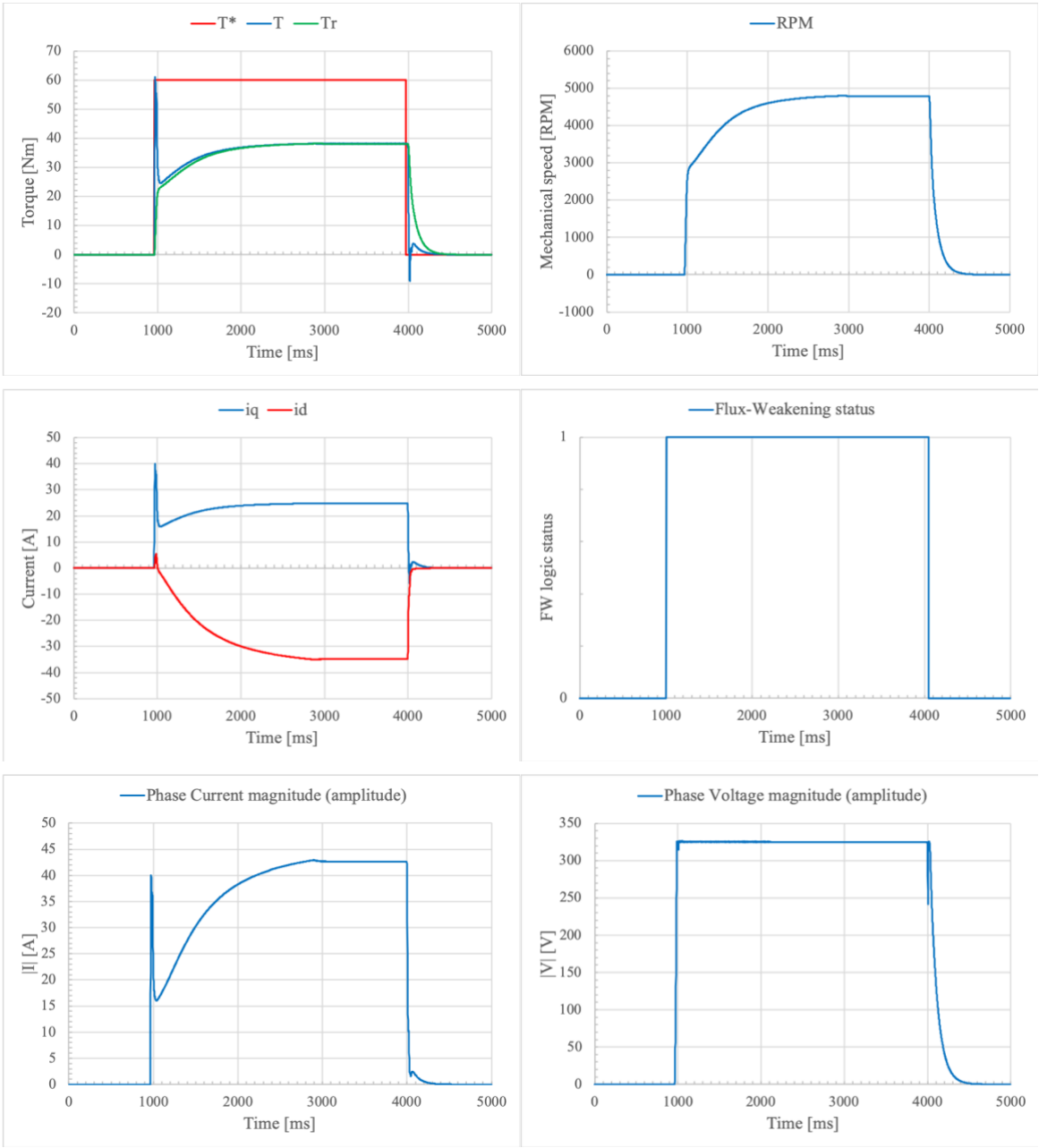

Figure 5.34: Results of SPMSM simulation, with a 100% *torque request and* $\gamma = 0.076\ Nm\ s/rad$.

5.4 BMS and dashboard simulation using CAN protocol

Once verified the correct behaviour of the IPMSM field-oriented control algorithm, including also the flux-weakening region in order to increase the speed range, the CAN bus is implemented in the real-time interface. This additional feature is related to automotive

applications of the engine control unit: inside the vehicle, as introduced in the first chapter, all the nodes exchange messages through the CAN bus. A reduced network is reproduced for the project, just for analysing how the frames are managed in LabVIEW environment. A battery electric vehicle is considered for the thesis project, so the created database – called *ECM* – reflects the possible received and delivered signals in a BEV engine control unit. The *ECM* file is exploited for associating a name and a short description to each message. Through the Vector CANalyzer tool and dedicated wire connections, a dashboard and a battery management system are simulated and interfaced with the SPARK board in Teoresi laboratory. Moreover, a blinking LED is configured on the hardware in order to verify the presence of error: red light if the execution is stopped, green if everything is correct. The previous real-time timed loop for the FOC and plant variables remains unchanged, only the additional LED control is inserted at the end of the diagram.

Concerning the CAN communication, first of all the database is deployed on the ECU through the NI-XNET Database Editor program. Inside the real-time scheme, the initial step is to open the FPGA VI reference and run it; the timing source is created, and the LED is switched off. Because the CAN blocks require a running VI, a flat sequence is used for assuring that the FPGA is totally configured and it is running, when the communication starts – this structure executes the frames in a sequential manner. In the second part of the flat sequence, the *ECM* file is opened, so the message names are extrapolated, and the X-NET session is launched. Moreover, the CAN interface is configured as CAN C, with a Baud rate equal to 500 kBaud, because the engine control unit has to manage time critical applications. A filter is inserted in the sequence: as described before, the number of messages in the bus could be substantial, but there is no identifier for the nodes. Consequently, each control unit should be able to receive only the messages which are fundamental for the proper working mode. The filter has this role, because the messages whose identifier is inserted in the filter setting array are the only readable ones. The other frames are totally neglected. This operation is fundamental for decreasing the board input traffic, in order to guarantee better performances. The last step is the creation of a CAN frame queue. In practice, this is a FIFO register used for respecting the timing requirements of the written messages. The ECU has to send different frames on the bus, so there is the risk of simultaneity. The arbitration mechanism resolves the conflict, but the least priority message is lost, and the corresponding information is deleted for that cycle. Moreover, the frames with the highest identifiers risk to be totally ignored during the communication. The queue is used for this purpose, because the created messages are not directly written on the bus, but they are saved in a sequential

manner in the FIFO block. Then, at each cycle one frame is extracted and written, so no information is wasted.

Once configured the network, three timed loops – with the same 1kHz timing source and the same period (1 ms) – are inserted in the real-time VI. The most important one manages the writing and reading phases, controlling also the transceiver state in case of absence of communication. The FPGA VI signals – rotor speed, estimated motor torque (the effective value is never available in the control algorithm), the external user requests and the limited reference values (obtained from the PI which manages the battery pack DC), the computed maximum torque (which decreases in flux-weakening region), the control status – are transformed into the corresponding CAN frames. The database provides all the information for correctly generating the message:

- the assigned frame name;
- the hexadecimal identifier (standard or extended);
- the subdivision of the data field in different signals, specifying for each of them the name, the startbit and the length. Also, the byte order (little-endian Intel or big-endian Motorola) is indicated;
- the value type, the reset value, the multiplicative factor, the offset, the maximum and the minimum, the unit of measure for all the signals that compose the frame;
- a short description of each signal.

In LabVIEW environment, one 8-byte array is used for creating the data field of a certain message, while the bundle block generates the CAN frame cluster by merging the fixed identifier, the extended Boolean indicator, the type and the previously composed data. The control and plant signals are passed through local variables and are opportunely converted.

An example is shown in figure 5.35 for the *MOT1* message: the double values are transformed in unsigned word and passed to the build array element. The rotor speed module doesn't require any further modification. On the other hand, the torque quantities are first converted in percentage values, expressed with respect to the fixed maximum torque parameter ($T_{max} = 231$ Nm) in the range [0%,100%]; then, they must be divided for the factor (0.392) indicated in the *ECM* file (fig. 5.36) in order to obtain consistent data. The idea is to create a cyclic message, so the number of iterations of the timed structure is used for sending *MOT1* every 10 ms. Because the while loop period is 1 ms, at each cycle the iteration variable increases and it passes through a quotient & reminder block, with a fixed divider equal to 10. When the reminder is equal to 9, the *MOT1* frame is inserted in the FIFO queue, otherwise no operation is executed – other messages with a different frequency could be meantime inserted in the register. The reminder is compared with the previous integer

value with respect to the desired period because during the first cycle the loop iteration is equal to zero.

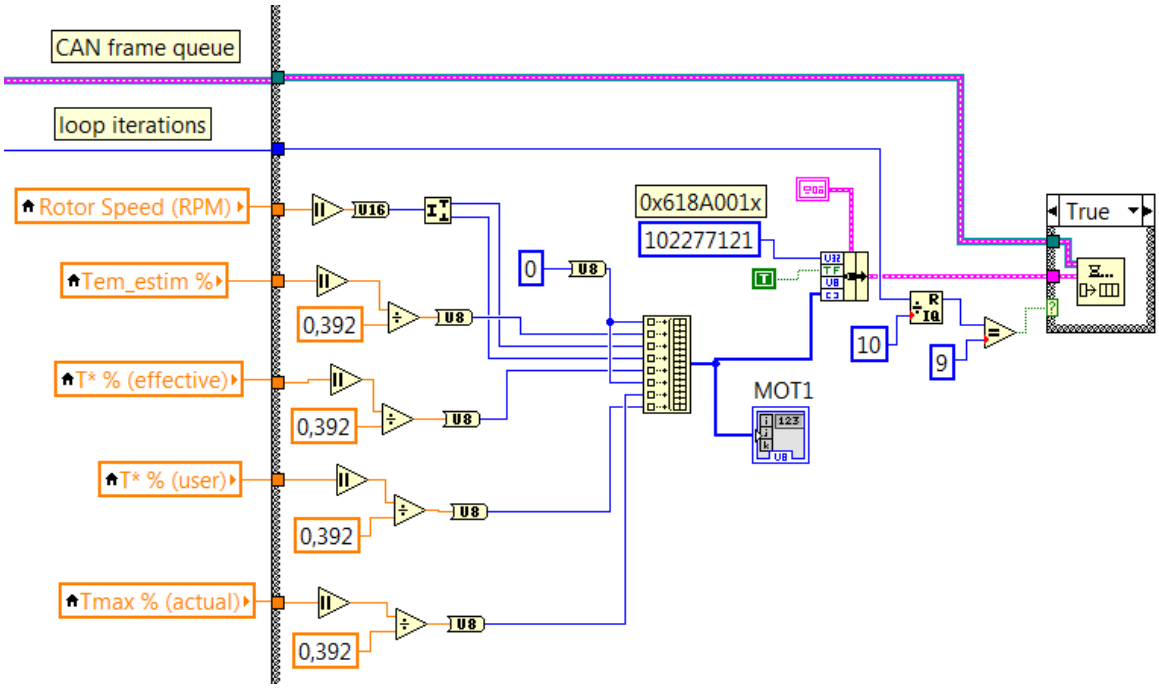

Figure 5.35: Generation of the cyclic message MOT1 inside the LabVIEW real-time interface.

MOT1 (0x618A001x)	Mess...	N	Startbit	Length...	Byte Order	Value Type	Initial...	Factor	Offs...	Min...	Max...	Unit
EngineTorqueDriverReqValidData	MOT1	-	2	1	Motorola	Unsigned	0	1	0	0	1	-
EngineTorqueValidData	MOT1	-	3	1	Motorola	Unsigned	0	1	0	0	1	-
FeedbackASR_ESCReq	MOT1	-	4	1	Motorola	Unsigned	0	1	0	0	1	-
EngineFrictionTorqueValidData	MOT1	-	5	1	Motorola	Unsigned	0	1	0	0	1	-
GasPedalPositionValidData	MOT1	-	6	1	Motorola	Unsigned	0	1	0	0	1	-
MaxEngineTorqueValidData	MOT1	-	7	1	Motorola	Unsigned	0	1	0	0	1	-
EngineTorque	MOT1	-	8	8	Motorola	Unsigned	0	0.392	0	0	99.96	%
EngineSpeed	MOT1	-	24	16	Motorola	Unsigned	0	1	0	0	102...	1/min
EngineTorqueDriverReq	MOT1	-	32	8	Motorola	Unsigned	0	0.392	0	0	99.96	%
EngineFrictionTorque	MOT1	-	40	8	Motorola	Unsigned	0	0.392	0	0	99.96	%
MaxEngineTorque	MOT1	-	48	8	Motorola	Unsigned	0	0.392	0	0	99.96	%
GasPedalPosition	MOT1	-	56	8	Motorola	Unsigned	0	0.392	0	0	99.96	%

Figure 5.36: Description of message MOT1 in the database ECM.

All the generated messages are inserted in the queue, which is passed to the CANwrite block. When the queue is null, the write operation is deactivated; when a frame is ready, it is sent to the bus. In the successive part of the loop, the bus is read in order to verify the presence of incoming frames. If no new messages are present for a configurable amount of cycles, the transceiver state is set to Sleep, waiting for updated signals. Obviously, due to the coexistence of different signals to be written on the CAN bus, the periodicity is not perfectly guaranteed. In the project, the maximum number of messages sent by the ECU is five: when a bigger complexity is required in automotive applications, more accurate

mechanisms are implemented in order to optimize the message writing and reading operations – especially in time critical cases. A second timed loop is used for associating a name to each message, based on the XNET database information, in order to obtain a more readable structure. The third structure acts as a filter, because it continuously updates an array where the read frames are saved. In fact, because the network messages are cyclic, it is more useful to save them in a single element and to update their timestamp and data field at each iteration. The error wires of each blocks are merged together and sent to the case structure which manages the LED, for showing the presence of errors. When the simulation is stopped, all the loops are interrupted sequentially, and the reference VI interface is closed.

On the CANalyzer tool side, first the CAN C communication is configured by selecting the Baud rate and the connector pins on the dedicated hardware. In the measurement setup, an interactive generator (IG) block is inserted for creating the cyclic message *mBMS_PP* where the maximum charging and discharging currents – and the corresponding powers – are set. This frame is used for simulating the BMS behaviour in the project. While in the previous phase, limits were configured directly from the user, now they are sent on the bus and received by the engine control unit. The latter uses the constraints for managing the actual battery pack and inverter direct current through the dedicated PI regulator. In the real-time interface, the inputs $I_{DC,pos}$ (corresponding to the signal *PP_I_dschrg)* and $I_{DC,neg}$ (*PP_I_chrg)* are extracted from the array where all the frames are collected. The power values are not used in the control algorithm, so they are simply neglected. In CANalyzer trace page, all the exchanged messages in the network can be visualized with their data fields and their periodicities. To simulate the dashboard, a front panel is created in order to graphically display the rotor mechanical speed; by using a generic image of an RPM indicator as background, the pointer moves depending on the effective ω_m – whose value is sent by the ECU real-time module. For completeness, the torque user request, the filtered reference value and the actual maximum torque are represented through loading bars. A negligible resolution error is present because the maximum percentage values is 99.960% – because 8 bits are used for each quantity – while the control algorithm can reach 100%. The Boolean *MAIN_CLOSE_REQ* signal is on – as well as the associated LED – when the control action is activated. One example is shown in figure 5.38, using the previously described interior permanent magnet synchronous motor FPGA VI: in this case, a 100% torque request arrives from the user and it is not limited because $PP\_I\_dschrg = 485$ A and $PP\_I\_chrg = -280$ A, so the battery pack DC never overcomes the limit. The user request and the effective request are consequently identical. The PMSM in flux-

weakening condition reaches a mechanical speed of 7914 RPM. The green LED shows that the control algorithm is working, while the maximum available torque is a variable which is equal to $T_{max} = 237$ Nm in MTPA condition and which decreases in FW. In fact – as discussed before – in constant power region the machine cannot deliver the maximum torque, because the current phasor is rotated for increasing the speed over the nominal value.

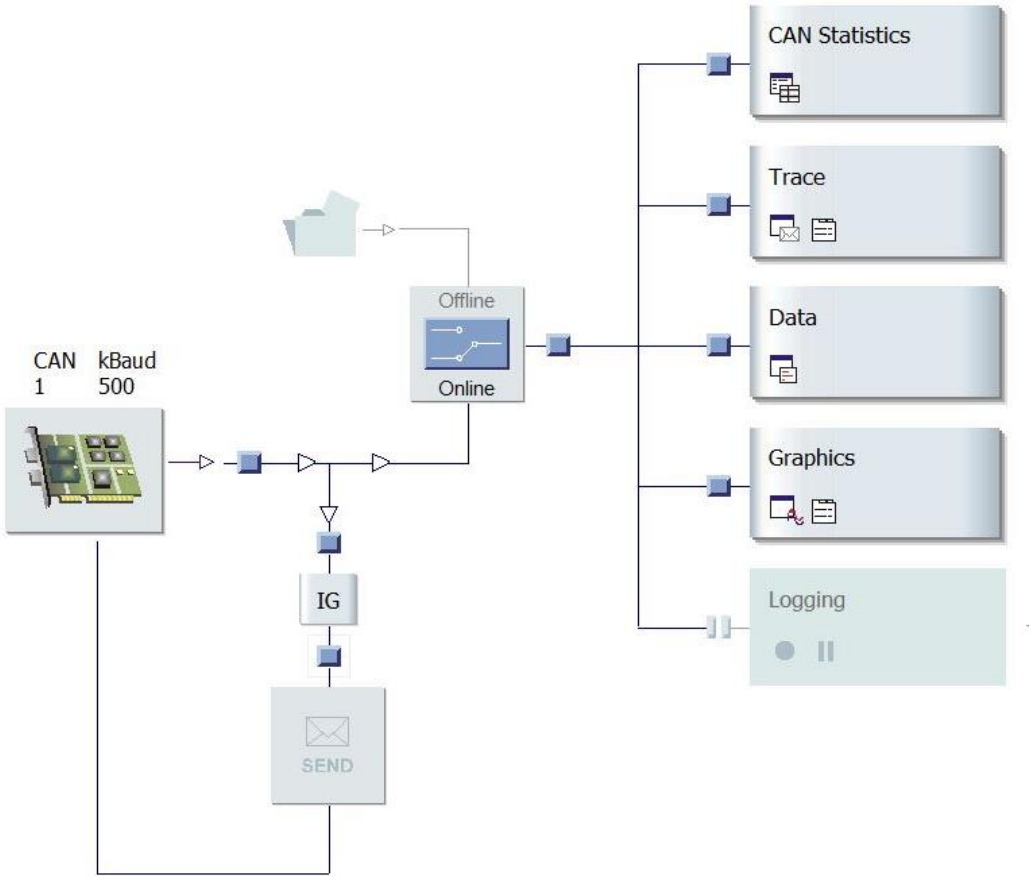

Figure 5.37: CANalyzer measurement setup interface.

The last step of the project is the creation of a real-time startup application. Once programmed in the design phase, the engine control unit should be able to run standalone the compiled block scheme – containing control and plant loops – and the communication. In the build specifications section, the FPGA VI is selected as startup VI, and all the necessary SubVIs – in particular for the CAN protocol – are included too. Then, the created application is built and deployed on the hardware, which is restarted for working autonomously from the computer host. Because the signals are not available on the real-time interface when the board is in this operating mode, the CAN network, the programmable LED – for controlling the errors – and dedicated text files are used in the debug phase. The mechanism is correctly implemented, and the Alma Automotive SPARK ECU is able to

communicate with the simulated dashboard and battery management system – providing the motor variables and receiving the DC constraints and speed or torque requests.

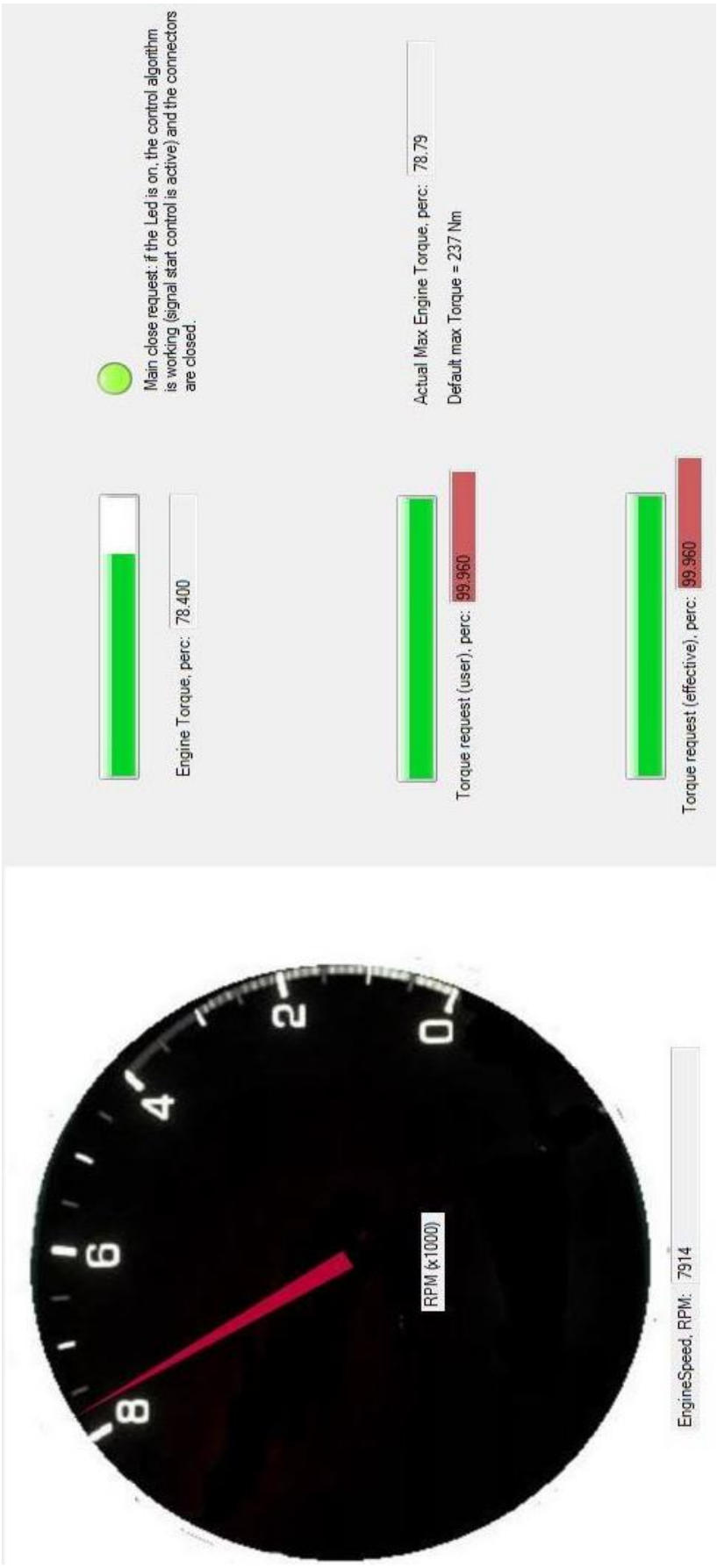

Figure 5.38: Example of front panel in CANalyzer, with a 100% torque request (the motor is in FW condition). The PI which regulates the battery DC is not working because the estimated direct current never reaches the charging and discharging limits.

Conclusion

The designed control algorithm is able to drive correctly both interior and surface-mounted permanent magnet synchronous motor models in presence of a resistance load – which can be fixed or speed dependent. It is also possible to increase the resultant mechanical velocity over the nominal value, as shown in the preceding charts. In fact, the flux-weakening mechanism is fundamental in order to improve the machine performance, especially in IPM structure: the theory affirms that the presence of saliency, due to the difference between direct and quadrature inductances, is exploited for reducing the air-gap magnetic field and consequently rising the speed. The torque decreases, and the power remains constant in the FW region. The obtained results confirm this analysis, showing also the correspondent current phasor rotation towards the direct axis. The application of IPM motors in electric and hybrid-electric vehicle is motivated from this advantage and from the higher torque and power density with respect to a SPMSM in identical operating condition. In case of BEVs, recent studies motivate the use of interior permanent-magnet solutions because the continuous evolution is reducing their price and, at the same time, improving their efficiency. Obviously, a complete electric passenger car still requires a non-negligible initial cost, linked in particular to the battery pack and to the motor driving system. Actually, also assisted switched reluctance synchronous motors are experiencing a substantial improvement, in order to make the most of reluctance torque contribution. Concerning the surface-mounted typology, it is adopted only for low-speed systems, so its control algorithm is useful just for a complete overview of PMSMs and not for practical examples.

In order to analyse the possible battery electric vehicle applications of the developed field-oriented control, the regulator for the battery pack – and ideal inverter – direct current is inserted at the beginning of the chain, for limiting the user requests. This approach reflects what happens in real electric powertrains, where the battery managements system continuously communicates with the engine control unit in order to send information about the energy source status. Consequently, the ECU – in this project the SPARK – is responsible for adapting its outputs to the imposed constraints. Once verified the correct implementation

of this mechanism, a sort of small CAN network is simulated: the BMS and dashboard behaviours are replicated in CANalyser tool for interfacing them with the board in order to send external requests or limit values and to display graphically the principal quantities. The introduction of CAN protocol inside the project is another fundamental step towards a possible automotive application. Finally, the speed loop in an additional feature useful for completely stopping the motor or for maintaining a constant velocity, i.e. a kind of cruise control system. By requiring a null reference speed when the system is running, the regenerative braking system is analysed too. The presence of a negative quadrature stator current – and consequently of a negative motor torque – allows the machine to work as a generator: the heat losses are reduced and the batteries can be refilled, by exploiting the kinetic energy.

Obviously, the project has limitations, in particular related to the motor model. In the plant, the degrading effects – i.e. heat losses, eddy currents, nominal magnetic flux variation, etc. – are totally neglected, because just the dynamic equations are converted into mathematical block schemes. Moreover, the limited hardware resources impose a constraint on the word dimension: an accurate resolution can be obtained, but a quantization error – typical of digital systems – will always affect the computed outputs. As example, the algorithm for the maximum torque per ampere region is based on interpolation because the arrays extracted from the LUTs must have a finite size. It is worth noting that the interconnection between the plant and the controller is totally ideal: the inverter is not inserted in the chain, so any modulation techniques is not required for driving the motor. PWM and SVPWM are just introduced in the theoretical part of the thesis, but they are not effectively simulated in the FPGA VI. The presence of both while loops in the Alma Automotive board is another limitation, because a considerable amount of resources is reserved to the motor model. A physical connection is not tested – except for the CAN bus – so the HIL condition is not perfectly verified: the hardware doesn't run the control algorithm alone and the interaction is guaranteed only within the same device.

A further improvement for the project is first of all the introduction of the inverter inside the scheme. In this way, the outputs of the controllers are managed as command voltages. For pulse-width modulation, the three-phase variables – obtained through the Clarke-Park inverse transformations – are compared with the sawtooth carrier signal, as shown in the generic example of chapter III. For reproducing the inverter legs, the comparison between the three modulating and the carrier waveforms produces the switch commands, with different duty cycles for each phase. Alternatively, the advanced space-vector algorithm could be inserted, using the $\alpha\beta$-axes voltages, in order to improve

performance and efficiency of the DC bus use, and to reduce distortion and torque ripple. Then, the motor acts as a low-pass filter, so the fundamental harmonic of the three waves can be extracted and the system can operate properly. The effects related to switching mechanism should be taken into account. Another important progress could be the realization of a complete hardware-in-the-loop validation. Because the real machine is not available, the plant model should run on a separate real-time host which is connected to the engine control unit. The latter executes only the field-oriented control autogenerated code, so in this way the HIL condition is totally guaranteed.

Regarding the realized block diagram for the IPM synchronous motor, the speed loop could be improved in terms of dynamic performance and range, for saturating the velocity if necessary. Furthermore, a hybrid solution for flux-weakening region certainly optimizes the computation of the *d*-axis stator current. The comparison between feedforward and feedback results reduces the uncertainty, requiring on the other side more resources due to the elevate computational effort. Moreover, the development of an algorithm dedicated to maximum torque per voltage (MTPV) could be useful for a further extension of the mechanical speed range. It has also been observed that when the motor enters the FW region it never demonstrates problems, while in the opposite case many peaks are present. Consequently, a different slope could be used, depending on the request variation. In order to verify the correct implementation of the weakening mechanism, a field observer could be inserted in the block scheme. Another important aspect which reflects a real application of the control algorithm is related to motor speed and angle. In the project, these values are simply passed as local variables, but this is not physically plausible, so a simulated encoder should be able to play this role. Finally, the battery management system could send information about the state of charge of the simulated energy source in order to verify that the system is effectively able to respond to user requests.

Bibliography

Akin, B., Bhardwaj, M., & Warriner, J. (2011, April), Texas Instruments, Retrieved from *Trapezoidal Control of BLDC Motors Using Hall Effect Sensors*: http:// www.ti.com/lit/an/sprabz4/sprabz4.pdf

Alma Automotive S.r.l., Retrieved from *SPARK - The open source ECU project*: https:// www.alma-automotive.it/public/sitemin/SPARK.pdf

Amin, F., *et al.* (2017, May), M*odelling and Simulation of Field Oriented Control based Permanent Magnet Synchronous Motor Drive System*, In *Indonesian Journal of Electrical Engineering and Computer Science, 6*(2), pp. 387-395.

Axsen, J., Burke, A. F., & Kurani, K. S. (2010), *Batteries for PHEVs: Comparing Goals and the State of Technology*, In G. Pistoia, *Electric and Hybrid Vehicles. Power Sources, Models, Sustainability, Infrastructure and the Market (pp. 405-427)*, Amsterdam, The Netherlands: Elseiver.

Bayindir, K., Gözüküçük, M., & Teke, A. (2011, February), A *comprehensive overview of hybrid electric vehicle: Powertrain configurations, powertrain control techniques and electronic control units*, In *Energy Conversion and Management, 52*(2), pp. 1305-1313.

Bhandari, P., Dubey, S., Kandu, S., & Deshbhratar, R. (2017, February), *Regerative Braking Systems (RBS),* In *International Journal of Scientific & Engineering Research, 8*(2), pp. 71-74.

Bird, B., King, K., & Pedder, D. (1993). *An Introduction to Power Electronics (Second Edition).* Chichester, West Sussex, United Kingdom: Wiley.

Blackman, J., & Monroe, S. (2013, January), Texas Instruments, *Retrieved from Overview of 3.3V CAN (Controller Area Network) Transceivers:* http://www.ti.com/lit/an/ slla337/slla337.pdf

Boglietti, A. (1995), *Concetti di base sulla macchina in corrente continua (Electrical Machines)*, Biella, Italy: Politecnico di Torino.

Buekers, J., Van Holderbeke, M., Bierkens, J., & Int Panis, L. (2014, December), *Health and environmental benefits related to electric vehicle introduction in EU countries,* In *Transportation Research Part D: Transport and Environment, 33*, pp. 26-38.

Chau, K., Wong, Y., & Chan, C. (1999, July). A*n overview of energy sources for electric vehicles*, In *Energy Conversion & Management, 40*(10), pp. 1021-1039.

Cheles, M. (2009), Microchip Technology Inc.*,* Retrieved from *Sensorless Field Oriented Control (FOC) for a Permanent Magnet Synchronous Motor (PMSM) Using a PLL Estimator and Field Weakening (FW)*: http://ww1.microchip.com/downloads/en/appnotes/01292a.pdf

Chin, Y., & Soulard, J. (2003), *A Permanent Magnet Synchronous Motor for Traction Applications of Electric Vehicles*, Presented at *IEEE Electric Machines and Drives Conference,* Madison, Wisconsin, United States.

Corrigan, S. (2016, May), Texas Instruments*,* Retrieved from *Introduction to the Controller Area Network (CAN)*: http://www.ti.com/lit/an/sloa101b/sloa101b.pdf

Cypress Semiconductor. (2017), Retrieved from *Coordinate Transform in Motor Control*: https://www.cypress.com/file/222111/download

Delucchi, M., & Lipman, T. (2010), *Lifetime Cost of Battery, Fuel-Cell, and Plug-in Hybrid Electric Vehicles*, In G. Pistoia, *Electric and Hybrid Vehicles. Power Sources, Models, Sustainability, Infrastructure and the Market (pp. 19-60),* Amsterdam, The Netherlands: Elseiver.

Eberle, U., & von Helmolt, R. (2010), F*uel Cell Electric Vehicles, Battery Electric Vehicles, and their Impact on Energy Storage Technologies: An Overview,* In G. Pistoia, *Electric and Hybrid Vehicles. Power Sources, Models, Sustainability, Infrastructure and the Market (pp. 227-245)*, Amsterdam, The Netherlands: Elseiver.

Ehsani, M., Gao, Y., & Emadi, A. (2010), *Modern Electric, Hybrid Electric, and Fuel Cell Vehicles. Fundamentals, Theory, and Design (Second edition),* Boca Raton, Florida, United States: CRC Press.

Ferraris, L. (1999), *Macchine Elettriche,* Turin, Italy: CLUT.

Ferreira, F., Ge, B., Quispe, E., & De Almeida, A. (2014), *Star- and Delta-Connected Windings Tolerance to Voltage Unbalance in Induction Motors,* Presented at *International Conference on Electrical Machines (ICEM),* Berlin, Germany.

Fitzgerald, A., Kingsley, C., & Umans, S. (2003), *Electric Machinery (Sixth Edition),* New York, New York, United States: McGraw-Hill.

Gaines, L. (2014, December), *The future of automotive lithium-ion battery recycling: Charting a sustainable course*, In *Sustainable Materials and Technologies, 1-2*, pp. 2-7.

Garland, N., Papageorgopoulos, D., & Stanford, J. (2012, December), *Hydrogen and fuel cell technology: Progress, challenges, and future directions*, In *Energy Procedia, 28*, pp. 2-11.

Ghazimoghadam, M., & Tahami, F. (2011), *Sensorless Control of Non-Salient PMSM using Asymmetric Alternating Carrier Injection,* Presented at *IEEE Symposium on Industrial Electronics and Applications*, (pp. 7-12), Langkawi, Malaysia.

Huynh, T., & Hsieh, M.-F. (2018, May), *Performance Analysis of Permanent Magnet Motors for Electric Vehicles (EV) Traction Considering Driving Cycles*, In *Energies, 11*(6).

Khajepour, A., Fallah, S., & Goodarzi, A. (2014), *Electric and Hybrid vehicles. Technologies, Modeling and Control: A Mechatronic Approach,* Chichester, West Sussex, United Kingdom: Wiley.

Khan, W. (2016), *Torque Maximizing and Flux Weakening Control of Synchronous Machines (Thesis),* Helsinki, Finland: Aalto University.

Kim, Y.-H., *et al.* (2015), *Comparison of IPM and SPM motors using ferrite magnets for low-voltage traction systems*, Presented at *The 28th International Electric Vehicle Symposium and Exhibition,* Goyang, South Korea.

Kohlrusz, G., & Fodor, D. (2011), *Comparison of scalar and vector control strategies of induction motors,* In *Hungarian journal of industrial chemistry Veszprém, 39*(2), pp. 265-270.

Krishnan, R. (2010), *Permanent Magnet Synchronous and Brushless DC Motor Drives,* Boca Raton, Florida, United States: CRC Press.

Kulkarni, S., & Thosar, A. (2013, June), *Mathematical Modeling and Simulation of Permanent Magnet Synchronous Machine*, In *International Journal of Electronics and Electrical Engineering, 1*(2), pp. 66-71.

Kumar, K., Michael, P., John, J., & Kumar, S. (2010, July), *Simulation and comparison of SPWM and SVPWM control for three phase inverter*, In *ARPN Journal of Engineering and Applied Sciences, 5*(7), pp. 61-74.

Lim, S. (2018, April), Texas Instruments, Retrieved from *Sensorless-FOC With Flux-Weakening and MTPA for IPMSM Motor Drives*: http://www.ti.com/lit/an/spracf3/spracf3.pdf

Lu, D., & Kar, N. (2010), *A Review of Flux-weakening Control in Permanent Magnet Synchronous Machines,* Presented at *IEEE Vehicle Power and Propulsion Conference,* Lille, France.

Mohan, N., Undeland, T., & Robbins, W. (2003), *Elettronica di Potenza. Convertitori e Applicazioni (Terza Edizione),* Milano, Italy: Hoepli.

Nagarajan, R., *et al.* (2016, September), *Implementation of SPWM Technique for Inverter*, In *International Journal of Advanced Research in Biology, Engineering, Science and Technology (IJARBEST), 2*(9), pp. 10-14.

National Instruments, Retrieved from *LabVIEW Environment Basics*: http://www.ni.com/getting-started/labview-basics/environment

National Instruments, Retrieved from W*hat Is the LabVIEW FPGA Module?*: http://www.ni.com/en-gb/shop/electronic-test-instrumentation/add-ons-for-electronic-test-and-instrumentation/what-is-labview-fpga-module.html

National Instruments, Retrieved from *What Is the LabVIEW Real-Time Module?*: https://www.ni.com/en-gb/shop/data-acquisition-and-control/add-ons-for-data-acquisition-and-control/what-is-labview-real-time-module.html

NXP Freescale Semiconductor (2012), Retrieved from *Permanent Magnet Synchronous Motor Control*: https://www.nxp.com/docs/en/brochure/BBPRMMAGSYNART.pdf

Ohm, D. (2000), Drivetech Inc., Retrieved from *Dynamic Model of a PM Synchronous Motor:* https://pdfs.semanticscholar.org/e2be/948549aaf744c73b36d303cf7165041222f4.pdf

Orecchini, F., & Santiangeli, A. (2010), *Automakers' Powertrain Options for Hybrid and Electric Vehicles,* In G. Pistoia, *Electric and Hybrid Vehicles. Power Source, Models, Sustainability, Infrastructure and the Market (pp. 579-636),* Amsterdam, The Netherlands: Elseiver.

Parmar, Y., *et al.* (2016, December), *Scalar control of Permanent Magnet Synchronous motor*, In *International Research Journal of Engineering and Technology (IRJET), 3*(12), pp. 364-366.

Prasad, E., Suresh, B., & Raghuveer, K. (2012), *Field Oriented Control of PMSM Using SVPWM Technique*, In *Global Journal of Advanced Engineering Technologies, 1*(2), pp. 39-45.

Raju, N., Islam, M., & Uddin, A. (2013, January), S*inusoidal PWM Signal Generation Technique for Three Phase Voltage Source Inverter with Analog Circuit & Simulation of PWM Inverter for Standalone Load & Micro-grid System*, In *International Journal of Renewable Energy Research, 3*(3), pp. 647-658.

Rusu, C., Birou, I., Radulescu, M., & Bara, A. (2014), *Developing Embedded Control System Platform for Testing PMSM Drives*, Presented at *International Conference and Exposition on Electrical and Power Engineering*, (pp. 677-682), Iasi, Romania.

Staffell, I., *et al.* (2018, December), *The role of hydrogen and fuel cells in the global energy*, In *Energy & Environmental Science, 12*(2).

Toshiba Electronic Devices & Storage Corporation (2018), Retrieved from *DC-AC Inverter Circuit*: https://toshiba.semicon-storage.com/info/docget.jsp?did=61546&prodName=GT30J341

Un-Noor, F., *et al.* (2017, August), *A Comprehensive Study of Key Electric Vehicle (EV) Components, Technologies, Challenges, Impacts, and Future Direction of Development*, In *Energies, 10*(8).

Velardocchia, M. (2019), *Fundamentals of Longitudinal Dynamics (Technologies for Autonomous Vehicles)*, Turin, Italy: Politecnico di Torino.

Wei, L. (2017), *Hybrid electric vehicle system modeling and control (Second Edition),* Chichester, West Sussex, United Kingdom: Wiley.

Weicker, P. (2014). *A systems approach to Lithium-Ion Battery Management.* Norwood, Massachusetts, United States: Artech House.

Xilinx Inc., Retrieved from *Field Programmable Gate Array (FPGA)*: https://www.xilinx.com/products/silicon-devices/fpga/what-is-an-fpga.html

Zhang, S., *et al.* (2012), *Permanent Magnet Technology for Electric Motors in Automotive Applications*, Presented at *2nd International Electric Drives Production Conference (EDPC),* Nuremberg, Germany.